Alfred-Wegener-Institut für Polar- und Meeresforschung
Forschungsstelle Potsdam
Arbeitsgruppe „Periglazialforschung“

Permafrost landform studies on Earth: Implications for periglacial landscape evolution and habitability on Mars

Dissertation
zur Erlangung des akademischen Grades
"doctor rerum naturalium"
(Dr. rer. nat.)
in der Wissenschaftsdisziplin „Terrestrische Geowissenschaften“

als kumulative Arbeit eingereicht an der
Mathematisch-Naturwissenschaftlichen Fakultät
der Universität Potsdam

von
Mathias Ulrich

Potsdam, 6. Juli 2011

“Given a phenomenon, A, whose antecedent we seek. First we ransack the memory for some different phenomenon, B, which has one or more features in common with A, and whose antecedent we know. Then we pass by analogy from the ancedent of B, to the hypothetical antecedent of A, solving the analogic proportion – as B is to A, so is the ancedent of B to the ancedent of A.”

Grove Karl Gilbert, 1886.

The inculcation of scientific method by example.

Am. Jour. Sci. 3d(31), 284-299.

"There is a theory which states that if ever anyone discovers exactly what the Universe is for and why it is here, it will instantly disappear and be replaced by something even more bizarre and inexplicable. - There is another theory which states that this has already happened."

Douglas Adams, 1980.

The Restaurant at the End of the Universe.

Pan Book Ltd., London.

Table of contents

Abstract

Periglacial landforms on Earth reflect cold-climate conditions in connection with permafrost (i.e. ground-ice-related) dynamics. Many geomorphological features, which are interpreted to be periglacial landforms, are in particular distributed in Martian mid-latitudes.

The aim of this thesis was to model geological and geomorphological evolution of Martian periglacial landscapes using the Earth analogous environments as reference, and to reconstruct processes and environmental conditions responsible for their formation. Therefore, spatial analyses of periglacial key regions on Earth and Mars using high-resolution remote-sensing data were supported by detailed terrestrial field investigations in NE Siberia (Russia) and on Svalbard (Norway). Morphometric analyses, modeling of process-controlling factors, and multivariate statistics were conducted with focus on specific periglacial relief features, i.e. depressions formed by permafrost degradation and polygonal patterned ground. Based on these findings the potential of permafrost environments on Mars to be habitable to life are discussed in particular for Utopia Planitia on the Martian northern hemisphere. In this context, the influence of liquid water in periglacial landscape evolution on Mars during its recent geological history is of special importance as liquid water is the major requirement for the existence, evolution, and preservation of any kind of life.

Permafrost degradation features (i.e. thermokarst) were investigated in ice-rich deposits in the Siberian Arctic as terrestrial analogues for asymmetric scalloped depressions in Martian volatile-(water-ice-) rich mantle deposits. Based on field studies, comparative insolation (i.e. thermal) modeling, and geomorphometric analyses an asymmetrical shape and a lateral retrogressive growth of permafrost-related depressions on Mars and Earth were recognized. The main controls are insolation and surface temperatures. In the case of the scalloped depression formation in Utopia Planitia on Mars, thermal modeling confirms that relatively short events of increasing sublimation or even thawing of ground ice during periods of high obliquity (i.e. tilt of the rotational axis) within the last 10 million years led to fast slumping processes on the steep pole-facing scalloped depression slopes. Meanwhile, the equator-facing slopes were flattened by continuous, though slow, ground ice sublimation and depression surface subsidence under lower obliquity conditions. Generally, the landscape morphology points to a dry origin of scalloped depressions on Mars. Surface features implying the former existence of flowing or standing water, which are clearly associated with thermokarst landscapes on Earth, do not exist in the investigated Martian region. The volume and the dimensions of the scalloped depressions on Mars, however, must be related to higher ground ice contents than the amounts proposed for Utopia Planitia. This conclusion became obvious as depth and size of terrestrial thermokarst depressions are clearly related to the ground-ice content of the sediments in which they are formed.

Geomorphometric analyses on Svalbard focused on polygonally patterned ground to draw a terrestrial analogue to small-scale polygonal structures in Utopia Planitia on Mars. Comparative quantitative terrain analyses based on high-resolution remote-sensing and topographic data were combined with terrestrial field data and multivariate statistics to determine the relationship of polygon geomorphometry to environmental conditions. The results reveal a similar polygon geomorphometry on Earth and Mars, which suggests a comparable genesis by thermal contraction cracking. Polygon morphology, however, is strongly related to local and regional landscape dynamics. This is reflected by differences in size and morphology of the polygons on Earth and Mars. Therefore, the effects of past and present environmental conditions on polygon formation had to be considered. The larger polygons on Svalbard and in Utopia Planitia are currently degrading and have probably been formed in past times when general climate conditions and in particular strong temperature gradients allow deep thermal contraction cracking. Smaller polygons represent young and recently-active low-centered polygons that were formed in fine-grained ice-rich material. In the case of the small low-centered polygons on Mars, the formation of ice wedge-like structures by the influence of transient liquid water could have occurred in micro-climatic niches in response to past orbital configurations. These patterns show the closest analogy to ice-wedge polygons on Svalbard. Regionally, the present appearance of polygons in Utopia Planitia is primarily the result of contemporary dry degradation processes (i.e. sublimation). In contrast, the thawing of ice wedges degrades high-centered polygons in Arctic permafrost regions (i.e. Svalbard). Furthermore, many of Svalbard's periglacial landforms, such as gullies, debris flow fans, polygonal terrain, fractured mounds, and rock glacier-like features are observed in similar proximity in mid-latitude landscapes on Mars suggesting the geologically recent action of glacial and periglacial processes. The landscape evolution would be controlled by obliquity and other orbital parameters such as eccentricity or the position of perihelion and is therefore assumed to be cyclic.

Finally, the insights gleaned from terrestrial analogue studies were summarized to discuss past and present subsurface and climate conditions in relation to periglacial landscape evolution on Mars. Specific climate periods were identified for the most recent Martian history (<10 million years), which meet the requirements of distinct orbital configurations (high obliquity (>35°), high eccentricity (>0.1), and northern summer at perihelion) during which thaw processes and liquid water could have had an influence on periglacial landscape evolution in Martian mid-latitudes. Liquid water involved in the evolution of permafrost landforms in Utopia Planitia might have allowed the development of habitable micro-climatic niches, which are strongly related to specific permafrost landform morphology.

Kurzfassung

Periglaziale Landschaftsstrukturen auf der Erde stehen in engem Zusammenhang mit kalt-klimatischen Umweltbedingungen. Die Geomorphologie solcher Landschaften wird durch die Dynamik von Grundeis im dauerhaft gefrorenen Untergrund (Permafrost) bestimmt. Viele geomorphologische Phänomene auf dem Mars, die insbesondere in dessen mittleren Breiten verbreitet sind, wurden ebenfalls als periglaziale Strukturen interpretiert.

Ziel dieser Arbeit war die Modellierung geologischer sowie geomorphologischer Entwicklung von periglazialen Landschaften auf dem Mars basierend auf der Studie terrestrischer Analoga. Darüber hinaus lag ein besonderer Schwerpunkt in der Rekonstruktion von Prozessen und Umweltbedingungen, welche die Entwicklung solcher Landschaften auf dem Mars beeinflussen. Unter Nutzung hoch aufgelöster Fernerkundungsdaten wurden periglaziale Schlüsselregionen auf der Erde und auf dem Mars anhand von morphometrischen Analysen, multivariater Statistik sowie der Modellierung prozess-kontrollierender Parameter räumlich analysiert. Ergänzend wurden Geländeuntersuchungen an periglazialen Indikatorstrukturen (Frostmuster-Polygonböden und Thermokarststrukturen) in Nordostsibirien und auf Spitzbergen durchgeführt, um diese als mögliche Mars-Analoga besser charakterisieren zu können. Ziel dieser Untersuchungen war die Eingrenzung möglicher habitabler (lebensfreundlicher) Zonen auf dem Mars anhand geologischer und geomorphologischer Bedingungen. Am Beispiel der auf der nördlichen Marshemisphäre gelegenen Region Utopia Planitia wurde die Habitabilität von Permafrostlandschaften abgeschätzt und diskutiert. Dabei ist der Einfluss von flüssigem Wasser in der geologisch jüngsten periglazialen Landschaftsentwicklung des Mars von besonderem Interesse, da flüssiges Wasser unerlässlich für die Existenz, Entwicklung und Erhaltung jeglicher Art von Leben ist.

Permafrostdegradationsstrukturen (Thermokarstsenken) wurden in sibirischen eisreichen Feinsedimenten als terrestrische Analoga für asymmetrisch geformte Senken auf dem Mars untersucht. Diese charakteristischen Marssenken (genannt *scalloped depressions*) bilden sich in Feinsedimenten, die als eisreiches Mantelmaterial interpretiert wurden. Auf der Basis von Feldstudien in Sibirien, vergleichenden Einstrahlungsmodellierungen sowie geomorphometrischen Analysen konnten eine typisch asymmetrische Form der Senken sowie ein lateral rückschreitendes Wachstum der Senken auf Erde und Mars nachgewiesen werden. Wesentliche Einflussfaktoren sind dabei direkte Sonnenbestrahlung und damit lokal steigende Oberflächentemperaturen. Im Falle der Marssenken in Utopia Planitia bestätigten die thermischen Modellierungen, dass verhältnismäßig kurze Ereignisse von zunehmender Sublimation oder des Auftauens des Grundeises zu kurzfristigen intensiven Rutschungen auf den steilen polwärts orientierten Senkenhängen geführt haben könnten. Dies geschah aller Wahrscheinlichkeit nach während Perioden hoher Obliquität (Neigung der Planetenachse) innerhalb der letzten 10 Millionen Jahre. Unterdessen wurden die äquatorwärts orientierten Hänge während Perioden geringerer Obliquität

durch eine sehr langsame Sublimation des Grundeises und der damit zusammenhängenden kontinuierlichen Absenkung der Oberfläche zunehmend verflacht. Im Allgemeinen deutet die Landschaftsmorphologie in Utopia Planitia aber auf einen trockenen Ursprung der Marssenken. Oberflächenstrukturen, die auf das ehemalige Vorhandensein von Fließgewässern oder stehenden Wassers hindeuten, die aber auf der Erde offenbar mit Thermokarstlandschaften verbunden sind, existieren in der untersuchten Marsregion nicht. Die Volumina und Ausmaße der Marssenken müssen allerdings im Zusammenhang mit weitaus höheren Grundeisgehalten entstanden sein, als sie heute in den obersten Bodenschichten in Utopia Planitia detektiert werden. Die Größe und Tiefe terrestrischer Thermokarstsenken steht in direktem Zusammenhang mit dem Grundeisgehalt der Sedimente, in denen sie gebildet werden.

Geomorphometrische Analysen auf Spitzbergen konzentrierten sich auf polygonale Frostmusterstrukturen, um einen Vergleich zu kleinskaligen polygonalen Strukturen auf dem Mars ziehen zu können. Quantitative Geländeanalysen, die auf hochauflösenden Fernerkundungsdaten basieren, wurden mit terrestrischen Felddaten und statistischen Verfahren zur Analyse multivariater Daten verknüpft, um das Verhältnis der polygonalen Geomorphometrie zu beeinflussenden Umweltbedingungen zu ermitteln. Die Ergebnisse offenbarten eine ähnliche Geomorphometrie der Polygone auf Erde und Mars. Daraus wurde eine vergleichbare Genese beider polygonaler Muster durch thermale Kontraktion des gefrorenen Bodens geschlossen. Jedoch hängt die Morphologie der Polygone stark mit der lokalen und regionalen Landschaftsdynamik zusammen. Dieses wird durch die Unterschiede von Größe und Morphologie der Polygone auf Erde und Mars deutlich. Folglich mussten die Effekte vergangener und gegenwärtiger Umweltbedingungen auf die Entstehung der polygonalen Strukturen betrachtet werden. Die größeren Polygone auf Spitzbergen und in Utopia Planitia unterliegen derzeit Degradationsprozessen und sind in vergangenen Zeiten unter anderen Klimazuständen gebildet worden als insbesondere stärkere Temperaturvariationen ein tieferes Eindringen von Frostspalten in den Permafrostboden ermöglichten. Kleinere Polygone mit im Vergleich zum umgebenden Rand tiefer liegenden Zentren (*low-centered polygons*), stellen junge und kürzlich aktive Strukturen dar, die in feinkörnigem eisreichen Material gebildet wurden. Im Falle der kleinen *low-centered* Polygone auf dem Mars könnten kurzfristige Tauprozesse und das Eindringen von vorübergehend flüssigem Wasser in Frostspalten während vergangener orbitaler Konfigurationen zur Bildung von eiskeil-ähnlichen Strukturen in bestimmten mikroklimatischen Nischen geführt haben. Diese polygonalen Muster zeigen die größte Analogie zu Eiskeilpolygonen auf Spitzbergen. Die gegenwärtige Erscheinung der Polygone in Utopia Planitia ist hingegen regional gesehen hauptsächlich das Resultat von aktuell vorherrschenden trockenen Grundeisdegradationsprozessen (d. h. Sublimation). Demgegenüber steht in arktischen Permafrostgebieten wie Spitzbergen die Entstehung von *high-centered* Polygonen (d. h. Polygone mit im Vergleich zum umgebenden Rand höher liegenden Zentren) durch das Auftauen von Grundeiskörpern (Eiskeilen). Viele der periglazialen Oberflächenstrukturen auf Spitzbergen wie

Erosionsrinnen, alluviale Fächer, polygonale Frostmuster, pingo-ähnliche und blockgletscher-ähnliche Strukturen wurden in vergleichbaren räumlichen Zusammenhängen in den mittleren Breiten des Mars beobachtet. Daraus lässt sich die geologisch junge Aktivität von periglazialen Prozessen auf dem Mars schließen. Die Landschaftsentwicklung wird vermutlich sehr stark durch die Obliquität und anderer orbitaler Parameter wie Exzentrizität und die Position des Perihelions beeinflusst und kann folglich als zyklisch angenommen werden.

Schließlich wurden die Erkenntnisse aus den terrestrischen Analogstudien zusammengefasst, um die gegenwärtigen und vergangenen Grundeis- und Klimabedingungen im Zusammenhang mit der periglazialen Landschaftsentwicklung auf dem Mars zu diskutieren. Spezifische Klimazeiträume konnten für die jüngere geologische Geschichte des Mars (<10 Millionen Jahre) identifiziert werden, in denen bestimmte orbitale Konfigurationen (hohe Obliquität (>35°), hohe Exzentrizität (>0,1) und Nordsommer im Perihelion) den Einfluss von Tauprozessen und flüssigem Wassers auf die periglaziale Landschaftsentwicklung innerhalb der mittleren Breitengrade des Mars ermöglicht haben könnten. Flüssiges Wasser, das in die Entwicklungsgeschichte der Permafrostlandschaften auf dem Mars einbezogen wurde, könnte zur Entwicklung habitabler mikroklimatischer Nischen im Permafrostboden geführt haben, die sehr stark mit der spezifischen Morphologie der periglazialen Strukturen in Utopia Planitia verbunden sind.

1. Introduction

Preface

This presented PhD thesis was realized within the framework of the research alliance "Planetary Evolution and Life", which is supported by the Helmholtz Association. The alliance focuses on the questions: Was there once, or is there still life on Mars or other extraterrestrial planets? What could be the linkage between the potential evolution of life and planetary geology and geomorphology? This question inspires the search for habitable zones outside the Earth and aims to identify the potential of different planetary environments to sustain life. Besides energy gained from inorganic/organic nutrients or from sunlight, the major requirement for the existence, evolution, and preservation of biological systems is access to liquid water. The identification of possible habitable zones depends, therefore, on knowing whether liquid water was available during the geological and geomorphological history of a certain planetary landscape. The most promising planet in our solar system to search for past and/or present liquid water activity is Mars. Several geomorphic features characteristic of water activity on Earth, e.g., outflow channels, deltas, and gullies, have been detected and investigated on Mars; therefore, it is nowadays widely accepted that water was active in the past on the Martian surface. Furthermore, we are now aware that Mars is a permafrost planet and that a large quantity of water on Mars exists in the subsurface today as ground ice. The surface of Mars shows many landforms that resemble terrestrial periglacial features. On Earth, such features reflect specific, continuous cold-climate conditions, and they are formed in connection with permafrost dynamics, commonly under the influence of freezing and thawing of water ice. Therefore, the investigations of potential Martian periglacial landforms, analogous to landforms found on Earth, contribute to understanding the history of water on Mars and to defining geological boundary conditions for possible habitable zones.

1.1 Scientific background

1.1.1 Permafrost, ground ice, and periglacial features on Earth and Mars

Permafrost is defined as any ground that remains at or below 0°C (~273 K) for at least two or more consecutive years, regardless of ice occurrence. Since the presence of mineral salts or higher pressure can depress the freezing point of water below 0°C, permafrost is not necessarily frozen [*Everdingen*, 2005; *French*, 2007]. Permafrost underlies more than 20% of the continental Earth's surface [*Bockheim*, 1995; *Zhang et al.*, 2005]. The dynamics of permafrost results in special frost-related structures, land-surface features, and processes summarized by the term "periglacial" [*Everdingen*, 2005]. Most of the frost-related processes, like frost cracking, cryoturbation, or solifluction, occur in the seasonally-changing uppermost part of the permafrost zone. One of the

most important attributes in periglacial landscape dynamics is the occurrence of ground ice. With respect to the geomorphology and topography of periglacial landscapes, four main types of ground ice can be distinguished; segregated ice, wedge ice, intrusive ice, and pore or interstitial ice [*Williams and Smith,* 1989; *Yershov,* 2004; *French,* 2007]. Segregated ice is the general term for ice accumulation in fine-grained soils with high ground-ice contents; it is formed by pressurized migration of water to the freezing front through the adjacent soil pores. It can be distinguished by its ice content and its structures from pore or interstitial ice, which cements the soil [*French,* 2007]. Large bodies of ground ice mainly occur in the upper part of frozen ground. Pingos (i.e. ice-cored mounds) contain intrusive ice cores that result from highly-pressurized water intrusion [e.g., *Gurney* 1998]. Ice-wedge bodies are developed when melt water fills frost cracks, a process that occurs almost every summer. These cracks are caused by thermal contraction of frozen ground, a process that results in polygonal patterned networks of frost cracks at the surface. Other types of massive ice bodies can also originate from, e.g., buried glacier ice. The thawing and degradation of permafrost that contains ground ice results in surface subsidence and the formation of characteristic depressions in the landscape (i.e. thermokarst).

According to the above definition of permafrost, Mars may be considered to be a permafrost planet that exhibits a wide variety of periglacial landscapes. As suggested by, e.g., *Shuster and Weiss* [2005], subsurface temperatures probably persisted below 0°C for most of Martian geological history. The presence of extensive near-surface ground ice on Mars was demonstrated conclusively using the measurements of the Gamma Ray Spectrometer (GRS), which detected a pole-ward increasing abundance of water-equivalent hydrogen concentration within the first meter of the subsurface [*Boynton et al.,* 2002; *Mitrofanov et al.,* 2002; *Feldman et al.,* 2004]. This was recently confirmed by *in-situ* detection of relatively pure water ice in the shallow subsurface at the Phoenix Lander site near the north pole [e.g., *Mellon et al.,* 2009; *Smith et al.,* 2009] and also by spectral analyses of water ice excavated from impact craters in a mid-latitude region [*Byrne et al.,* 2009]. These findings correspond to ice-stability models that suggest stable ground ice can exist near the surface only at higher latitudes (>50-60°N/S) under the current Martian climate, but ice could generally be stable at depths below 1 m at latitudes down to ~40-45°N/S [e.g., *Mellon and Jakosky,* 1995; *Mellon et al.,* 2004]. Therefore, the depth of the ground-ice (i.e. permafrost) table varies in relation to the geographic distribution. The models also suggest that the stability of near-surface ground ice on Mars depends on the variations of Martian orbital parameters. If Mars' obliquity (i.e. tilt of the rotational axis) exceeds 32° (today ~25°) ground-ice becomes globally stable [*Mellon and Jakosky,* 1995]. Since the orbital parameters change chaotically and the value of the mean obliquity in the Martian past was probably higher than today [*Laskar et al.,* 2004], ground ice is believed to have exerted a significant influence on Martian landscape evolution.

The release of low-resolution Mariner 9 and Viking data allowed a morphological analogy to be drawn between several periglacial Martian landforms and terrestrial permafrost features as early

as the 1970's [e.g., *Sharp,* 1973; *Carr and Schaber,* 1977; *Lucchitta,* 1981; *Rossbacher and Judson,* 1981]. With the advent of high-resolution data (i.e. from the Mars Orbiter Camera, MOC, and the High Resolution Imaging Science Experiment, HiRISE), these early notions were confirmed and new geomorphological evidence was found to support the hypothesis that periglacial processes might have played an important role in shaping the younger Martian landscapes [e.g., *Baker,* 2001; *Malin and Edgett,* 2000; *Mangold et al.,* 2004; *Levy et al.,* 2009a]. However, the origin of Martian ground ice is still under debate. Most of the studies concerning ground-ice-related landforms have focused on their formation in young geological units (Late Amazonian-aged; Figure 1.1) of the mid- and high-latitudes. These observations are in agreement with hypotheses of obliquity-driven subaerial deposition of ice-rich material during recent geological times [e.g., *Head et al.,* 2003; *Levrard et al.,* 2004; *Madeleine et al.,* 2009]. Other authors have discussed climatic and latitude-dependent water exchange by vapor diffusion into and out of the subsurface regolith [e.g., *Mellon et al.,* 2004; *Schorghofer and Aharonson,* 2005; *Schorghofer,* 2007].

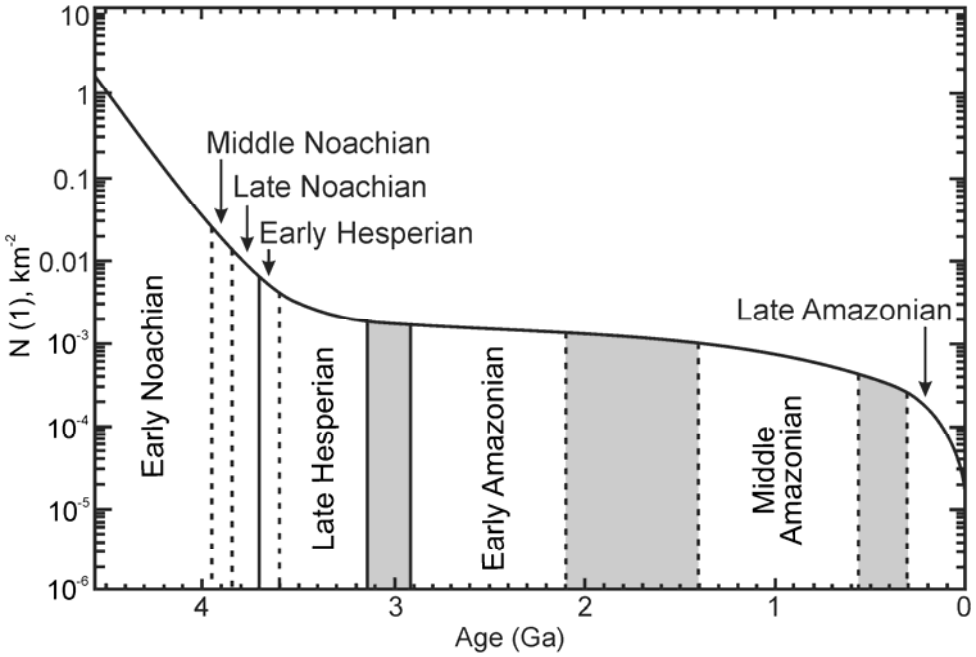

Figure 1.1: Mars stratigraphy based on cratering chronology [modified after *Hartmann and Neukum,* 2001]. The major time periods (Noachian, Hesperian, and Amazonian) are separated by solid lines. Grey areas mark time uncertainties in period transitions.

1.1.2 The Martian mid-latitude landscapes and Utopia Planitia

An exciting aspect with regard to the distribution of Martian permafrost landforms is the fact that features which are interpreted to be formed in relation to ground ice (e.g., thermal-contraction-cracking polygons, small rimless depressions, gullies, viscous flow features, and pingo-like features) are clustered in a latitudinal belt between ~30° and ≥60° (Figure 1.2) and often formed in

areas which appear smooth on a kilometer scale where they are not degraded. Deposits covering these areas are identified on the basis of Mars Orbiter Laser Altimeter (MOLA) and MOC data and interpreted as a tens-of-meters–thick, fine-grained, ice-rich mantle layer, which drapes over older, rougher terrain [*Kreslavsky and Head*, 2000, 2002; *Mustard et al.*, 2001; *Head et al.*, 2003].

This study focused on the western part of Utopia Planitia situated within the northern Martian lowlands (30°N-60°N and 80°E-120°E; Figure 1.2). The area is part of the Utopia basin, which was possibly formed by a giant impact during the (pre-) Noachian period (~4.5 to ~3.7 Ga) [*McGill*, 1989; *Thomson and Head*, 2001; *Tanaka et al.*, 2005]. During the Hesperian (~3.7 to ~3.0 Ga; Figure 1.1) the region was influenced by tectonic and volcanic activities, and in the transition to the Amazonian (<3.0 Ga) the basin was filled by outflow channel deposits and/or sediments deposited in large standing water bodies [*Head et al.*, 2001]. In particular, the late Amazonian (<300-600 Ma; Figure 1.1) was characterized by air-fall deposition of ice-rich materials, which were subsequently reworked by periglacial processes [e.g., *Tanaka et al.*, 2005]. The area was chosen for analogue studies because it has been well known since the Viking 2 mission landed in 1976 at 47.7°N and 134.1°E. More importantly, the region is unique, because many landforms interpreted to have formed in relation to ground ice are clustered there, in particular in western Utopia Planitia (Figure 1.2).

For instance, small rimless depressions, recently described as scalloped depressions (Figure 1.2B), were interpreted by *Sharp* [1973] as ground-ice degradation features. Many varieties of small-scale polygonal structures are widely distributed (Figure 1.2E) [e.g., *Seibert and Kargel*, 2001], and small fractured mounds are suggested to be analogues to terrestrial pingos (Figure 1.2D) [e.g., *Soare et al.*, 2005; *de Pablo and Komatsu*, 2009]. Furthermore, the occurrence of gullies (Figure 1.2C) in the comparatively few impact craters of Utopia Planitia point to the recent activity of liquid water [*Soare et al.*, 2007; see e.g., *Malin and Edgett*, 2000, and *Dickson and Head*, 2009 for discussions of Mars-wide gully origin]. Climatically, Utopia Planitia is situated right at the border of currently stable ground ice. The mean surface temperatures range between ~180 K (~-90°C) in winter and ~240 K (~-30°C) in summer [*Morgenstern et al.*, 2007] and the quantity of ice in the upper ground (<1 m) in the region detected by the GRS is estimated to be about 7 wt% (see also Figure 1.2A) [*Feldman et al.*, 2004]. However, the role of liquid water and thaw processes in the landscape evolution of Utopia Planitia is still under debate. For instance, *Levy et al.* [2009b] favor prolonged “dry” desert periglacial conditions in which sublimation is the dominant permafrost degrading factor and liquid water is excluded, while e.g., *Soare et al.* [2007, 2008] and *Soare and Osinski* [2009] proposed a “wet” periglacial landscape evolution in which standing water bodies existed and thawing was the dominant degrading factor.

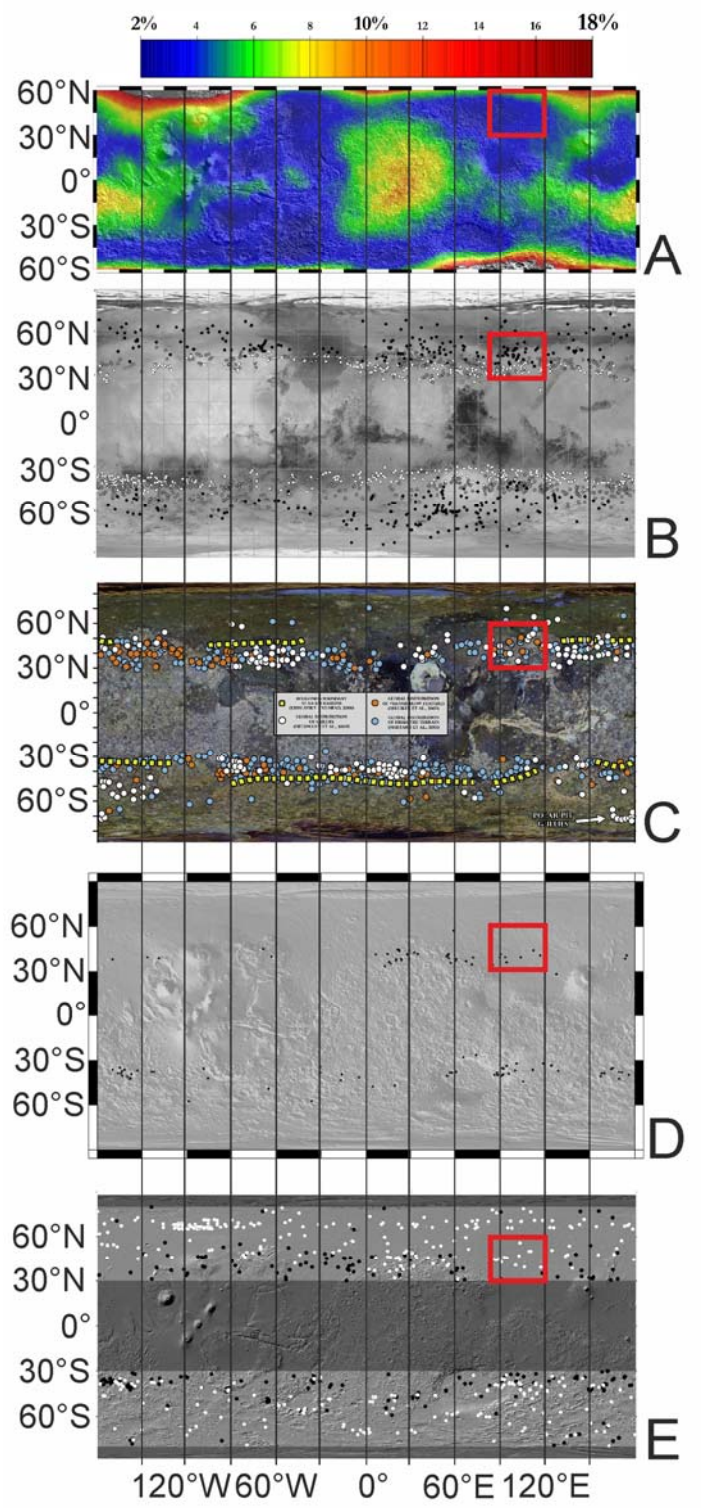

Figure 1.2: Distribution of water and selected periglacial features on Mars. Maps are compiled and modified from the literature. The investigated region is marked by the red rectangle (see text). Note some symbols are not mentioned; they refer to data presented in the individual papers and are not covered by this work. (A) water-equivalent hydrogen content determined by GRS [*Feldman et al.*, 2004]. (B) Distribution of different types of degraded terrain. Black dots represent mantled and scalloped terrain [*Zanetti et al.*, 2010]. (C) Global distribution of gullies (white dots) and viscous flow features (orange dots) [*Dickson and Head*, 2009]. (D) Distribution of fractured mounds (black dots) partly interpreted as pingo-like features [*Dundas and McEwen*, 2010]. (E) White dots indicating satellite images in which features were interpreted to be thermal-contraction-crack polygons [*Levy et al.*, 2009a].

1.1.3 Terrestrial periglacial landscapes as Martian environmental analogues: Introduction to the study sites in Siberia and on Svalbard

During the long tradition of terrestrial analogue studies in planetary science [see e.g., *Sharp*, 1988], cold-climate polar landscapes have often been considered to be the most useful terrestrial analogues to Martian climate. With respect to the prolonged cold and dry conditions on present-day Mars, in particular, the cold deserts of the Antarctic Dry Valleys are suggested to be the closest environmental analogues to Mars (Figure 1.3) [e.g., *Anderson et al.*, 1972; *Marchant and Head*, 2007].

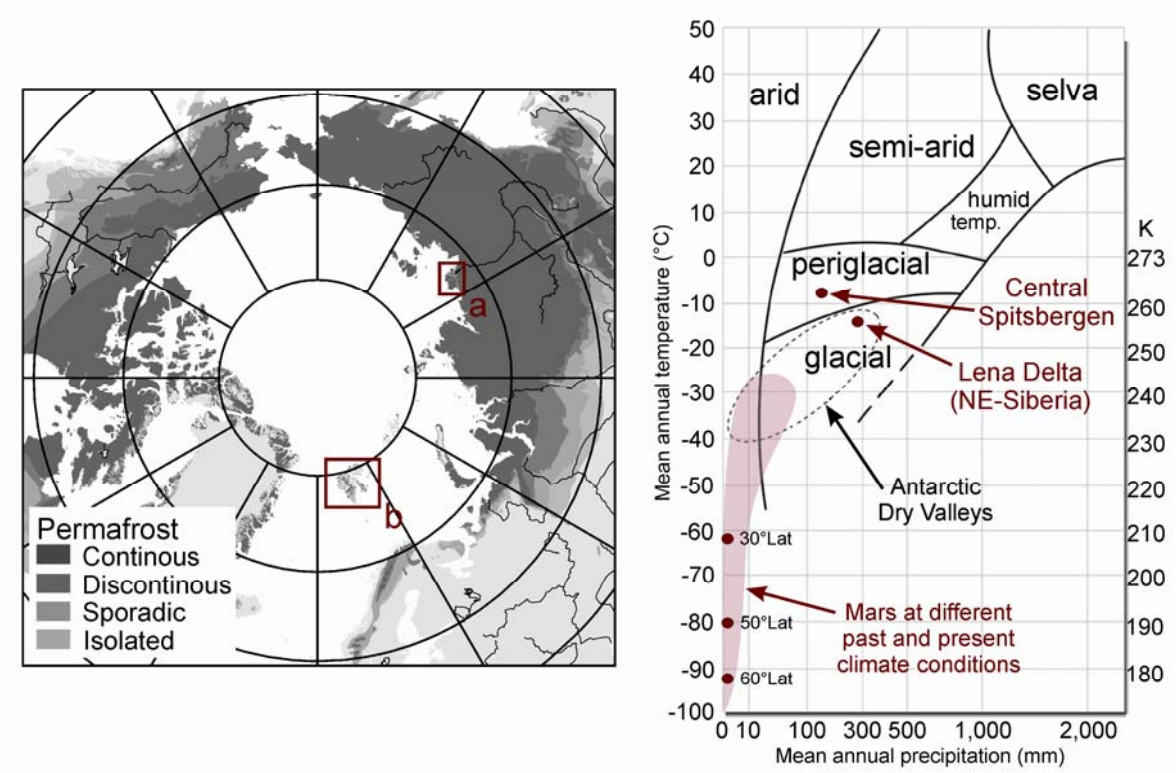

Figure 1.3: Left: Location of the terrestrial study sites marked with red squares. Map of permafrost distribution after *Brown et al.* [1998] (a) The Lena Delta in NE Siberia. (b) The Svalbard Archipelago. Right: Morphogenetic regions for climate-related landforms on Earth; modified from *Baker* [2001] and *Marchant and Head* [2007]. The transparent red area represents Mars at different latitudes and surface pressures (present and inferred past).

Many authors have studied Antarctic permafrost geomorphology and ecology to obtain insights into climate and subsurface conditions, landforms, and possible microbial activity on Mars [e.g., *Gilichinsky et al.*, 2007; *Marchant and Head*, 2007; *Levy et al.*, 2009c, 2010a]. However, besides the necessary costly and complicated logistics required to access the Antarctic Dry Valleys, the valleys lack some periglacial features whose analogues can probably be seen on Mars (e.g., pingos and thermokarst features). Arctic regions are often more easily accessible, and provide numerous periglacial landforms in close spatial proximity that have already been compared to similar landforms on Mars. For instance, polygonal structures on the Arctic coastal plains of North

America and in the Canadian high Arctic regions have been compared by e.g. *Seibert and Kargel* [2001] and *Mangold* [2005], and quantitatively analyzed by e.g. *Haltigin et al.* [2010]. The distribution of possible pingos on Mars was assessed by *Burr et al.* [2009] after a comprehensive literature review of and morphological comparisons with Arctic pingos. *Balme and Gallagher* [2009] used retrogressive thaw slumps on Herschel and Ellesmere islands, Canadian Arctic, as terrestrial analogues for morphologically similar landforms in a Martian equatorial region. From the same region, certain polygonal patterns were inferred to be analogues to sorted stone circles on, e.g., Ellesmere Island in Canada [*Balme et al.,* 2009]. *Morgenstern et al.* [2007] suggested the periglacial landscapes in Siberian ice-rich deposits are terrestrial analogues to the polygonally-fractured mantling material and its thermokarst-like depressions in Martian mid-latitudes.

For this study Kurungnakh Island in the south-central Lena Delta (NE Siberia, Russia) and the Adventdalen in Central Spitsbergen (Svalbard, Norway) were chosen, as both areas are located in the zone of continuous permafrost (Figure 1.3) and offer a diverse inventory of periglacial landforms in close spatial proximity. Kurungnakh Island represents a typical thermokarst-influenced lowland permafrost landscape with a widespread distribution of large thermokarst depressions, ice-wedge polygons, and pingos. The climate of the Lena Delta is true arctic. The mean annual air temperature is about -13.5°C and the mean annual precipitation reaches ~300 mm [*ROSHYDROMET,* 2009]. Kurungnakh Island consists of fine-grained sediments with very high ice contents of up to 90% by volume. The U-shaped valley named Adventdalen represents a mountainous arctic permafrost landscape and is located in the dry central regions of Spitsbergen, the largest island of Svalbard. The annual precipitation reaches only ~180 mm and the mean annual air temperature is around -6°C [*Hanssen-Bauer and Førland,* 1998] (Figure 1.3). The bedrock massifs bordering the valley are characterized by Jurassic and Cretaceous sandstones, siltstones, and shales, but fine-grained loess-like deposits are widely distributed on the valley bottom [*Bryant,* 1982; *Dallmann et al.,* 2001]. Typical periglacial features which can be found in the Adventdalen include different kinds of patterned ground, pingos, and rock glaciers. Both study sites are easily accessible for field work. The periglacial inventory of both terrestrial study sites and their comparative morphological and geological similarities to Martian mid-latitude mantle deposits make them very useful morphological analogues.

1.1.4 Climatic and astrobiological relevance of potential Martian periglacial landscapes

Pure liquid water is generally unstable everywhere on the present Martian surface because of very low pressure and low temperature (Figure 1.4) and the question of whether transient liquid water currently exists, for instance as salty solutions or thin films, is still under debate [e.g., *Haberle et al.,* 2001; *Möhlmann,* 2005; *Tosca et al.,* 2011]. Despite the instability of liquid water, many probably-young landforms, in particular gullies and periglacial features, have been

interpreted as the results of processes involving liquid water [e.g., *Costard and Kargel*, 1995; *Malin and Edgett*, 2000; *Seibert and Kargel*, 2001; *Reiss et al.*, 2010]. Therefore, they must have formed either under current short-time and small-scale special environmental conditions or as a result of past processes that occurred when Martian environments were more favorable to the thawing of ice and to the existence of stable liquid water.

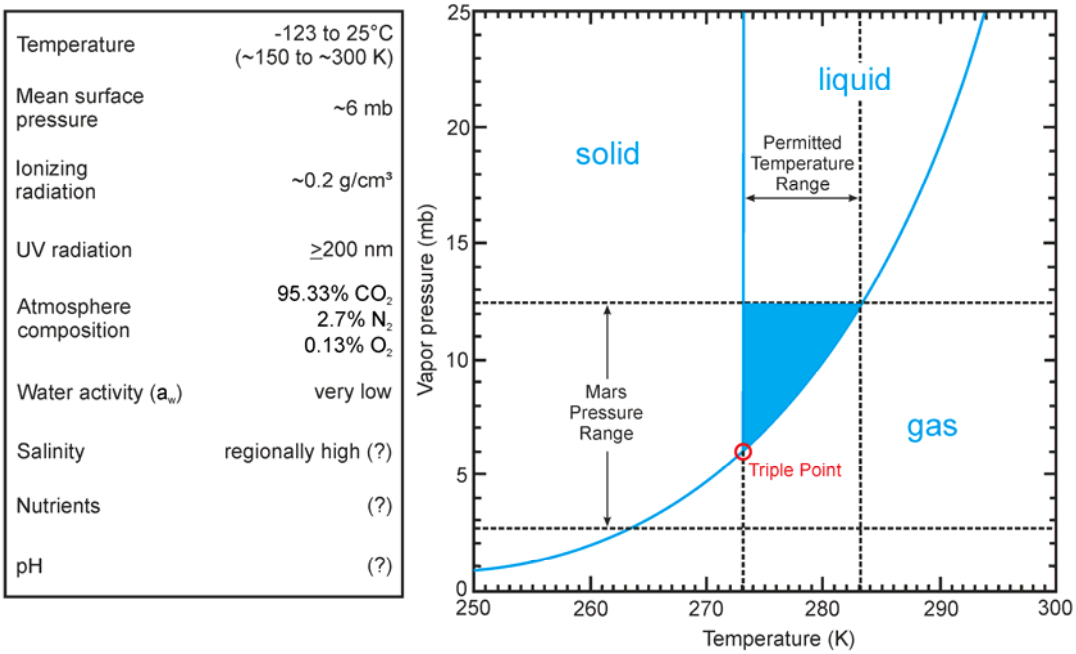

Figure 1.4: Left: Current mean environmental conditions on the entire Martian surface, modified after *Horneck* [2000]. Right: Water-phase diagram shows the stable phase of water (gas, liquid, or solid) over a range of pressure and temperature [modified after *Haberle et al.*, 2001]. Transitions between the phases are represented by the blue line. All three phases can co-exist at the triple point (~273 K, 6.1mb). The range of pressure and temperature that would currently permit the presence of pure liquid water on Mars is shown by the blue area: Pressure above 6.1mb, temperature between 273 K (below 273 K water sublimates or freezes) and 284 K (above 284 K water boils).

Significant and chaotic changes of past Martian climate were precisely modeled for the last 20 Ma by *Laskar et al.* [2004]. Insolation increased, in particular on the mid- and high-latitudes, and temperatures probably rose above 273 K, especially if obliquity reached higher values [e.g., *Costard et al.*, 2002]. Furthermore, during obliquity changes the Martian climate is also sensitive to variations of eccentricity (i.e. orbit deviation from a perfect circle) and climatic precession (i.e. orientation of the rotation axis at summer solstice) [*Laskar et al.*, 2002; *Paige*, 2002]. Therefore, investigating periglacial landforms and estimating the degree of influence exerted by liquid water on their formation allows us to obtain insights into past and present environmental and climate conditions. With regard to the potential depth of the Martian water-ice cryosphere [i.e. several kilometers; *Clifford et al.*, 2010], permafrost on Mars represents a large water reservoir outside the polar caps. Beyond its role as a geomorphological agent, its exploration is also important for

astrobiological studies because it possibly provides protective niches where life may have survived or evolved [e.g., *McKay,* 1997; *Horneck,* 2000].

1.2 Aims and approaches

The comparison of Martian and terrestrial permafrost features is the general objective of this thesis. To obtain reference values and the information needed to interpret remote-sensing data, the consideration and understanding of terrestrial analogues is essential. Knowing the processes that formed a terrestrial analogue might allow us to infer the processes that formed a similar feature on a different planet under study [see discussion by *Baker*, 2008]. Up to now, many analogue studies have been based primarily on descriptive (qualitative) comparisons. Therefore, the overarching approach of this thesis is the morphometric analysis of periglacial structure in key regions on Mars and Earth using high-resolution remote-sensing data and the analysis of local environmental conditions that control terrestrial periglacial morphology. For this purpose, quantitative terrain analyses are combined with geomorphological and sedimentological field data (Figure 1.5). The first main goal of this thesis is to model the geological and geomorphological evolution of certain periglacial landscape features with respect to past and present Martian environmental conditions.

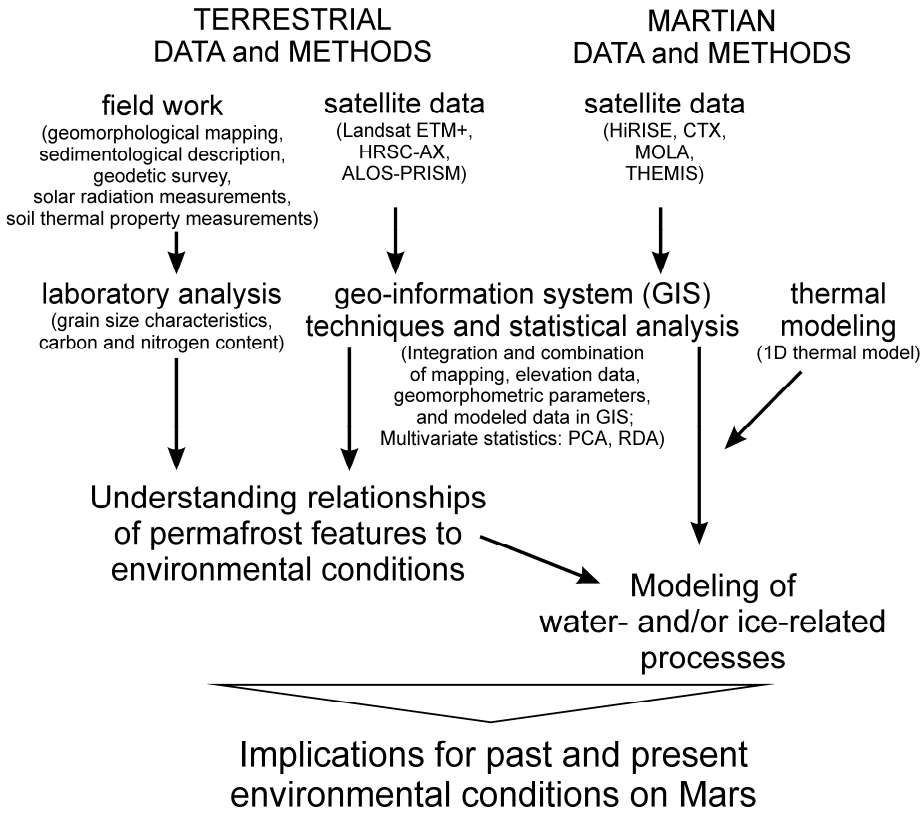

Figure 1.5: Flowchart of methodical approach used in this thesis (ETM+, Enhanced Thematic Mapper Plus; HRSC, High Resolution Stereo Camera; PRISM, Panchromatic Remote-sensing Instrument for Stereo Mapping; CTX, Context Camera; THEMIS, Thermal Emission Imaging System; PCA, Principal Component Analysis; RDA, Redundancy Analysis).

The following questions shall be answered to reach the first goal:

- Which environmental parameters are directly or indirectly related to the formation and appearance of specific periglacial features on Earth?
- What can be inferred from the known controlling environmental parameters of terrestrial permafrost landforms for analogous landforms on Mars?
- What are the similarities of and differences between diverse morphological analogues?
- How does the morphometry and geomorphology of Martian landforms reflect past and present subsurface and environmental conditions?

The second goal is to estimate the potential for permafrost landscapes on Mars to be habitable environments. In order to reach this goal the following questions are to be answered:

- How is the influence of liquid water connected with the influence of thawing ground ice on Martian permafrost landforms during current and past climate periods?
- Can we define periods with favorable climate conditions that allow thaw processes and the presence of liquid water, and what is the duration of those periods?
- What can be inferred from past and/or present environmental conditions on Mars with regard to the allowed environmental range for the existence of any biological system?

1.3 Thesis organization

1.3.1 Overview of chapters

This cumulative dissertation consist of an introductory chapter (Chapter 1) providing scientific background and the aims and objectives of this thesis, followed by three main chapters (Chapters 2-4), and a synthesis (Chapter 5). The three main chapters and the appendix contain original research papers, which have been designed for publication in international peer-reviewed journals (Table 1.1). These papers are published in the *Journal of Geophysical Research – Planets* (Chapter 2), accepted for publication in *Geomorphology* (Chapter 3), submitted to *Icarus* (Chapter 4), and accepted for publication in an issue of the *Geological Society London, Special Publications* (Appendix).

Chapter 2 deals with the investigations of thermokarst landforms in Siberian ice-rich deposits as analogues to asymmetrically-shaped Martian scalloped depressions. On the basis of field studies within a large thermokarst depression in the Lena Delta (NE Siberia) and comparative geomorphometric analyses and insolation (i.e. thermal) modeling using high-resolution and thermal-infrared satellite data, the geomorphology and the factors influencing both types of depressions are examined and compared [*Ulrich et al.*, 2010].

In Chapter 3, the results of an analogue study of terrestrial polygonally-patterned ground are demonstrated and compared to small-scale polygonal structures on Mars. The relationship of

polygon geomorphometry to local environmental conditions in the Adventdalen (Central Spitsbergen) and western Utopia Planitia (Mars) are analyzed by a combination of terrestrial field data, quantitative terrain analyses, and multivariate statistics [*Ulrich et al.,* in press].

Chapter 4 summarizes the insights gleaned from terrestrial analogue studies into permafrost landforms on Mars and is focused on the potential habitability of Martian mid-latitude periglacial landscapes. Specific periods in the Martian past are identified when thaw processes and liquid water were probably important in periglacial landscape evolution. Implications of past and present environmental conditions are discussed with respect to the potential survival of microorganisms. Finally, possible habitable niches that might exist in Martian permafrost landforms are described [*Ulrich et al.,* submitted].

The appendix contains a discussion of diverse periglacial landforms on Mars and Earth and proposes different landscape evolution scenarios for Martian mid-latitude craters, which are inferred from studies of analogous periglacial landforms on Svalbard [*Hauber et al.,* 2011].

In Chapter 5, results and implications of the individual thesis papers are synthesized and discussed, as well as critically viewed from a the methodological side. Furthermore, Chapter 5 provides a look forward to further analogue studies and permafrost investigations on Mars.

Table 1.1: Overview of publications presented within this thesis

Chapters	Publications
Chapter 2	Ulrich, M., Morgenstern, A., Günther, F., Reiss, D., Bauch, K.E., Hauber, E., Rössler, S., Schirrmeister, L., 2010. Thermokarst in Siberian ice-rich permafrost: Comparison to asymmetric scalloped depressions on Mars. *Journal of Geophysical Research 115,* E10009. doi:10.1029/2010JE003640.
Chapter 3	Ulrich, M., Hauber, E., Herzschuh, U., Härtel, S., Schirrmeister, L., in press. Polygon pattern geomorphometry on Svalbard (Norway) and western Utopia Planitia (Mars) using high-resolution stereo remote-sensing data. *Geomorphology*.
Chapter 4	Ulrich, M., Wagner, D., Hauber, E., de Vera, J.-P., Schirrmeister, L., submitted. Habitable periglacial landscapes in Martian mid-latitudes. *Icarus*.
Appendix	Hauber, E., Reiss, D., Ulrich, M., Preusker, F., Trauthan, F., Zanetti, M., Hiesinger, H., Jaumann, R., Johansson, L., Johnsson, A., Van Gasselt, S., Olvmo, M., 2011. Landscape evolution in Martian mid-latitude regions: insights from analogues periglacial landforms in Svalbard. In: Balme, M.R., Bargery, A.S., Gallagher, C.J., Gupta, S. (Eds.), *Martian Geomorphology*. Geological Society, London, Special Publications 356, 111-131. doi:10.1144/SP356.7.

1.3.2 Authors´ contribution

As first author, I reviewed the relevant literature, analyzed and interpreted the data, and initiated, wrote, and coordinated the manuscripts. The co-authors participated in field work, contributed data, and/or critically reviewed and discussed early manuscript drafts. Lutz Schirrmeister and Ernst Hauber contributed to the organization of the three manuscripts and

advised me throughout the whole process. Dennis Reiss provided valuable help dealing with Martian remote-sensing data and Karin Elke Bauch performed the thermal modeling for the Martian study site in *Ulrich et al.* [2010]. Ulrike Herzschuh and I jointly developed and conducted the statistical analyses of morphometric datasets in *Ulrich et al.* [in press]. Dirk Wagner made decisive contributions to *Ulrich et al.* [submitted] based upon his expertise in permafrost microbiology. The paper by *Hauber et al.* [2011] was coordinated and drafted by Ernst Hauber. I organized and contributed to the field work and I was involved as a co-author in internal reviews and writing of the final manuscript.

2. Thermokarst in Siberian ice-rich permafrost: Comparison to asymmetric scalloped depressions on Mars

Mathias Ulrich[1], Anne Morgenstern[1], Frank Günther[1], Dennis Reiss[2], Karin E. Bauch[2], Ernst Hauber[3], Sebastian Rössler[4], Lutz Schirrmeister[1]

[1]Alfred Wegener Institute for Polar and Marine Research, Research Unit Potsdam, Potsdam, Germany
[2]Institut für Planetologie, Westfälische Wilhelms-Universität Münster, Münster, Germany
[3]Institute for Planetary Research, German Aerospace Center (DLR), Berlin, Germany
[4]Limnological Institute, Technical University of Munich, Iffeldorf, Germany

Journal of Geophysical Research 115, E10009. doi:10.1029/2010JE003640.

Abstract

On Earth, the thawing of permafrost deposits with high ground ice content results in massive surface subsidence and the formation of characteristic large thermokarst depressions. Slope asymmetries within thermokarst depressions suggest lateral growth, which occurs due to thermoerosion and gravimetric mass wasting along these slopes. It has been proposed that rimless, asymmetrically-shaped depressions (called scalloped depressions) on Mars were formed by insolation-driven ground ice sublimation. We investigated a large thermokarst depression in Ice Complex deposits in the Siberian Arctic as a terrestrial analogue for scalloped depressions in Martian volatile-rich mantle deposits. Our results from field studies, insolation modeling, and geomorphometric analyses suggest lateral thermokarst development in a northern direction. This conclusion is obvious due to steeper slope angles of the south-facing slopes. Insolation and surface temperatures are crucial factors directly influencing thermokarst slope stability and steepness. Comparative analyses of Martian scalloped depressions in Utopia Planitia were conducted using high resolution (HIRISE, CTX) and thermal infrared (THEMIS) satellite data. By direct analogy, we propose that the lateral scalloped depression development on Mars was primarily forced on the steep pole-facing slopes in the equator-ward direction. Insolation modeling confirms that this must have happened in the last 10 Ma during an orbital configuration of higher obliquity than today. Development would have been maximized if the orbit was both highly oblique and highly eccentric, and/or the Martian summer coincided with perihelion. Relatively short events of increasing sublimation or even thawing of ground ice led to fast slumping processes on the steep pole-facing slopes.

2.1 Introduction and background

The visual similarity of terrestrial thermokarst depressions and Martian scalloped depressions implies comparable periglacial origins linked to extensive degradation of ground ice. Assumed thermokarst development cannot be transferred one-to-one to scalloped depressions, but the study of analogous terrestrial thermokarst properties within a well-known environment contributes to an improved understanding of periglacial landscape evolution on Mars considering prevailing Martian hydrological and climatic conditions. Following *Morgenstern et al.* [2007], the Siberian Ice Complex landscape is suggested as a terrestrial analogue for Martian degraded volatile-rich mantle deposits [*Kreslavsky and Head,* 2000; *Mustard et al*., 2001]. Thermokarst-affected landscapes are widely distributed in Northeast Siberian ice-rich permafrost deposits called Ice Complexes. Thermokarst as a process of permafrost degradation is caused by disturbances of the thermal equilibrium in the upper permafrost zone and results in surface subsidence and characteristic landforms in Arctic lowlands [*Czudek and Demek*, 1970; *Soloviev,* 1973; *French,* 2007]. Such disturbances can have long-term regional causes (e.g., climate changes) but may also result from temporally and spatially limited non-climatic reasons (e.g., destruction of the vegetation cover, local erosion). Large thermokarst depressions of several square kilometers (i.e. alasses), often filled with lakes and separated by flattened hills, are the most striking landscape elements (referred to as Yedoma) in parts of the Siberian Arctic lowlands [*Grosse et al*., 2006, 2007; *Schirrmeister et al*., 2008]. Particularly, the high ground ice content (up to 90% by volume) of Ice Complex deposits formed during the late Pleistocene by various periglacial processes [*Schirrmeister et al*., 2008] is a crucial factor for the development of large thermokarst depressions because surface subsidence is related to ice volume loss [e.g., *Romanovskii et al.,* 2000]. Generally, the development took place in several stages [*Czudek and Demek*, 1970; *Soloviev,* 1973; *Romanovskii et al.,* 2000] and was probably initiated by the warmer and moister climate conditions during the Late Glacial to Early Holocene transition (10 – 12 ka) [*Grosse et al.,* 2007]. Increasing insolation in the northern hemisphere due to Earth's orbital parameter variations [*Berger and Loutre,* 1991] was probably an important factor for the major landscape changes during this time [*Grosse et al.,* 2007]. Initially, rapid enlargement of water bodies corresponds to massive thawing of ice-rich deposits under deepening thermokarst lakes. After lake drainage, surface subsidence results in large thermokarst depressions with steep slopes [*Czudek and Demek*, 1970; *Soloviev,* 1973; *Everdingen,* 2005]. Further deepening might be prevented if ground-ice-depleted material forms an insulating layer at a later stage. Lateral growth of thermokarst basins occurs due to thermoerosion along the slopes (i.e. thermoabrasion) and gravimetric mass wasting. Preliminary studies indicate a specific asymmetric morphometry of these permafrost degradation features in Siberian ice-rich deposits suggesting spatially-directed thermokarst processes [*Morgenstern et al.,* 2008a] but the potential driving processes are still unclear.

Comparably shaped depressions and permafrost degradation features on Mars were first interpreted as thermokarst in origin by *Sharp* [1973]. These 'scallops' or scalloped depressions are rimless depressions (a few hundred meters to several kilometers in diameter), which can coalesce to form large areas of scalloped terrain that exhibit a north-south asymmetrical shape, opposed on both hemispheres with the steeper slopes pointing polewards [*Morgenstern et al.,* 2007; *Lefort et al.,* 2009*,* 2010; *Zanetti et al.,* 2010]. They are present in Mars' mid-latitude regions in close proximity to a volatile-rich (i.e. water-ice-rich) mantle layer tens of meters thick, which was deposited during variations in Mars' orbital parameters (i.e. obliquity and eccentricity) [*Kreslavsky and Head,* 2000, 2002; *Mustard et al*., 2001; *Head et al*., 2003]. Various authors have studied the surface morphology of scalloped depressions on Mars and suggested formation processes controlled by solar insolation, which resulted in an asymmetric sublimation of ground ice with respect to the aspect (i.e. North – South) [*Morgenstern et al.,* 2007; *Lefort et al.,* 2009, 2010; *Zanetti et al.,* 2010] or an origin by ponding water comparable to terrestrial drained-thermokarst lake depressions [*Costard and Kargel,* 1995; *Soare et al.,* 2007, 2008].

In this work, techniques for comparatively analyzing scalloped and thermokarst depression properties are combined with terrestrial field studies to emphasize similarities in and differences between these morphological analogues. In the next section (section 2.2) overviews of the investigated terrestrial and Martian areas are given separately to highlight the similarity of these sites, including the geomorphological and geological characteristics. Section 2.3 reviews data acquisition during field work and the methods used to determine geomorphometry and thermal properties, first of the terrestrial thermokarst depression, and then of the Martian scalloped depressions. Next we present results of geomorphometric analyses of the investigated thermokarst depression including observations made during field work and new results from insolation modeling (section 2.4.1). Comparable results of geomorphometric analyses and insolation modeling of Martian scalloped depressions are presented later in the same section (section 2.4.3). Finally, we discuss properties of terrestrial thermokarst depression asymmetry and the implications for spatially-directed development of Martian scalloped depressions (section 2.5). The main questions of this study are: (i) Which parameters control thermokarst morphology on Earth, and what can be inferred for scalloped depressions on Mars from terrestrial thermokarst topography, morphometry, and volume? (ii) What is the influence of solar insolation on terrestrial thermokarst development (a factor that has been suggested as a main driving process for scallop formation on Mars)? and (iii) Which conclusions can be drawn from the development of scalloped depressions for the climate history and ground ice (i.e. permafrost) conditions on Mars?

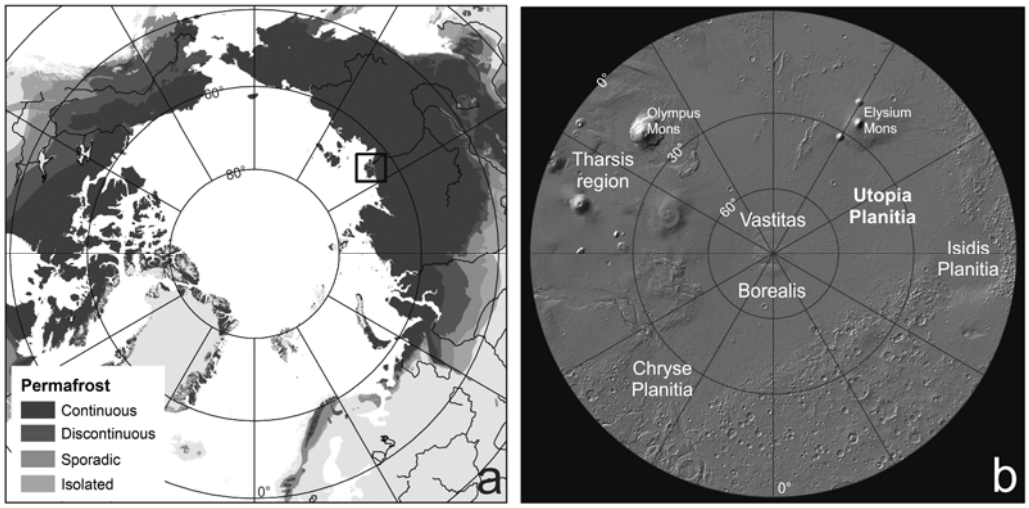

Figure 2.1: (a) Circum-Arctic permafrost distribution and location of the Lena Delta (rectangle) in NE Siberia (Russia) within the zone of continuous permafrost. Map based on *Brown et al.* [1998]. (b) Location of Utopia Planitia on the northern hemisphere of Mars (MOLA shaded relief).

2.2 Regional setting

2.2.1 Earth

Kurungnakh Island located in the southcentral Lena Delta was chosen as the terrestrial study area because it is representative of thermokarst in Ice Complex sediments (i.e. Yedoma) and is easily accessible for field work. The Lena Delta is situated in northeastern Siberia within the zone of continuous permafrost (Figure 2.1a), which at this location is several hundred meters thick and hundreds of thousands of years old. The climate is true arctic, characterized by very low mean annual air temperatures of about -13.5°C and low mean annual precipitation of around 300 mm. [*ROSHYDROMET,* 2009]. Kurungnahk Island is part of the third Lena Delta terrace [*Grigoriev,* 1993] which mainly consists of erosional fragments of a broad accumulation plain composed of late Pleistocene permafrost deposits [*Schirrmeister et al., 2003*] situated north of mountain ridges bordering the delta to the south (Figure 2.2a). The island covers an area of about 350 km² and reaches a maximum elevation of 55 m a.s.l. (Figure 2.2b).

The sediments are composed of two stratigraphically different units. The lower unit consists of sandy sediments with gravimetric ice contents of about 25 wt% related to the dry sediment weight. The deposits are 15 to 20 m thick and were accumulated between 100 and 50 ka [*Krbetschek et al.,* 2002; *Wetterich et al.,* 2008]. The upper unit overlies the sandy deposits discordantly and is composed of Ice Complex deposits. The Ice Complex section is about 15 to 20 m thick and consists of fine-grained deposits with ice supersaturation due to the very high gravimetric ice contents (up to 150 wt%) [*Wetterich et al*., 2008]. The ice occurs in the form of huge ice-wedges and segregation ice. Thus, the total amount of ice contained in the Ice Complex can reach 90 % by

volume. The syngenetically-formed ice wedges are 5-7 m wide and about 20 m deep, indicating long-term stable landscape conditions. The Kurungnakh Ice Complex deposits accumulated between 50 and 17 ka [*Schirrmeister et al.*, 2003; *Wetterich et al.*, 2008].

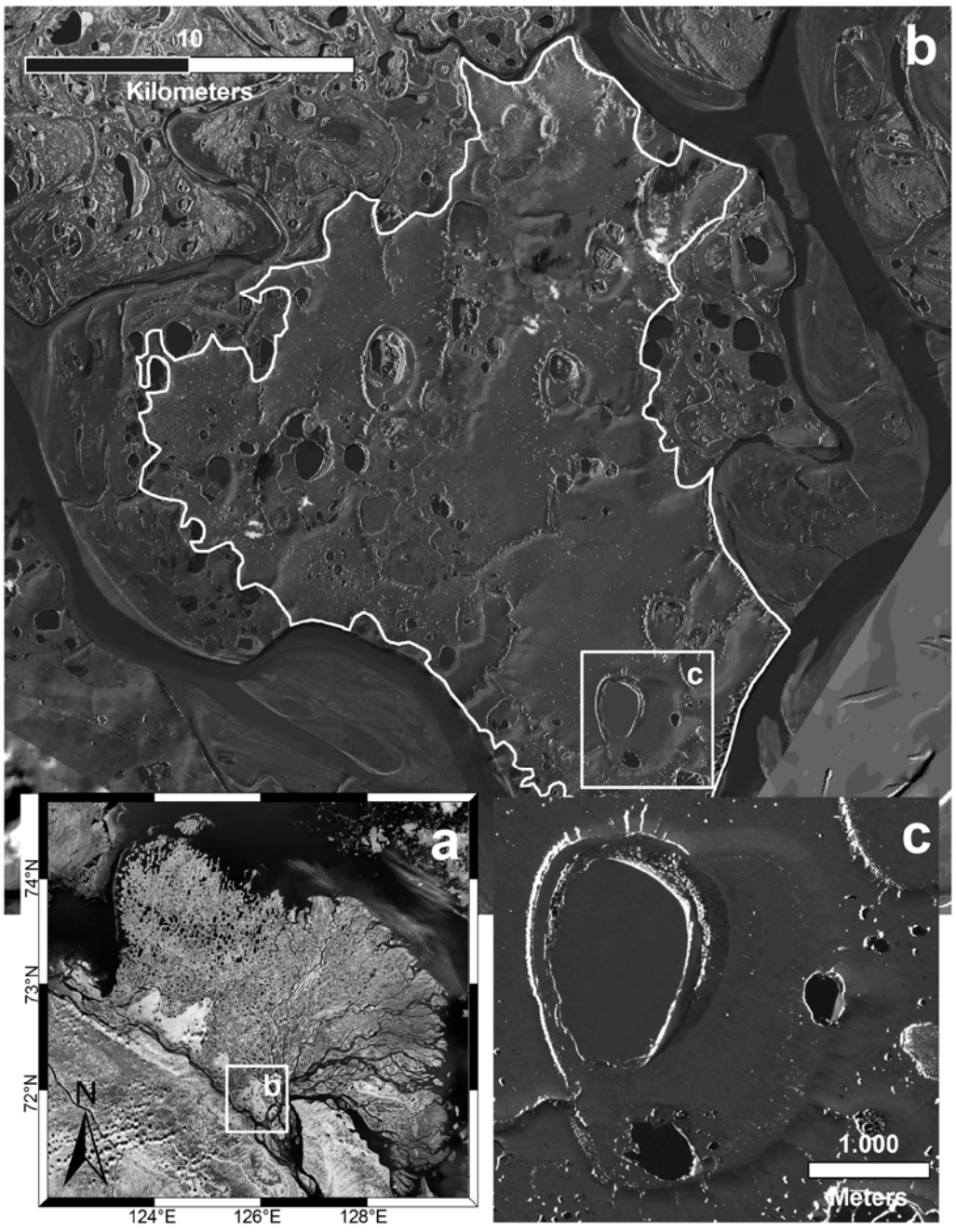

Figure 2.2: Regional setting of the terrestrial study site. (a) Lena Delta. Brighter colours indicate Ice Complex remnants in the south of the Delta (GeoCover 2000 NASA). (b) Thermokarst landscape on Kurungnakh Island in the southcentral Lena Delta; the grey line marks the distribution of Ice Complex deposits that have built the island (ALOS PRISM image, Date: 21 September 2006, over DEM shaded relief) (c) The Kurungnakh Island thermokarst depression on which this work is focused (ALOS PRISM subset).

Today the formerly consistent Ice Complex mantle is interrupted by thermokarst depressions filled by limnic and boggy deposits indicating Ice Complex degradation during the Late Glacial to Early Holocene period (ca. 12 to 8 ka). The surface of Kurungnakh Island is characterized by a highly dissected thermokarst landscape (Figure 2.2b) dominated by large thermokarst depressions (i.e. alasses) with diameters of up to ~3 km and depths of up to ~30 m, which often coalesce to form large thermokarst valleys. The border of the island is frequently cut by thermoerosional gullies. More than 50 % of the island area is occupied by thermokarst features, with about 38 % covered by alasses. The depressions show steep, often asymmetrical slopes in the N-S direction and flat bottoms. About 8 % of the island's area is covered by thermokarst lakes. Within the depressions they are mostly situated at the margins. At higher elevations, the surface of the Yedoma hills is drier, better drained, and contains only small lakes and polygonal ponds. The occurrence of polygonal structures of ice wedge systems depends on the individual drainage situation. Generally, the bottoms of thermokarst depressions are dominated by low-center polygons, while high-center polygons are common on slopes or on the better-drained hill positions. The terrestrial studies described here are particularly focused on a characteristic, ca. 7.5 km² large thermokarst depression in the southeast of Kurungnakh Island (Figure 2.2c).

2.2.2 Mars

For comparison with our terrestrial study area, we selected an area in the northern Martian hemisphere in western Utopia Planitia (UP) (Figure 2.1b). This area is part of the Utopia Basin (Figure 2.3a) and was possibly formed by a giant impact during the pre-Noachian period (4.5 - 4.1 Ga) [*McGill,* 1989; *Tanaka et al.,* 2005; *Carr and Head,* 2009]. The area is covered by the Vastitas Borealis interior unit (ABv_i) which underlies the Astapus Colles unit (ABa) nearby [*Tanaka et al.,* 2005]. The ABa unit is relatively young on the Martian time scale (Late Amazonian, 2 – 0.4 Ma), and is interpreted as an ice-rich mantle deposit tens of meters in thickness [*Kreslavsky and Head,* 2000, 2002; *Mustard et al*., 2001; *Head et al*. 2003; *Carr and Head,* 2009]. The ABv_i unit is of Early Amazonian age (< 3.0 Ga) and consists of outflow channel sediments and subsequently reworked ice-rich deposits [*Tanaka et al.,* 2005]. The region is characterized by various landforms of periglacial origin, e.g., polygonal structures, scalloped depressions, and small mounds [e.g., *Soare et al.,* 2005, 2007, 2008; *Morgenstern et al.,* 2007; *de Pablo and Komatsu,* 2009; *Burr et al.,* 2009; *Lefort et al.,* 2009; *Levy et al.,* 2009a]. There are strong morphological similarities between the western UP landforms and terrestrial periglacial landforms. Although the Gamma Ray Spectrometer (GRS) on Mars Odyssey shows that this area is relatively free of water ice in the upper surface layer (about 1 m) [*Boynton et al*., 2002; *Feldman et al.,* 2004], the presence of possible periglacial features suggests the existence of volatile-rich (i.e. ice-rich) mantle deposits [e.g., *Morgenstern et al.,* 2007; *Lefort et al.,* 2009].

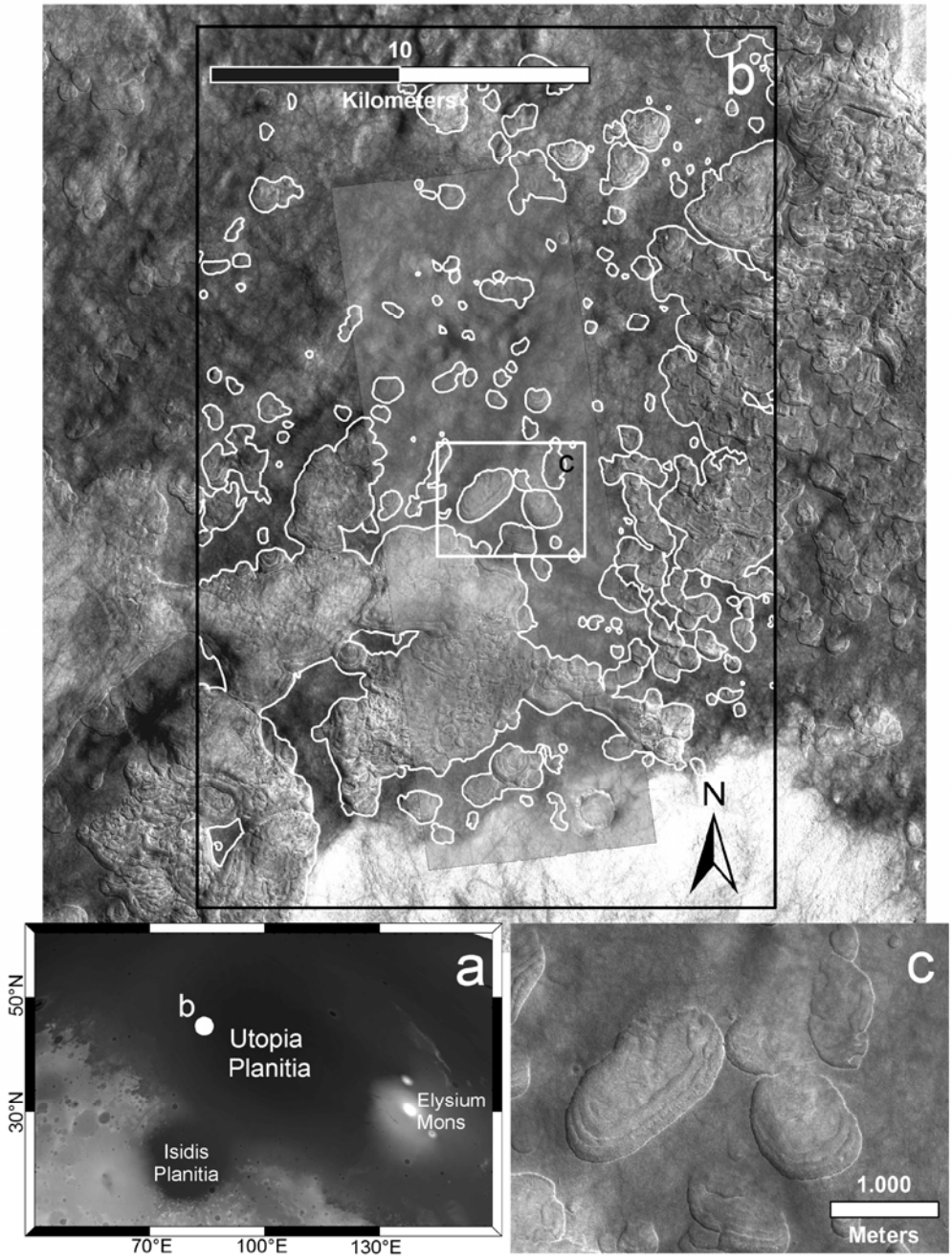

Figure 2.3: Regional setting of the Martian study site. (a) The studied location in western Utopia Planitia (MOLA DEM in sinusoidal projection). (b) Mapped scalloped terrain within the self-defined study site (white borders) (HiRISE image: PSP_001938_2265 on CTX image: P02_001938_2263_XI_46N267W). (c) Example of a larger single asymmetrically-shaped scalloped depression (HiRISE subset).

For direct comparison with the terrestrial study site an area of about 350 km² in western UP was defined (Figure 2.3b) that is representative of scalloped and periglacial terrain on the northern plains of Mars. According to *Morgenstern et al.* [2007], 24% of the area between 40 – 50°N and 80 – 85° E is degraded by scalloped depressions with an increasing coverage from North to South. Our area of focus is centered at 46°N and 92°E and is located around the footprint of the HiRISE image PSP_001938_2265. It represents an area similar to the central section of the area described by

Morgenstern et al. [2007], which is located between an almost non-degraded, smooth, and flat surface in the north, and an area in the south where the mantling material has been completely removed. The elevation of our study area ranges between -4600 m in the north and -4500 m in the south as indicated by topographic information from Mars Orbiter Laser Altimeter (MOLA) data [*Smith et al.,* 2001]. The area is characterized by a generally smooth and flat surface with polygonal structures and isolated scalloped depressions beside larger coalesced and nested regions of completely removed mantle material (Figure 2.3b).

2.3 Data and methods

2.3.1 Terrestrial data

2.3.1.1 Field data

Field work was conducted during a field campaign on Kurungnakh Island (Lena Delta) in summer 2008 to investigate terrestrial thermokarst depression morphometry and surface characteristics and their controlling factors. For quantitative land surface analyses and detailed description of the thermokarst depression morphology a high resolution digital elevation model (DEM) was necessary. Therefore, a tacheometric field survey was carried out using a ZEISS ELTA C30 tacheometer with an electro-optical distance measurement device. Altogether, 2663 points representing the thermokarst depression were measured and stored in a coordinate-point database which allows interpolation to a raster dataset.

Another important aim of the fieldwork was to characterize and map different relief units and geomorphological features by their distinct surface properties. Relief features (micro- and meso-relief, slope characteristics), vegetation properties (coverage, height, vitality), hydrological conditions (soil/surface moisture, drainage situation, water bodies), and active-layer depth measured by a steel rod were recorded at more than 280 sites covering the total area of the investigated thermokarst depression and the adjacent undisturbed uplands This ground-truth dataset was derived as a training and reference set for further remote-sensing analyses.

Downwelling shortwave solar radiation was measured on differently-exposed thermokarst depression slopes and surfaces. Measurements were conducted between 9 and 22 August 2008 at 19 locations using a Pyranometer CS300 from Campbell Scientific, Inc. Basic cloud cover corrections were done using an algorithm developed by *Laevastu* [1960] and visual cloud cover observations. Several evaluations of the cloud correction algorithm at different sites [e.g., *Reed,* 1977; *Frouin et al.,* 1988; *Kumar et al.,* 1991] showed good results for the formula used, as well as for the lower sun elevations [*Reed,* 1977] that occur in Arctic environments. Finally, only measurements between noon and 4 pm were used and averaged for each location.

2.3.1.2 GIS and remote-sensing analyses

For calculating a hydrologically-correct DEM within ArcGIS™ (ESRI) the TOPOGRID algorithm by *Hutchinson* [1989] was used. A grid cell size of 3 m was chosen for the output DEM to reflect small-scale morphological characteristics. Vertical accuracy of the DEM was tested by comparing height values from the calculated DEM to the original point database. The root mean square error (RMSE) averaged 0.28 cm, indicating high accuracy of the model. The DEM was used to extract morphometric parameters (slope angle, aspect, elevation, curvature) within ArcGIS™ for a quantitative terrain analyses. Each parameter was calculated on a cell-by-cell basis, fitting a plane composed of a 3x3 cell neighborhood. Furthermore, the GIS-calculated volume of the alas being investigated was used for estimating relationships between ground ice contents, surface subsidence, and thermokarst deposit sedimentation.

Solar radiation influencing the thermokarst morphology is of special interest in this work. We used the solar radiation analysis tool provide by ArcGIS™ to calculate insolation for the area of the thermokarst depression on Kurungnakh Island and specific point-locations therein. The toolset is based on an algorithm developed by *Rich et al.* [1994]. Total global radiation was calculated for an arbitrary time as the sum of direct and diffuse radiation after generating upward-looking viewsheds based on each grid cell in the DEM. The solar radiation toolset performs sunmap calculations to determine direct solar radiation originating from each sky direction. Diffuse radiation was calculated using a skymap, which represents a hemispherical view of the entire sky defined by zenith and azimuth angle. The sunmap, the skymap, and the viewshed are then combined to calculate total solar radiation. The theory of the solar radiation tool is described in detail by *Fu and Rich* [1999].

Model parameters were adjusted according to atmospheric and meteorological conditions in the central Lena Delta region [e.g., *Boike et al.,* 2008]. Thus, a standard overcast diffuse model was used in which the radiation flux varies with the zenith angle. Transmittivity and diffuse proportion parameters were set to account for average sky conditions and cloud cover in the study area during summer. The tacheometer DEM was used as topographic input, and insolation was calculated for an estimated snow-free time span of 90 days between 1 June and 30 August 2008. The radiation in the investigated artic region is usually highest during this time and low before and after, when the sun's angle is lower. Furthermore, snow is usually melting by the end of May and starts to accumulate in September [e.g., *Williams and Smith,* 1989; *Boike et al.,* 2008].

Thermal infrared (IR) data acquired by Landsat ETM+ (Band 6, 10.4 – 12.5 µm, 60 x 60 m) were used to analyze spatial patterns of thermal emittance within the thermokarst depression and to extract at-sensor brightness temperatures for relative estimations of seasonal surface temperature differences within the thermokarst depression. An algorithm presented by *Chander et al.* [2009] was used to convert at-sensor spectral radiance to temperature. Averaged at-satellite temperatures were extracted for thermokarst depression slopes from 250 random points on 5 images acquired

from June to September during the 2000 to 2002 period. One image acquired in June 2001 features cloud cover in the northeast of the thermokarst depression. Therefore, points covering this area were not included.

2.3.2 Martian data

Comparative analyses of the Martian scalloped depression were done using High Resolution Imaging Science Experiment (HiRISE) data [*McEwen et al.,* 2007] and Context Camera (CTX) data [*Malin et al.,* 2007] from the Mars Reconnaissance Orbiter (MRO). HiRISE provides data with a very high spatial resolution of 30 cm/pxl and the possibility of 3D views by stereo pairs. About 30 surveyed HiRISE images of UP contained possible Martian ground ice degradation features; the stereo pair PSP_001938_2265 and PSP_002439_2265 was selected for detailed analyses because these images contain large scalloped depressions representative of the UP region. Further topographic information was derived from a DEM of 1 m/pixel based on this stereo pair [*Kirk et al.,* 2008] and MOLA tracks [*Smith et al.,* 2001]. The CTX image P02_001938_2263, with a spatial resolution of about 6 m/pxl, was used for albedo estimations of the study site. Brightness temperatures for the selected region were derived from Thermal Emission Imaging System (THEMIS) infrared data [*Christensen et al.,* 2004]. All data were stored in a geographical information system (GIS), processed in sinusoidal projection with a center longitude of 90.0°E, and used for manual mapping of scalloped terrain.

In order to investigate the insolation and resulting temperatures on the scalloped terrain, especially on the depression slopes, in the region under investigation, a 1D thermal model was employed, which includes the effect of surface slopes, as described by *Bauch et al.* [2009]. The model was originally used to determine temperatures on the lunar surface and has been modified to fit Martian conditions with boundary conditions similar to the model by *Kieffer et al.* [2000]. Absorption and scattering in the atmosphere depend on the optical depth ($\tau = 0.5$), single-scattering albedo ($\omega = 0.9$), and an asymmetry dust factor ($G = 0.7$), for which we used parameters based on Viking and Pathfinder observations. Based on our CTX data an albedo of $A = 0.16$ was chosen. According to *Mellon et al.* [2000] and *Putzig et al.* [2005], a thermal inertia of $I = 300$ J m^{-2} s$^{-1/2}$ K^{-1} was assumed for the western UP region. The thermal conductivity was set to 1.6 W m^{-1} K^{-1}, which corresponds to a fine-grained permafrost soil with a porosity of 40 % [*Williams and Smith,* 1989]. Insolation strongly depends on the planet's orbit; therefore, we used results from *Laskar et al.* [2004] as input parameters for obliquity, eccentricity, and longitude of perihelion at different times in Martian history. Three scenarios were used to distinguish daily surface temperatures during summer (solar longitudes $L_s = 90°$) on the gentle equator-facing scalloped depression slope, on the steep pole-facing scarp, and on a flat surface in the investigated region. In addition to the present insolation conditions, modeling was conducted for the most recent period of 35.0° obliquity around 0.865 Ma with an eccentricity of 0.059 and a solar longitude of perihelion of 309.5°, and the most

recent period of 46.8° obliquity around 5.641 Ma with an eccentricity of 0.03 and a solar longitude of perihelion of 141.2°.

2.4 Results

2.4.1 Terrestrial thermokarst depression morphometry, geomorphology, and surface features

The DEM of the studied alas on Kurungnakh Island covers an area of 7.5 km² and shows the meso-scale morphology of the investigated thermokarst depression in detail (Figure 2.4a). Several asymmetries are obvious from analyses of geomorphometric parameters, confirming observations made during the field work (Figure 2.5). Elevation, slope angle, aspect, and plan and profile curvature are used to identify and describe specific thermokarst depression properties.

The depression is generally elongated in the N-S direction with a longitudinal axis of 3.3 km and a diagonal axis of 2.5 km. About 28 % of the depression area consist of slopes >2°, with the west-facing slopes occupying the largest area (Figure 2.4c). The thermokarst depression slopes clearly differ in their morphology and surface characteristics (Figure 2.5). The slope map (Figure 2.4b) indicates an asymmetrical shape in the NNW – SSE direction. While the steepest slope sections (7° to 20°) are prevalent on south- and east-facing slopes, the north- and west-facing slopes mostly show gentler slopes (2° to 7°) (Figure 2.4d). The south- and southeast-facing slopes in the north and northwest of the thermokarst depression (Figure 2.4b) and in the north of the small eastern lake (Lake 2 in Figure 2.4a) show the steepest slopes. These steepest slope sections are also represented by highly divergent (very convex) profiles on the upper slopes and highly convergent (very concave) profiles on the lower slope (Figure 2.6a and 2.7a). The slopes end sharply on the basin floor (Figure 2.5a).

Concerning the relationship of slope steepness to instability, the high relief energy is further represented by high profile curvature values of the south- and southeast-facing slopes (Figure 2.6a and 2.7b). These observations suggest a laterally-directed thermokarst basin development. The west- and north-facing slopes and minor parts of the south- and the east-facing slopes are flat and more rectilinear (Figure 2.6a and 2.7b) and are characterized by less convexity in the upper slopes and less concavity in the lower slopes (Figure 2.7a). The comparatively low relief energy suggests higher slope and surface stability of the west- and north-facing slopes. The lack of denudation (i.e. areal erosion and slope retreat) is confirmed by the area-wide distribution of well-developed hummocks (about 40 cm high) and terrace-like solifluction lobes (Figure 2.5b, c). These slopes are also distinguishable by a higher frequency of deep thermoerosional gullies, clearly visible in the planiform curvature map of the depression (Figure 2.6b). Despite minor parts of the south-facing slope north of Lake 1, the other slopes are smoother in planiform curvature (Figure 2.6b).

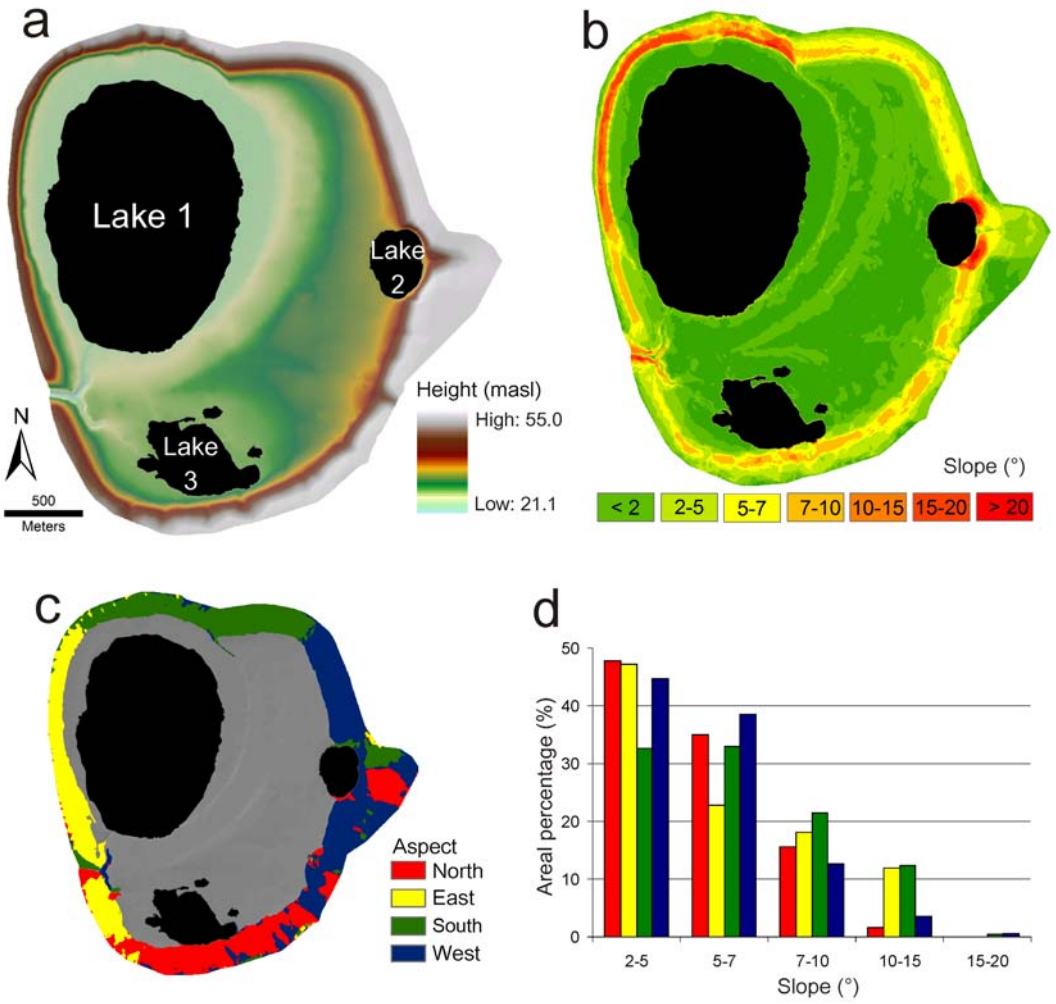

Figure 2.4: (a) DEM derived from tacheometric measurements (ground resolution 3m). (b) Slope map of the thermokarst depression. The asymmetrical shape resulting from the south/southeast exposure of the steepest slopes is obvious. Note that the lake terraces within the basin floor are subparallel, and are elongated at the largest lake. (c) Aspect of the thermokarst depression slopes >2° and located >30 m a.s.l. This mask was used for further calculations of slope properties. (d) Area of different slope exposure versus slope degree (color code same as that used in 4c). The diagram shows that north- and west-facing slopes tend to be shallower. Steeper slopes are prevalent on south- and southeast-facing slopes, though east-facing slopes differ in their profiles from the northern part (steeper) to the southern part (shallower) (see also Figure 2.5d).

Slopes clearly differ in their vegetation cover and surface moisture (Figure 2.5). The generally drier south-facing slopes are dominated by dwarf shrubs, lichens, and dry mosses. Hummocks are less pronounced here. In contrast, the southeast-facing part of the western depression margin is covered by fresh green vegetation consisting of dwarf shrubs, grasses, and herbs. Tussocks of cotton grass beside mosses are abundant on the north- and west-facing slopes. The lower sections of these slopes are particularly affected by high surface moisture.

The Ice Complex uplands surrounding the depression decrease in elevation from 55 m a.s.l. above the west-facing slope to 37 m a.s.l. above the east-facing slope. Different basin floor levels in the DEM are clearly obvious, indicating different stages of surface subsidence (Figure 2.4a). The

basin floor is slightly inclined, from 28 m a.s.l. in the east to 21 m a.s.l. in the northwest, over three terraces, which are concentrically arranged around the largest lake (Lake 1), probably tracing former lake levels. The total thermokarst subsidence ranges from 27 to 16 m (mean 21.5 m). The three large lakes within the thermokarst depression are located on different terrace levels. Lake 1 is located on the lowest level in the northwest of the depression, while Lake 2 is situated on the highest terrace level and Lake 3 on a middle level (Figure 2.4a). The former, probably N-S elongated elliptical shape of the alas is now interrupted by the basins of Lake 1 and Lake 2.

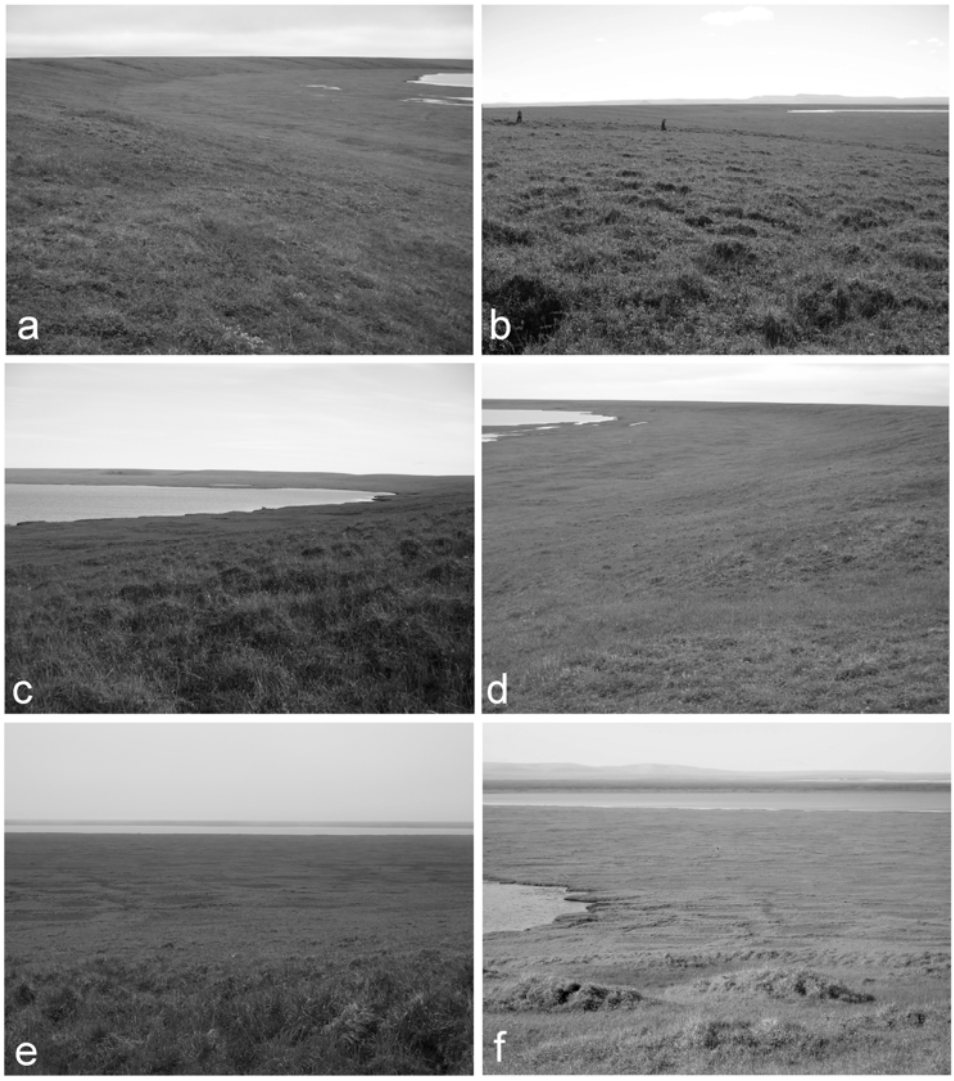

Figure 2.5: Surface characteristics of the differently-exposed thermokarst depression slopes and examples of ice-wedge polygons within the alas. (a) The steep south-facing slope ends abruptly at the basin floor. View to the northeast. (b) Hummocky micro-relief on the slightly inclined rectilinear west-facing slope. View to the south. (c) View over Lake 3 to the east over the north-facing slope which is characterized by hummocks and solifluction lobes caused by the poor drainage. (d) View to the south over the flattened southern part of the east-facing slope. (e) Orthogonal low-centered polygons oriented on the south-facing slope in the north of Lake 1. The polygonal micro-relief is flatter towards the lake. View to the south. (f) Ice-wedge degradation on the shore of Lake 2.

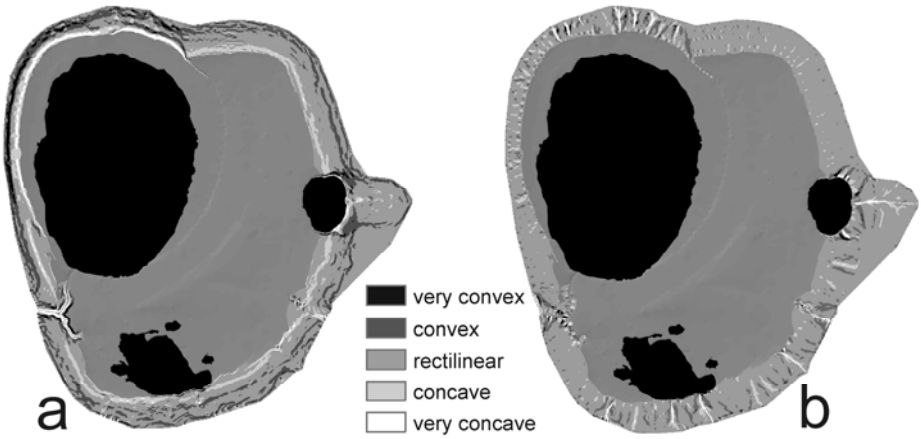

Figure 2.6: Curvature maps of the thermokarst depression slopes are calculated as the second derivative of the surface. The basin floor is not considered and is illustrated by the DEM shaded relief. (a) Profile curvature indicates the rate of potential slope gradient change. (b) Planiform curvature indicates the rate of aspect change along a contour.

According to field observations, the different terraces are clearly distinguishable in relief features, drainage situation, and vegetation. This is particularly obvious for the development of ice-wedge polygonal structures. Oriented polygons on the shore of Lake 1 and on the slopes suggest renewed ice wedge growth after the alas was formed (Figure 2.5e). Distinct orthogonal low-center polygons with diameters of about 20 m are randomly distributed over large parts of the highest basin floor level. Well-drained polygon rims, often covered by dwarf shrubs, are raised ≥50 cm above the centers. The centers are covered by moss and cotton grass and often contain polygonal ponds. Ice wedge degradation results in high-center polygons with deep troughs on the western shore of Lake 2 (Figure 2.5f) and at the mouth of larger thermoerosional valleys, which terminate in the thermokarst basin. Generally, the drainage degrades towards Lake 3 and Lake 1. The reduced micro-relief of the polygons results in indistinct patterns with larger and commonly orthogonal (but sometimes pentagonal or hexagonal) polygons at some locations. While the very moist centers are covered by sedges, the hardly elevated rims are only distinguishable because the vegetation changes from sedges to peat mosses.

Average active-layer depths within the basin floor range between 36 and 82 cm, with the deepest values occurring on the lowest basin floor level around Lake 1. Only small differences in active-layer depth were measured between the different exposed slopes, where average depths are 38-49 cm on south- and east-facing slopes, and 37-42 cm on west- and north-facing slopes. Differences in active-layer depths seem to be caused by micro-morphological conditions rather than by the aspect. Generally, smaller active-layer depths occur in organic soils under insulating non-vascular vegetation (i.e. mosses and lichens) because the heat flux is reduced in summer, especially if these soils are dry [e.g., *Williams and Smith,* 1989; *Anisimov and Reneva*, 2006; *French* 2007]. For instance, active-layer depth within the moist center of low-center polygons located on the basin floor could be twice the depth on the rims. Drier and mostly flat high-center

polygons show little differences in active-layer depth between the center and the trough. On the slopes, differences occur especially in hummocky terrain. Average active-layer thickness on the hummocks ranges from 46 cm on south-facing slopes to 55 cm on east-facing slopes. Between hummocks, depths range from 27 cm on west-facing slopes to 35 cm on east-facing slopes.

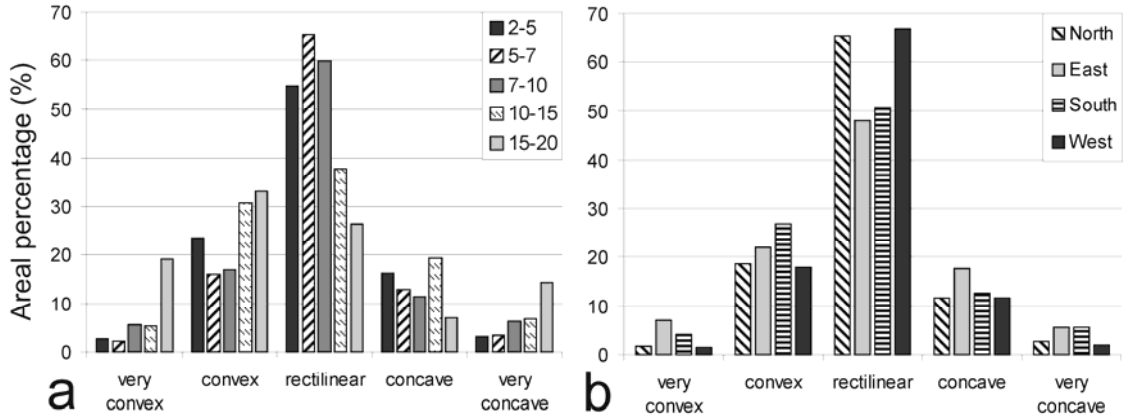

Figure 2.7: (a) A plot of the percent area of different slope degrees versus profile curvature shows that the steepest slopes (10 – 20°) consistently exhibit higher convexity and concavity values. (b) a plot of the area of different slope exposures versus profile curvature indicate comparatively higher curvature values for south- and east-facing slopes and lower relief energy on north- and west-facing slopes.

Thermokarst depression development is related to massive surface subsidence. The depths of thermokarst depressions, and therefore the amount of subsidence, are strongly related to the ground ice content. The sediment material in a thawing Ice Complex below a deepening thermokarst lake remains at the lake bottom as a taberal deposit (i.e. taberite) [e.g., *Grosse et al.*, 2007] and could be exposed today, refrozen on the basin floor after the lake drained. Thus, the thickness of sediment remaining after an Ice Complex has thawed decreases if the ground ice content of the Ice Complex increases. Using the dimensions of the depression as extracted from the DEM and simple geometrical calculations of the base, top, height, and volume of an upside-down truncated cone, the thickness of taberal deposits can be estimated. An appropriate truncated cone for the investigated depression has a bottom radius of 1304 m and a top radius of 1518 m (Figure 2.8). Using the Cut/Fill tool of ArcGIS^{TM}, a lost volume of about 130.4 x 10^6 m³ was calculated, representing the volume of thawed ground ice. A corresponding cone height of 20.8 m was calculated (H1 in Figure 2.8), which accurately represents the mean depth of the thermokarst depression (see above) and, therefore, the current total thermokarst subsidence. The volume and thickness of the Ice Complex deposits previously existing at the site of the thermokarst depression can be calculated using different possible total Ice Complex ground ice contents (70, 80, and 90 vol.%) arising from measured gravimetric ground ice contents of frozen sediments [*Schirrmeister et al.*, 2003; *Wetterich et al.*, 2008] and estimated contents of ice wedge and segregation ice. Calculated Ice

Complex thicknesses which would have existed to build the present depression are shown in Figure 2.8. These are 23.1 m at 90 vol.% (H2), 26.6 m at 80 vol.% (H3), and 29.7 m at 70 vol.% (H4). This would imply present taberite thicknesses of 2.3 m for 90 vol.% (h2), 5.2 m for 80 vol.% (h3), or 8.9 m for 70 vol.% (h4). The most realistic calculations suggest 90 vol% ground ice content, close to taberite thicknesses observed by *Grosse et al.* [2007]. However, accumulation of lake sediments, possible erosion of material, as well as the subaerial accumulation of sediments on the basin floor after lake drainage and/or peat formation after surface stabilization [*Romanovskii et al.*, 2000; *Grosse et al.*, 2007; *Ulrich et al.*, 2009] cannot be ruled out.

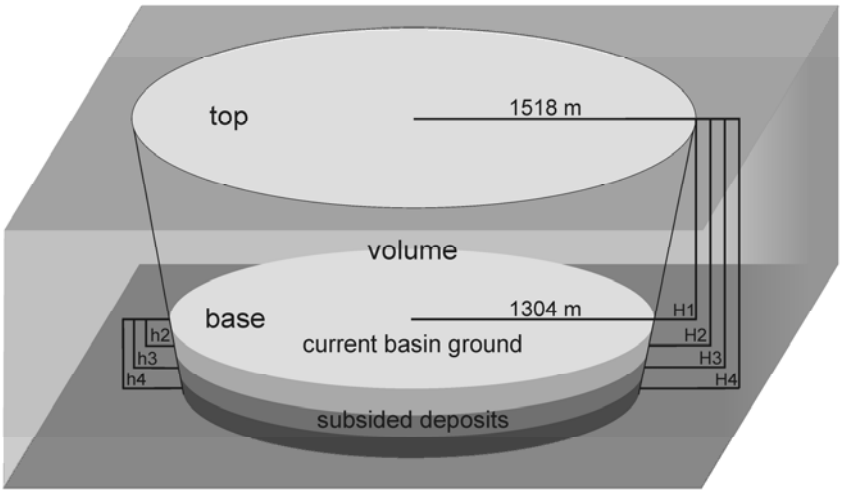

Figure 2.8: Geometrical representation of an upside-down truncated cone used for modeling subsided deposits (i.e. taberite), which is based on DEM data. Possible thicknesses of taberal deposits depending on ground ice contents are h2 for 90 vol%, h3 for 80 vol%, and h4 for 70 vol%. Calculated cone height representing the current mean depth of the depression is given by H1. Ice Complex thicknesses with different ground ice contents, which would have formerly existed to build the present thermokarst depression, are H2 with 90 vol%, H3 with 80 vol%, and H4 with 70 vol%. Explanations: see text.

2.4.2 Insolation and thermal properties of terrestrial thermokarst depression

Areas of high incoming radiation are clearly distinct from areas of low radiation in the solar insolation map of the thermokarst depression (Figure 2.9). Influences of the basin morphology are obvious. The south-facing slopes are exposed to much higher radiation rates than the north-facing slopes. West-facing slopes show higher total rates than east-facing slopes. Calculated radiation values over the modeled period range from ~259 kWh/m² (daily mean of ~120 W/m²) on south-facing slopes to ~193 kWh/m² (daily mean of ~89 W/m²) on north-facing slopes for the modeled time period between June and August (Figure 2.9). Furthermore, Figure 2.10 suggests the highest calculated radiation values occur at slope angles between 10 and 20° on the south-facing slopes, while lower and medium values were generally calculated for lower degrees of slope (2° to 7°). In particular, the highest radiation values correspond to the steepest south-facing slopes north of both Lake 2 and Lake 1. Generally, these findings were confirmed by the field measurements (Figure

2.9). The highest downwelling shortwave radiation (averaging from 503 to 530 W/m²) was measured on south-facing slopes (Figure 2.9). Lower measurements were acquired on the east- and north-facing slopes (from 297 to 471 W/m²). However, inaccuracies caused by varying measurement conditions and cloud-cover correction potentially exist in the recorded data and must be considered.

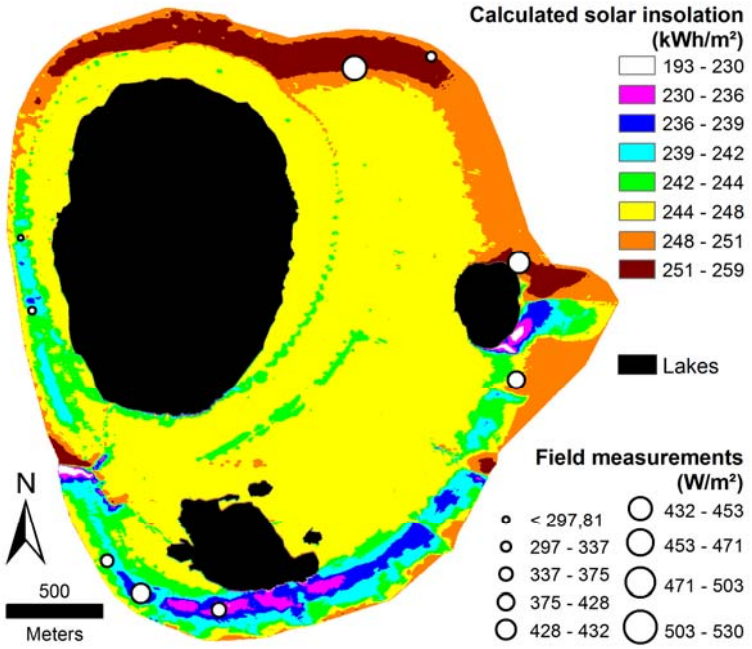

Figure 2.9: The relationship of calculated solar insolation to thermokarst depression topography is shown as the amount of radiation between 1 June and 30 August 2008. At each location, downwelling shortwave radiation field measurements are shown as instantaneous values.

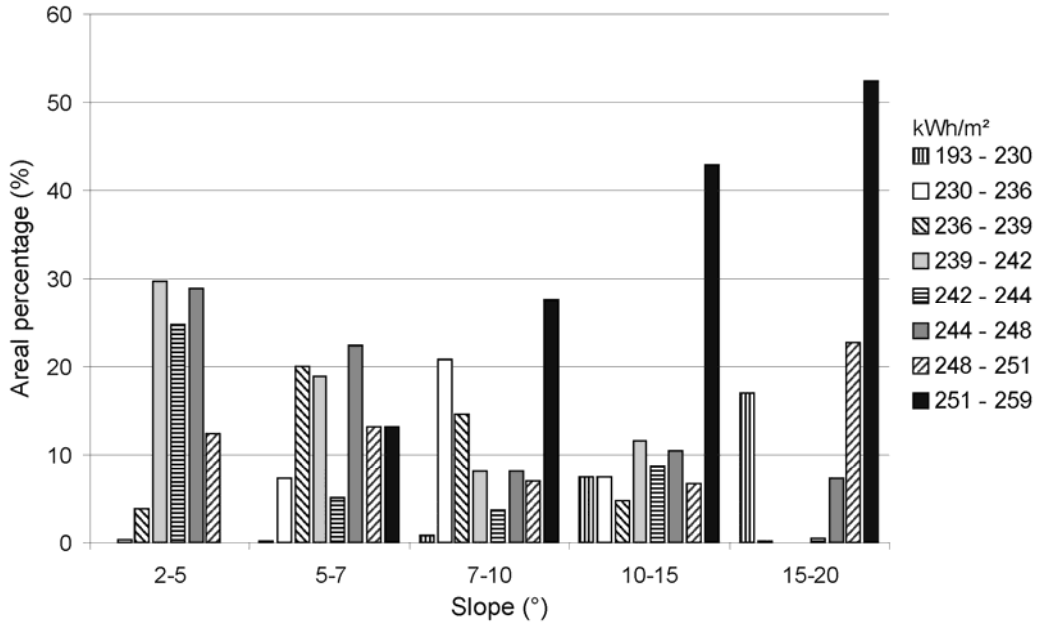

Figure 2.10: Relationship between degree of slope and modeled solar radiation. Highest insolation values are clearly related to steepest slopes. Amounts of insolation (kWh/m²) are equal to those found in Figure 2.9.

Additionally, the modeled insolation could be validated using Landsat ETM+ thermal data (Figure 2.11). Soil surface temperatures are related to environmental conditions such as solar radiation, snow cover, and/or prevailing wind. Furthermore, they are important in determining morphological conditions on Arctic slopes [e.g., *French* 1970]. The seasonal temperature variations clearly differ on different slopes of the thermokarst depression (Figure 2.11a-e). Temperatures are always highest on south-facing slopes and lowest on north-facing slopes. In addition, higher values were derived on the west- than on the east-facing slopes between July and August (Figure 2.11f). In absolute terms, the highest temperatures were reached at the beginning of August. A strong temperature increase could be observed from June to July, and a comparable decrease from August to September. This correlates with the general regional temperature pattern [*Boike et al.* 2008]. The derived relative temperatures decrease to near 0°C in September on parts of the north-facing slopes (Figure 2.11e). Only the south-southeast-facing slope shows higher temperatures at this time. Thus, the temperature distribution on the thermokarst depression slopes is consistent with the modeled solar insolation.

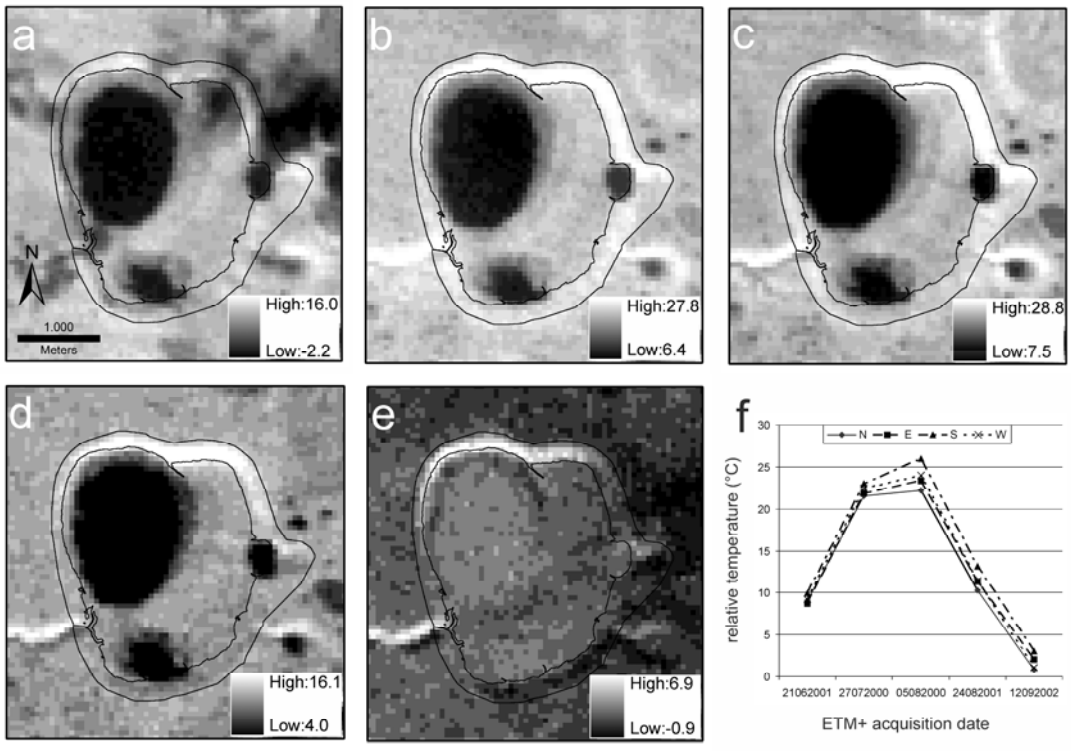

Figure 2.11: Changes over time in Landsat ETM+ thermal data (Band 6, 10.4 – 12.5 µm, 60 x 60 m) for the investigated thermokarst depression. Temperatures in °C (see legends on the bottom right of each panel) are only relative, derived after *Chander et al.* [2009], and should not be seen as absolute values. Black outlines mark the area of basin slopes. Acquisition dates and times: (a) 21 June 2001, 3:17 UTC; (b) 27 July 2000, 3:25 UTC; (c) 05 August 2000, 3:18 UTC; (d) 24 August 2001, 3:16 UTC; (e) 12 September 2002, 3:15 UTC. (f) Temperature trend for the different slope exposure extracted and averaged from randomly-distributed points.

The scatter plots in Figure 2.12 show Landsat-derived temperatures for 250 random points versus modeled solar insolation. Insolation data were modeled on each point for an hour around the acquisition time and date of the satellite imagery. The correlation coefficients shown for each plot indicate moderate to good correlations, particularly for August and September. The best fit was derived for 24 August 2001 (Figure 2.12). Temperature differences within the thermokarst depression are probably most connected to varying insolation in late summer. However, the influence of DEM-measured topography during insolation modeling must be considered, because the complex surface conditions are only partly reflected in the comparatively low-resolution Landsat at-satellite temperatures. This is particularly obvious in the scatter plots where the modeled insolation varies for points with equal temperatures. The highest variations and therefore the lowest correlation coefficients are observed for 21 June 2001 (Figure 2.12). Insolation is typically highest during June, but soil-surface temperatures are comparatively low in early summer [*Boike et al.*, 2008]. Finally, the control of temperature by geomorphology and seasonal differences between the slopes become obvious in the Landsat satellite data.

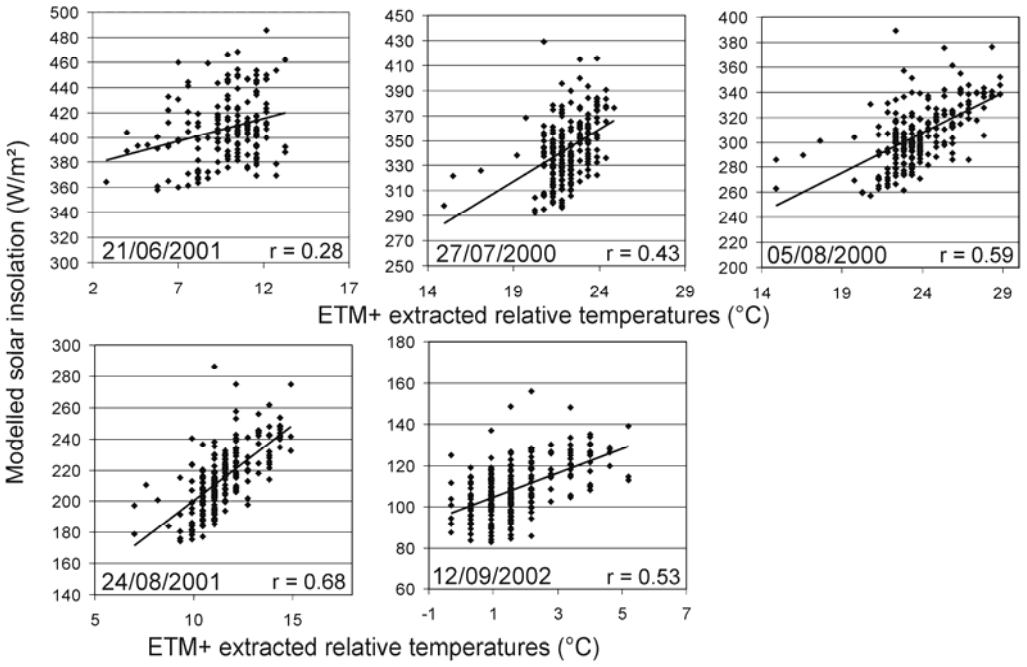

Figure 2.12: Landsat ETM+ extracted temperatures versus modeled solar insolation. The correlation coefficient (r) and the satellite acquisition date are shown for each plot. The solid line indicates the 1:1 line. Note the different axis scales corresponding to the seasonal temperature conditions.

2.4.3 Morphological properties of scalloped depressions on Mars

The morphology of scalloped depressions has been described by numerous authors for the northern [e.g., *Morgenstern et al.,* 2007; *Soare et al.,* 2007, 2008; *Lefort et al.,* 2009] and southern [e.g., *Lefort et al.,* 2010; *Zanetti et al.,* 2010] hemispheres of Mars. Thus, the studied area in

western UP (Figure 2.3) is representative and was primarily selected for comparison to the terrestrial investigation area (Figure 2.2). About 38 % of the UP area is characterized by the formation of scalloped terrain (Figure 2.3b) and consists of typical rimless, irregularly-shaped depressions (Figure 2.3c). The size of single isolated depressions ranges from an area ~0.004 km², 80 to 100 m in diameter, to an area of ~2 km², 1 to 2 km in diameter. The mapped area of the largest complex of coalesced scalloped depressions covers 68 km², though further expanding outside the mapped area. Smaller isolated depressions are generally bowl-shaped and completely surrounded by more-or-less steep slopes (Figure 2.13a). Depths extracted from HiRISE DEM data [*Kirk et al.*, 2008] (Figure 2.13) are on average ~5 m. Larger single depressions in the study area are 20 to 25 m deep and show the typical north-south asymmetrical shape with steep and always concave-upward north (pole)-facing slopes, and gentle convex-to-concave south (equator)-facing slopes (Figure 2.13b and c).

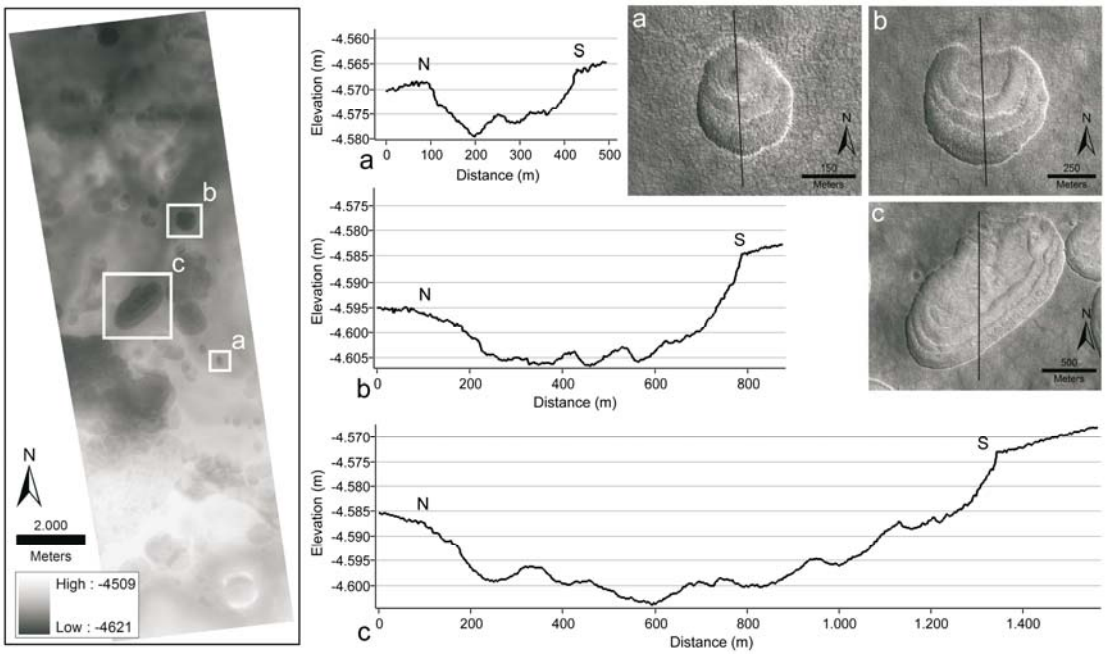

Figure 2.13: HiRISE DEM (1 m/pixel, stereo pair: PSP_001938_2265_PSP_002439_2265) showing the location of typical single-scalloped depressions in the investigated Martian area that reflect different stages of scallop development. (a) Small, fairly symmetrically-shaped depression shows one or two ridges. (b) Medium-sized scalloped depression with very steep concave north-facing slope and slightly inclined convex south-facing slope. Three distinct ridges are visible. (c) Large depression with a flattened profile. The slope asymmetry is visible. Four curvilinear ridges exhibit a step-like profile.

DEM-derived slope angles are 10 to 30° for the steep pole-facing scarps and typically 2 to 4° for the opposite, gentle slopes. The floors of larger isolated depressions and complexes of coalesced depressions are characterized by curvilinear step-like ridges, which are elongated subparallel to the steep scarps; these ridges exhibit asymmetrical profiles, with the steeper side facing the scarp. The number of ridges increases with the size of the depression (Figure 2.13),

which was interpreted by *Lefort et al.* [2009] to reflect different stages of scarp retreat. The coalescence of the depressions to scalloped terrain is influencing large areas in UP (Figure 2.14). Coalescing scallops extend over different elevation levels (Figure 2.14a). Convex slope breaks are typical of the interfaces between coalesced scallops (Figure 2.14b). Inter-depression areas are characterized by a multiphase lowering without any incision [*Balme and Gallagher*, 2009]. No channels have been observed that would connect separate scalloped depressions. On Mars, they have only been found in association with much older, Hesperian-aged thermokarst depressions [*Warner et al.*, 2010].

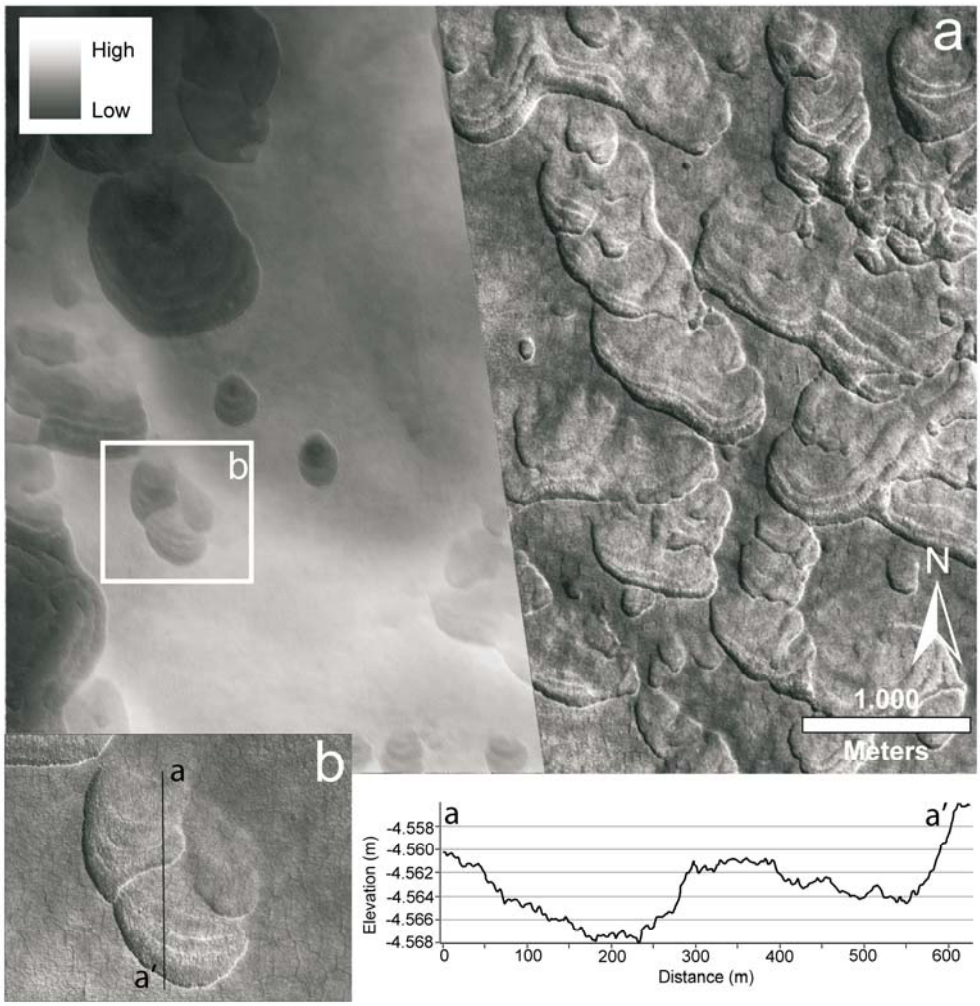

Figure 2.14: (a) Scalloped terrain in the investigated area in Utopia Planitia resulting from the coalescences of scalloped depressions by areal expansion. Smaller isolated depressions in different stages of development are visible nearby (part of the HiRISE DEM on CTX image subset P02_001938_2263_XI_46N267W). (b) An example of small coalesced scalloped depressions and the DEM derived topographic profile highlight a multiphase lowering without connecting channels.

The region is characterized by distinct polygonal patterned ground [e.g., *Lefort et al.*, 2009; *Levy et al.*, 2009a]. The scalloped terrain is well-defined from the adjacent non-degraded uplands by the type of polygonal structures. The uplands show comparatively large irregular random

orthogonal polygons. HiRISE data indicate mean diameters of 40 to 60 m (Figure 2.15). The flat to slightly-elevated centers are surrounded by well-pronounced and partly deep-appearing troughs. These polygonal structures seem to be truncated by scallop development. Troughs are often traceable over the scarps but disappear towards the deeper parts of the depression. In contrast, inside the scalloped depressions there are orthogonal high- to low-center polygons, which are almost 10 m in mean diameter (Figure 2.15). The strong orientation of polygons parallel to steep north-facing slopes is noteworthy; this might be caused by primary cracking perpendicular to the scarp front. The distinct character of the polygonal structures inside and outside of scalloped depressions suggests remarkable differences in ground and atmospheric conditions during polygon formation, as has been explained for terrestrial regions by e.g., *Lachenbruch* [1962, 1966], *Yershov* [2004], and *French* [2007].

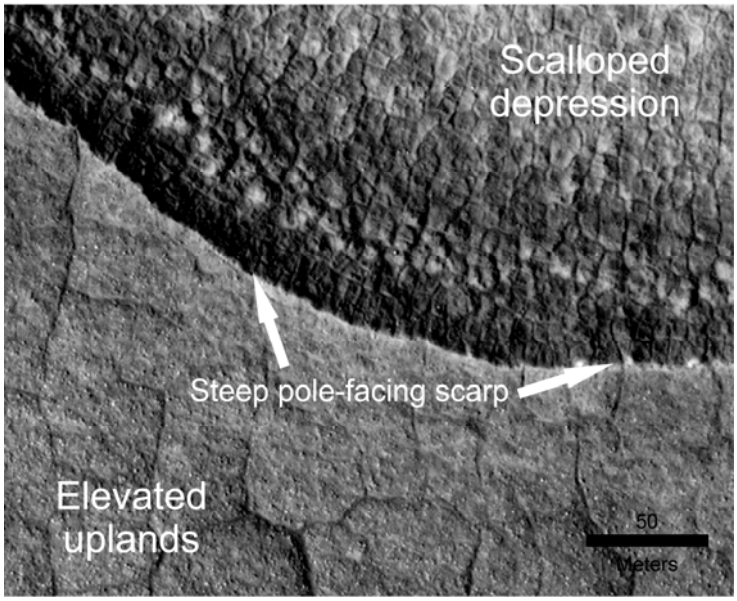

Figure 2.15: Example of polygonal patterned ground inside the scalloped depressions and on the adjacent uplands (HiRISE image subset: PSP_001938_2265).

2.4.4 Insolation and thermal properties of scalloped depressions within the Martian mantle terrain

Lefort et al. [2009] and *Zanetti et al.* [2010] have suggested that temperature differences between the north- and south-facing slopes of the Martian scallops result in enhanced heating of the equator-facing slopes. Therefore, previous interpretations were focused on enhanced scallop development at these slopes [*Morgenstern et al.,* 2007; *Lefort et al.,* 2009, 2010; *Zanetti et al.,* 2010]. Three THEMIS-IR images from the Mars Odyssey orbiter [*Christensen et al.,* 2004] covering a time period from early spring to middle summer show seasonal temperature variations in the study area (Figure 2.16a-c). The temperature changes over time demonstrated in the THEMIS-IR show that the uplands warm at a remarkably faster rate than does the scalloped terrain, allowing the scalloped depressions to be distinguished from the uplands by their lower temperatures (Figure 2.16a-c, e). Temperature differences within the scallops on the depression

slopes are relatively low though all images are acquired at local solar times (LST) in the afternoon. In early spring (L_s = 21.95°, LST = 17.07), temperatures range from ~203 K within the depressions to ~227 K on exposed upper slopes and the adjacent uplands (Figure 2.16a). In late spring (L_s = 75.58°, LST = 17.83), temperatures have already reached ~239 K on the adjacent uplands (Figure 2.16b); these temperatures are not exceeded in middle summer (Figure 2.16c). During summer (L_s = 130.27°, LST = 17.82), only the steeper upper parts of the exposed slopes, passing into the uplands, are warmer (by about 2 K) than the opposite slope and the areas within the scallops (Figure 2.16c). However, the temperature range is greater in spring (~215 to ~239 K) than in summer (~224 to ~237 K).

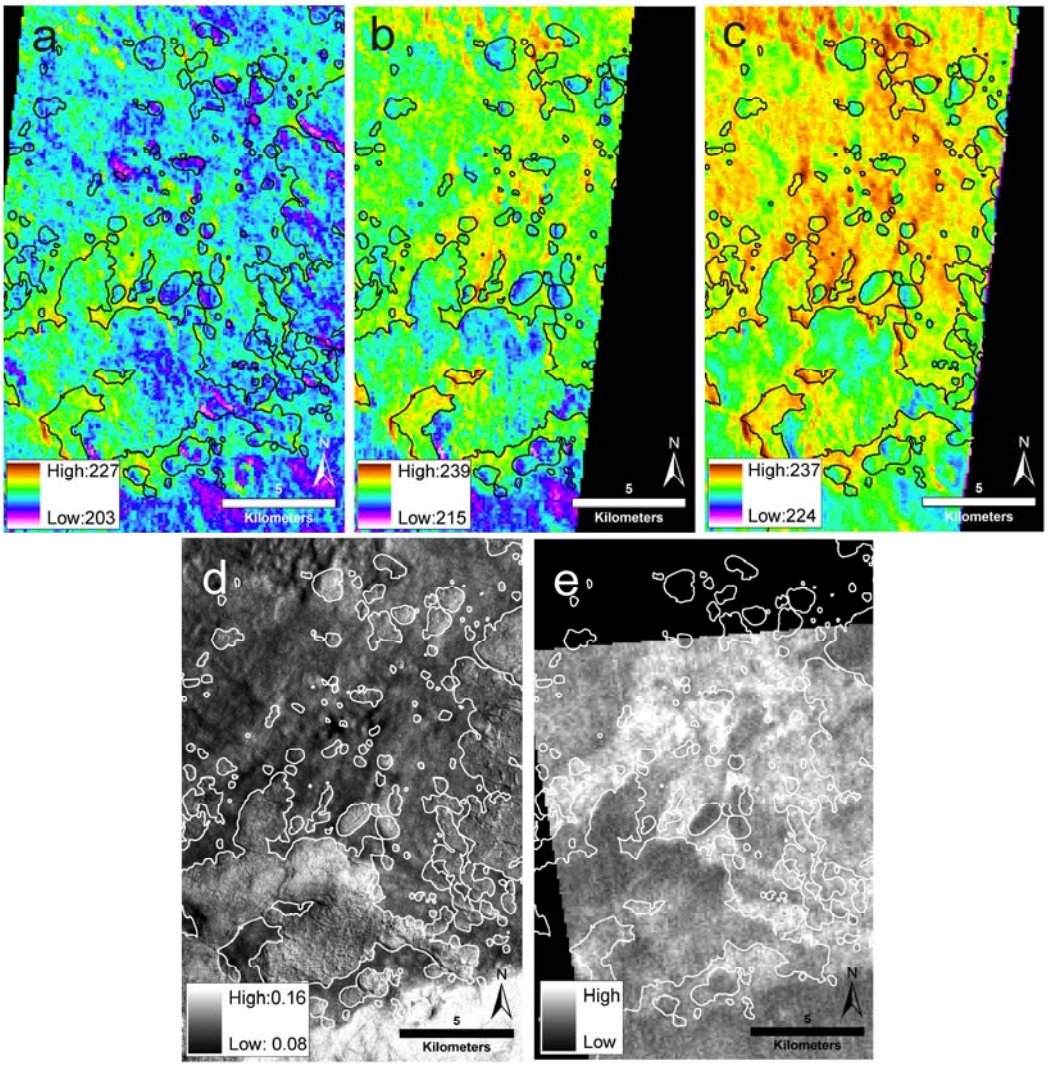

Figure 2.16: (a – c) Daytime temperature variations for the investigated Utopia Planitia area from early spring to middle summer. The changes over time show that the undegraded uplands warm faster than the scalloped terrain (black outlines). Temperatures are given in Kelvin. (a) Early spring (THEMIS-IR image I27105029, LS: 21.95 LST: 17.07). (b) Late spring (THEMIS-IR image I28565002, LS: 75.58 LST: 17.83). (c) Summer (THEMIS-IR image I21689005, LS: 130.27 LST: 17.82). (d) CTX-derived albedo (Lambert albedo) indicates a distinct contrast between the scalloped terrain (white outlines) and the adjacent uplands (CTX image P02_001938_2263_XI_46N267W). (e) The higher nighttime temperatures of the undegraded uplands are clearly visible (THEMIS-IR image I03386003, LS: 70.28 LST: 4.24).

CTX-derived albedo further indicates a distinct contrast between the depressed scalloped terrain and the non-degraded uplands. The higher albedo within the scalloped terrain (Figure 2.16d) suggests different thermal properties of the material inside the depressions and on the adjacent uplands. Nighttime THEMIS-IR data showing the higher temperatures of the non-degraded uplands during night (Figure 2.16e) confirms this assumption. The more compact and (judging by the albedo [Figure 2.16d]) darker material of the uplands would possess higher thermal inertia (i.e. the ability of material to store and conduct heat) than the more unconsolidated fine-grained material within the depressions [e.g., *Mellon et al.* 2000; *Putzig et al.* 2005]. Accelerated warming of the non-degraded uplands caused by the general exposure of the area can be ruled out because the area gently rises towards the south.

Generally, the results from insolation modeling (Figure 2.17) suggest that the typical asymmetric morphology of the scalloped depressions and their formation can be explained by variations in Mars´ orbital parameters. During present orbital configurations, maximum daily surface temperatures on the gentle, equator-facing slopes of the scallops are permanently higher than on the steep pole-facing scarps, due to the higher insolation (Figure 2.17a). In the case of increasing obliquity (i.e. 35° and more), temperature differences between the slopes remain relatively constant but absolute temperatures increase and exceed the melting point of water with certainty only on the equator-facing slopes and flat surfaces (Figure 2.17b). Over periods of high obliquity (>45°) the results show that the pole-facing slopes receive higher insolation than the equator-facing slopes, and temperatures are higher in the morning and evening hours (Figure 2.17c). During the day, temperatures on the pole-facing scarps and the equator-facing slopes are equal and range from well above to right at the melting point of water. The modeling was tested for varying orbital configurations as well. Temperatures on all surfaces can be noticeably higher if high obliquity coincides with high eccentricity, especially if the Martian northern hemisphere summer coincided with perihelion at the same time. The results are similar to results mentioned by *Paige* [2002]. For instance, for a period around 4.816 Ma with an obliquity of 34.8° and a high eccentricity of 0.10 the temperature differences between the slopes are similar to the scenario presented in Figure 2.17b, but absolute temperatures are 10 K higher on all slopes and exceed the melting point of water on the pole-facing slopes as well as on the equator-facing slopes. Otherwise, for a period around 9.112 Ma with a high obliquity of 46.3 and higher eccentricity of 0.08, comparable to the scenario presented in Figure 2.17c, temperatures were around 10 K lower because the solar longitude of perihelion was far from the summertime at this time. However, these specific orbital configurations have rarely occurred during the last 20 Ma [*Laskar et al.*, 2004].

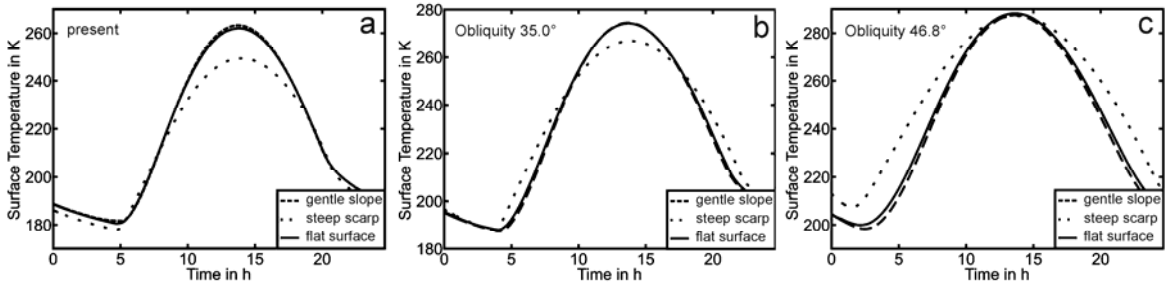

Figure 2.17: Modeled maximum daily surface temperatures during summer (LS: 90°) in the investigated region in western Utopia Planitia for a 20° pole-facing scarp, a 3° equator-facing slope of a scalloped depression, and a flat surface. Temperatures are calculated for three orbital configurations (obliquity, eccentricity, and longitude of perihelion) according to *Laskar et al.* [2004]. (a) Present insolation conditions; obliquity: 25.2°, eccentricity: 0.09, longitude of perihelion: 251.0. (b) Insolation conditions at 0.865 Ma. (c) Insolation conditions at 5.641 Ma.

2.5 Discussion

2.5.1 Terrestrial characteristics of slope asymmetry and spatially directed thermokarst development

The morphometric analyses on Kurungnakh Island confirm a spatially-directed thermokarst development process in ice-rich deposits, as already postulated using remote-sensing analysis [*Morgenstern et al.* 2008a]. Based on the general basin form, the slope asymmetry, and the lake configuration as well as the lake terrace arrangement (Figure 2.4a), a lateral thermokarst development in a northern direction is hypothesized. The results suggest solar insolation (Figure 2.9) and surface temperatures (Figure 2.11) as crucial factors controlling thermokarst slope instability and steepness. The highest amounts of solar insolation and the highest temperatures on south-facing slopes force lake migration in a northern direction and, therefore, the lateral orientation of thermokarst development. In the case of the investigated thermokarst depression, Lake 1 interrupts the former contour of the thermokarst basin, which probably was regularly elliptical. Furthermore, Lake 2 is propagating into the slope, probably in a northern direction as well.

The steepness of the south- and southeast-facing thermokarst depression slopes indicates the geomorphological activity. Denudative processes (i.e. solifluction) have not yet resulted in a flattening of these slopes, as has happened on the west- and north-facing slopes where the widespread distribution of hummocks suggests slope stability. The slope instability of steep south- and southeast-facing slopes is also indicated by the high relief energy represented by the high profile curvature of these slope sections (Figures 2.6a and 2.7). Slope retreat and subsidence probably dominates thermoerosional gully formation here, as seen in the planiform curvature map (Figure 2.6b). The field observation of an area (several square meters in size) on the south-facing slope north of Lake 2 with disturbed vegetation and slope movement, comparable to retrogressive

thaw slumps, supports these assumptions, and clearly reflects the present slope instability (Figure 2.18). Furthermore, spatial and temporal analyses of remote-sensing data show a retreat rate of the south- and southeast-facing slopes of a few centimeters per year north of Lake 1 during the last forty years [*Günther,* 2009] and a measurable shift (by a few meters) of Lake 1 and Lake 2 to the north.

Differently-exposed slopes receive varying amounts of radiation. Only small differences in active-layer depth (<7 cm) as a function of aspect were observed. If the heat transfer to the ground varies as a function of slope and aspect, then these variations result in thawing of Ice Complex deposits at the base of the active layer and in subsidence of the ground surface, rather than in variable thaw depths [*Overduin and Kane,* 2006].

Generally similar observations supporting our work were made by *Czudek and Demek* [1970] for large thermokarst depressions in Central Yakutia (Siberia), where south-facing slopes are commonly steeper because erosion is more effective there and the slopes are thawed to greater depths. In contrast, as was observed in our study as well, north-facing slopes are moister and more gently inclined. A possible control of spatial thermokarst development by insolation has been mentioned by several Russian authors, although no quantitative validations were presented. *Soloviev* [1962] explains the elongation of thermokarst basins in northern and eastern directions by more intense warming and erosion of slopes exposed to the south and west. *Boytsov* [1965] also points out the influence of direct solar radiation on the pace of thermoabrasion of differently-exposed slopes. In general, south-southwest facing slopes receive the highest energy as air and water temperatures are highest during times when the afternoon sun is directed at these slopes. Thermoabrasion is more pronounced here and accounts for an elongation of a thermokarst lake basin in north-northeastern directions. This pattern can be altered by the severe morning fog or afternoon cloud cover typical for some regions, which will have a weakening effect on slope warming and lateral basin growth.

Steep head-wall retreat and retrogressive thaw-slump activity mainly forced by solar radiation and sensible heat flux were identified by *Lewkovicz* [1986], and recently confirmed by *Grom and Pollard* [2008] using microclimatic investigations on a southerly-oriented active thaw slump in the Canadian high Arctic. Insolation as primary agent of slope asymmetry in artic asymmetrical valleys was already suggested by *Crampton* [1977], who described steeper south-facing slopes in numerous asymmetrical valleys in the Mackenzie River region of Canada. Similar observations were made by *French* [1970]. The steepness of southwest-facing slopes was explained by higher loss of latent heat due to the exposure of these slopes to prevailing winds, and thus warmer and moister conditions on the opposite slopes. These conditions result in a higher extent of mass-wasting (solifluidal) processes on northeast-facing slopes, where material is preferentially transported into the river and the streams are therefore pushed to the southwest-facing slopes. In response, the slope is undercut and steepened. It must be noted that theories of asymmetrical valley

development are difficult to apply to thermokarst slope asymmetry, because erosion and accumulation processes of a flowing river are of prime importance. However, the influence of ponding water on thermokarst depression development must be considered [e.g., *Czudek and Demek*, 1970; *Romanovskii et al.,* 2000]. The most effective process is the lateral bank erosion of a standing water body. Wind has been suggested as the driving agent of oriented thaw lake expansion due to wind-driven currents and wave activities [e.g., *Carson, 2001*; *Côté and Burn,* 2002; *Hinkel et al*., 2005; *French,* 2007]. However, great differences exist in wind data from several meteorological stations within the Lena Delta area, and there is little knowledge about the detailed conditions and factors that might be involved in lake-orientation processes in the Delta [*Morgenstern et al*. 2008b].

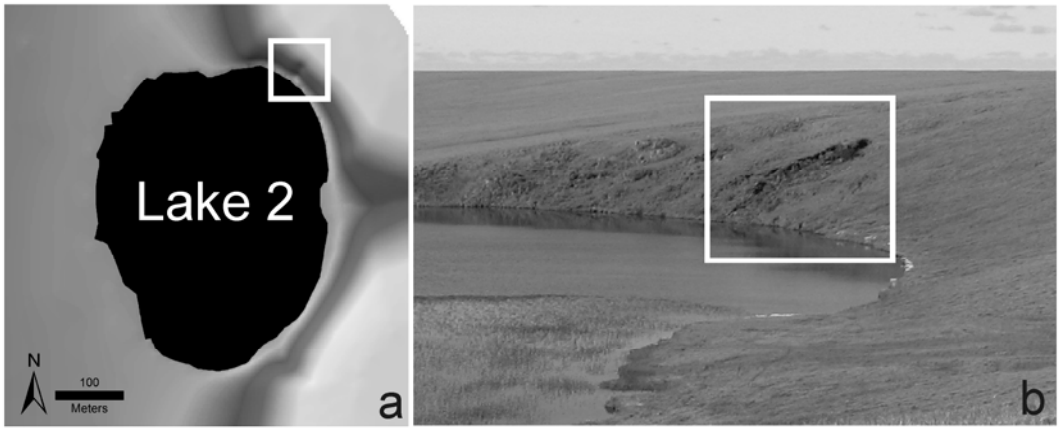

Figure 2.18: Slope movement and instability indicated by an area of disturbed vegetation on the steep south-facing thermokarst depression slope north of Lake 2 (white rectangle). (a) Subset of the DEM (see Figure 2.4a). (b) Photograph of the lake and the described area. View to the north-northwest.

According to *Soloviev* [1973] and *Romanovskii et al.* [2000] the following scenario of landscape evolution at our thermokarst study site can be proposed: An approximately north-south elongated depression was filled and formed by a large thermokarst lake in an early stage during the late Glacial to early Holocene period. The fast-growing thermokarst lake thawed and deepened into the ice-rich deposits beneath, resulting in strong thermokarst subsidence [*Grosse et al.,* 2007]. Taberal deposits remaining at the lake bottom probably range in thickness from 2.3 to 8.9 m today. The current volume and dimension of the thermokarst depression accurately reflects the high ground ice content, as was shown above. Further deepening of the thermokarst depression is probably restricted by the lower boundary of Ice Complex deposits and the underlying ice-depleted sandy sequence at 20 m a.s.l. [*Schirrmeister et al.,* 2003; *Wetterich et al.,* 2008], an elevation level which has already been reached by the largest lake. Large and deep thermokarst depressions are also common in the northern Lena Delta in sandy deposits with lower ice contents [*Grigoriev,* 1993; *Schwamborn et al.,* 2002; *Ulrich et al.,* 2009]. Therefore, further thermokarst subsidence

cannot be excluded. After the primary lake was drained, two secondary lakes (Lake 1 and Lake 3) remained within the incidental thermokarst depression. Lake 1 migrated over the basin floor in several stages in a north-northwest direction, deepening into the basin floor and undercutting the slope as indicated by different terrace levels within the depressions (Figure 2.4a). This process was strongly influenced by high insolation and higher temperatures on south-southeast-facing slopes. Lake 2 drained into the thermokarst depression later from an adjacent small depression. Currently, this lake is migrating to the north-northeast. The steepest slope angles and disturbed vegetation cover caused by the highest insolation values and comparatively higher temperatures (Figure 2.9 and 2.11) on the slope north of the lake confirm ongoing lateral thermokarst development (Figure 2.18). As the soil thermal energy balance is disturbed, slope instability, steepness, and therefore lateral thermokarst development are forced by solar insolation.

2.5.2 Implications for scalloped depression development on Mars

On Earth, steeper south-facing thermokarst depression slopes are geomorphologically more active. This activity is forced directly by solar insolation and, therefore, higher temperatures in the investigated thermokarst depression on the Ice Complex remnants of Kurungnakh Island. Less erosional activity of north-facing slopes is indicated by areal flattening due to solifluction and cryoturbation processes in the terrestrial permafrost region [e.g., *Williams and Smith,* 1989; *French,* 2007]. By direct analogy, this implies that lateral scallop development on Mars is primarily forced on the steep pole-facing scarps in an equator-ward direction. This would have happened primarily during periods of high obliquity (35- 45° and more) (Figure 2.17).

The relationship of obliquity changes to increasing erosion on mid-latitude pole-facing crater slopes due to gully formation has already been suggested by various authors, predominantly for the Martian southern hemisphere [e.g., *Costard et al.,* 2002; *Dickson et al.*, 2007; *Head et al.,* 2008; *Morgan et al*., 2010]. In the northern hemisphere there is a shift of gully orientation at 40°N from pole-facing slopes to equator-facing slopes, suggesting that obliquity-driven insolation is not the only factor controlling gully formation [*Kneissl et al.,* 2009]. However, a genetic linkage between obliquity-driven volatile-rich mantle formation on pole-facing slopes and gully erosion in the northern hemisphere is proposed by e.g., *Bridges and Lackner* [2006]. The morphometrical characteristics of the equator-facing scalloped depression slopes in UP (convex curvature, slightly inclined, flat) imply the absence of strong erosional processes as suggested by *Lefort et al.* [2009], but instead suggest areal flattening and likely current surface stabilization (Figure 2.13).

Slow-to-absent morphological processes in the current stage of scalloped depression formation are also suggested by the thermal properties and albedo data, which always show lower temperatures and higher albedo of the scalloped terrain compared to the adjacent uplands within the investigated area (Figure 2.16). Nevertheless, our results support the general insolation model

suggested by *Morgenstern et al.* [2007] and *Lefort et al.* [2009], which suggests the formation of scalloped depressions by insolation-driven ground ice sublimation.

Different interpretations of scalloped depressions as residues of thermokarst lakes or alas depressions [e.g., *Costard and Kargel*, 1995; *Soare et al*., 2007, 2008] are not consistent with the definition of alas development on Earth [e.g., *Everdingen,* 2005] despite visual similarities. Evidence for thermokarst lake or alas formation due to ponding water cannot be identified in scalloped depressions on Mars [e.g., *Lefort et al.,* 2009; *Zanetti et al.,* 2010]. The ridges within the depressions were interpreted by *Soare et al.* [2007, 2008] as stages of alas growth; "the shallowest step represents the most recently formed part of the alas, whereas the deepest step indicates an older presence" [*Soare et al.*, 2007]. If a lake is migrating on a thermokarst depression bottom and deepens due to thawing of ground ice and combined subsidence, then the highest lake terrace represents the oldest stage and the lowest the youngest. The ridges within the scallops which are trending subparallel to the proposed scarp retreat must have an opposite form if a lake is migrating and eroding the scarp as was described above for the terrestrial thermokarst depression (see also Figure 2.4). Furthermore, terrestrial thermokarst depressions and thermokarst lakes are usually connected by channels and narrow valleys (see also Figure 2.2). The drainage of thermokarst lakes, which results in the formation of thermokarst depressions (i.e. alasses), occurs via thermoerosional valleys [e.g., *Hill and Solomon*, 1999; *Grosse et al*., 2007]. Such features implying the former existences of flowing water between or the drainage of standing water bodies do not exists in Martian scalloped terrain (Figure 2.14). The landscape geomorphology in UP points to a dry origin of the scalloped depressions. The coalescence to scalloped terrain took place by areal expansion and multiphase lowering without channel incision. *Warner et al.* [2010] show evidence for wet thermokarst, i.e. thermokarst-like depressions connected by narrow channels. However, these features are much older and are, therefore, not further discussed here. In contrast, wet thermokarst degradation analogous to terrestrial retrogressive thaw slumps and thaw lakes is proposed by *Balme and Gallagher* [2009] for a study site in Athabasca Vallis near the Martian equator. The region is characterized by shallow basins, which are linked by fluvial-like channels. Retrogressive erosional scarps occur along the margins of the basins. With many of these scarps dendritic channels are associated. *Balme and Gallagher* [2009] suggest an origin during warmer conditions in the recent past including the thawing of ground ice by standing water bodies followed by surface subsidence and the lateral erosion by thaw slumps.

With respect to former studies [*Morgenstern et al.,* 2007; *Lefort et al.,* 2009; *Zanetti et al.,* 2010], the formation theory of scalloped depressions is modified here in particular for the volatile (ice)-rich UP deposits (Stage 0 in Figure 2.19). Scallop formation started at weak points like large thermal contraction cracks [*Zanetti et al.*, 2010] or the small-relief surface depressions proposed by *Lefort et al.* [2009]. During low to moderate Martian obliquity a small depression, symmetric in cross section, was formed by homogeneous ground ice sublimation and subsequent subsidence of

the ice-depleted surface material (Stage 1 in Figure 2.19). If temperatures were very low and ice thawing was unlikely [e.g., *Costard et al*., 2002; *Hecht,* 2002], the comparatively slow process of ground ice sublimation would have led to a consistent and homogeneous subsidence. Within the investigated area, small isolated depressions (around 100 m in diameter) that are not asymmetric but rather bowl-shaped represent an initial scallop stage. At this time, during which the orbital configuration was comparable to that of the present day, insolation and temperatures were permanently higher on the equator-facing depression slopes than on the pole-facing slopes (Figure 2.17a). The continuous ice sublimation led to an areal flattening of the equator-facing slopes and further deepening of pre-existing depressions, while the pole-facing slopes steepened because they were permanently shaded and stabilized by ice-cementation (Stage 2 in Figure 2.19). When Mars` obliquity was changed to higher values and insolation increased (Figure 2.17b), scallop development moved in an equator-ward lateral direction (Stage 3 in Figure 2.19). Increasing insolation on the pole-facing slopes would have forced slope instability and erosion by enhanced ground ice sublimation or even thawing. This suggestion has already been proposed as a possible stage of scalloped depression development by *Lefort et al.* [2009]. When the ice was lost as the major cementing material, the upper material layer of the pole-facing slope was interrupted (further destabilized) in weak areas such as in the cracks of the large polygons on the adjacent uplands, and slumped into the depression (Stage 3 in Figure 2.19). In this process the sediment mass slid on the still-frozen material beneath. Simultaneously, the sediment mass block-rotated around a horizontal axis in such a way as to tilt the former surface backward. Furthermore, this process led to a concave scarp profile and subparallel ridges with steeper sides facing the scarp, and the lateral movement and growth of the scallops in an equator-ward direction (Stage 4 in Figure 2.19).

Modeling results show that this process must have been maximized by ground ice thawing when Mars obliquity reached >45° (Figure 2.17c and 2.19). Maximum temperature events especially occurred if orbital eccentricity was high and/or the Martian northern summer coincided with perihelion (see above). The equator-facing slope was probably stabilized at a specific stage if the ice-depleted material formed an insulating layer which prevented further sublimation. However, the slumping processes were likely fast, brief events of increasing sublimation or even thawing on pole-facing scarps because these slopes were not flattened like the opposite slopes. The scarp was stabilized again because ice cement still existed inside after the uppermost material layer had slumped. The retrogressive growth stopped when Mars´ obliquity tilted back to low degrees. The material was stabilized at the basin floor; strong thermal contraction cracking occurred at lower temperatures, while primary cracking developed perpendicular to the weak areas formed by the scarp front (Figure 2.15) as is known from similar processes in terrestrial permafrost regions [e.g., *Lachenbruch*, 1962, 1966; *Yershov*, 2004]. Such events happen periodically, as evidenced by increasing numbers of ridges with increasing scalloped depression sizes (Figure 2.13). The notion that each ridge may represent a single period of high obliquity [*Lefort et al*., 2009] is difficult to

confirm, since such strong and comparatively fast slumping processes should happen more often during times of high obliquity and the favorable orbital configurations are rare [*Laskar el al.*, 2004].

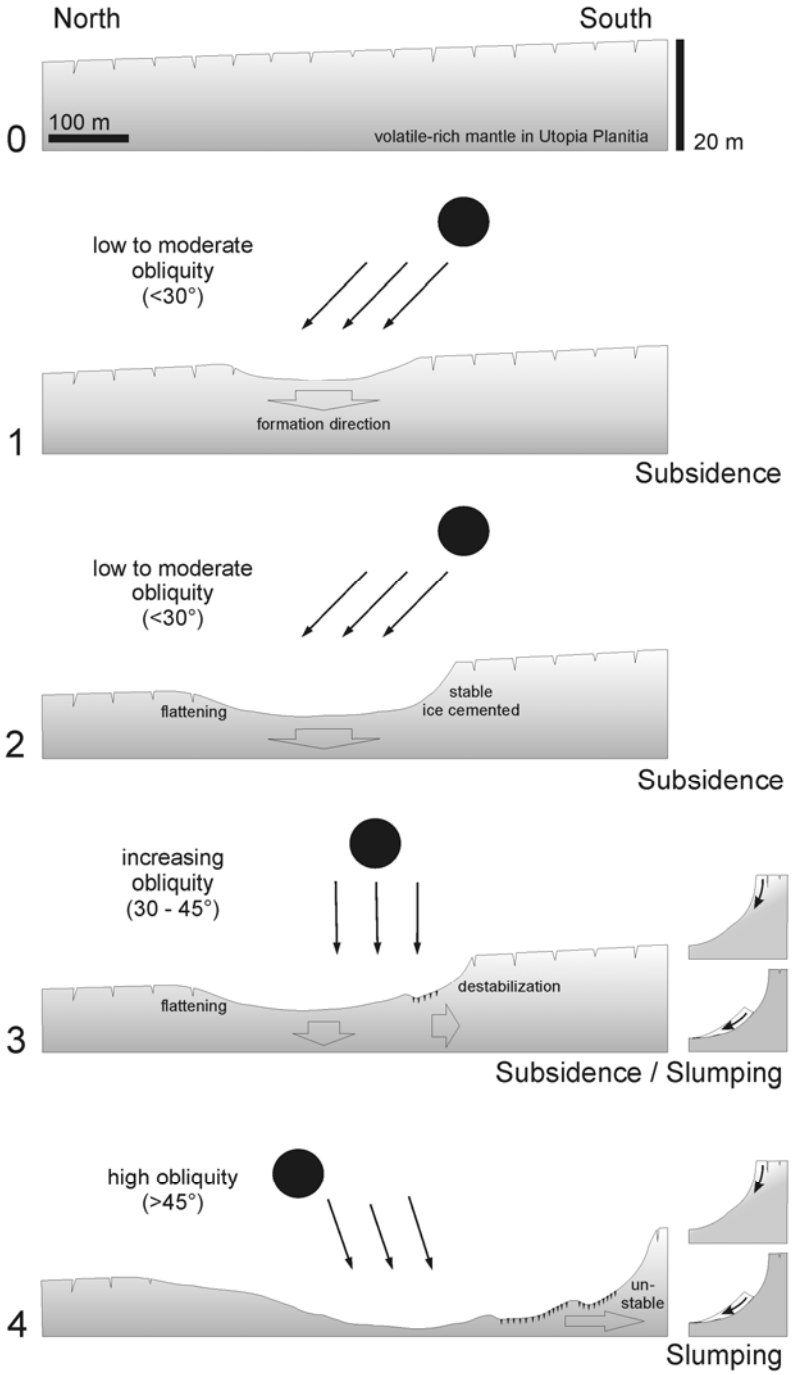

Figure 2.19: Schematic model for scalloped depression formation in Utopia Planitia including changes of Mars´orbital parameters. Stage 0: Surface of volatile (ice)-rich mantling deposits [*Kreslavsky and Head,* 2000; *Mustard et al.,* 2001]. Stage 1: Homogenous ground ice sublimation resulted in an initial scallop stage. Stage 2: An asymmetrical depression was built by areal flattening of the equator (south)-facing slope and due to ice-cementation of the steepened pole (north)-facing slope. Stage 3: Initiation of scalloped depression retrogressive growth in equator-ward direction by destabilization of the pole-facing slope due to obliquity-driven temperature increase. Stage 4: Maximization of equator-ward lateral scalloped depression formation during high obliquity periods.

The depths of scalloped depressions originated primarily by subsidence and suggest high ground ice contents of the volatile (ice)-rich mantle material, although this material could be partly removed by eolian processes [e.g., *Lefort et al.*, 2009, 2010; *Zanetti et al.*, 2010]. However, the asymmetrical shape of the scallops in UP does not correspond to the prevailing wind direction in summer (from S to SSW) [*Morgenstern et al.*, 2007], when scallop formation activity is likely to be most intense. Additionally, eolian dunes and dust devil tracks suggesting eolian erosion were not observed in the investigated area. The volume and the dimensions of the scalloped depression must be related to ground ice contents, which were presumably higher than the amounts proposed in the literature [e.g., *Boynton et al.*, 2002; *Feldman et al.*, 2004].

Age determinations of the scalloped depression development are difficult to make. The occurrence of suitable orbital configurations in the last 10 Ma suggests that the largest single scalloped depression and the coalesced part of the scalloped terrain could have formed within this time period, but younger stages of higher obliquity as well the additional coincidence with favorable orbital configurations (high eccentricity and/or summer coinciding with perihelion) suggest scallop formation at least in the last 5 Ma as well. The model results propose that, at the most recent stages of high obliquity around 5.641 and 9.112 Ma, ground ice thawing may have forced scallop development and scallops could have developed in a few hundred thousand years. However, because the slumping process at the pole-facing slope must be a fast and abrupt event, the subsidence of the depression surfaces by sublimation must occur at a very slow rate [*Lefort et al.*, 2009]. Furthermore, we think that scalloped depression formations probably remain dormant, preserved by the atmospheric conditions at low obliquity periods like the present, because the scalloped depressions appear unweathered and young.

2.6 Conclusions

Thermokarst formation on Earth is strongly influenced and driven by standing water bodies. Direct comparison to Martian scalloped depressions is therefore problematic. However, studies of analogous thermokarst depressions in Ice Complex deposits in the Siberian Arctic and investigations of the influence of solar insolation on terrestrial thermokarst morphology have improved our understanding of insolation-driven scallop development on Mars. The asymmetry of terrestrial thermokarst depression slopes with steeper slopes facing south (i.e. the equator) is confirmed by geomorphometric analyses. Both the results of insolation modeling and thermal Landsat satellite data imply a strong influence of incoming radiation on slope morphology. We propose a lateral development of thermokarst depressions and lake migration in a northern direction in the Ice Complex remnants in the Lena Delta.

For the development of Martian asymmetric scalloped depressions, retrogressive growth in an equator-ward direction is postulated. The schematic model of the formation of scalloped

depressions in UP shows a climatically-controlled evolution. Our insolation modeling of scalloped depressions in UP supports the hypothesis that fast and abrupt slumping processes at the steep pole-facing scarps have occurred during periods of increasing obliquity within the last 10 Ma. The lateral scallop formation was maximized by possible ground ice thawing during periods of high obliquity, and when certain orbital configurations coincided. The equator-facing slopes were flattened by continuous, though slow, ground ice sublimation and depression surface subsidence. When Mars´ orbit tilted back to low degrees of obliquity sublimation of ground ice was minimized and lateral scalloped depression formation stopped. The material was stabilized at the basin floor and strong thermal contraction cracking occurred.

Acknowledgements

This research has been partly supported by the Helmholtz Association through the "Planetary Evolution and Life" research alliance. Field work was carried out within the framework of the Russian-German Lena 2008 expedition. We express our grateful appreciation to all colleagues involved in logistical and scientific support. The continuing efforts and support of the HiRISE and CTX teams in making their data publicly available and the ALOS project and ESA for providing ALOS data within the framework of the "LEDAM" project (awarded by ESA ADEN, PI Lantuit, ID 3616) are gratefully acknowledged. We thank Randolph L. Kirk (USGS, Flagstaff, USA) and colleagues for kindly providing a HiRISE DEM for our Martian study site. The paper benefited by English proof-reading and valuable comments from Candace S. O'Connor (UAF, Fairbanks, Alaska) as well as by highly constructive suggestions from an anonymous reviewer.

3. Polygon pattern geomorphometry on Svalbard (Norway) and western Utopia Planitia (Mars) using high-resolution stereo remote-sensing data

Mathias Ulrich[1], Ernst Hauber[2], Ulrike Herschuhr[1], Stefanie Härtel[3], Lutz Schirrmeister[1]

[1]Alfred Wegener Institute for Polar and Marine Research, Research Unit Potsdam, Potsdam, Germany
[2]Institute for Planetary Research, German Aerospace Center (DLR), Berlin, Germany
[3]Institute for Geography, University of Leipzig, Germany

Accepted for publication in Geomorphology

Abstract

Polygonal systems formed by thermal contraction cracking are complex landscape features widespread in terrestrial periglacial regions. The manner in which cracking occurs is controlled by various environmental factors and determines dimension, shape, and orientation of polygons. Analogous small-scale features are ubiquitous in Martian mid- and high-latitudes, and they are also inferred to originate from thermal contraction cracking. We studied the geomorphometry of polygonally-patterned ground on Svalbard to draw a terrestrial analogy to small-scale polygonal structures in scalloped terrain in Martian mid-latitudes. We performed a comparative quantitative terrain analysis based on high-resolution stereo remote-sensing data (HRSC-AX and HiRISE) in combination with terrestrial field data and multivariate statistics to determine the relationship of polygon geomorphometry to local environmental conditions. Results show that polygonal structures on Svalbard and in Utopia Planitia on Mars are similar with respect to their size and shape. A comparable thermal contraction cracking genesis is likely. Polygon evolution, however, is strongly related to regional and local landscape dynamics. Individual polygon dimensions and orthogonality vary according to age, thermal contraction cracking activity, and local subsurface conditions. Based on these findings, the effects of specific past and current environmental conditions on polygon formation on Mars must be considered. On both Earth and Mars, the smallest polygons represent young, recently-active low-centered polygons that formed in fine-grained ice-rich material. Small, low-centered Martian polygons show the closest analogy to terrestrial low-centered ice-wedge polygons. The formation of composite wedges could have occurred as a result of local geomorphological conditions during past Martian orbital configurations. Larger polygons reflect past climate conditions on both Earth and Mars. The present degradation of these polygons depends on relief and topographical situation. On Svalbard

the thawing of ice wedges degrades high-centered polygons; in contrast, the present appearance of polygons in Utopia Planitia is primarily the result of contemporary dry degradation processes.

3.1 Introduction and background

Many landforms on Mars show similarities with periglacial features on Earth. On Earth these landforms reflect the effects of cold-climate conditions often in connection with permafrost dynamics. However, some of the periglacial features on Mars seem inconsistent with the prevailing Martian hydrological and climatic conditions because, like on Earth, water must have played an important role during their formation. The study of their characteristics, distribution, and spatial associations would therefore allow conclusions to be drawn about the climate history of Mars; thus, such study can be used to indicate past and present environmental conditions. For instance, polygonal surface structures are a widespread phenomenon in periglacial landscapes on both Earth and Mars. This allows several conclusions to be drawn by analogy, but leaves open an important question: Are these structures morphological analogues only, or is there a genetic relationship between them?

Patterned ground with polygon diameters ranging from meters to tens of kilometers has been described for many years on Mars [e.g., *Luchitta,* 1981; *Mellon,* 1997; *Seibert and Kargel,* 2001; *Mangold,* 2005; *van Gasselt et al.,* 2005; *Levy et al.,* 2009a, 2010a]. While medium-sized (diameter >100 m) and giant polygons (several kilometers in diameter) are suggested to originate by tectonic processes [e.g., *Hiesinger and Head*, 2000; *Yoshikawa,* 2003] or by desiccation in the case of medium-sized polygons [*El Maarry et al.,* 2010], many authors have inferred that small-scale patterns (<100 m in diameter) are formed as thermal contraction polygons, analogous to terrestrial ice- and sand-wedge polygons [e.g., *Seibert and Kargel,* 2001; *Mangold,* 2005; *Mellon et al.,* 2008; *Levy et al.,* 2009a, 2010a]. Recently, it could be shown by mechanical modeling that the maximum size of polygons formed by thermal contraction is limited to a few decameters [*El Maarry et al.,* 2010].

Generally, the average diameters of thermal contraction polygons on Earth range between a few meters and a few decameters. Low-centered polygons can be distinguished from high-centered polygons. Low-centered polygons are commonly characterized by outlining furrows, which are delineated by raised rims. Upturning rims form as a result of thermal expansion and lateral displacement of the active-layer (i.e. the upper soil layer which thaws seasonally) material above a growing ice or sand wedge [*Mackay,* 1980]. High-centered polygons are the result of ice-wedge degradation followed by the enlargement and deepening of the polygon-outlining troughs [e.g., *Washburn,* 1979]. Ice-wedge polygons are the most common type of thermal contraction polygons in more humid arctic regions. In hyper-arid polar deserts (e.g., the Antarctic ice-free areas, Canadian high Arctic), liquid water is lacking and cracks are commonly filled by eolian material or

sand, building sand-wedge polygons [e.g., *Péwé,* 1959; *Sletten et al.,* 2003; *Bockheim et al.,* 2009] (Table 3.1). If local conditions favor the occasional support of moisture, composite wedges can develop [*Murton,* 1996]. Special types of sand-wedge polygons described from the Antarctic Dry Valleys are high-centered sublimation polygons [*Marchant et al.,* 2002; *Marchant and Head,* 2007]. However, sand-wedge polygons can hardly be distinguished from ice-wedge polygons in the plan view [*Black,* 1976].

Table 3.1: Literature-based compilation of climate and subsurface conditions in relation to various thermal contraction polygon properties.

Indicator	Control factors	Effects	Reference
polygon formation	air and soil temperature, grain size	in silt, clay, and peat: < -3°C in sand and gravel: -8 to – 10 °C	*Washburn* [1979]; *Romanovskii* [1985]; *Yershov* [2004]
	insulation	limiting the continuous frost cracking	*Washburn* [1979]; *French* [2007]
polygon diameter	temperature gradient	large gradient → harsher climate → smaller polygons	*Yershov* [2004]; *French* [2007]
	rheology of frozen ground	heat conductivity (grain size, ice content) → fine-grained, high ice content → smaller polygons	*Lachenbruch* [1962, 1966]
polygon form	stress free zones	orthogonal → near the cooling surface hexagonal → in larger distance	*Romanovskii* [1977]
	ground homogeneity	hexagonal patterns – stress balance	*Lachenbruch* [1962]; *French* [2007]
	stage of development	secondary cracking → polygon subdivision → more regular and orthogonal	*Lachenbruch* [1966] *French* [2007]
polygon orientation	stress relief	oriented if stress-free vertical surfaces exist (i.e. anisotropy of strength)	*Lachenbruch* [1962]
polygon nets	drainage	small nets → < 27° slope large nets → to 31° slope	*Washburn* [1979]
ice or sand wedge formation	atmospheric and ground humidity	high aridity → sand wedge polygons	*Péwé* [1959]; *Black* [1976]; *French* [2007]
ice-wedge polygon formation	soil temperature, grain size	in clay → < -2 °C, in gravels → < -6°C	*Romanovskii* [1985]

The term polygon is here used *in sensu Washburn* [1979], *Yershov* [2004], and *French* [2007] as a form of patterned ground indicative of continuous cold climates and the presence of permafrost. These polygonal networks are formed by thermal contraction fissures [*Lachenbruch,* 1962, 1966] after an initial crack is reactivated recurrently [*Mackay,* 1974, 1992] and widened through subsequent filling by water, sand, or soil [*Péwé,* 1959; *Black,* 1976; *Sletten et al.,* 2003; *French,* 2007]. The frozen ground cracks under volumetric tension due to long cold periods and a severe soil temperature drop in winter [*Yershov,* 2004; *Christiansen,* 2005; *Fortier and Allard*,

2005]. This in turn depends on the coefficient of thermal expansion which is larger in ice-rich sediments than in ice-free sediments [*Lachenbruch,* 1962] (Table 3.1). The strength and direction of stress vectors during thermal contraction, which determine dimension, shape, and orientation of thermal contraction polygons, are controlled by various factors such as air and ground temperature variations, subsurface conditions (i.e. rheology, water/ice content), topography, and stress-free vertical surface (e.g., breaks, other cracks, terrain edges, talik rims). Some of these factors are summarized in Table 3.1; these factors offer the possibility of estimating the subsurface and climate conditions that existed during polygon formation by geomorphometric properties.

Although no clear evidence for the processes responsible for the formation of small-scale polygons on Mars can yet be presented, the distribution of these polygons at middle to high latitudes [*Mangold,* 2005; *Levy et al.,* 2009a] and their spatial relationship to ground ice on Mars [*Mangold et al.,* 2004] suggest that these landforms are formed by thermal contraction cracking, which is controlled by specific periglacial climatic and subsurface conditions [*Levy et al.,* 2010a]. Furthermore, the relationship of likely active thermal contraction polygons to periglacial landscape features in a geomorphologic context compared to terrestrial analogues allows conclusions to be drawn about small-scale polygon origin on Mars. However, even if most of the conclusions about Martian polygon evolution are very detailed and plausible they frequently offer only qualitative explanations. Only a few studies have been done regarding polygon geomorphometry on Mars using quantitative methods [e.g., *Rossbacher,* 1986; *Pina et al.,* 2008; *Dutilleul et al.,* 2009; *Haltigin et al.,* 2010]. Therefore, based on very-high-resolution stereo remote-sensing data, comparative quantitative terrain analysis in combination with geomorphological and sedimentological field data from terrestrial polygons were used to verify the hypothesis that polygonal structures on Earth and Mars, which are similar in appearance, originate from comparable processes. Additionally, a multivariate statistical approach has been applied to validate and compare the relationship of polygon geomorphometry to the topographical conditions of various polygonal sites from a mid-latitude region on the Martian northern hemisphere and an analogous high-arctic region in central Spitsbergen (Svalbard) [*Hauber et al.,* 2011; *Hauber et al.,* in press]. The main objective of this paper is, first to highlight the relationship between geomorphometric parameters of thermal contraction polygons and site-specific topographical and subsurface conditions on Earth. Second, this understanding will be applied to give insights into formation processes and subsurface conditions of small-scale polygonal patterned ground on Mars by comparison of their associated geomorphometry. Bearing in mind the regional geomorphological context of diverse polygonal fields within periglacial landscapes, this work is focused on Adventdalen (Svalbard) and on the scalloped terrain in Utopia Planitia (Mars).

3.2 Characterization of study areas

3.2.1 Svalbard (Adventdalen)

The Svalbard archipelago, and in particular its largest island, Spitsbergen (Figure 3.1), exhibits a diverse inventory of periglacial landforms in close spatial proximity. Svalbard is situated in the zone of continuous permafrost [*Brown et al.,* 1998], which is widespread primarily outside the 60%-glacier-covered area [*Humlum et al.,* 2003]. Permafrost thickness ranges from 100 m in the valleys to around 450 m in the mountains [e.g., *Liestøl,* 1976; *Isaksen et al.,* 2001]. Permafrost ages on Svalbard are estimated to be late Holocene in the valleys and the coastal areas [*Humlum et al.,* 2003]. The permafrost temperature on Svalbard is -2.3°C to -5.6°C [*Christiansen et al.,* 2010], and active-layer thickness varies from a few decimeters to 1.5 m depending on vegetation, snow cover, and subsurface conditions [*Sørbel et al.,* 2001].

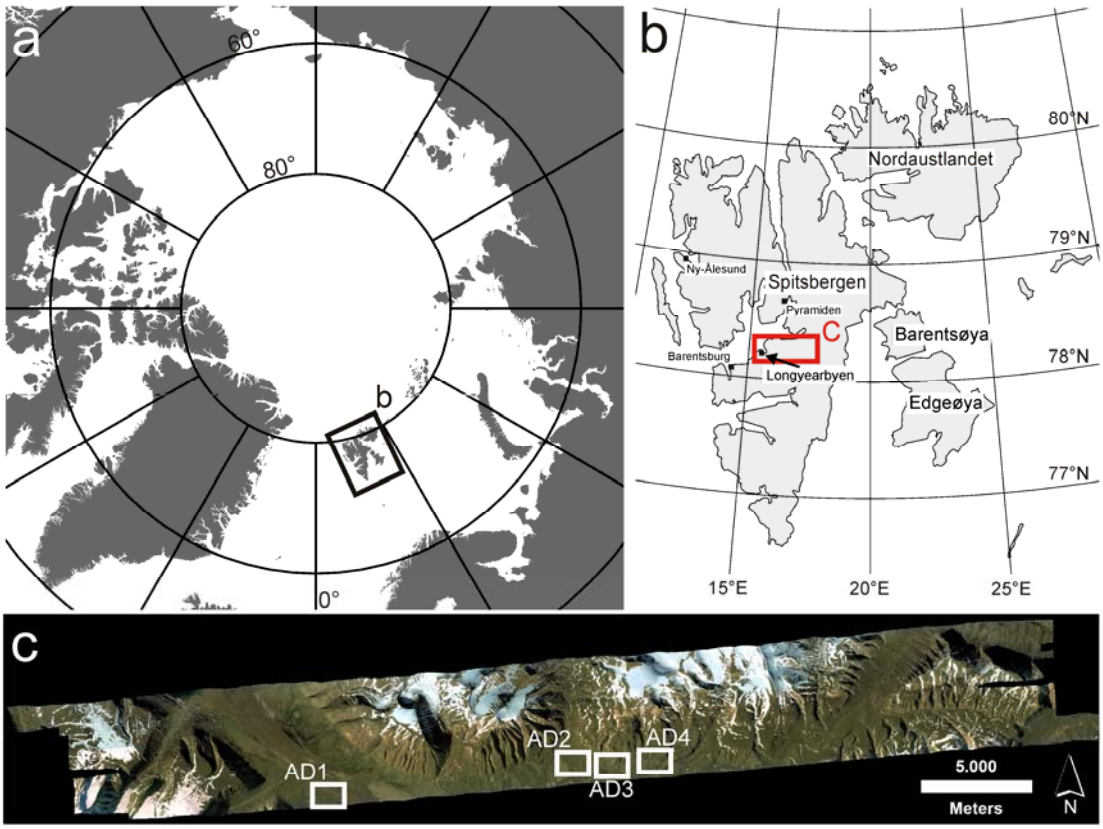

Figure 3.1: Context maps of the terrestrial study area. (a) Location of the Svalbard archipelago in the Arctic. (b) Map of Svalbard and its largest island Spitsbergen with the Adventdalen area marked by the black box. (c) HRSC-AX true-color image mosaic of the Adventdalen region with the location of the investigated polygonal fields shown. Elevation increases from site AD1 to site AD4.

The main study area is Adventdalen in Central Spitsbergen (Figure 3.1b), a ~30 km long and ~4 km wide U-shaped valley, which extends eastward from Svalbard's main town Longyearbyen (78°13'00''N, 15°38'00''E). The area, deglaciated around 10 ka BP [*Mangerud et al.,* 1992], is

one of the driest regions on Svalbard. The annual precipitation reaches only ~180 mm and the mean annual air temperature (MAAT) is around -6°C [*Hanssen-Bauer and Førland,* 1998]. The geology of the Adventdalen area is characterized by Jurassic and Cretaceous sandstones, siltstones, and shales. Most of the bedrock massifs bordering Adventdalen belong to the Helvetiafjellet and Carolinefjellet formations [*Dallmann et al.,* 2001]. On the valley bottom, fine-grained loess-like deposits, most likely derived by deflation and local deposition of fluvial sediments, cover exposed terraces [*Bryant,* 1982]. The patchy vegetation cover is dominated by mosses, herbs, and shallow shrubs. On exposed dry areas, which are affected by wind action, the vegetation is very sparse. The valley bottom is characterized by pingos (i.e. ice-cored mounds) and ice-wedge polygons. Studies of polygonal patterned ground in the Adventdalen range from geomorphological and sedimentological surveys [e.g., *Matsuoka and Hirakawa,* 1993; *Sørbel and Tolgensbank,* 2002] to thermal contraction cracking monitoring [e.g., *Matsuoka,* 1999; *Christiansen,* 2005].

Our study focuses on four polygon fields (AD1-AD4) distributed across almost the whole of Adventdalen (Figure 3.1c). The sites were chosen in the field in accordance with changes in morphology, topography, and related surficial sediment material given in the map of *Tolgensbakk et al.* [2001], which is explained in detail by *Sørbel et al.* [2001]. Site AD1 is located between 11 and 15 m a.s.l. on a river terrace near Longyearbyen. This site, which has been well investigated by researchers of the University Center of Svalbard (UNIS), is characterized by low-centered polygons [*Christiansen,* 2005]. Site AD2 is located between 79 and 114 m a.s.l. and consists of high-centered polygons. High-centered polygons also characterize the sparsely-vegetated site AD3 (82 to 112 m a.s.l.). Site AD4 is located at the highest elevation between 139 and 169 m a.s.l.

3.2.2 Mars (Utopia Planitia, UP)

The Martian study site was selected on the northern hemisphere of Mars in western Utopia Planitia (UP) (Figure 3.2) due to the availability of appropriate data (see section 3.3.2.) and our previous studies [*Ulrich et al.,* 2010]. Furthermore, various periglacial-like features have been observed in the region, e.g., polygonal structures, scalloped depressions, and small mounds [e.g., *Soare et al.,* 2005; *Morgenstern et al.,* 2007; *Burr et al.,* 2009; *de Pablo and Komatsu,* 2009; *Lefort et al.,* 2009; *Levy et al.,* 2009b; *Ulrich et al.,* 2010; *Séjourné et al.,* 2011]. These landforms are associated in a geomorphological context, suggesting the existence of ice-rich ground [e.g., *Morgenstern et al.,* 2007; *Lefort et al.,* 2009; *Ulrich et al.,* 2010]. Present surface temperatures in the region have been detected to range from ~180 K in winter to ~240 K in summer [*Morgenstern et al.,* 2007], but thermal modeling indicates they could reach ~260 K during summer [*Ulrich et al.,* 2010]. Geologically, the region is characterized by two main units: the Vastitas Borealis interior unit (ABv_i), which underlies the Astapus Colles unit (ABa) [*Tanaka et al.,* 2005]. The ABa unit is interpreted as a fine-grained volatile-rich (i.e. ice-rich) mantling layer tens of meters thick which was deposited during recent variations in Mars' orbital parameters (i.e. higher obliquity) [e.g.,

Kreslavsky and Head, 2000, 2002; *Mustard et al.,* 2001; *Head et al.,* 2003]. The older ABv_i unit consists mainly of outflow channel sediments and subsequently reworked ice-rich deposits [*Tanaka et al.,* 2005].

Generally, the region is characterized by a relatively smooth and flat surface. The most conspicuous landforms in western UP are asymmetrically-shaped scalloped depressions, which are interpreted as ground ice degradation features [e.g., *Morgenstern et al.,* 2007; *Lefort et al.,* 2009; *Ulrich et al.,* 2010; *Séjourné et al.,* 2011]. Isolated depressions (a few hundred meters to several kilometers in diameter) alternate with coalesced scalloped terrain and nested areas of completely removed mantel material (Figure 3.2b). About 24 % of this region is covered by scalloped terrain [*Morgenstern et al.,* 2007]. Polygonal patterned ground is widespread in western UP [e.g., *Seibert and Kargel,* 2001; *Lefort et al.,* 2009; *Levy et al.,* 2009b]. Small high- and low-centered polygons (about 10 m in diameter) are associated with the scalloped depressions, showing an internal arrangement that is typical of all well-pronounced scalloped depressions. Large polygons (up to 80 m in diameter) are distributed on the non-degraded plain uplands.

In this work, we focused on four different polygon fields (named UP1 to UP 4), which are located in and around a medium-sized scalloped depression (Figure 3.2c). This depression is about 800 m in diameter and 20 m deep, centered at ~92.12N and ~46.07E.

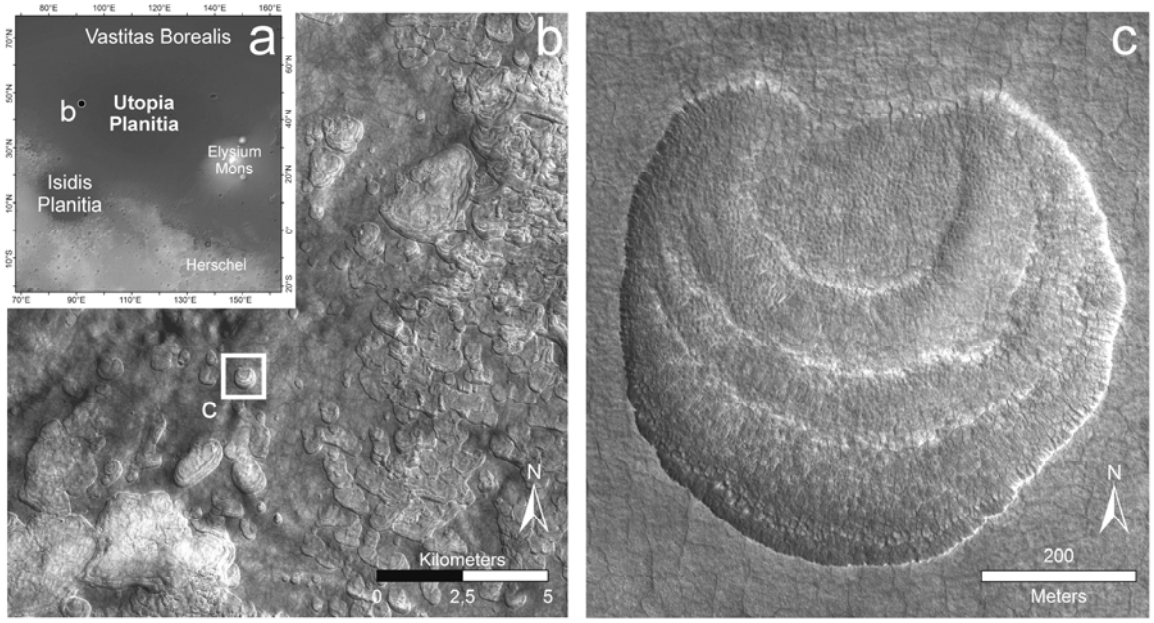

Figure 3.2: Regional setting of the Martian study site. (a) Location of Utopia Planitia on the Martian northern hemisphere. (b) Investigated area in western Utopia Planitia. The region is characterized by single scalloped depressions and extended areas of coalesced scalloped terrain (CTX image subset: P02_001938_2263_XI_46N267W). (c) The scalloped depression and the associated polygonal structures on which this study is focused. The depression is characterized by a gentle south-facing slope and a steep north-facing scarp. Four elongated ridges within the depression are oriented subparallel to the north-facing slope. (HiRISE image subset: PSP_001938_2265 ; see also Fig.13b of *Ulrich et al.* [2010])

3.3 Methods and data

3.3.1 Field work and laboratory analyses

Field work on Svalbard was conducted by making measurements and observations of various periglacial landforms, analyzing soil properties, and collecting soil samples during July-August 2009 [see also *Hauber et al.,* 2011; *Hauber et al.,* in press]. The observed and measured parameters are used as a ground-truth dataset for remote-sensing analyses. In total, nine soil profiles were described and sampled at different polygon fields in the Adventdalen. At each site, active-layer samples were taken from centers and troughs of randomly-selected polygons. *In situ* measurements of active-layer thermal properties were done using a KD2 Pro Thermal Properties Analyzer (Decagon Devices Inc.), and soil water content was measured using a Hydrosense probe (Campbell Scientific Inc.). At site AD1, sediment samples from a polygon center (Figure 3.1) taken by *Härtel and Christiansen* [2010] were also used in order to complete the dataset for sedimentological analyses.

Grain-size analyses were carried out using a Laser Particle Analyzer (Beckmann Coulter LS 200) for the fine fraction (< 1 mm). The coarse fraction (>1 mm) was sieved additionally with an ATM sonic sifter separator (ATM Corporation, Milwaukee, WIS). Total carbon (TC), total organic carbon (TOC), and total nitrogen (TN) contents were determined with a CNS-Analyzer (Elementar Vario EL III).

3.3.2 Remote sensing data

Very-high-resolution images and topographic information about periglacial landforms on Svalbard were acquired in July and August 2008 with HRSC-AX, which is an airborne version of the HRSC (High Resolution Stereo Camera) currently orbiting Mars [*Jaumann et al.,* 2007]. Color orthoimages (20 cm/pixel) and corresponding Digital Elevation Models (DEMs) with a cell size of 50 cm and a vertical accuracy of 20 cm are available for seven regions on Svalbard [*Hauber et al.,* 2011; *Hauber et al.,* in press]. HRSC-AX data from Central Svalbard were used for quantitative terrain and remote-sensing analyses. HRSC-AX is a multi-sensor push-broom instrument with nine CCD line sensors mounted in parallel. High-resolution stereo, multicolor, and multi-phase images are obtained simultaneously. True-color and false-color orthoimages are obtained by the four color channels (blue, green, red, and near-infrared). Based on the five stereo channels, which provide five different views of the ground, digital photogrammetric techniques are applied to reconstruct the topography. The stereo capability of the HRSC-AX allows the systematic production of high-resolution DEMs. The principles of HRSC data processing and application are described by e.g., *Wewel et al.* [2000], *Scholten et al.* [2005], and *Gwinner et al.* [2009, 2010].

Martian polygonal structures were analyzed using High-Resolution Imaging Science Experiment (HiRISE) data [*McEwen et al.,* 2007]. HiRISE provides data that have a quality and

scale comparable to HRSC-AX, with a very high spatial resolution of 30 cm/pixel and the possibility of 3D views by stereo pairs. The method of producing of high-resolution DEMs based on stereo pairs is available [*Kirk et al.,* 2008]. However, detailed analyses, mapping, and extraction of geomorphometric parameters was restricted to the stereo pair PSP_001938_2265 and PSP_002439_2265 and the corresponding DEM with a grid spacing of 1 m. To our knowledge, this is the only HiRISE DEM covering scalloped terrain and related polygonal structures in UP, because HiRISE stereo pairs cover only very small parts of the Martian surface and are very difficult to process [*Kirk et al.,* 2008; *McEwen et al.,* 2010].

3.3.3 GIS Analysis and polygon mapping

Polygons were manually digitized within ArcGIS™ from panchromatic HiRISE and HRSC-AX data using the corresponding DEMs and DEM-derived slope maps as well as 3D views (i.e. in case of the HiRISE data) for better visualizing polygon edges, fissures, troughs, and intersections. Only clearly-recognizable polygon fissures and troughs which could be reliably interpreted as non-erosional linear structures have been mapped along the centerline (Figure 3.3). In case of the terrestrial high-centered polygons, the polygon interiors were also mapped along the highest points of the trough shoulders. The distance from each polygon trough shoulder to the shoulder edge of its nearest neighbor was then calculated automatically in ArcGIS™, allowing estimates of minimum polygon trough widths at each site. Furthermore, locations where two polygon-bounding troughs intersect were marked with points and the distributions of four- and three-ray intersections were distinguished (Figure 3.3). Theoretically, a polygonal field which is characterized by a higher frequency of connected four-ray intersections could be specified as an orthogonal polygon pattern even if the polygon geometry was primarily determined by the conjunction angle [e.g., *Lachenbruch,* 1962; *French,* 2007].

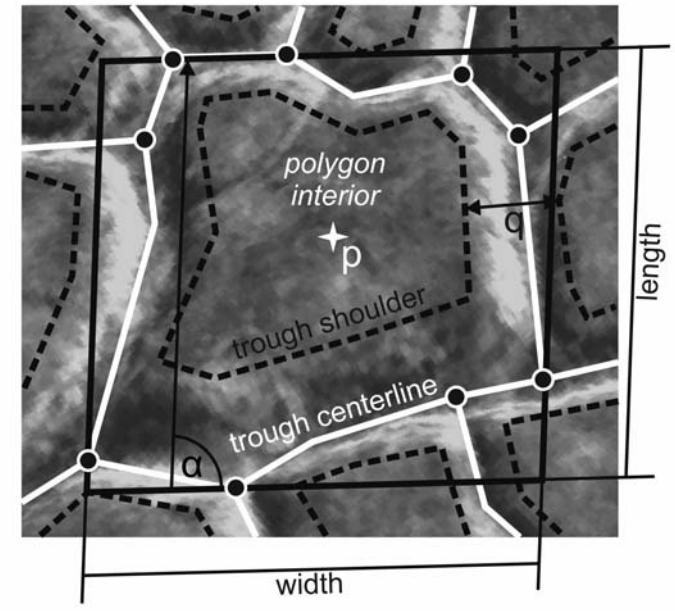

Figure 3.3: Scheme of extracted geomorphometric parameters using the example of a high-centered polygon in the Adventdalen. Based on those characteristics, additional parameters could be calculated (see also Table 3.2). The centerline (i.e. the cracks that outline the low-centered polygons) surrounds the area. The length of the centerline represents the perimeter. Trough intersections are illustrated by the black dots. (p) polygon center point, (q) calculated minimum polygon trough width, (α) polygon main angle (i.e. direction of polygon elongation). Oblique 3-D view based on HRSC-AX topography data.

A polygon was considered in the dataset if it was completely enclosed by troughs or cracks and if there was no doubt during mapping as to whether the visible lineaments corresponded to the original polygon form. Problems appear, for instance, at degraded surfaces, or where slope deposits are superimposed upon troughs. In those cases, the original polygon geometry was often difficult to identify precisely despite the high image resolution.

For each recorded polygon, geomorphometric parameters (Figure 3.3) and topographical properties were extracted within ArcGIS™ and added to an attribute table. Dimension parameters include *area* (A), *perimeter* (P), *length* (L), *width* (W), and *size* (S) (Table 3.2). The *size* was calculated as equivalent to the diameter (Yoshikawa, 2003). Three shape factors were calculated, including *circularity* (FF), *aspect ratio* (AR), and *thickness ratio* (Th) (Table 3.2). All shape factors have values between 0 and 1. The smaller the value, the thinner (i.e. more elongated) is the polygon. Topographical properties (i.e. elevation, slope angle, and slope aspect) were extracted for the center point of each polygon after smoothing the HiRISE DEM and the HRSC-AX DEM to 10 m/pixel, taking into account small-scale changes in topography. Moreover, to investigate the relationship of the slope direction to the orientation of polygon elongation, the main angle of the longest axis of a minimum-area-bounding rectangle was calculated for each polygon, which is at least 15 % longer than broader. This bounding rectangle schematically represents the original orientation of polygon elongation (Figure 3.3). Fairly-symmetrical polygons which are not 15% longer than they are broad were not considered. Calculated angles range between 0° and 180°, where 0° corresponds to a polygon directed from east to west, 90° corresponds to a north-south direction, and 180° represents a west-to-east direction. Therefore, the slope aspect, represented by values ranging between 0° and 360°, was converted to values ranging between 0° and 180°, and thereafter represents the direction of slope angle.

3.3.4 Numerical analysis

Multivariate statistics in terms of ordination methods were applied to the remote-sensing datasets from Spitsbergen and Mars. First, principal component analyses (PCAs) were performed to assess the relationships among the polygon shape and the dimensional variables (Table 3.2). Second, redundancy analyses (RDAs, partial-RDAs) including environmental parameters as explanatory variables (Table 3.2) were applied to identify factors that could significantly explain variations in polygon shape and dimension. In preparation for the multivariate analyses, datasets were organized for each polygon site that contained all the studied polygons, dimension parameters, shape factors, and polygon main angles as response variables as well as topographical properties as environmental (i.e. explanatory) variables (Table 3.2). First, a data exploration was carried out to check the data distribution and relationships between the variables, and to calculate the statistical characters, such as mean, median, maximum (Max), and minimum (Min) values, or standard deviation (SD) and skewness (SK) for comparing of the different polygon sites. Circular

data, such as aspect and polygon main angle, were transformed by trigonometric functions [e.g., *Roberts,* 1986] (Table 3.2). Aspect transformation was accomplished by creating two variables, *northness* (No) and *eastness* (Ea). Polygon main angle values (0-180°) were transformed to cosine representation (*CosMA*), ranging thus from 1 to -1. Elevation is represented by the *relative height* (RH); the lowest-level polygon within each polygon site was set to RH = zero.

Table 3.2: Geomorphometric parameters and topographical properties which were extracted and calculated for each considered polygon and used as variables in multivariate statistics. See also Figure 3.3.

Variable (Abbreviation)	Unit or Scale	Source (Explanation)	Type
Response variables			
Area (*A*)	Square meter	HRSC-AX, HiRISE	Dimension
Perimeter (*P*)	Meter	HRSC-AX, HiRISE	Dimension
Size (*S*)	Meter	$= \sqrt{(4A/\pi)}$	Dimension
Length (*L*)	Meter	HRSC-AX, HiRISE (largest diameter)	Dimension
Width (*W*)	Meter	HRSC-AX, HiRISE (smallest diameter)	Dimension
Circularity (*FF*)	0 to 1	$= 4\pi A / P^2$	Shape
Aspect Ratio (*AR*)	0 to 1	$= W / L$	Shape
Thickness Ratio (*Th*)	0 to 1	= the polygon area versus the area of its minimum bounding rectangle	Shape
CosMA	-1 to 1	= cosine representation of polygon main angle values	Orientation of polygon elongation
Explanatory variables			
Relative Height (*RH*)	Meter (above fixed point)	DEM	Topography
Slope (*Slo*)	Degrees	DEM	Topography
Northness (*No*)	-1 to 1	= cos (Aspect), DEM	Topography
Eastness (*Ea*)	-1 to 1	= sin (Aspect), DEM	Topography

PCA and RDA were performed on standardized data (i.e. all variables have equal weights) using BRODGAR version 2.6.5. (Highland Statistics Ltd., UK). These ordination techniques are commonly used in ecological data analysis [*Zuur et al.,* 2007]. PCA is a comparatively simple method used to visualize correlations between variables. RDA is an extension of the PCA; it

models the response variables as a function of the explanatory variables. The ordination axes and algorithm in RDA are based on the PCA.

Ecological data which originate from neighboring objects in the same physical environment are often spatially autocorrelated, because the objects interact and are often more alike than objects which are far apart from each other. Spatial autocorrelation within our dataset, which could result in a lack of stochastic independence, was addressed using principal coordinates of neighbor matrices (PCNM) analyses [*Borcard and Legendre,* 2002; *Borcard et al.,* 2004]. This method allows spatial patterns to be detected and quantified over a wide range of scale by creating spatial variables. Using the Cartesian coordinates (X, Y) of each polygon center, a set of spatial variables was generated for each polygon site. These analyses yielded up to 400 PCNM variables per site. To assess the amount of variance that is explained by the "pure" non-spatially-structured environmental variables, the effect of the spatial variables could then be partialled out by the use of variance partitioning through partial-RDA for each polygon dataset [e.g., *Borcard et al.,* 1992; *Zuur et al.,* 2007; *Sweetman et al.,* 2010]. First, a series of RDAs were run constrained to each spatial and environmental variable. Only variables which explained a significant (p-value < 0.05) amount of variance in the polygon dataset were considered for further analyses. The statistical significance was tested continually by Monte Carlo permutation tests using 999 unrestricted permutations. Thereafter, we applied a separate RDA with a forward-selection procedure for all significant spatial and environmental variables to identify the most important variables that could ultimately explain variations in polygon dimension and shape among sites. Collinearity among the variables could be excluded, as all the highest variance inflation factors (VIFs) were less than 5. Finally, variance partitioning in a series of partial RDAs was conducted for each polygon site: i) on all forward-selected spatial and all forward-selected environmental variables; ii) on all forward-selected spatial variables, using the forward-selected environmental variables as covariables; and iii) on all forward-selected environmental variables, using the forward-selected spatial variables as covariables. The amount of variance in each polygonal network that is explained by the pure environmental variables effect, the pure spatial variables effect, the shared effect, and the amount of unexplained variance could then be determined using the cumulative eigenvalues as the percentage of total inertia (i.e. variance) explained by each of these calculations.

3.4 Results

3.4.1 Geomorphology and morphometry of Adventdalen polygons

Four polygonal fields were mapped with a total of 688 polygons (Figure 3.4 and Table 3.3). These fields are distinguishable with respect to their dimensions, geomorphology, and the associated surficial material. For each polygonal site, the characteristics of geomorphometric parameters are summarized in Table 3.4.

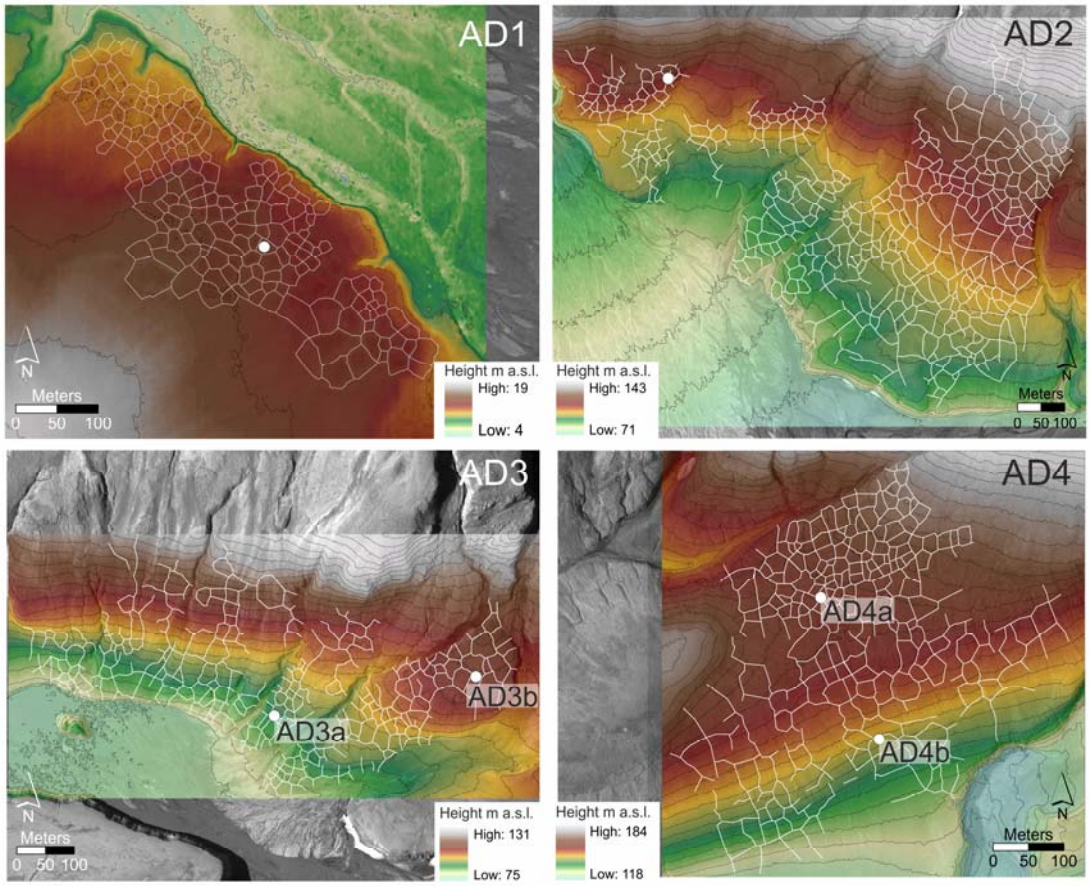

Figure 3.4: Mapped polygonal fields in the Adventdalen (Svalbard). HRSC-AX DEM subsets on panchromatic HRSC-AX images illustrate the topography at each site. Contours are given by the gray lines at 2 m intervals. The white dots mark the location of the investigated active-layer profiles. Profiles of diverse polygons at one site are labeled additionally (see Fig. 3.7).

Site AD1 is located on the front of a recently inactive alluvial fan, which is cut by the Adventelva River. The area is exposed generally in a north-northeastern direction (Figure 3.4). The polygonal field is formed in eolian deposits [*Tolgensbakk et al.*, 2001], which cover this part of the fan and is characterized by some orthogonal but mostly pentagonal and hexagonal low-centered polygons (Figure 3.5). Nearly 90% of the counted furrow intersections belong to the three-ray type (Table 3.3). The polygons are outlined by comparatively shallow (<40 cm deep) and narrow (<100 cm wide) furrows. Typically, the low-centered polygons are characterized by pairs of slightly-raised rims beside the furrows. Open cracks could be observed within the furrows during field work. Sizes of individual polygons range from 8.1 m to 50.8 m (mean 19.7 m). A shift to smaller dimensions can be seen in positive skewness (SK) of the dimension variables (Table 3.4). The vegetation cover shows a zonal distribution, with grasses and mosses in less-well drained centers. Dry and sparse vegetation covers the raised rims. However, not all of the mapped polygons are characterized by distinct low-lying centers. In these cases, the center can be described as rather flat, and the drainage situation is improved.

The AD2 polygonal field formed in glaciofluvial sediments [*Tolgensbakk et al.,* 2001]. Its high-centered polygons are located on a terraced gentle slope (mean slope angle =3°), which is exposed in a south-southwest direction (Figure 3.4). The upper slope and the terrace transitions show steeper slope angles (up to 9°). Polygon sizes range from 9.4 m to 65.1 m (mean 29.7 m) (Table 3.4). Bigger polygons occur on gentle slope sections and smaller polygons on the steeper parts (Figure 3.5). In general, the polygonal field shows a pentagonal to hexagonal lattice. Only 4% of the mapped intersections belong to the four-ray type, which is the lowest percentage of this type of all mapped polygon sites (Table 3.3). The majority of polygonal troughs at site AD2 are less pronounced than at sites AD3 and AD4, especially in gentler, lower slope sections. The mean of the calculated minimum trough widths is 1.4 m, but the width can reach maxima of 4.2 m. Trough depths of 0.5 m on average were measured in the HRSC-AX DEM. Depths of more than 1 m could be observed in the field on steeper slope sections. Upon visual inspection of the DEM, polygons that appear bigger seem to be clearly elongated parallel to the slope contour and exist primarily in the lower slope sections (Figure 3.4). The calculated shape variables for site AD2 cannot be differentiated clearly from those of the other Adventdalen sites apart from a slightly larger variance of the values (Table 3.4). The vegetation cover at site AD2 is more or less closed but thins out up the slope and on exposed lower slope parts. The well-drained elevated polygon centers show hummocks covered by dry grasses, herbs, and shrubs, while grasses, mosses, and shrubs in the troughs appear to be more succulent. The shoulders of big troughs are often disrupted and only sparsely vegetated.

According to *Tolgensbakk et al.* [2001], the AD3 polygonal field is spread on solifluction and autochthonous weathered material. The mean size of the high-centered polygons is 25.4 m (ranging from 10.4 m to 51.7 m) (Table 3.4). About 93 % of all observed intersections belong to the three-ray type. This site is also located on a terraced slope. However, the southerly exposed slope is partly steeper (mean slope angle =4.9°) than the slope at site AD2. It rises shortly and sharply from the Adventelva River, and it is more frequently incised by fluvial channels (Figure 3.4). The polygonal field is cut by the river as well. A general trend in the distribution of larger polygons as a function of steeper slope sections could not be observed. Polygons at this site are rather regularly distributed with respect to their dimension and shape. The troughs, however, are more pronounced. The mean of the calculated minimum width at site AD3 is 2.3 m, ranging to maxima of 4.6 m (Table 3.3). Most of the measured trough depths ranged between 0.3 m and more than 1 m; the deeper troughs drain into the fluvial channels. Trough shoulders are disrupted by trough-parallel fractures (Figure 3.5). The site is characterized by generally drier surface conditions, but these change sharply in the eastern part and in the up-slope direction. The relatively closed but low-standing vegetation cover on the elevated polygon centers changes to exposed vegetation-free areas; only low grasses and dry mosses can be found in the polygon troughs.

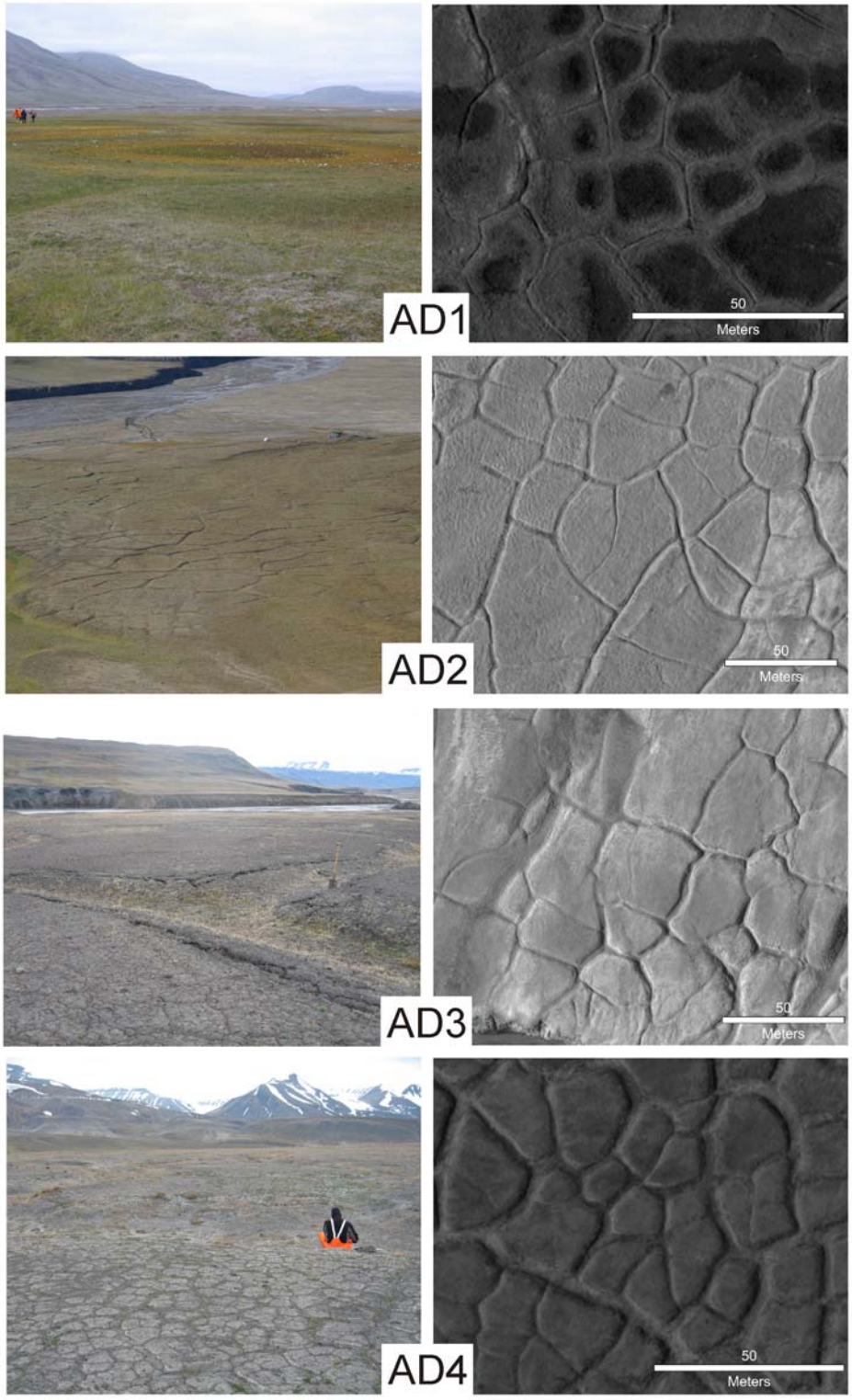

Figure 3.5: Photograph and HRSC_AX close-up of each polygonal field in the Adventdalen elucidate the site-specific differences in geomorphology. Low-centered polygons at site AD1 are formed in eolian deposits on an inactive alluvial fan. High-centered polygons at the sites AD2, AD3, and AD4 are formed in glaciofluvial sediments, solifluction and autochthonous weathered material, and autochthonous weathered material, respectively. The person in the photograph of site AD4 is sitting on the shoulder of a huge polygon trough, which can be seen in the lower left of the HRSC_AX close-up (Photographs of AD1 and AD2 by H. Hiesinger, AD3 and AD4 by M. Ulrich).

AD4, the most elevated polygonal field (Figure 3.4) in the Adventdalen (between 139 and 169 m a.s.l.), is formed in autochthonous weathering material [*Tolgensbakk et al.,* 2001] and characterized by remarkably wide and deep troughs and very sparse vegetation cover (Figure 3.5). The mean of the calculated minimum trough width is 2.9 m, but widths range to maxima of 7.5 m. The manually-measured depth of the troughs is between 0.5 m and >1 m. The size of the high-centered polygons ranges between 9.8 m and 47.7 m (mean 24.2 m) (Table 3.4). Smaller, rather hexagonal polygons are located on an elevated terrace, which is characterized by a very dry surface (Figure 3.5). Secondary cracks can be observed within the polygon centers. They were probably formed by desiccation when the surface dried after spring snowmelt. The terrace continues on a south-southeast exposed slope which is inclined toward the Adventelva River. The mean slope angle is 3.5° but can reach about 10° in the lower slope sections. Down the slope, vegetation cover becomes denser and polygon dimensions increase. Here the polygons show an orthogonal lattice in some places. About 9% of all polygon intersections at site AD4 belong to the four-ray type (Table 3.3).

Table 3.3: Overview and characteristics of all mapped polygonal sites and corresponding trough intersections.

Location	ID	Type	N	Covered area (m^2 x 10^3)	Trough intersections	3-ray (%)	4-ray (%)
Adventdalen	AD1	low center	185	63	387	90.2	9.8
Adventdalen	AD2	high center	241	186	698	96.0	4.0
Adventdalen	AD3	high center	103	58	381	92.9	7.1
Adventdalen	AD4	high center	159	80	426	91.3	8.7
AD total			688	387	1892		
Utopia Planitia	UP1	high center	453	477	1293	92.4	7.6
Utopia Planitia	UP2	low center	756	58	1751	82.9	17.1
Utopia Planitia	UP3	high center	579	63	1562	86.4	13.6
Utopia Planitia	UP4	low center	566	30	1110	87.4	12.6
UP total			2354	628	5716		
Total			3042	1 015	7608		

All high-centered polygonal fields are located on inclined surfaces. We found a small but significant correlation (r=0.32; *p*-value<0.05) between minimum polygon trough width and slope angle for all Adventdalen high-centered polygons. At all Adventdalen sites polygons are elongated in two main directions, subparallel to the contour of the slope and subparallel to the direction of

slope angle (Figure 3.6). The majority of polygons at site AD1 are elongated perpendicularly to the direction of slope angle. The majority of polygons at site AD3 and in particular at AD4 are predominantly elongated subparallel to the slope angle direction. For site AD2, a relative balance of orientation is shown in Figure 3.6 in contrast to the visual observations (see above; Figure 3.4).

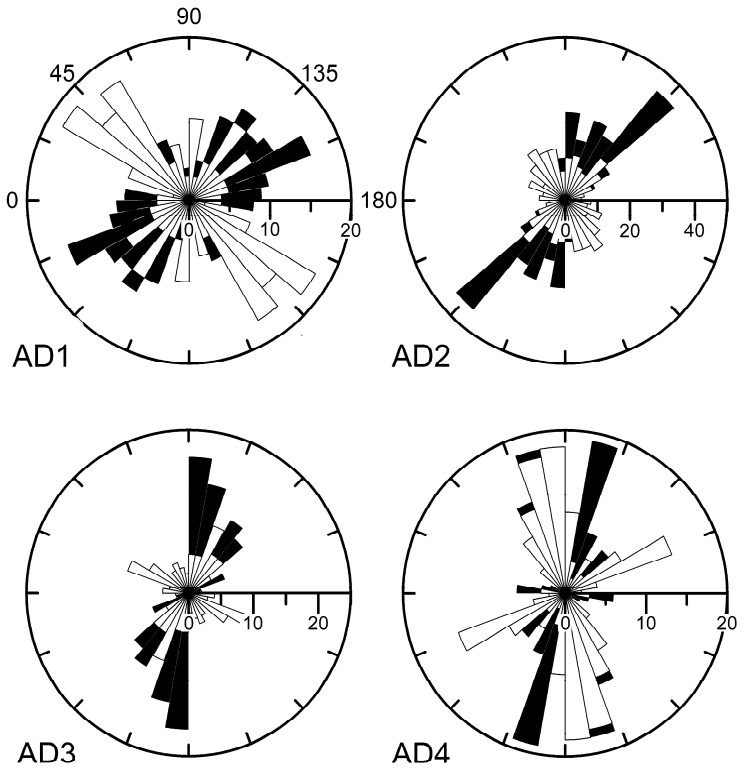

Figure 3.6: Orientation of polygon elongation (white) in relation to the direction of slope angle (black) for each terrestrial polygonal field. The ray length represents the number of polygons that fall within a specific angular region. Ray size (binning) is 10 degrees. Note that the x-axes are differently scaled and the rays are vertically mirrored for better visualization.

3.4.2 Sedimentology of the Adventdalen polygons

The sedimentological results for ten active-layer profiles of individual polygons representative of each polygonal field are summarized in Figure 3.7. Sediment data are presented for the trough and the center of one polygon at site AD2 and AD4a, respectively (Figure 3.4). Due to varying surface conditions down-slope at site AD4 an additional analysis is shown for an active-layer pit in a polygon trough (AD4b). Because of heterogeneous surface conditions at site AD3, the center and trough of two polygons were surveyed. At site AD1, samples from the topmost 100 cm of an active-layer pit and a permafrost core (Figure 3.4) were analyzed to complete the dataset. Field measurements of thermal conductivity and ground temperature were done exemplarily at sites AD2, AD3, and AD4a. These measurements were used additionally to distinguish the various polygon fields as well as the trough and center of separate polygons.

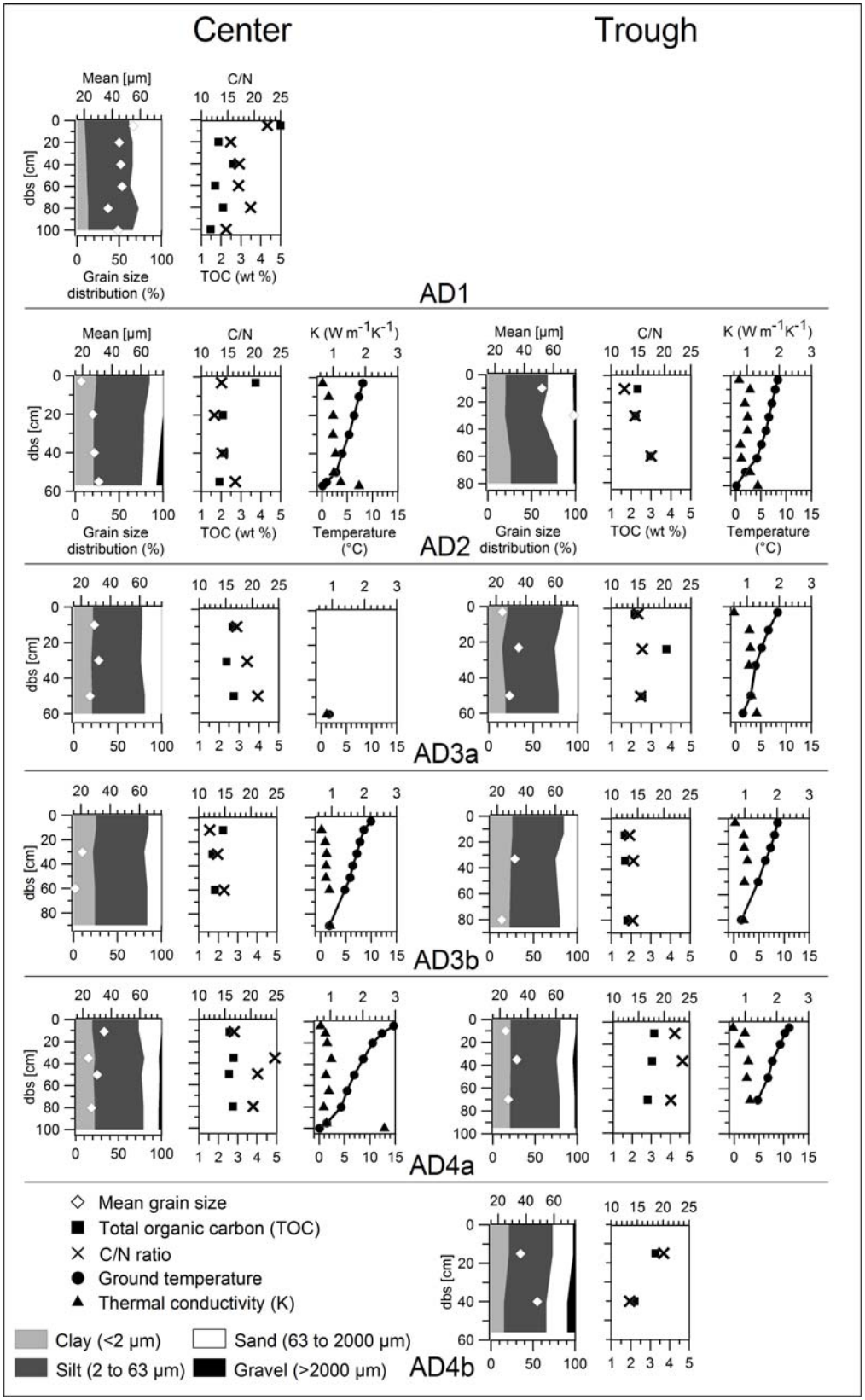

Figure 3.7: Active-layer sediment data and thermal properties from centers and troughs of selected polygons at each Adventdalen polygonal field (for locations see Figure 3.4). Parameters are plotted against depth below surface (dbs). Note the different scales of the y-axes. The bottom end of the grain-size distribution signatures represent the active-layer depths, except for AD1 in which an active-layer depth of around 60 cm was observed. The thermal conductivity and ground temperature data have been averaged over 3-4 measurements at different depths.

All active-layer profiles are characterized by poorly sorted, clayish to fine-sandy silts with varying amounts of gravel and low TOC values (Figure 3.7). The TOC/TN ratios are relatively wide (between 12 and 25). Except for the polygon center pit at site AD1, all profiles were dark-grayish to grayish-black in color and unstratified. No signs of underlying ice wedges could be found at sites AD2, AD3, or AD4. Active-layer depths at all sites ranged between ~60 cm and ~100 cm. The deepest active layer of ~100 cm (Figure 3.7) was measured where the vegetation cover was absent and the surface appeared mostly dry. In comparison to the other sites, the AD1 profile shows less clay but higher sand contents corresponding to the mapped loess-like sediments of *Tolgensbakk et al.* [2001] and the material is better sorted. The AD4b trough profile contains the highest gravel content, particularly at the bottom (Figure 3.7). Furthermore, measurable proportions of gravel could be determined for sites AD2 and AD4a, corresponding to the glaciofluvially-formed and autochthonously-weathered surface material suggested by *Tolgensbakk et al.* [2001]. At site AD2 only, the trough profile reveals considerably higher grain size mean values, corresponding to higher sand contents than in the related polygon center profile (Figure 3.7).

The measured thermal properties reflect the sedimentological similarities of the four sites. The temperature decreases to about 0°C towards the permafrost table. Thermal conductivity values range around 1.0 $Wm^{-1}K^{-1}$ at all sites, increasing slightly with depth, and show higher values (up to 2.6 $Wm^{-1}K^{-1}$) in the upper centimeters of the permafrost due to the ice content (e.g., the center of AD4a in Figure 3.7). The typical relationships of decreasing thermal conductivity with increasing organic carbon content and of increasing thermal conductivity with increasing soil moisture [e.g., *Williams and Smith,* 1989; *French,* 2007; *Yershov,* 2004] are confirmed by our measurements.

3.4.3 Geomorphology and morphometry of Utopia Planitia (UP) polygons

Polygonal networks in western UP show a zonal distribution that is associated with scalloped terrain. The study of the different polygonal networks allows detailed local analyses in a relatively limited spatial context. Therefore, we focused on one depression, representative of the geomorphological context of scalloped terrain and polygonal structures in UP (Figure 3.8). In total, four different types of polygonal networks including 2354 polygons were mapped (Table 3.3) and classified in and around this depression (UP1 to UP4). Similar to the terrestrial polygons in the Adventdalen, the Martian polygons are uniform with respect to their shape factors (Table 3.4). Only UP3 polygons reveal a slightly larger variance of the shape factor values and a little larger negative SK in *circularity*, which statistically would indicate less-elongated polygons (Table 3.4).

The upper level, representing the non-degraded mantle material in the surroundings of the scalloped depression, is characterized by a random network of large irregular polygons (UP1) (Figure 3.8). These polygons range from almost flat to high-centered. The sizes of the mapped UP1 polygons ranges from 13.1 m to 88.1 m (mean 34.3 m) (Table 3.4). Large troughs most commonly 3 m to 4 m wide (max. >10 m) outlines the polygons. Narrow, indistinct cracks in polygon centers

form small secondary polygons. The HiRISE DEM indicates trough depths of more than 1 m. The polygonal network at site UP1 shows an orthogonal to hexagonal lattice (Figure 3.9). About 93% of the trough intersections belong to the three-ray type (Table 3.3). All elongated (i.e. >15% longer than wide) UP1 polygons are oriented mainly in the N-S or E-W direction (Figure 3.10). The surface around the depression is almost flat. Numerous boulders are distributed randomly in the area [see also *Lefort et al.,* 2009]. The polygon troughs seem to be filled with fine-grained dark deposits (Figure 3.9). Differences of UP1 polygon shapes and dimensions were observed in relation to the topography around the scalloped depression. The polygons in the southern and southwestern more-elevated area are more distinct and bigger, their outlining troughs are clearly visible, and their centers are rather flat. In contrast, polygons in the north and northeastern lower area are smaller, very bumpy, and appear much more degraded; often only long north-south-trending troughs are visible (Figure 3.8). This topographic zonation of the upland polygons could be observed elsewhere in the investigated region.

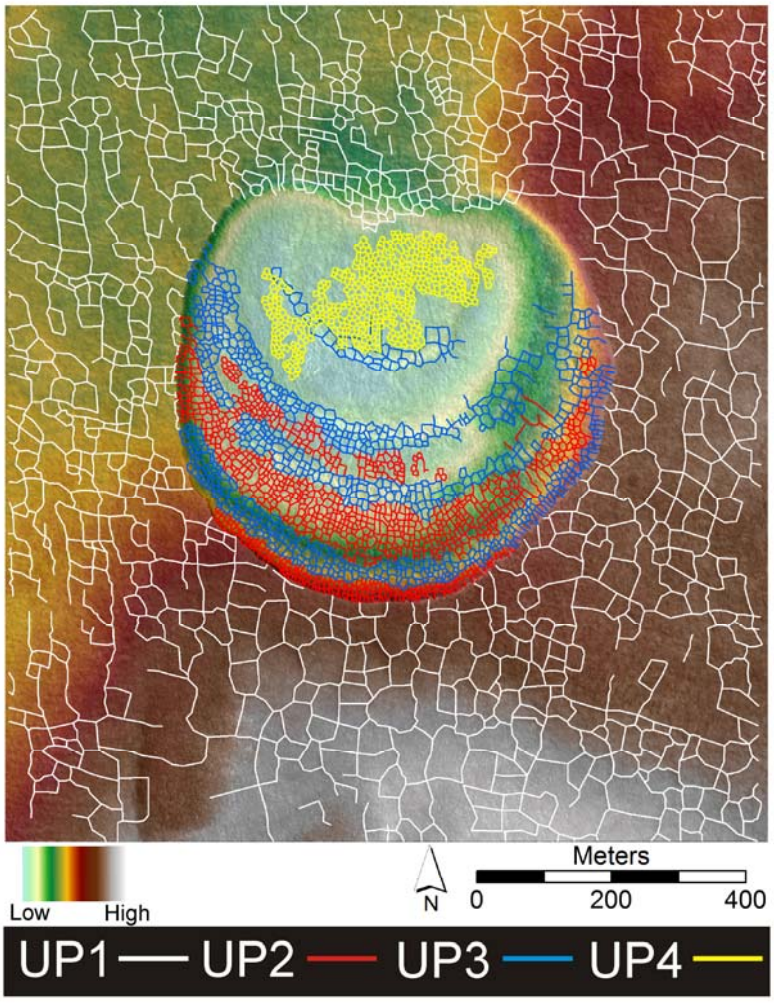

Figure 3.8: Mapped polygonal field in western Utopia Planitia. The polygons that make up the polygonal fields UP2, UP3, and UP4 are indicated by colors in the scalloped depression. Topography is illustrated by a HiRISE DEM subset (1 m/pixel, stereo pair: PSP_001938_2265_PSP002439_2265).

Table 3.4: Calculated statistical characteristics of the geomorphometric parameters for each polygonal field in the Adventdalen (AD) and Utopia Planitia (UP). (units and scales correspond to Table 3.2)

		AD1	AD2	AD3	AD4	UP1	UP2	UP3	UP4
Area	Min	50.9	69.7	84.9	75.1	135.6	15.6	14.7	10.0
	Max	2029.0	3328.6	2100.5	1785.7	6098.7	206.6	513.0	151.9
	Mean	340.1	771.1	558.5	506.7	1053.4	76.7	109.2	52.4
	Median	268.4	594.3	447.2	82.7	816.1	69.5	91.6	50.1
	SD	261.6	534.7	378.2	331.0	830.3	35.5	65.2	18.4
	SK	3.0	1.7	1.7	1.3	2.1	1.0	1.9	1.4
Perimeter	Min	30.4	35.2	39.9	37.2	46.8	16.3	16.6	13.2
	Max	177.1	245.5	170.7	178.1	298.4	59.8	92.9	51.2
	Mean	69.8	108.3	90.8	87.1	124.2	34.4	40.5	28.7
	Median	65.0	100.5	87.2	82.7	117.9	33.6	38.9	28.2
	SD	23.8	38.3	28.3	28.6	46.5	7.8	11.1	5.3
	SK	1.6	0.8	0.9	0.7	0.9	0.5	1.0	1.0
Size	Min	8.1	9.4	10.4	9.8	13.1	4.5	4.3	3.6
	Max	50.8	65.1	51.7	47.7	88.1	16.2	25.6	13.9
	Mean	19.7	29.7	25.4	24.2	34.3	9.6	11.4	8.1
	Median	18.5	27.5	23.9	23.5	32.2	9.4	10.8	8.0
	SD	6.6	10.0	8.2	7.8	12.8	2.2	3.2	1.4
	SK	1.5	0.7	0.9	0.6	0.9	0.5	0.9	0.5
Length	Min	11.4	13.3	14.8	13.4	18.8	6.4	6.1	5.1
	Max	65.3	96.2	61.7	71.3	109.4	24.5	35.7	22.6
	Mean	25.6	40.9	33.5	32.3	46.2	12.9	15.1	10.7
	Median	24.2	37.4	31.7	30.3	43.8	12.3	14.7	10.3
	SD	9.0	14.9	10.1	10.7	16.9	3.0	4.1	2.2
	SK	1.6	1.2	0.8	0.8	0.8	0.8	1.0	1.4
Width	Min	7.0	10.2	9.6	9.9	12.3	4.1	4.2	3.8
	Max	49.8	79.4	51.4	57.0	82.7	18.2	27.9	13.1
	Mean	19.9	28.7	25.1	24.6	35.0	10.0	11.6	8.1
	Median	18.6	27.2	23.4	23.8	33.4	9.9	11.1	8.0
	SD	6.7	10.3	8.4	8.0	13.6	2.4	3.6	1.4
	SK	1.5	1.2	0.9	0.6	0.9	0.4	0.9	0.2
Circularity	Min	0.58	0.47	0.57	0.58	0.41	0.41	0.21	0.46
	Max	0.91	0.91	0.91	0.92	0.92	0.92	0.92	0.92
	Mean	0.79	0.75	0.77	0.76	0.76	0.78	0.78	0.78
	Median	0.81	0.76	0.78	0.77	0.76	0.78	0.79	0.80
	SD	0.06	0.08	0.08	0.07	0.08	0.07	0.08	0.08
	SK	-0.83	-0.74	-0.49	-0.29	-0.77	-0.74	-1.46	-0.83
Aspect ratio	Min	0.41	0.37	0.45	0.46	0.37	0.35	0.37	0.37
	Max	1.00	0.99	0.98	0.99	0.99	0.99	1.00	1.00
	Mean	0.79	0.72	0.75	0.77	0.76	0.79	0.77	0.77
	Median	0.80	0.72	0.76	0.78	0.77	0.80	0.79	0.78
	SD	0.12	0.14	0.12	0.13	0.13	0.12	0.12	0.12
	SK	-0.50	-0.19	-0.48	-0.44	-0.35	-0.65	-0.60	-0.57
Thickness ratio	Min	0.29	0.24	0.30	0.26	0.29	0.23	0.15	0.27
	Max	0.76	0.84	0.70	0.80	0.85	0.88	0.86	0.79
	Mean	0.53	0.49	0.51	0.51	0.55	0.52	0.53	0.54
	Median	0.52	0.49	0.52	0.51	0.55	0.51	0.52	0.54
	SD	0.09	0.10	0.10	0.10	0.11	0.10	0.11	0.11
	SK	-0.11	0.11	-0.15	0.19	0.05	0.13	-0.02	-0.08

The small-scale polygons within the scalloped depressions were classified as mixed-center polygons by *Levy et al.* [2009a]. Three different types of polygonal networks were identified (UP2, UP3, and UP4) (Table 3.3) in connection with the internal morphology of the scalloped depression (Figure 3.8). Stripes of low-centered (UP2) and high-centered (UP3) polygons with narrow troughs and cracks alternate concentrically from the north-facing scarp to the depression bottom (Figure 3.9). These stripes of polygons are distinctly oriented along the scarp. The polygon troughs and cracks are mainly oriented perpendicular and parallel to the scarp. The relationship can also be seen from the direction of polygon elongation, reflecting the horseshoe shape of the north-facing slope (Figure 3.10). The orientation of polygon elongation is much more closely parallel to the slope angle on the steeper parts of the north-facing slope (slope angles ~14°). Low-centered polygons (UP2) show a more distinct orientation than high-centered polygons (UP3). The ridges within the depression are characterized by high-centered polygons with peaked and domed as well as flat elevated centers (UP3) (Figure 3.9b). The size of high-centered polygons ranges between 4.3 m and 25.6 m (mean 11.4 m) (Table 3.4). These polygons are orthogonal, but hexagonal geometries exist as well. About 14% of the counted trough intersections belong to the four-ray type (Table 3.3). Four concentric zones of high-centered polygons corresponding to four internal ridges were mapped in the depression (Figure 3.8). The smallest and most distinct high-centered polygons exist on the less-pronounced ridge close to the scarp edge. Low- to flat-centered polygons with a mean size of 9.8 m (4.5 m to 16.2 m) (Table 3.4) are spread between the ridges (UP2) (Figure 3.9). The polygons closest to the scarp edge are characterized by distinct low-lying centers. Pairs of raised rims beside the outlining cracks are visible (Figure 3.9a). These strongly-oriented polygons with a clear orthogonal shape exhibit a very homogenous size distribution. The highest percentage of four-ray intersections (~17%) among all Martian or terrestrial polygonal fields could be observed within this network (see Table 3.3).

The south-facing slope is also characterized by patterns of low-lying centers (UP4) (Figure 3.9c). These patterns overlay a larger polygonal network, indicating residues of upland polygons in this comparatively shallower part of the depression (Figure 3.8). The centers of these very small polygons are outlined by raised single ridges (Figure 3.9c). Cracks, which typically outline low-centered polygons, were not identified. The polygon sizes at site UP4 range from 3.6 m to 13.9 m (mean 8.1 m) (Table 3.4). The network is characterized by an orthogonal to hexagonal lattice. About 87% of the mapped intersections at UP4 are of the three-ray type (Table 3.3). The orientation of polygon elongation is mainly north-south and normal to the average direction of slope angle (Figure 3.10). The striking spatial arrangement of the small-scale polygons within the scalloped depression is also visible in other well-pronounced single depressions in the region.

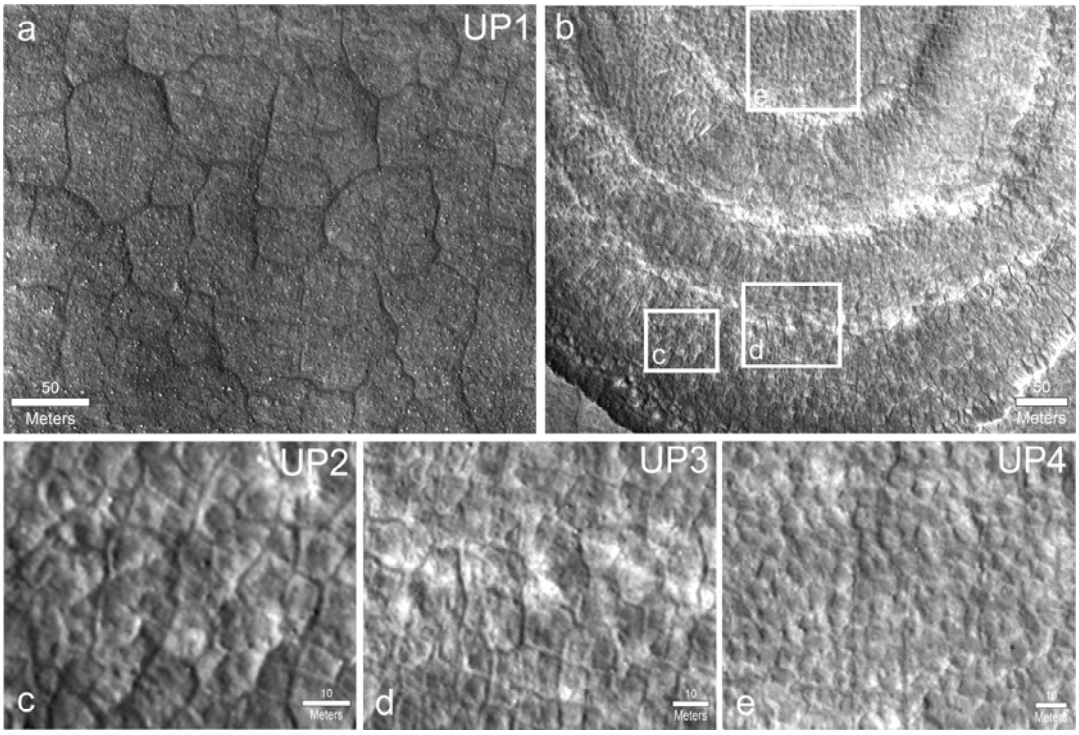

Figure 3.9: Close-up of each polygonal field in Utopia Planitia. (a) Large flat- to high-centered polygons on the uplands in the south of the scalloped depression. (b) Context of the polygonal network connected to the internal morphology of the scalloped depression. (c) Low-centered polygons with raised ridges flanking outlining fissures. (d) High-centered polygons on one of the interior scallop ridges. Smaller examples can be seen close to the north-facing scarp on the upper left image. (e) Low-centered polygons with single raised ridges overlying a larger polygonal network on the south-facing slope of the scalloped depressions. Cracks that outline the polygons are not visible. (Each subset from HiRISE image: PSP_001938_2265).

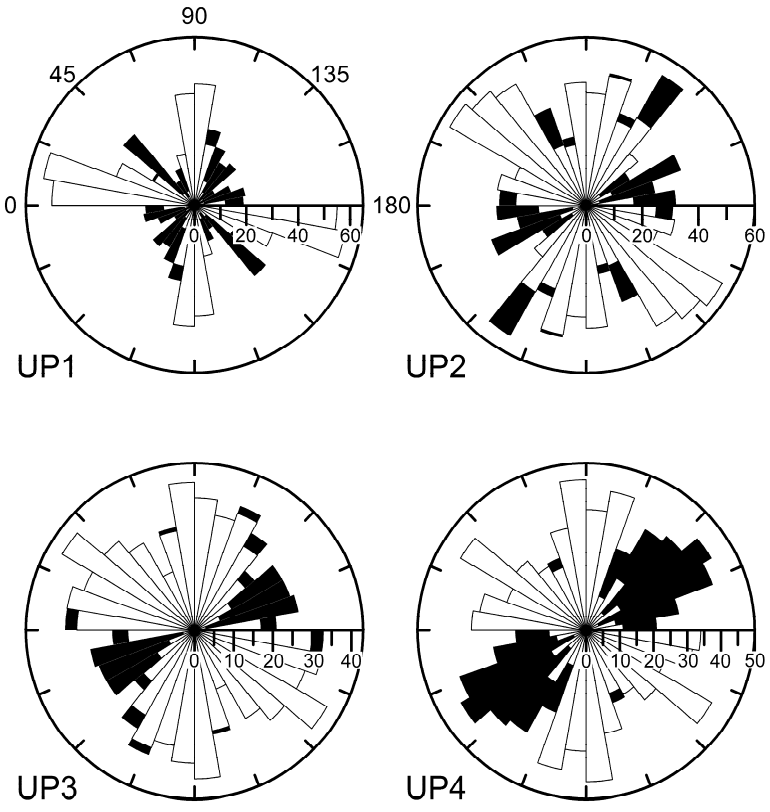

Figure 3.10: Orientation of polygon elongation (white) in relation to the direction of slope angle (black) for each Martian polygonal field. The ray length represents the number of polygons that fall within a specific angular region. Ray size (binning) is 10 degrees. Note that the x-axes are differently scaled and the rays are vertically mirrored for better visualization.

3.4.4 Results of the multivariate statistics

Principal component analyses (PCAs) were conducted and revealed similar results for all polygonal fields. Thus, PCA results are summarized using the example of a combined dataset which includes all investigated sites. The response variables extracted for each polygon (Table 2) are clearly separated on the first two PCA axes. Together, the cumulative percentage of eigenvalues reveals that 79% of the total variance is explained by PC1 and PC2. Variables representing polygon dimension are clearly correlated to PCA axis 1, explaining more than half of the variance (54%) in the polygon dataset. The PCA axis 2 is related to variables representing polygon shape. About 25% of the total variance is explained by this axis. The PCA reveals no correlation between dimension variables (PC1) and shape variables (PC2). The variable *CosMA*, representing direction of polygon elongation (Table 2), contributes only a little to the explained variance although a negative correlation to the shape factor variables was expected.

In order to identify the specific environmental parameters that predominantly explain polygon shape and dimension, several constrained ordination analyses (RDAs, partial-RDAs) were performed. Variance partitioning (i.e., partial-RDA) with PCNM-analysis-derived spatial variables (see Section 3.3.4) was used to filter out spatially-structured effects (i.e., autocorrelation) in the environmental variables. Small but significant portions of the explained variance in most of the polygon dataset are primarily related to the elevation effect (i.e., *RH*), and secondarily to aspect (i.e., *Ea*) and slope angle. Figure 11 presents the results of variance partitioning. The bar plots illustrate the unexplained amount of variance in the dataset, as well as the amount explained by non-spatially-structured (i.e., pure) environmental factors, by the spatial variables alone, and by the spatially-structured components shared by the environmental and spatial variables. Large amounts of the explained variance are related to spatial factors, because neighboring polygons are often quite similar and polygon formation depends on the spatial position. RDA triplots are only exemplarily shown for sites AD3 and UP1 (Figue 12). All significant environmental and spatial variables (named PCNM) are plotted in relation to the response variables. Environmental and spatial variables which lost their significance after forward selection are marked. For site AD3, 7.4% of the explained variance is attributed to the pure elevation effect (Figure 11). *Ea* was excluded after forward selection. *RH* shows clear correlation with the shape *FF*, *AR*, and *Th* (Figure 12a), but only a small correlation to the dimension variables. For site UP1, 6.3% of the explained variance is attributed to the pure effect of *RH* and *Slo*. *No* was excluded after forward selection (Figure 11). In the corresponding RDA triplot (Figure 12b), polygon dimension variables are positively correlated with *RH* but negatively correlated with the slope angle. Generally, a similar positive correlation of *RH* to the dimension variables is calculated in all site-specific RDAs in which *RH* was significant after forward selection (see Figure 11). A negative correlation is obvious only for sites AD4 and UP3. Furthermore, in site UP3, aspect represented by *Ea* has more explanatory power as *RH*. *Slo* and *No* were excluded here after forward selection. For site AD2,

only *Slo* was significant after forward selection and *Ea* was excluded. Even if only very little variance can be explained by the pure effect of *Slo* after variance partitioning for this site (Figure 11), slope angle shows a distinct correlation to the shape factors in the associated RDA triplot. After forward selection for site UP2, all environmental variables, which were significant before, must be excluded. Therefore, the explained variance at this site can only be attributed to the spatial variables. The highest amounts of variance (>80%) unexplained by either the environmental or the spatial variables were found for sites AD2 and UP4.

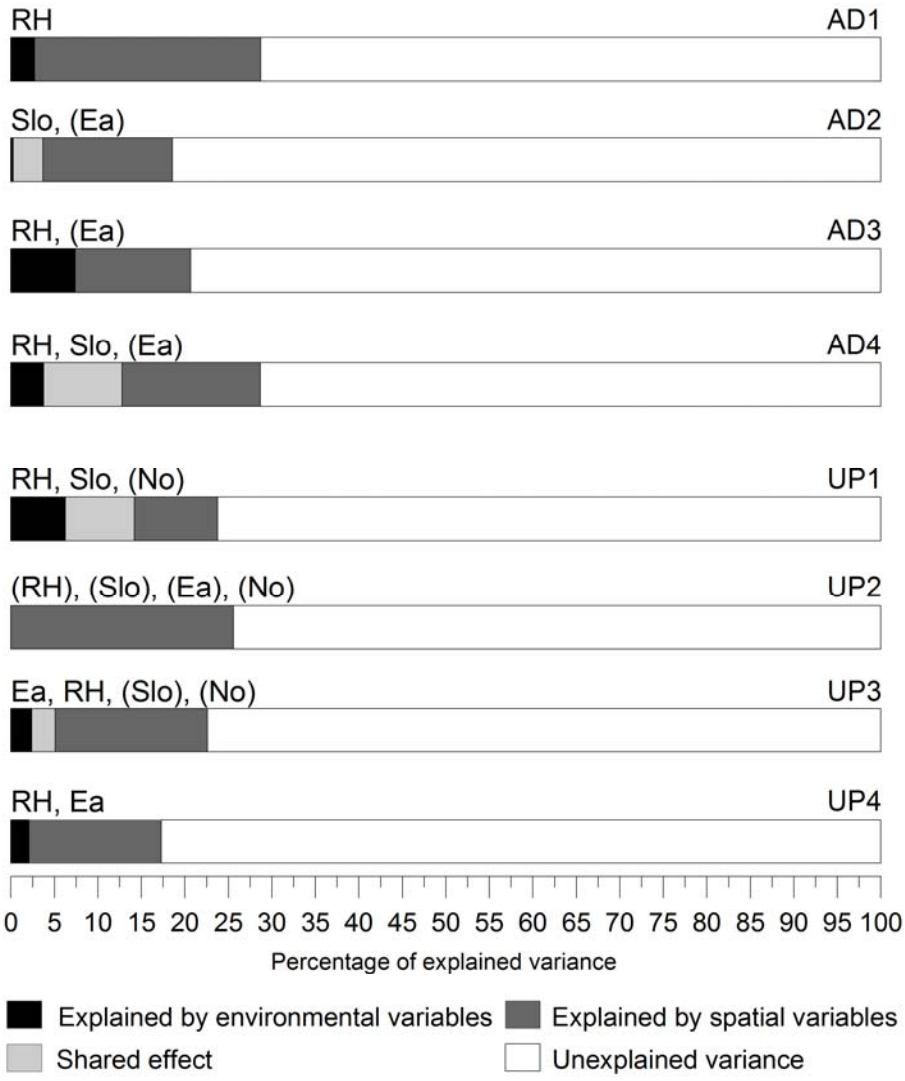

Figure 3.11: Results of variance partitioning for each investigated terrestrial (AD1-AD4) and Martian (UP1-UP4) polygonal field. For each site the bar plot shows the different explained proportions of variance. The environmental variables explaining significant amounts of variance are listed on the left above the plots. Variables which were finally excluded after forward selection are given in parentheses. Variable abbreviations are used according to Table 3.2. For further explanations see text.

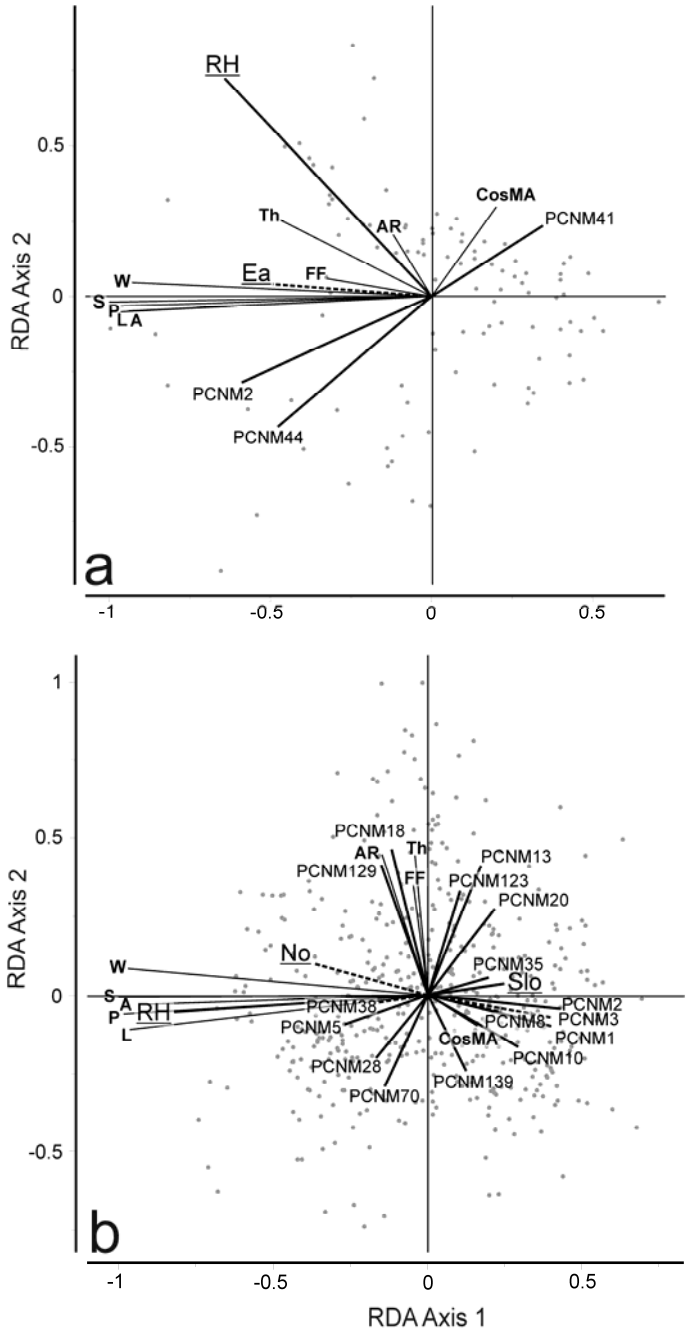

Figure 3.12: Example of redundancy analysis (RDA) triplots for (a) site AD3 and (b) site UP1 showing the relationship of significant environmental (thick solid lines, underlined letters) and significant spatial (PCNM, thick solid lines, simple letters) variables to the response variables (thin solid lines, bolded letters). Environmental variables which were excluded after forward selection are illustrated as dotted lines. The grey dots illustrate the locations of polygon samples. Abbreviations are used according to Table 3.2.

3.5 Discussion

3.5.1 Relationship between geomorphometry and genesis for the terrestrial polygons

The four polygonal fields in the Adventdalen are homogeneous with respect to their geomorphometric parameters. The statistical characteristics of *FF*, *AR*, and *Th* are similar for all sites (Table 3.4). However, the differing surface morphologies and dimensions indicate different stages of evolution (Table 3.5). The smallest and youngest polygons exist in the lower Adventdalen on flat terraces near the Adventelva River (site AD1). These are recently-active low-centered ice-

wedge polygons. Active thermal contraction cracking is proven, and relatively large ice wedges exist below the wider furrows at site AD1 [*Matsuoka and Hirakawa,* 1993; *Christiansen,* 2005]. The ongoing activity of thermal contraction cracking has resulted in progressive polygon subdivision (Table 3.5), expressed by a higher frequency of four-ray intersections compared to site AD2, AD3, and AD4 (Table 3.3). Therefore, these polygons are regular in shape and smaller in size [*Lachenbruch,* 1966]. The largest high-centered polygons were observed in the central valley at site AD2. The dimensions of the observed high-centered polygons decrease from the central valley to the upper Adventdalen, but ages are probably increasing. The dating of pingo and ice-wedge material suggests that periglacial landform formation in the lower Adventdalen was initiated about 3000 yr BP [*Svensson,* 1971; *Jeppesen,* 2001]. The late Holocene age of polygons in the lower Adventdalen (e.g., AD1) is likely, as they are located below the uppermost Holocene marine limit (~70 m above the present sea level). The relative sea level had fallen to the present-day position not until about 4300 yr BP [*Lønne and Nemec,* 2004]. Certainly, pingo ages have been identified to increase up the valley to about 7000 yr BP [*Yoshikawa and Nakamura,* 1996; *Ross et al.* 2007; *Meier and Thannheiser,* 2009; and references therein]. In general, this points to an older periglacial landform formation in the upper Adventdalen. Smaller high-centered polygons in the upper Adventdalen (AD4) have probably resulted from comparatively more permanent activity in the Holocene and thus enhanced polygon subdivision. The widths of the outlining troughs definitely increase in the up-valley direction to site AD4. This observation is in agreement with *Malmström et al.* [1973] who found the oldest and best-developed troughs on the highest terraces in this region. Furthermore, the same authors suggest a direct correlation between the width of ice wedges and the width of the overlying troughs. Based on the observed lack of ice wedges just below the active layer and of frost cracks extending through the active layer, which are regarded as indicators of wedge activity [e.g., *Romanovskii,* 1985; *Mackay,* 1992], the high-centered polygons in the central and upper Adventdalen are classified as inactive. The degradation and thawing of ice wedges has resulted in wide and deep troughs. This is supported by the relationship between larger trough widths and steeper slope angle. The evolutionary change from low-centered to high-centered polygons caused by ice-wedge degradation [e.g., *Washburn,* 1979; *Mackay,* 2000] might be reinforced on slopes by increasing drainage along the polygon-outlining troughs [*Fortier et al.,* 2007]. This degradation factor dominates the recent development of the high-centered polygons in the middle and upper Adventdalen and prevents active frost cracking (Table 3.5); this is also true because snow accumulating in the deep troughs would have an insulating effect, preventing crack initiation [e.g., *Mackay,* 1974, 1992]. Crack formation is influenced by micro-climate, micro-relief, vegetation, and snow cover, and therefore by specific temperature conditions [*Christiansen,* 2005; *Fortier and Allard,* 2005], which further complicates the discussion of differing cracking activity in the Adventdalen. The change in cracking activity is thought to reflect a change in climate [*French,*

2007]. Conditions more favorable to frost cracking than those of today (e.g., lower ground temperatures) probably existed in the middle and upper Adventdalen earlier in the Holocene.

The sedimentological properties of all active-layer profiles are relatively uniform, reflecting less variability in surficial material than suggested by *Tolgensbakk et al.* [2001]. Only small differences due to varying gravel contents were observed between the sites. Higher contents of gravel, in particular at the high-centered polygon sites in the upper Adventdalen, would be in agreement with current inactive thermal contraction cracking, because coarser-grained sediments require lower ground temperatures for cracking (< -6°C) [*Romanovskii,* 1985] than the existing average permafrost temperatures on Svalbard (-2.3°C to -5.6°C) [*Christiansen et al.,* 2010]. Furthermore, we found that the smallest polygons are associated with the homogenous silty loess-like deposits in the lower Adventdalen (AD1). The largest polygons are associated with higher gravel contents in the middle valley (AD2), i.e., with more compositionally heterogeneous sediments. This agrees with the suggestion of *Lachenbruch* [1962, 1966], that smaller regular polygons are related to homogenous fine-grained sediments with higher ground-ice contents due to the larger expansion coefficient and higher thermal stress. In contrast, larger irregular polygons are related to heterogeneous coarser-grained sediments (see also Table 3.1). Thus, we assume relatively high ground-ice contents at site AD1. At site AD4, the polygon size changes in accordance with the hillslope gradient and a change in grain-size distribution. Larger polygons, located down-slope, are associated with the highest measured contents of gravel (AD4b in Figure 3.7). By comparison, on the more elevated and horizontal parts, smaller polygons have formed in material with lower gravel contents and smaller mean grain size (AD4a; see also Figure 3.5). Furthermore, the polygonal network is rather irregular and shows a non-orthogonal lattice at its elevated parts. Down the slope, the larger polygons are mainly orthogonal (Figure 3.4). The relationship of ground material homogeneity to the orthogonality of polygonal systems is a further topic of debate (see Table 3.1). Most authors suggest that non-orthogonal (i.e. hexagonal) and complex systems are formed in homogenous material, while orthogonal lattices are related to heterogeneous material [*Lachenbruch,* 1962; *French,* 2007]. Such relationships could not be confirmed by our observations in the Adventdalen. With regard to the intra-site differences at AD4, orthogonal polygons are associated with more heterogeneous ground material down the slope. The regular AD1 polygonal network with partly orthogonal structures (Figures 3.4 and 3.5, Table 3.5) formed in homogenous ground material (see above).

The direction of polygon elongation was measured to estimate the direction of primary cracking. The majority of polygons within all polygonal fields are elongated (i.e. they are 15% longer than wide); only a few polygons are characterized by their similar width and length. Theoretically, if first-order cracks are long and subsequently subdivided by shorter secondary cracks, as has been modeled by *Plug and Werner* [2001], the primary cracks would determine the direction of polygon elongation in most cases.

Table 3.5: Compilation of morphometric criteria as well as past and present formation processes in the studied terrestrial and Martian polygonal fields. Question marks refer to processes which are not entirely clarified. For instance, composite-wedge formation at the Martian sites UP2 and UP3 would have occurred only during high-obliquity conditions in the past.

	Earth				Mars			
	AD1	AD2	AD3	AD4	UP1	UP2	UP3	UP4
Shape	similar	similar	similar	similar	similar	similar	similar	similar
Average Size	< 20m	< 30m	< 30m	< 30m	> 30m	< 10m	< 20m	< 10m
Polygon center	Low	High	High	High	High	Low	High	Low
Orientation to stress-free vertical surfaces	No	No	No	No	No	Strong near the topographic scarp	Strong near the topographic scarp	No
Network orthogonality	Partial	More complex	More complex	Partial on steeper slope sections	Partial	Distinct near the topographic scarp	Distinct near the topographic scarp	More complex
Origin of mean polygon elongation	Random	Random	Gravitational	Gravitational	Gravitational?	Gravitational and stress release at vertical surface	Gravitational and stress release at vertical surface	Random
Polygon subdivision	Medium, increasing	Low, Stopped	Low, stopped	Medium, stopped	Low, stopped	High, increasing?	High, stopped	Medium, stopped
Wedge formation	Ice-wedge	Ice-wedge	Ice-wedge	Ice-wedge	Sand-wedge?	Sand-wedge, Composite-wedge?	Sand-wedge, Composite-wedge?	Sand-wedge?
Current dominant process	Active cracking, Ice-wedge growth	Degradation by thawing of ice-wedges	Degradation by thawing of ice-wedges	Degradation by thawing of ice-wedges	Sublimation of ground-ice within polygon troughs	Active cracking (limited to favorable local conditions), Sand-wedge growth?	Sublimation of ground-ice within polygon troughs	Sublimation of ground-ice within polygon centers
Origin	Thermal contraction cracking	Thermal contraction cracking	Thermal contraction cracking	Thermal contraction cracking	Thermal contraction cracking	Thermal contraction cracking	Thermal contraction cracking	Thermal contraction cracking?

A distinct orientation of polygon elongation with respect to the direction of slope angle could be determined for the Adventdalen polygons (Figure 3.6). However, all polygonal networks are randomly formed *in sensu Lachenbruch* [1962, 1966] and are therefore not oriented to stress-free vertical zones such as the shore of the Adventelva River. But at the sites where the polygonal fields are formed on steeper slopes, in particular at sites AD3 and AD4 (Figure 3.4), the primary cracking seems to have occurred normal to the contour as polygon elongation is mainly parallel to the slope angle (Figure 3.6). *Mackay and Burn* [2002] reported similar primary crack orientation on the slopes of a drained lake site in the western Canadian Arctic. At our AD1 Adventdalen site, where the polygonal field is formed on a very gentle slope and in a rather flat area, polygon elongation is mainly parallel to the contour. A similar relationship was visually observed for the gentle slope sections at site AD2. These observations led to the assumptions that the gravitational effects on steeper slopes affect the direction of primary thermal contraction cracking and, furthermore, the orientation of polygons, because the secondary cracking occurs along the contour [*Mackay and Burn,* 2002].

The statistical analysis reveals differences within the individual polygonal fields in accordance with the site-specific conditions. Thus, the polygon geomorphometry is related to topographical conditions. The results of our multivariate statistics show that polygon dimension and shape are related to the location within a polygonal field, as expressed by the highly significant influence of the variable *RH* on almost all polygonal fields (Figure 3.11). This variable probably represents unmeasured or statistically unconsidered factors that vary along a hillslope gradient within the polygonal field, such as ground-ice and moisture contents, thermal conductivity (e.g., influenced by snow and vegetation cover), or grain-size distributions. Aspect and slope-angle conditions play a minor role in the statistics of our polygon dataset. This is unexpected, as subsurface and micro-climate conditions also change with slope angle and aspect and should have an influence on initial thermal contraction cracking and subsequent polygon formation [e.g., *Lachenbruch,* 1966; *Mackay,* 2000; *Mackay and Burn,* 2002]. Furthermore, interrelationships of slope conditions and polygon shape or dimension could be observed, as was discussed above. However, this was only slightly apparent in the statistics for the AD2 and AD4 Adventdalen sites (see Figure 3.11).

3.5.2 Comparability of terrestrial and Martian polygonal structures

The investigated polygonal structures in western UP on Mars share the geomorphological and morphometrical characteristics of the Adventdalen polygons. By comparing diverse geomorphometric criteria, several points are discussed by analogy (Table 3.5). The polygonal structures of western UP belong to the category of small-scale patterns, according to classifications of the wide variety of polygonal structures on Mars [e.g., *Mangold,* 2005; *Levy et al.,* 2009a]. Besides the analogy to the terrestrial polygons, the thermal contraction cracking origin is more likely than other origins such as desiccation cracking, as the landscape assemblage in the region

points to a dry origin and there is no evidence of former lakes [*Ulrich et al.,* 2010] or water-rich sediments essential for desiccation [*El Maary et al.,* 2010]. The statistical properties indicate that the shape of the observed Martian and terrestrial polygons are similar (see Table 3.4). Additionally, the sizes of the UP polygons are comparable to those of the Adventdalen polygons and fall within the range of maximum fracture spacing under current climate conditions on Mars (<75 m) [*El Maary et al.,* 2010]. They are also significantly smaller than polygons of tectonic origin [e.g., *Hiesinger and Head,* 2000]. Thus, we can conclude that they originated by thermal contraction cracking in connection with near-surface ground ice [*Mellon,* 1997; *Mangold et al.,* 2004] (Table 3.5). The morphological differences between the observed Martian polygons reflect different ages, thermal contraction cracking activity, and local environmental conditions, similar to their terrestrial analogues. In both cases, flat- to high-centered polygons are separated by distinct outlining troughs. The trough widths and depths of the large high-centered polygons (UP1) as well as their older appearance suggest that the Martian upland polygons have undergone continuous degradation [*Lefort et al.,* 2009]. In contrast to the Adventdalen high-centered polygons, where the trough expansion is related to ice-wedge degradation, it is suggested that the enlargement of polygon troughs on present-day Mars occurred by progressive sublimation of interstitial ice exposed after initial thermal contraction cracking [*Mangold,* 2005; *Levy et al.,* 2010a]. Examples of such high-centered sublimation polygons are known from Beacon Valley, Antarctica [*Marchant et al.,* 2002]. These high-centered polygons are formed on sediments which cover massive ice bodies (e.g., a stagnant glacier) by thermal contraction and the absence of a liquid phase. Polygon troughs are formed as sublimation is enhanced within the cracks due to the higher porosity and permeability of material trapped therein [*Marchant and Head,* 2007]. From the abundance of high-centered polygons on Mars, *Levy et al.* [2009a] estimated that sublimation of ground ice in the absence of liquid water is the dominant formation process of Martian polygon morphology. This is consistent with the current very cold and dry climate on Mars. The geomorphology of the polygonal network observed at site UP1 is more likely to have resulted from interstitial ice sublimation than from ice-wedge degradation in the current stage of climate.

Our data indicate a comparable frequency of three-ray intersections in the terrestrial and Martian high-centered polygons (Table 3.3), which is a sign of a lower degree of polygon subdivision (Table 3.5) by ongoing cracking and, therefore, older ages. This interpretation is supported by the larger polygon dimensions, which suggest older features formed under past environmental conditions [e.g., *Mangold et al.,* 2004; see also next section]. No clear relationship was observed between a higher frequency of three-ray intersections and mainly hexagonal polygon geometry. Within the terrestrial and Martian polygonal fields, which exhibit more than 90% three-ray intersections, orthogonal polygons are ubiquitous as well. The high frequency of three-ray intersections further points to a random formation of the polygonal networks (e.g., AD2 and UP1), as four-ray intersections are more typical of orthogonal polygons oriented at topographical edges

[e.g., *Lachenbruch,* 1966; *Romanovskii,* 1977], like in the UP2 and UP3 Martian polygonal networks (Figure 3.9c,d).

A striking feature of the UP1 polygons is the distinct two-directional polygon elongation (i.e. N-S and E-W) which shows only a small relationship to the slope angle direction (Figure 3.10). *Yoshikawa* [2003] reported a similar observation in UP for slightly larger polygons and interpreted the predominantly N-S crack orientation as a sign of tectonic origin. Because the region is gently rising to the south, the observed orientation of polygon elongation would be in agreement with the notion (for terrestrial polygons) that the gravitational effect of the slope influences thermal contraction cracking, controlling crack initiation even if the slope angle is very low [*French,* 2007]. The two-directional polygon elongation could therefore be explained by even a very low slope angle (Table 3.5). The primary cracking occurred in equal parts along and perpendicular to the contour. Other possible explanations exist, such as energy transfer by warmer winds coming from a southern direction during summer [*Morgenstern et al.,* 2007]. Winds could possibly increase temperature gradients and thus crack propagation in N-S-trending troughs, resulting in perpendicular secondary cracks forming in the E-W direction.

Like the terrestrial low-centered polygons (AD1), the small Martian polygons (UP2) are characterized by pairs of raised rims beside the outlining fissures. The low-centered polygons on the south-facing scalloped depression slope (UP4) are exceptional, since they are characterized by single outlining ridges without fissures between them (Figure 3.9e). The UP2 polygons, particularly those situated close to the steep north-facing wall of the scalloped depression (Figure 3.9c), show close similarities to the active low-centered polygons (AD1) in Adventdalen. In direct analogy, their fresh appearance as compared to the upland UP1 polygons, their small size, and their clear orthogonal lattice point to recently-active thermal contraction cracking processes due to homogenous fine-grained ice-rich material [*Lachenbruch,* 1962, 1966; *Lefort et al.,* 2009]. Besides the distinct orthogonality of the UP2 polygons, the orientation of polygon elongation (Figure 3.10 and Table 3.5), which is clearly parallel to the slope angle, suggests the primary cracking occurs perpendicular to the contour as the result of stress release at the scarp edge, and is further induced by the gravitational stress of the slope (Figure 3.13). Similar observations are reported by *Levy et al.* [2009a] for polygons present in Martian gully alcoves and by *Mangold* [2005] who also relates the orientation of orthogonal polygons inside Martian crater walls to the effect of slope. The orientation changes to a random orthogonal system at the foot of crater flanks. This is in agreement, first, with the observed changes in the character of the Martian UP2 and UP3 polygons to a random and increasingly complex network towards the depression bottom (Figure 3.13). Second, a similar change in polygon geometry was described for site AD4 in the Adventdalen where orthogonal structures are mainly grouped on steeper slope sections.

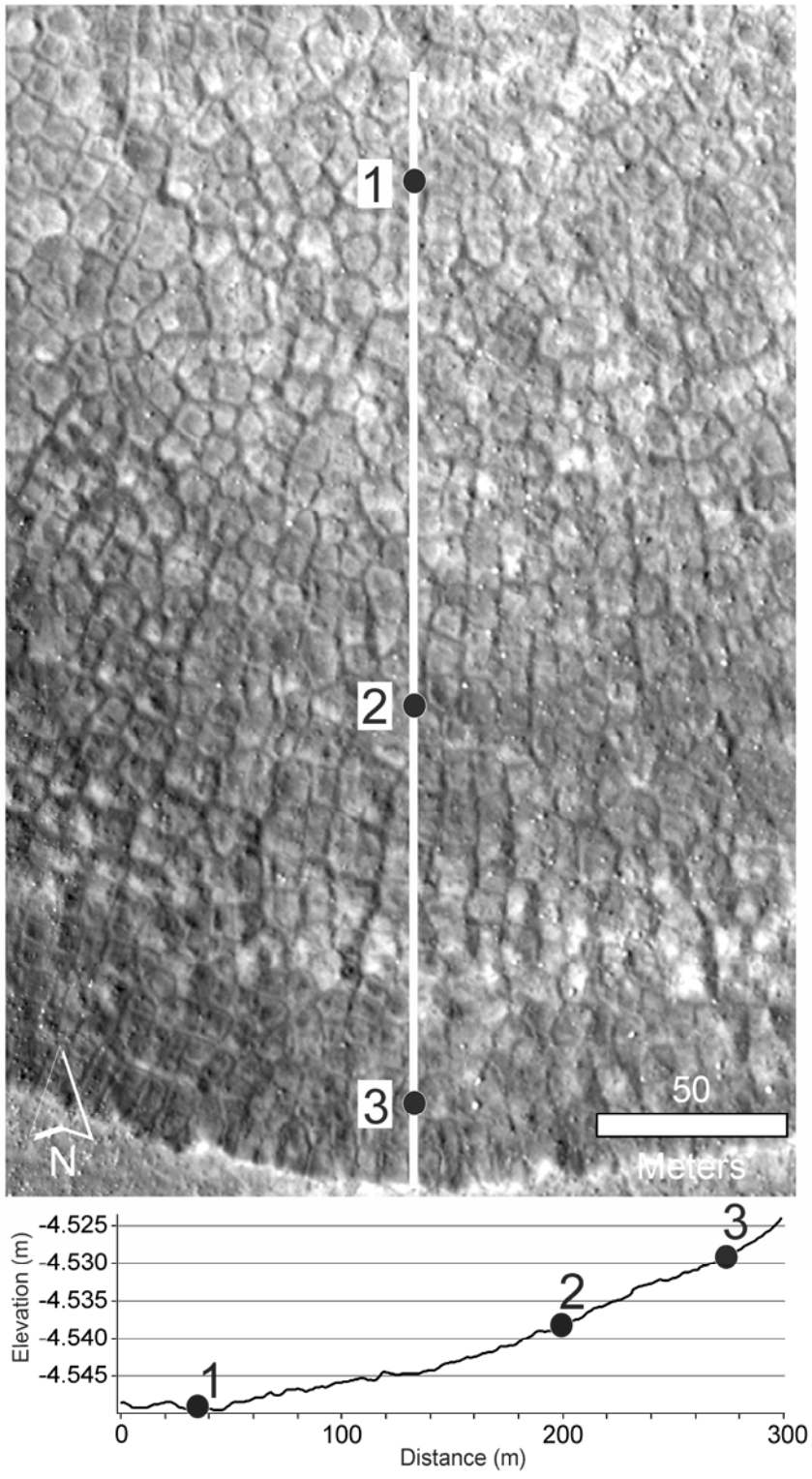

Figure 3.13: HiRISE subset showing small polygons of UP2 and UP3 character on the north-facing slope of a large scalloped depression adjacent to the main study site. This example is representative of how polygon morphology changes in response to the slope angle and the distance to the scarp edge. Polygons are clearly orthogonal and cracks are strongly oriented at point 3. Polygons become increasingly randomly distributed, their orthogonality decreases, and troughs (i.e. cracks) widen towards the depression bottom (point 1). The location of the DEM-derived topographic profile (below) is marked by the white line in the image. (HiRISE image: PSP_001938_2265).

The above suggestion for the highly significant influence of the variable *RH* within the multivariate statistics (Section 3.5.1) also applies to the Martian polygonal fields. This is particularly obvious for the UP1 polygonal field (see Figures 3.11 and 3.12) as the statistics confirm the visual observation explained in Section 3.4.3, i.e., that polygons in the lower area north of the depression are a little smaller, very bumpy and appear more degraded compared to the UP1 polygons south of the depression. Slightly varying ground-ice conditions or even small-scale changes in albedo would have led to different polygon morphologies. Another interesting detail is the statistically higher influence of aspect (represented by the variable *Ea*) as compared to *RH* on the polygonal characteristics at site UP3 (Figure 3.11). The polygon geomorphometry changes with increasing degradation of the UP3 polygons towards the depression bottom because sublimation would be significantly lower on a north-facing slope than on a south-facing slope due to reduced insolation (Figure 3.9b). These interpretations of the multivariate statistical results highlight the helpfulness of this approach in interpreting initial polygon geomorphometry as a function of site-specific conditions. Moreover, these discussions demonstrate the relationship of secondary polygon morphology to individual topographic conditions.

3.5.3 Genesis of Mars polygons and environmental implications

Based on our terrestrial studies and considering the landscape assemblage in UP, some implications for the formation of the Martian polygonal structures can be drawn (Figure 3.14). The large upland polygons (UP1) are probably very old and were formed after the deposition of the mantling material during conditions of high obliquity [*Kreslavsky and Head,* 2000, 2002; *Mustard et al.,* 2001; *Head et al.,* 2003]. An old age is also indicated by the fact that these polygons are truncated by the scalloped depressions (see Figure 3.2c). Troughs are often traceable across the steep north-facing scarps [*Lefort et al.,* 2009; *Ulrich et al.,* 2010] and the original polygonal network is visible in shallow depressions nearby or on south-facing slopes (see Section 3.4.3), where the lowering of the surface has not yet reached the maximum depths of the cracks [*Lefort et al.,* 2009]. The sizes of the polygons indicate very deep thermal contraction cracking, which must be related to strong temperature gradients [*Lachenbruch,* 1962, 1966]. It was shown by thermal modeling that summer temperatures in this region could reach 273 K even at obliquities of 35°, but such temperatures are more likely at higher obliquity [*Ulrich et al.,* 2010]. Very high temperatures in summer followed by an extreme temperature drop in winter could have led to deep crack penetration and the formation of larger polygons. Larger polygons, however, are also formed in material with lower ice content [*Lachenbruch,* 1966] as was discussed for the terrestrial polygons (see also Table 3.1). No clear relationship between polygon dimension and ground-ice content, which increases with latitude [e.g., *Feldman et al.,* 2004], could be observed on Mars [*Mangold et al.,* 2004; *Mangold,* 2005*; Levy et al.,* 2009a]. The size of the upland polygons (UP1) is consistent with the findings of the Gamma Ray Spectrometer (GRS) that only ~4 to ~10 wt% water-ice

equivalent exists currently in the upper surface layer (<1 m depth) in the regions between 45°S and 45°N [*Boynton et al.,* 2002; *Mitrofanov et al.,* 2002; *Feldman et al.,* 2004]. If higher ground-ice contents than in the upper layer occur deeper than 1 m, which was inferred from the dimension of the scalloped depressions [*Morgenstern et al.,* 2007; *Ulrich et al.,* 2010], seasonal thermal waves should not reach this depth at the present time [*Mellon*, 1997; *Mangold et al,* 2004]. Thus, the process of thermal contraction cracking which formed the UP1 polygons is likely inactive today (Table 3.5 and Figure 3.14). Only small shallow cracks observed within some polygon centers were likely to have been formed subsequently. It is not clear, however, how much ground ice existed during times of higher obliquity when these polygons were formed and ground ice was more stable in the upper surface layer than it is today [e.g., *Hecht,* 2002; *Head et al.,* 2003]. Currently, UP1 polygons are more influenced by degradation through sublimation. This process would be enhanced by the dark fine-grained material trapped within the polygon troughs. Furthermore, the enrichment of fine material within the large cracks could have led to the formation of sand-wedge-like structures [e.g., *Sletten et al.,* 2003*; Bockheim et al.,* 2009] (Table 3.5).

The small Martian polygons (UP2, UP3, and UP4) were formed after the depression formed and must therefore be relatively young (Figure 3.14). If scallop formation is comparatively young, as stated e.g., by *Ulrich et al.* [2010], these polygons are not older than 5 Myr and are most likely much younger [e.g., *Levy et al.,* 2009a, b, 2010a]. Based on the geomorphometry of the low-centered polygons located on the north-facing slope of the depression (i.e. UP2), it was concluded that thermal contraction cracking is active there (Table 3.5) and that these polygons formed in fine-grained ice-rich material. This is in agreement with the suggestion of *Lefort et al.* [2009] that they formed in connection to an ice table, which is closer to the surface there than on the uplands and deepens towards the south-facing slope. The lower amount of insolation on the north-facing slope results in higher ground-ice stability. This would explain currently active thermal contraction cracking despite lower temperature gradients on this permanently-shaded part of the depression [*Lefort et al.,* 2009]. However, if ice-cemented material were to be exposed after scarp erosion [see *Ulrich et al.,* 2010], initial cracking could have occurred immediately afterwards (Figure 3.14) and the small polygons could have been formed within a few tens of years [*Mackay and Burn,* 2002]. The cracks would then fill with wind-blown material, forming sand-wedges. Furthermore, if thawing of ground-ice enhanced the scarp erosional process during higher obliquity conditions [*Ulrich et al.,* 2010], a small occasional water supply likely led to the formation of composite wedges [e.g., *Murton,* 1996] and thus the development of upturning ridges beside the cracks. As the ice-table deepens towards the depression bottom [*Lefort et al.,* 2009] and the ground-ice content is lowered accordingly, the activity of the UP2 polygons decreases or even ceases entirely at a greater distance from the scarp [e.g., *Mellon,* 1997] (Table 3.5 and Figure 3.14).

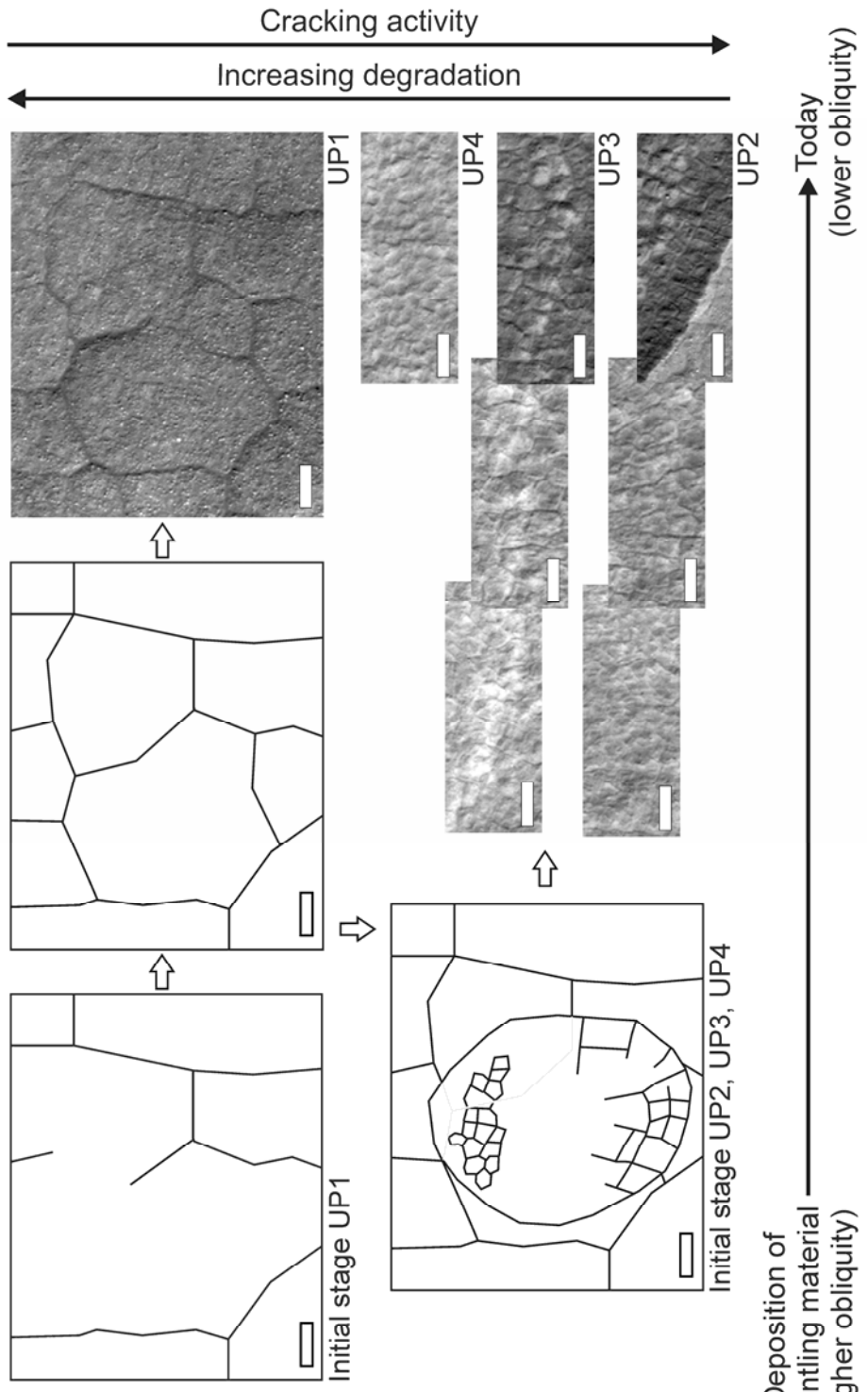

Figure 3.14: Schematic model of suggested polygon evolution in western Utopia Planitia, Mars, from a time of high obliquity conditions until today. Images on the right represent the current stages. The series of three images for UP2 and UP3 illustrate the development of small low- and high-centered polygonal networks, alternating arranged within a scalloped depression from north (left) to south (right) (for explanations see also Section 3.4.3). All scale bars are 20 m. North is up. (Details of PSP_001938_2265).

The high-centered polygons on the ridges inside the depression (UP3) are proposed to have originated by similar processes as the UP2 polygons, although they represent older evolutionary stages in context of the equator-ward lateral depression formation and scarp erosion [*Ulrich et al.,* 2010; *Séjourné et al.,* 2011]. After the ridges were formed, their exposed position led to an initial enhancement of sublimation within the previously-formed crack pattern, especially if composite

wedges existed below the cracks. Accordingly, the age of the UP3 polygons increases towards the depression bottom (Figure 3.14). They are further influenced by intensified erosion and degradation and thus changing geomorphology due to the aspect of the internal ridges as was identified by the statistics. The changing geomorphometry of the polygonal UP2 and UP3 networks within the depression (Table 3.5) is in agreement with the proposed lateral scarp formation in the equator-ward direction [*Ulrich et al.,* 2010; *Séjourné et al.,* 2011]. While the UP2 and UP3 polygons are slightly smaller, more regular, orthogonal, and more subdivided on the north-facing slope, they are bigger, much more degraded, more irregular, and rather hexagonal on the depression bottom towards the south-facing slope (Figures 3.13 and 3.14). Moreover, the morphology of upturning ridges beside the outlining cracks of the low-centered UP2 polygons is consistent with the recent growth of sand wedges or even the hypothesis of composite-wedge formation during more benign conditions in the past. *Levy et al.* [2009b] suggested an alternative formation hypothesis to explain the elevation of mixed-center polygon shoulders. The location of sublimation would shift inside a polygon; sublimation would be enhanced within the polygon interior as the troughs become insulated from further deepening by the thickening of ice-depleted material therein, while the centers remain less-efficiently insulated. This could be an explanation for the UP4 polygonal network on the south-facing slope where no cracks and only single outlining ridges could be observed. The UP4 polygons show close similarities to the "brain terrain" discussed by *Levy et al.* [2009b]. After a small initial crack network, superimpose upon the remnants of the upland polygonal cracks, was formed by permanent insolation and therefore relatively higher temperature gradients (Figure 3.14), it is conceivable that the pattern was modified relatively quickly according to *Levy et al.* [2009b] by continuous ground-ice sublimation and subsidence of ice-depleted material. The UP4 polygonal field could be an expression of the flattening and recent surface stabilization by permanent insolation and continuous but slow ground-ice sublimation on the south-facing scalloped depression slope [*Ulrich et al.,* 2010].

In summary, from the comparison of polygon geomorphometry alone it seems problematic to classify the Martian polygons as ice-wedge, sand-wedge, or sublimation polygons, not least because the Adventdalen polygons also show close similarities to sand-wedge or sublimation polygons in Antarctica [e.g., *Péwé,* 1959; *Marchant et al.,* 2002; *Sletten et al.,* 2003; *Bockheim et al.,* 2009; *Levy et al.,* 2010a]. If we consider the evolution of the UP polygons in the geomorphological context of the scalloped depression formation, it becomes obvious, however, that sand or even composite wedges are likely to be formed and that all the different polygonal fields represent different evolutionary stages within the landscape formation process (Figure 3.14). Differing local and regional changes in climate and ground-ice conditions are reflected in their geomorphology and geomorphometric characteristics. Recent polygon development in western UP seems to be limited to the effects produced when small-scale local conditions allow active thermal contraction cracking (Table 3.5). Regionally, the UP polygons have been influenced by dry

degradation processes such as ground-ice sublimation. As this is a very slow process, the polygon evolution in UP is currently almost stagnant compared to polygon evolution stimulated by the fast-changing environment in Adventdalen.

3.6 Conclusions

Thermal contraction polygons in different stages of evolution on Svalbard were used as terrestrial analogues to elucidate the processes of small-scale polygon formation in western Utopia Planitia, Mars. Quantitative terrain analyses on the basis of very-high-resolution remote-sensing data indicate a comparable thermal contraction cracking genesis of the small-scale polygons investigated on Mars, and allowed us to infer specific atmospheric and subsurface conditions which exist or which existed in the past in relation to polygon formation on Mars. Both in Adventdalen and on Mars, polygon evolution is strongly related to regional and local landscape dynamics. On Earth and on Mars larger polygons were formed in the past during times when more favorable conditions allowed deep thermal contraction cracking. These polygons are currently degrading. The formation of composite wedges could have occurred in response to past orbital configurations of Mars, which led to the development of small low-centered polygons on north-facing scalloped depression slopes. These patterns show the closest analogy to ice-wedge polygons in Adventdalen. However, their location within the scalloped depressions probably allowed active thermal contraction cracking and possibly sand-wedge growth under current Martian climate conditions. On Earth ice-wedge polygons form due to the existence of liquid water, and are subsequently degraded by ground-ice thawing, while the present appearance of Martian polygons is primarily the result of dry degradation processes (i.e. sublimation).

The multivariate statistical approach was successfully applied to quantitatively validate the relationship between polygon geomorphometry and topographical parameters. Comparatively few environmental parameters could be extracted out of DEMs and used in the statistics as explanatory (i.e. environmental) variables, which results in the relatively high amount of unexplained variance in the polygon dataset. In future work, further parameters reflecting not only topography but also subsurface and climate conditions should be included in the statistics. Furthermore, in cooperation with other quantitative methods like spatial point pattern analysis (SPPA) [e.g., *Dutilleul et al.,* 2009; *Haltigin et al.,* 2010], a more detailed understanding of diverse polygonal geomorphometry can be achieved and linked to individual formation processes.

Our results demonstrate the difficulty of addressing the question of what factors govern the size and shape of polygons. These results emphasize the complex interaction of various factors such as air and ground temperature variations, subsurface conditions, and topography. More detailed analyses of physical properties influencing polygon evolution should be performed, and the individual subsurface and climatic conditions of genetically differing polygonal structures must be

included in future quantitative terrain analyses. Field surveys of analogue morphologies in terrestrial permafrost environments are the necessary complement and provide the ground truth for remote-sensing data analyses.

Acknowledgements

This research has been partly supported by the Helmholtz Association through the "Planetary Evolution and Life" research alliance. Field work on Svalbard would not have been possible without logistical support by the AWIPEV German-French research station. UNIS and the Norwegian Polar Institute generously provided transport and safety equipment for the field campaign in Adventdalen. Special thanks go to the other members of our field team, Harald Hiesinger, Dennis Reiss, Michael Zanetti (University of Münster), Lars Johansson, and Andreas Johnsson (University of Gothenburg). The analytical lab work was significantly supported by Ute Bastian (AWI Potsdam). We thank Matthias Grott (DLR Berlin) for assistance and fruitful discussions about the KD2 measurements. The efforts of all colleagues involved in HRSC-AX image acquisition and processing, in particular Frank Trauthahn and Frank Preusker (DLR Berlin), are highly appreciated. The continuing efforts and support of the HiRISE and CTX teams in making their data publicly available are gratefully acknowledged. We also thank Randy Kirk (USGS, Flagstaff, USA) and colleagues for kindly providing a HiRISE DEM of our Martian study site. The paper benefited by English proof-reading and valuable comments from Candace S. O'Connor (UAF, Fairbanks, Alaska). Finally, we would like to thank Goro Komatsu, Victor R. Baker, and the editor Takashi Oguchi for their reviews and helpful comments.

4. Habitable periglacial landscapes in Martian mid-latitudes

Mathias Ulrich[1], Dirk Wagnerr[1], Ernst Hauber[2], Jean-Pierre de Vera[2], Lutz Schirrmeister[1]

[1]Alfred Wegener Institute for Polar and Marine Research, Research Unit Potsdam, Potsdam, Germany
[2]Institute for Planetary Research, German Aerospace Center (DLR), Berlin, Germany

Submitted to Icarus

Abstract

Subsurface permafrost environments on Mars are considered to be zones where extant life could have survived. For the identification of possible habitats it is important to understand periglacial landscape evolution and related subsurface and environmental conditions. Many landforms that are interpreted to be related to ground ice are located in the Martian mid-latitudinal belts. This paper summarizes the insights gained from studies of terrestrial analogues to permafrost landforms on Mars. The potential habitability of Martian mid-latitude periglacial landscapes is exemplarily deduced for one such landscape, that of Utopia Planitia, by a review and discussion of environmental conditions influencing periglacial landscape evolution. Based on recent calculations of the astronomical forcing of climate changes, specific climate periods are identified within the last 10 Ma when thaw processes and liquid water were probably important for the development of permafrost geomorphology. No periods could be identified within the last 4 Ma which met the suggested threshold criteria for liquid water and habitable conditions. Implications of past and present environmental conditions such as temperature variations, ground-ice conditions, and liquid water activity are discussed with respect to the potential survival of highly-specialized microorganisms known from terrestrial permafrost. We conclude that possible habitable subsurface niches might have been developed in close relation to specific permafrost landform morphology on Mars. These would have probably been dominated by lithoautotrophic microorganisms (i.e. methanogenic archaea).

4.1 Introduction and background

The identification of possible habitable zones on extraterrestrial planets is one of the major challenges in planetary research. This quest is based predominantly on the search for zones outside the Earth where liquid water exists or has existed in the past. The occurrence of water is one of the major requirements for the existence, evolution, and preservation of biological systems. Habitability is generally defined as a measure of an environment's potential, past or present, to

sustain any kind of life as we know it [e.g., *Des Marais et al.,* 2003]. *Kminek et al.* [2010] defined the lower limits of temperature and water activity (a_w) on Mars to which terrestrial organisms are able to replicate or extant Martian life could have survived to −25°C and 0.5, respectively, and defined the geomorphologic features, which meet these requirements under present-day conditions as special regions, such as gullies or the deep subsurface. Periglacial (i.e. cold-climate) features, for instance, are not considered to be special regions [*Beaty et al.,* 2006; *Kminek et al.,* 2010].

Mars is the most promising celestial body to search for water and habitable zones. Investigations of specific geomorphologic features (e.g., outflow channels, deltas, paleolakes) led authors to infer that water was active on the surface in the geological history of Mars [e.g., *Carr,* 1996; *Baker,* 2001]. The almost global distribution of hydrated minerals on the very old (Noachian-Hesperian) Martian surfaces of the low- and mid-latitude highlands further suggests diverse surface alterations in the distant past under the influence of water [e.g., *Bibring et al.,* 2006, *Chevrier and Mathé,* 2007]. Based on these observations, it has often been suggested that life or the remnants of life (e.g. spores, organic detritus, fossil microorganisms) should be sought in the geologically oldest regions on Mars due to the assumption that conditions on early Mars (>3.8 Ga) were more favorable to the origin of biological systems [*McKay and Stoker,* 1989; *Farmer and Des Marais,* 1999]. The present atmospheric conditions (i.e. very low pressure, low temperatures, hyper-aridity, high radiation) generally do not allow the permanent existence of liquid water and life on the Martian surface [*Kminek et al.* 2010]. If life still exists, it must have survived in well-protected ecological niches, which are still unknown [e.g., *Horneck,* 2000].

Subsurface permafrost environments on Mars represent one possibility where highly-specialized microorganisms could have survived or may still exist [e.g., *Chapelle et al.,* 2002; *Gilichinsky,* 2007; *Morozova et al.,* 2007]. Most of the water on Mars probably exists today as ground ice in the subsurface. This is supported by the findings of the Gamma Ray Spectrometer (GRS) on Mars Odyssey, which detected an increasing abundance of water-equivalent hydrogen (interpreted as ground ice) towards the Martian poles [*Boynton et al.,* 2002; *Mitrofanov et al.,* 2002; *Feldman et al.,* 2004]. The habitability of Martian high latitudes has been discussed by e.g., *Jakosky et al.* [2003] and *Stoker et al.* [2010]; the mid-latitudes could be of particular importance with respect to the search for life, because they represent a transition zone [*Kreslavsky and Head,* 2002]. On the one hand, ground ice is permanently stable in the very cold polar regions [*Mellon et al.,* 2004] and liquid water could probably occur only temporarily as salty solutions (i.e. cryobrines) under present-day climate conditions [e.g., *Rennó et al.,* 2009; *Möhlmann,* 2010a]. On the other hand, temperatures could reach 273 K (H_2O melting point) in the equatorial regions, but water and ground ice are unstable and will sublimate even from several meters deep in the ground because of very low atmospheric pressure [*Mellon and Jakosky,* 1995; *Mellon et al.,* 2004]. Many landforms which are primarily distributed in the mid-latitudes (between ~30° and ≥60°), such as gullies and periglacial features (e.g., polygons, scalloped depressions, fractured mounds, viscous

flow features) [e.g., *Malin and Edgett,* 2000; *Mangold,* 2005; *Burr et al.,* 2009; *Levy et al.,* 2009a; *Dundas and McEwen,* 2010], are interpreted to have formed in the presence of transient surface water and/or the occasional thawing of ground ice which has occurred due to the extreme variations of Mars orbital configurations within the Late Amazonian [*Costard et al.,* 2002; *Dickson et al.,* 2007; *Ulrich et al.,* 2010]. Surface features possibly indicative of thawing, however, are not restricted to mid-latitudes, and have been found at high latitudes [*Gallagher et al.,* 2011] and even near the equator [*Balme and Gallagher,* 2009]. Young periglacial landforms that resemble cold-climate (i.e. permafrost) features on Earth are of particular astrobiological interest because, first, they suggest the presence of ground-ice dynamics during their formation and, second, permafrost is known to be a rich habitat for cold-adapted microbial communities [reviewed in *Gilichinsky and Wagener,* 1995; *Wagner,* 2008]. It is particularly interesting to discuss the habitability of regions on Mars where many possibly-periglacial landforms are spatially related, for instance Utopia Planitia (UP) or Martian mid-latitude craters [see *Hauber et al.,* 2011], because in those regions it is necessary to consider the geomorphological context of diverse landscape features.

The main purpose of this paper is to discuss the potential habitability of mid-latitude permafrost environments on Mars. Martian mid-latitudes in general are potentially interesting for habitability studies, and UP is the particular area we chose to focus on in our investigation of this topic. Based on the literature and on our own previous studies [*Ulrich et al.,* 2010, in press], which were strongly guided by terrestrial analogue field work, diverse landforms are integrated to propose a conceptual scenario for periglacial landscape evolution. With focus on the formation theories of diverse permafrost landforms in western UP, the potential climate-related influence of water and/or thawing ground ice during climate changes within the last 10 Ma will be considered. Finally, we will discuss the overlap of past and present environmental conditions on Mars within the allowed environmental range for growth or survival of certain microorganisms in order to define possible habitable niches.

4.2 Permafrost conditions of Utopia Planitia

Possible periglacial landforms on Mars have been studied since the Viking era (late 1970`s). Their formation was interpreted to have occurred in association with Martian ground ice [e.g., *Lucchitta,* 1981; *Rossbacher and Judson,* 1981]. With the advent of high-resolution images acquired by the Mars Orbiter Camera (MOC, between 1997 and 2006) and the High Resolution Imaging Science Experiment (HiRISE, since 2006), the western UP region (centered at ~45°N; Figure 4.1), in particular, became the focus of periglacial investigations (see Table 4.1) because the landscape assemblages (e.g., scalloped depressions, polygonal patterned ground, and pingo-like features; Figure 4.2) show morphological analogies to permafrost landscapes on Earth [e.g., *Morgenstern et al.,* 2007; *Soare et al.,* 2008; *Burr et al.,* 2009*; Ulrich et al.,* 2010] (Figure 4.1c, d).

However, the role of liquid water in the evolution of the UP landscape is still under debate (Table 4.1).

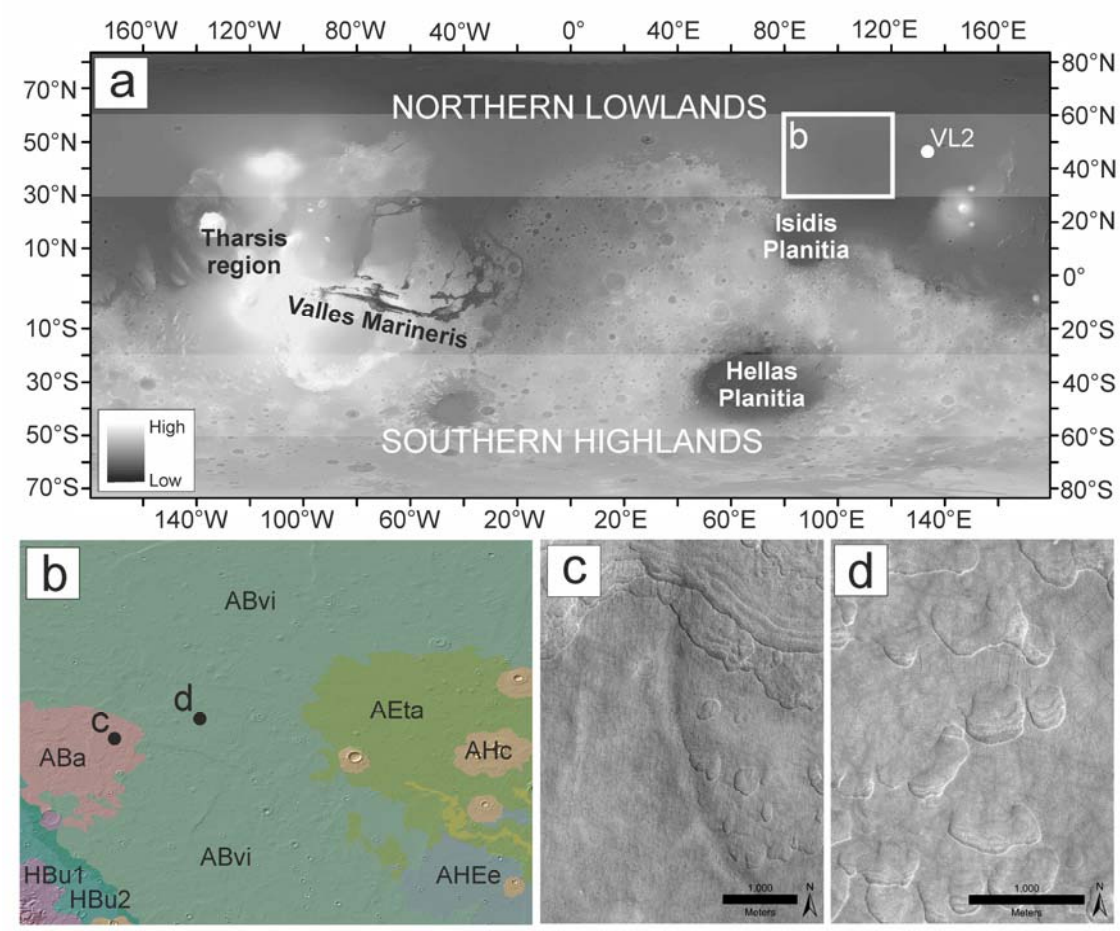

Figure 4.1: Regional setting of Utopia Planitia. (a) MOLA DEM on shaded relief shows the area located in the western part of the Utopia basin on which this work is focused (white rectangle). All periglacial features discussed and compiled from the literature in Tab. 1 are clustered between 30°-60°N and 80°-120°E. The mid-latitudinal belts are highlighted. VL2, Viking Lander 2 site. The "High-Low" scale refers to elevation. (b) Geological map of western Utopia Planitia. According to *Tanaka et al.* [2005], the geological units with decreasing age are; Early Hesperian: HBu1=Utopia Planitia 1 unit. Late Hesperian: HBu2=Utopia Planitia 2 unit, AHEe=Elysium rise unit. Early Amazonian: ABvi=Vastitas Borealis interior unit, AEta=Tinjar Valles a unit. Late Amazonian: ABa=Astapus Colles unit. AHc=Crater unit. Examples of landscape assemblages are shown by HiRISE portions for (c) the ABa unit and (d) the ABvi unit.

4.2.1 Latitude-dependent mantle deposits

UP is part of the Utopia Basin (Figure 4.1a), which was probably formed by a giant impact during the (pre-) Noachian period (~4.5 to ~3.7 Ga) [*McGill,* 1989]. During the Hesperian (~3.7 to ~3.0 Ga), the region underwent significant modifications by volcanic and tectonic activities. At the end of the Hesperian in transition to the Amazonian (<3 Ga) the basin was filled by outflow channel deposits; these deposits were subsequently reworked to form the Vastitas Borealis units, which underlay the region today [see *Tanaka et al.*, 2005, and references therein].

The Late Amazonian was characterized by depositions of an ice-dust mixture, building a tens-of-meters-thick ice-rich sediment mantle that spreads over the mid- to high latitudes on both hemispheres and covers the Vastitas Borealis units on the northern hemisphere [e.g., *Kreslavsky and Head,* 2000; *Mustard et al.,* 2001; *Head et al.,* 2003]. This mantle was identified on the basis of Mars Orbiter Laser Altimeter (MOLA) and MOC data. It forms layered deposits covering older, rougher terrain, which appear to be smooth where they are not degraded [*Kreslavsky and Head,* 2000; *Mustard et al.,* 2001] (see Figure 4.2b, e). The degradation of the ice-rich mantle increases towards the equator and is attributed to insolation-driven sublimation of ground ice [*Mustard et al.,* 2001; *Milliken and Mustard,* 2003, *Morgenstern et al.,* 2007]. This process has created a distinctive appearance and specific surface morphologies, especially in the regions between 30° and 60°; this suite of characteristics has been referred to as "dissected mantle terrain" (DMT) by *Milliken and Mustard* [2003]. In the western UP, the Astapus Colles unit (ABa), which overlies the Vastitas Borealis interior unit (ABv_i), represents parts of the DMT [*Tanaka et al.,* 2005] (Figure 4.1b). Many periglacial features are widespread on the ABa unit (Figure 4.1c) and the surrounding ABv_i unit (Figure 4.1d), reflecting the assumed presence of ground ice.

The poleward-increasing hydrogen content in surface soils detected by GRS, which is mainly interpreted as a signal of ground ice [e.g., *Feldman et al.,* 2004], supports these theories of mantle formation. Extreme variations in Martian orbital parameters and the related changes in insolation intensity are thought by many authors to be the driving force for the cyclical deposition and mobilization of volatiles [e.g., *Head et al.,* 2003; *Levrard et al.,* 2004; *Madeleine et al.,* 2009]. *Laskar et al.* [2004] precisely calculated orbital parameter variations and corresponding insolation changes for the last 10 to 20 Ma. Insolation and surface temperatures are often suggested to vary with the obliquity cycle (~120 ka). Moreover, variations are related to eccentricity (cycle of 95 to 99 ka) and the perihelion precession (51 ka cycles) [*Laskar et al.,* 2002]. During high-obliquity conditions water-ice is removed from the polar reservoirs, transported equator-ward, and deposited as a mantle consisting of an ice-dust mixture; in contrast, during low obliquity conditions, like the present, interstitial ice within the upper surface layer becomes unstable, sublimates, and is transported pole-ward. Thus the mantle becomes progressively degraded between 60° and 30° [e.g., *Mustard, et al.,* 2001; *Milliken and Mustard,* 2003]. Alternatively, *Levrard et al.* [2004] and *Madeleine et al.* [2009] propose that under prolonged high-obliquity conditions volatiles are transported from the poles to the equatorial regions, building tropical mountain glaciers. During moderate obliquity (~25° to 35°), this equatorial ice reservoir sublimates and the water is then redistributed pole-ward and accumulates as air-fall deposition (i.e. precipitation) of ice and dust [*Levrard et al.,* 2004]. The volatile cycling in response to orbital variations led *Head et al.* [2003] to infer that the surface of Mars is influenced by ice ages, and that Mars currently exits in an interglacial period. According to the orbital parameters, the most recent ice ages occurred during high obliquity periods less than ~5 Ma ago [*Head et al.,* 2003; *Levrard et al.,* 2004].

Table 4.1: Literature-based compilation of records focusing on Utopia Planitia and landforms in which water, ground ice, and/or glacier ice are suggested to have played a role during formation

Form	Interpreted process	Suggested liquid water activity	Relative age	Data	Author
Ground-ice degradation features					
Scalloped depressions	- insolation-driven ground-ice sublimation - volume loss and surface collapse	Low	Late Amazonian	HRSC, THEMIS-VIS, MOC, MOLA	*Morgenstern et al.* [2007]
Scalloped depressions	- evaporation and drainage of melt-water ponds	Very high	Late Amazonian	MOC	*Soare et al.* [2007]
Pits along pedestal craters	- sublimation of volatiles	Low	Amazonian	CTX, MOLA THEMIS-VIS	*Kadish et al.* [2008]
Lobate, scalloped and rimless depressions	- episodic loss of ponded water by evaporation or drainage	Very high	Late Amazonian	MOC, THEMIS-VIS, HiRISE	*Soare et al.* [2008]
Scalloped depressions	- insolation-driven ground-ice sublimation - localized thawing and slumping events - volume loss and surface collapse	Low to middle	Late Amazonian	HiRISE, MOC, THEMIS-IR	*Lefort et al.* [2009]
Scalloped depressions	- insolation-driven ground-ice sublimation - surface subsidence and lateral growth - slumping processes due to increasing sublimation and occasional thawing	Low to middle	Late Amazonian	HiRISE, CTX, THEMIS-IR, MOLA	*Ulrich et al.* [2010]
Scalloped depressions	- ground-ice sublimation - surface subsidence and lateral growth - increasing sublimation at interior-polygon troughs	Low to middle	Late Amazonian	HiRISE, MOLA	*Séjourné et al.* [2011]
Polygonal patterned ground					
Small-scale polygonal structures	- thermal contraction cracking - ice-wedge growth	Middle to high	Amazonian	MOC	*Seibert and Kargel* [2001]
Small-scale polygonal structures	- thermal contraction polygons - ice wedges - after slow loss of ponded water	Very high	Late Amazonian	MOC, MOLA	*Soare et al.* [2005]
Small-scale polygonal structures	- thermal contraction cracking - enhanced degradation of N-S trending cracks by warm winds during summer	Low	Late Amazonian	HRSC, THEMIS-VIS, MOC, MOLA	*Morgenstern et al.* [2007]
Small-scale polygonal structures	- ice-wedge polygons - freeze and thaw cycles included	Very high	Late Amazonian	MOC, THEMIS-VIS, HiRISE	*Soare et al.* [2008]
Small-scale polygonal structures	- thermal contraction polygons at different stages of evolution - modification by sublimation	Low to middle	Late Amazonian	HiRISE, MOC, THEMIS-IR	*Lefort et al.* [2009]
"Brain terrain" and small-scale polygonal structures	- thermal contraction cracking - differential sublimation and topographic inversion	Very low	Late Amazonian	HiRISE	*Levy et al.* [2009b]
Small-scale polygonal structures	- thermal contraction polygons at different stages of evolution - uncertain filling of cracks - degradation by sublimation	Low to middle	Late Amazonian	HiRISE, MOLA	*Séjourné et al.* [2011]
Small-scale polygonal structures	- thermal contraction polygons at different stages of evolution - sand-wedge formation - current degradation by sublimation - formation of composite wedges by occasional ground ice thawing	Low to middle	Late Amazonian	HiRISE	*Ulrich et al.* [in press]

Table 4.1: (*Continued*)

Form	Interpreted process	Suggested liquid water activity	Relative age	Data	Author
Pingo-like structures					
Small crater-floor mounds	- hydrostatic (closed-system) pingos - formed after the presence and drainage of ponded water by ground-ice aggradation	Very high	Late Amazonian	MOC, MOLA	*Soare et al.* [2005]
Small fractured and flat-topped mounds	- analogue to terrestrial pingos - uncertain process - presence of ground ice and subsurface liquid water is suggested	High	Amazonian	HiRISE, CTX MOC	*Dundas et al.* [2008]
Raised rim landforms	- collapsed hydrostatic (closed-system) pingos	Very high	Late Amazonian	MOC, THEMIS-VIS, HiRISE	*Soare et al.* [2008]
Dome, cone, and ring-shaped features	- open-system (hydraulic) pingos at different stages of evolution - melting ground ice due to deep subsurface heat source	High	Amazonian	MOC, THEMIS-VIS, HRSC, MOLA	*de Pablo and Komatsu* [2009]
Others					
Gullies	- meltwater migration through a thawed ice-rich regolith to gully alcoves	Very high	Late Amazonian	MOC	*Soare et al.* [2007]
Lobate flows, concentric crater fills, arcuate ridges	- glacial origin	Low	Late Amazonian	MOC, MOLA, THEMIS-VIS/NIR, HiRISE, CTX	*Pearce et al.* [2011]

4.2.2 Ground-ice and environmental conditions

In contrast to the DMT hypotheses, *Mellon et al.* [2004] present ground-ice stability models for Mars and suggest that the behavior of ground ice is controlled by a climate- and latitude-dependent water exchange which occurs via vapor diffusion into and out of the subsurface regolith. Ground ice is currently not stable within the upper surface layer in UP, but the region is located near the modeled boundary of the global mean ground-ice stability zone [e.g., *Mellon and Jakosky*, 1995]. The permafrost table is assumed to be stable at a depth of about 1-2 m; this is true especially if ice-cemented layers are insulated by dry, ice-depleted surface deposits [*Mellon et al.*, 2004]. However, the permafrost table could be much closer to the surface and ground ice could be stable due to more favorable local conditions like shaded pole-facing slopes or areas with higher albedo and/or lower thermal inertia (the ability of material to store and conduct heat) [*Mellon et al.*, 2004; *Schorghofer and Aharonson*, 2005]. The quantity of ice in the upper ground (<1 m) in UP detected by the GRS is estimated to be about 7 wt%, e.g., at the Viking Lander 2 (VL2) site (47.7°N, 134.1°E) (see Figure 4.1a) [*Feldman et al.*, 2004]; this estimate is, however, much more than the amount directly measured at VL2 (Table 4.2). Generally, hydrogen concentrations detected by GRS between 40° and 60° latitude on both hemispheres are in the range of 4 wt% to 20 wt% water equivalent [*Boynton et al.*, 2002; *Mitrofanov et al.*, 2002; *Feldman et al.*, 2004].

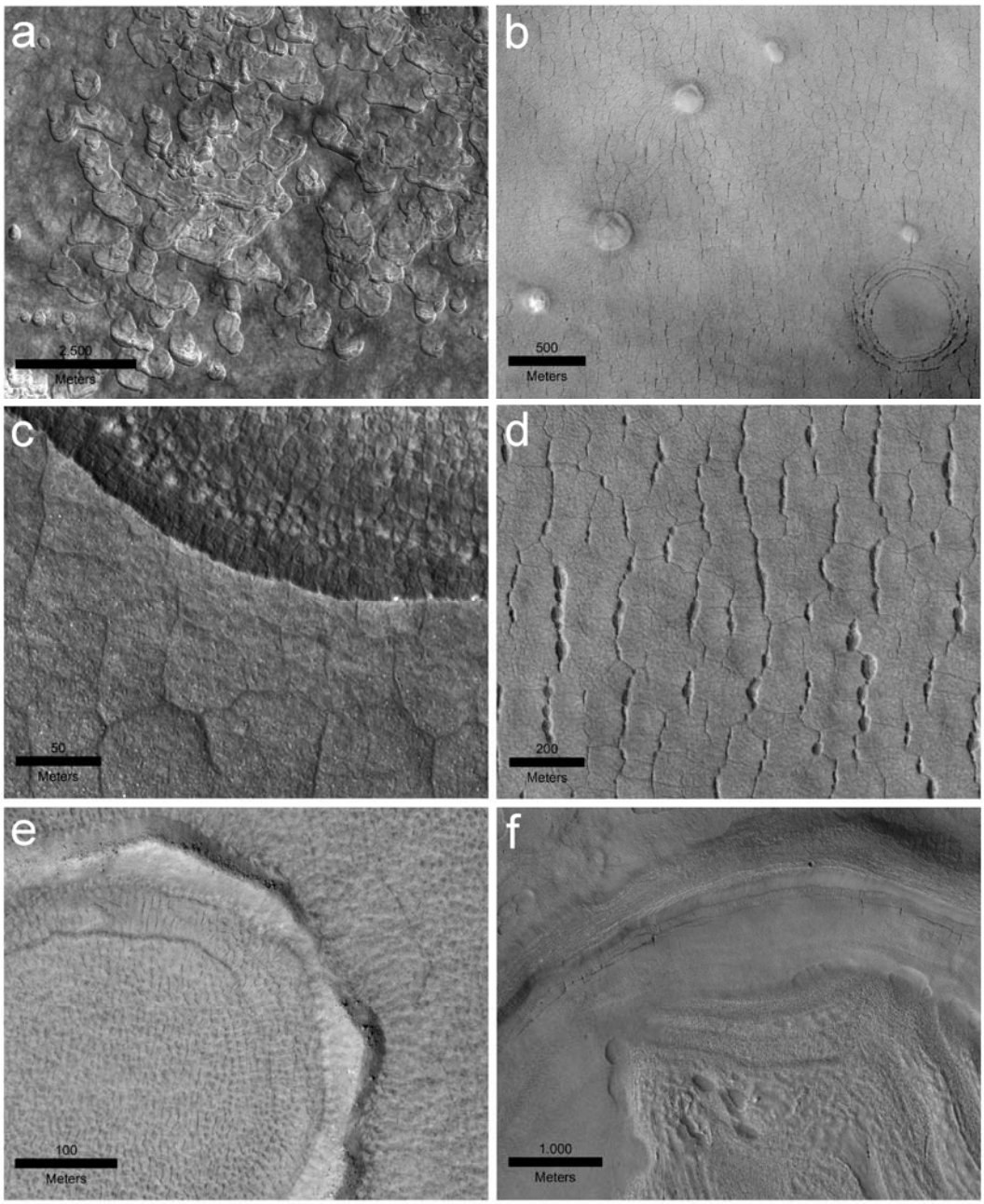

Figure 4.2: Examples of periglacial-like landforms in Utopia Planitia (see also Table 4.1). (a) Scalloped terrain with coalesced asymmetrical depressions extending over different elevations (CTX image: P02_001938_2263_XI_46N267W; 46.37°N, 91.10°E). (b) Group of small fractured mounds interpreted to be analogues to terrestrial pingos (ice-cored mounds) and a polygonal network. Note in the lower right radial and concentric cracks are probably formed due to a subsurface structural weakness caused by a mantle-covered crater (HiRISE Image: PSP_006804_2220; 40.00°N, 83.04°E). (c) Polygonal structures in and around scalloped depressions. Larger polygons on the non-degraded uplands, truncated by the depressions, can be distinguished from small low- and high-centered polygons on a north-facing scalloped depression slope (upper part of the image) (HiRISE image: PSP_001938_2265; 45.00°N, 92.10°E). (d) Polygonal network with well-pronounced N-S trending troughs and pit chains (HiRISE image: PSP_002202_2250; 40.00°N, 84.44°E). (e) and (f) Other features of possible glacial and periglacial origin, which are linked to climate-related accumulation of ice-rich material and landscape modification. (e) Filled crater and "brain terrain" (HiRISE image: PSP_006962_2215; 40.00°N, 90.09°E). (f) Concentric crater fill, rimless depressions, and "brain terrain" described by *Levy et al.* [2009b] (HiRISE image: PSP_002782_2230; 40.00°N, 90.03°E). North is always up.

Morgenstern et al. [2007] showed that the present mean surface temperatures in the western UP region range from ~180 K in winter to ~240 K in summer and thermal modeling indicates that temperatures could reach ~260 K during summer [*Ulrich et al.,* 2010]. This is consistent with the *in situ* observations at the VL2 site (Table 4.2). About 24 cm below the surface, however, temperatures fall to about 222 K [*Kieffer,* 1976] and would probably continue to decrease rapidly to ~180 K in an ice-cemented soil layer as was modeled by *Mellon et al.* [2004] for a latitude of 55°S. Thus, if similar deposits exist for the UP region, temperatures therein would be far below the current Martian frost point of water (typically ~198 k) and temperature fluctuations would probably be restricted to the uppermost soil layers [*Mellon et al.,* 2004; *Schorghofer and Aharonson,* 2005]. If liquid water exists, it could therefore only be stable in an extremely salty solutions (i.e. a cryobrine) [see e.g., *Möhlmann,* 2010a; *Tosca et al.,* 2011] or as thin films of adsorption water [e.g. *Möhlmann,* 2005]. Combining VL2 surface pressure data, which consistently show values above the triple point of water (6.1 mbar, ~273 K; see Table 4.2), temperature data from the Viking orbiter, and MOLA topography data, Lobitz et al. [2001] estimate that pure liquid water could be stable currently in the form of thin films at some locations during 5% of the Martian year. *Haberle et al.* [2001] point out that pressure values in the northern lowland are indeed above 6.1 mbar but temperatures never exceed 273 K and water could therefore not be stable against freezing or evaporation above 30°N. Thus, even if transient liquid water could exist on the surface or even in the subsurface today, it would not act as a geomorphological agent although it could have implications for biological systems. However, as the occurrence of ground ice is the major requirement for liquid water, these discussions elucidate the reality that minor variations in the Martian climate may be sufficient to re-start a water-influenced periglacial landscape evolution in UP. As modeled by *Mellon and Jakosky* [1995], an obliquity exceeding 27° (today ~25°) is required for ice to be stable at latitudes ≥30° and higher and ground ice becomes globally stable at an obliquity exceeding 32°. Thus, most authors (see Table 4.1) suggest that the periglacial landscape dynamics in UP were primarily forced under higher obliquity conditions than exist at present; at that time, ground ice was stable near the surface even in the mid-latitudes, and more favorable climate conditions would have allowed temperatures to increase above the melting point of water (i.e. 273 K) [*Costard, et al.,* 2002; *Kreslavsky et al.,* 2008; *Ulrich et al.,* 2010].

4.2.3 Periglacial Features

4.2.3.1 Scalloped depressions

Asymmetrically-shaped scalloped depressions with steeper slopes facing pole-wards are the most remarkable landforms in western UP (Figure 4.2a). According to *Morgenstern et al.* [2007] about 24% of the area between 40°N-50°N and 80°E-85°E is characterized by scalloped depressions with an increasing coverage from north to south. These small (<3 km wide), shallow (<30 m deep), and rimless depressions have been observed on the southern hemisphere (i.e. Malea

Planum) as well, and show an opposed shape [e.g., *Lefort et al.*, 2010]. Often these depressions coalesce into entire areas of scalloped terrain. Scalloped, rimless, and flat-floored depressions are thought to be the results of ground-ice degradation. Generally, there is an ongoing debate regarding their formation (see also Table 4.1). Some authors suggest ground-ice sublimation as the main formation process, which is driven by insolation and is enhanced on equator-facing slopes [e.g., *Morgenstern et al.*, 2007; *Lefort et al.*, 2009]. A climatically-controlled evolution in which ground-ice sublimation and surface subsidence is combined with an equator-ward lateral development by possible ground-ice thawing on pole-facing slopes during periods of high obliquity is discussed by *Ulrich et al.* [2010] and *Séjourné et al.* [2011]. Others have interpreted the depressions as residues of thermokarst lakes, which would have formed by the thawing of ground ice and the evaporation of ponded water during more benign climate conditions [*Costard and Kargel*, 1995; *Soare et al.*, 2007, 2008]. According to *Lefort et al.* [2010], the northern scallops are older than the southern analogs which formed in less ice-rich and thinner mantle deposits. Generally, as *Milliken and Mustard* [2003] have pointed out, we know that the scalloped terrain did not erode through the entire DMT because the underlying bedrock or substrate is not exposed. This suggests that the mantle in regions influenced by scalloped depressions is probably thicker than the mantle found at lower latitudes [*Milliken and Mustard*, 2003; *Morgenstern et al.*, 2007].

4.2.3.2 Polygonal patterned ground

Polygonal structures are widespread on Mars, especially at mid- and high-latitudes. There is a general consensus that, analogous to terrestrial ice- or sand-wedge polygons, the small-scale polygons (<100 m in diameter) originated by thermal contraction cracking in connection with ground ice, and their distribution is controlled by climate factors [e.g., *Mellon*, 1997; *Mangold*, 2005; *Levy et al.*, 2009a]. However, there is an ongoing debate about whether ice wedges could have been preserved below some small-scale polygonal structures (Table 4.1). *Levy et al.* [2009a] have pointed out that under current atmospheric conditions sand-wedge and sublimation polygons dominate the Martian surface.

The UP region is characterized by distinct small-scale polygonal structures (Figure 4.2c, d), clearly related to the scallop morphology [e.g., *Ulrich et al.*, in press]. These structures exist in different formation stages due to the varying subsurface and climate conditions. The non-degraded uplands surrounding the scalloped depressions show large flat to high-centered polygons, which are outlined by deep and wide troughs. Within the scallops, strips of small low- and high-centered polygons alternate concentrically from the steep north-facing slopes to the depression bottoms (Figure 4.2c). Low-centered polygons show especially strong similarities to active low-centered ice-wedge polygons on Earth [*Seibert and Kargel*, 2001; *Soare et al.*, 2005; *Séjourné et al.*, 2011]. In contrast, *Levy et al.* [2009b] propose that the concentration of low-centered polygons within the

scalloped depressions indicates that locally-enhanced sublimation of ground ice has occurred, and that the formation of these polygons originated by topographic inversion after the sublimation was intensified inside a polygon.

Table 4.2: Some measured and assumed environmental conditions at the Viking Lander 2 site (47.7°N, 134.1°E), representative for UP

Parameter conditions	Quantity / Amount	References
Surface and soil temperatures		
daily	183 to 268 K	Measured at VL2 [*Kieffer*, 1976]
seasonal	~180 to ~240 K ~180 to ~260 K	*Morgenstern et al.* [2007] *Ulrich et al.* [2010]
~24 cm below surface	~222 K	*Kieffer* [1976]
Permafrost table (~1-2 m below surface)	~180 K	*Mellon et al.* [2004]
Upper ground-ice (<1 m)		
Water-equivalent hydrogen	~7 wt%	GRS detection [*Feldman et al.*, 2004]
Soil water content	~2 wt%	Measured at VL2 [*Anderson and Tice*, 1979]
Pressure (daily mean)	~7.5 mbar in summer to ~10 mbar in winter	Measured at VL2 [*Hess et al.*, 1980]
Nutrients (C, H, N, O, P, S)	Available from atmosphere	All compiled as inferred by *Stoker et al.* [2010]
Chemical energy source for microorganisms	Perchlorate and reduced iron	
Salinity	High	
a_w	Very low	
pH	Slightly alkaline	

4.2.3.3 Pingo-like features

Pingos are perennial frost mounds that indicate the presence of permafrost. They are formed by the growth of a massive ice-core and the subsequent up-doming of the overlying terrain surface [see *Gurney*, 1998, and references therein]. Important preconditions for pingo formation are the pressurized migration of liquid water through unfrozen zones within permafrost and, thus, the occurrence of unconsolidated, permeable ground layers [*Gurney*, 1998; *Dundas and McEwen*, 2010; *Grosse and Jones*, 2011]. Pingos are generally conical with circular to elliptical outlines; diameters range up to 600 m and they can be several tens of meters in height [*Gurney*, 1998]. Fractures (i.e. dilation cracks) have often developed in the overlying surface by the radially-

outward displacement of material, and central depressions are commonly formed on collapsing pingos [*Mackay,* 1987].

Small fractured mounds, domes, and ring-shaped features at many sites on Mars were interpreted to be pingos or collapsed pingos [see *Burr et al.,* 2009; *Dundas and McEwen,* 2010; and references therein] (see Table 4.1). Concerning the pingo-like features in UP (Fig. 4.2b), *Burr et al.* [2009] pointed out that the question of the water source required for pingo formation remains open. On Earth hydrostatic closed-system pingos are widespread in arctic lowlands and have formed mostly within drained thermokarst depressions [*Grosse and Jones,* 2011] by re-freezing of unfrozen zones from all sides following water migration under hydrostatic pressure. Hydrologic open-system pingos are mostly distributed in areas with topographic relief (e.g., valleys of east Greenland and Svalbard) and formed by pressurized (artesian) water from a hydraulic head [e.g., *Yoshikawa,* 1993].

Besides the hypotheses of obliquity-driven formation of pingos in a "wet" periglacial environment [*Soare et al.,* 2005, 2008], *de Pablo and Komatsu* [2009] propose a possible magma chamber under the Utopia basin as a heat source for melting ground ice. However, based on a Mars-wide inventory of fracture mounds using HiRISE data, *Dundas and McEwen* [2009] concluded that fractured mounds on the floors of mid-latitude craters morphologically most closely resemble terrestrial pingos [see also *Hauber et al.,* 2011] and suggest that pingo-like features in UP are more likely formed by latitudinally-controlled erosion processes [*Dundas and McEwen,* 2009].

4.3 Permafrost as microbial habitat on Earth

Among all extreme terrestrial habitats [*Rothschild and Mancinelli,* 2001], permafrost is the most promising analogue for a potential life habitat on Mars [e.g. *Gilichinsky et al.,* 1995]. Studies of microbial diversity in permafrost and cold-climate environments show that terrestrial permafrost is colonized by high numbers of very specialized cold-adapted (psychrophilic) microorganisms [*Wagner,* 2008]. They have existed for several million years independent of photosynthetic energy production and can be still active with very low amounts of unfrozen water [e.g., *Rivkina et al.,* 2000; *Gilichinsky et al.,* 2007]. Moreover, the cold and freeze tolerance of permafrost-derived bacteria seems to be associated with salt tolerance [*Vishnivetskaya et al.,* 2000; *Gilichinsky et al.,* 2005; *Morozova and Wagner,* 2007].

In light of the present-day Martian climate and subsurface conditions, Antarctic dry permafrost is often suggested as the most probable analogue environment to Mars. *Gilichinsky et al.* [2007] reported that microorganisms occur in Antarctica as deep as several meters in ~5 Ma old, dry, frozen deposits, and that they are still metabolically active at ground temperatures between −18°C and −28°C. In addition, *Rivkina et al.* [2000] and *Vishnivetskaya et al.* [2000] isolated bacteria from 2-3 Ma old Siberian permafrost deposits at ~25 m and ~40 m depth, respectively, in ground

temperatures of about −10°C. The activity of methanogenic archaea for instance is also evident in 24-m-deep Siberian Late Pleistocene ice-rich sediments [*Griess et al.,* in prep].

In spite of the extreme habitat conditions in deeper permafrost zones, the active layer, especially, is subjected to drastic variations of environmental conditions (e.g., temperature, salinity, soil pressure, moisture, oxygen) due to strong seasonal changes in air temperature (approx. between −50°C and +30°C), snow cover, and related freeze and thaw cycles [e.g., *Yershov*, 2004]. Differences in micro-relief formed by cryogenic processes in the active layer also influence the composition and activity of microbial communities [e.g., *Wagner et al.,* 2005; *Liebner et al.,* 2008]. Detailed analyses of microbial community compositions within the active layer of a low-centered ice-wedge polygon in the Siberian Lena Delta, for instance, revealed great abundance and diversity, a diversity as large as or even greater than the diversity seen in soil ecosystems existing in more moderate conditions [*Wagner et al.,* 2005].

With respect to Mars and its potential habitability, the biological activity at low temperatures in relation to low a_w is of special interest [*Kminek et al.,* 2010]. Several studies show that microbial communities isolated from permafrost environments are able to remain metabolically active down to −20°C (~250 K) [*Rivkina et al.,* 2000; *Jakosky et al.,* 2003]. According to *Beaty et al.* [2006] and *Kminek et al.* [2010], no microbial reproduction below −20°C and below a_w=0.5 has been demonstrated so far. However, it is well known that microorganisms may survive or be active at temperatures far below −20°C [see e.g., *Horneck,* 2000; *de Vera et al.,* 2010]. Besides resistance to low temperature and a high desiccation tolerance, the metabolic (e.g., potential to grow lithoautotrophic without any organic carbon source) and genetic (e.g., regulation of specific genes, initialization of repair mechanisms) potential of the microorganisms is important to survive and adapt to changing environmental conditions like in terrestrial or Martian permafrost ecosystems. Such organisms are most likely to be analogous to any organism that could exist under Martian environmental conditions [e.g., *Chapelle et al.,* 2002; *Morozova et al.,* 2007]; this will be discussed in detail below.

4.4 Habitability during events of periglacial landscape evolution in UP

The formation of a volatile-rich mantle deposit (consisting of an ice and dust mixture) under higher obliquity conditions is considered to be the starting point for a simple conceptual model of periglacial landscape evolution in UP. Strong seasonal temperature gradients allowed deep thermal contraction cracking more or less simultaneously, which led to the ubiquitous formation of large polygonal systems on the former UP surface. This event was followed by the degradation of ground ice, which caused volume loss and surface subsidence and resulted in the formation of rimless, scalloped depressions. Different stages of ice loss and lateral basin growth are marked by interior

step-like ridges elongated subparallel to the steep north-facing scarps. The scalloped depression formation, in turn, is postdated by the development of different small low- and high-centered polygonal patterns located within the depressions. Finally, fractured mounds (i.e. pingo-like features) would have been formed simultaneously with the three events just described, because they are almost free standing and not located within scalloped depressions but are crossed by radial cracks (see Figure 4.2b).

According to *Ulrich et al.* [2010, in press], almost all periglacial landforms in UP were formed in relation to high ground-ice contents and partly to by ground-ice thawing and the existence of transient liquid water. However, the absolute timing and duration of these events are still unknown, in particular the length of periods with temperatures around 273 K that would have allowed the existence of liquid water. Mars experienced a period of high mean obliquity (~35° ± 10°) around 10 to 5 Ma ago, with a transition period around 5-4 Ma to modern conditions of lower mean obliquity (~25° ± 10°) [*Laskar et al.,* 2004]. When the obliquity is high (>35 to 45°), ground ice could be stable near the surface in the mid-latitudes and surface temperatures could reach 273 K during summer due to increased insolation [*Mellon and Jakosky,* 1995; *Costard et al.,* 2002; *Ulrich et al.,* 2010]. Such favorable conditions would be more probable, however, if the orbit was both highly oblique and highly eccentric and the Martian summer coincided with the perihelion. In accordance to *Paige* [2002], summer temperatures remain well above the melting point of water throughout the Martian day if obliquity approaches 45°, eccentricity approaches 0.11, and the summer in one of both hemispheres coincides with perihelion. Based on Martian climate models and our model results [*Ulrich et al.,* 2010], we estimate that a minimum threshold for liquid water and habitable conditions will occur in UP if an obliquity higher than 35° coincides with an eccentricity higher than 0.08 (more likely >0.1), and the northern Martian summer (solar longitude L_s = 90°-180°) occurs at perihelion. Using the calculations from *Laskar et al.* [2004], such distinct periods could be determined for the last 10 Ma (Figure 4.3). For the time before 4 Ma ago, 28 such periods were distinguished. These periods cover time spans between 1,000 and 14,000 consecutive years and return at intervals of between 41,000 and 1.38 million years. The shortest recurrence intervals of about 41,000 to 48,000 years occurred between ~9.82 Ma and ~9.45 Ma ago. If the eccentricity threshold is set to 0.1, only 7 such periods remain. The latest periods of 1,000 and 4,000 consecutive years that meet these requirements started 4.330 Ma and 4.439 Ma ago, respectively. One period occurred between 7.864 Ma and 7.855 Ma and 4 periods of 1,000 to 12,000 consecutive years occurred between ~9.76 Ma and ~9.45 Ma ago (Figure 4.3). At these times, potentially habitable conditions most likely existed regionally in UP during summer, and liquid water was probably stable for long enough to act as a periglacial agent, assuming a mean atmospheric pressure identical to that of today (Table 4.2) or even higher [see *Phillips et al.,* 2011]. In particular, the periods 7.864 Ma to 7.855 Ma ago and ~9.76 Ma to ~9.45 Ma ago correspond with estimated times of active layer processes in the mid-latitudes [*Kreslavsky et al.,* 2008]. During

periods when eccentricity was also higher than 0.08, habitable conditions could have occurred, at least locally, under specific relief conditions, like exposed slopes.

These results should not be regarded as definitive and precise predictions of when Mars was habitable. Instead, they are meant to provide a temporal estimate of how long and in which intervals liquid water might have occurred in the Late Amazonian. Besides the climate-driven temperature changes, seasonal and diurnal changes must also be considered in future discussions of habitability during the last 10 Ma on Mars. As was shown by *Ulrich et al.* [2010], night-time temperatures drop to ~200 K even at >45° obliquity, and below 200 K at ~35° obliquity. Similar variations may be expected for seasonal temperature changes.

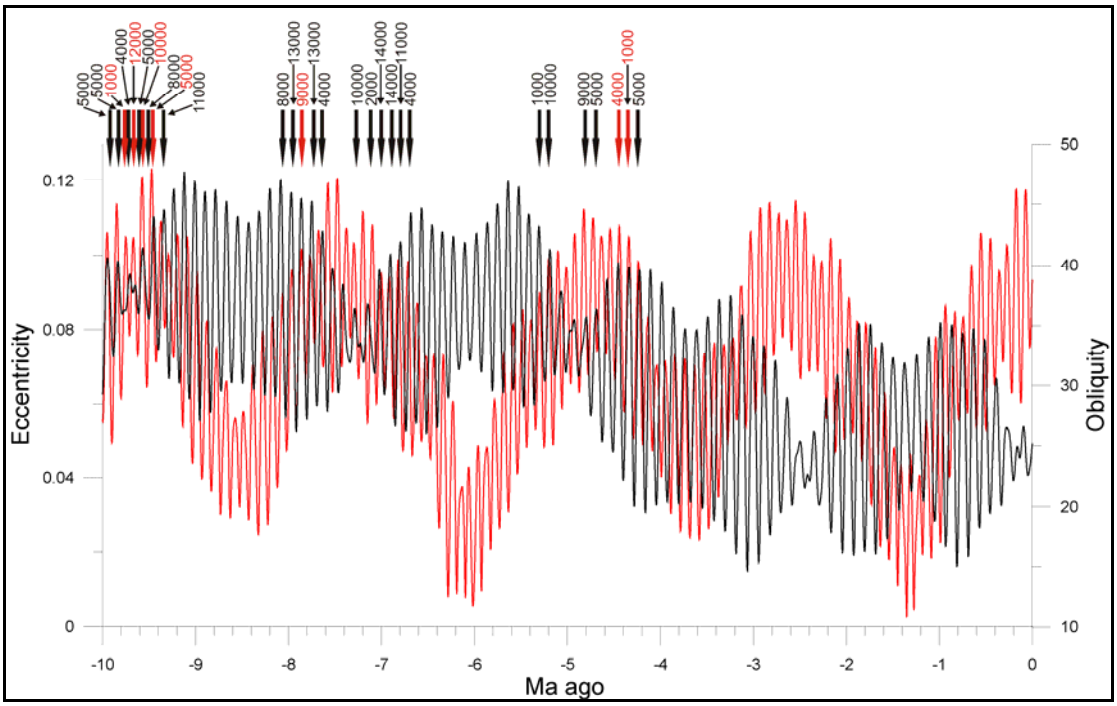

Figure 4.3: Variations in Mars' obliquity (black line) and eccentricity (red line) for the last 10 Ma [data from *Laskar et al.*, 2004] and possible habitable periods in which the northern summer (Ls 90 – 180°) coincided with perihelion, the obliquity was above 35°, and the eccentricity was above 0.08 (black arrows) or above 0.1 (red arrows). Numbers above the arrows indicate the period's duration if these conditions occurred successively every 1000 years, the minimum time step modeled by *Laskar et al.* [2004].

In the last 4 Ma, the threshold criteria for liquid water and habitable conditions discussed above were never met. Although several excursions to higher obliquity (~35°) might have facilitated temperatures of >273 K during summer, these excursions did not coincide with a higher eccentricity (Figure 4.3). It is therefore questionable whether liquid water could have existed during such periods to act as a geomorphic agent. The morphology of gullies in the mid-latitudes, however, has been frequently interpreted as the result of liquid water activity and the origin of these gullies has been dated to fairly recent times [e.g., ~300 ka ago, *Reiss et al.*, 2004; <2.4 Ma ago, *Schon et al.*, 2009a].

If periglacial landforms in UP are related to the existence of liquid water, the influence of water was restricted to conjuncture periods of favorable orbital parameters as shown in Figure 4.3. The existence of locally habitable conditions would therefore be closely connected to the geomorphological situation during the formation of individual permafrost features. Specific locations probably provide climatic niches which exhibit a relatively higher likelihood of habitable conditions (Figure 4.4).

The morphology of scalloped depressions suggests high ground-ice contents. These depressions are formed by spatially-varying ground-ice conditions and changes in insolation and temperature, which lead to local thawing within the depressions. In particular, the steep pole-facing slopes receive the highest insolation rates, and temperatures can be well above 273 K at high obliquity conditions (~45°). Night-time temperatures are warmer on these slopes than on flat surfaces or on equator-facing slopes [*Paige,* 2002; *Ulrich et al.,* 2010]. Today, pole-facing slopes in scalloped depressions are less insolated and permanently shaded, which results in lower temperature gradients and higher ground-ice stability near the slope surface. This would diminish deeper subsurface desiccation [e.g., *Mellon et al.,* 2004]. The unique appearance of the polygonal structures in and around the scalloped depressions in UP suggests that higher temperatures and stronger seasonal temperature gradients existed during their formation. It is conceivable that habitable conditions could exist in particular within polygonal cracks, if an occasional water supply supported the formation of ice-wedge-like polygons during high obliquity conditions, especially on the steeper pole-facing depression slopes [*Kreslavsky et al.,* 2008] (Figure 4.4). Considering that drier conditions [see *Levy et al.,* 2009a,b] existed during the formation of the larger polygons around the scallops, deep thermal contraction cracks partly filled with fine-grained material [*Lefort et al.,* 2009] would provide weakness zones where thermal waves and higher temperatures could reach deeper subsurface layers (Figure 4.4). Furthermore, seasonal thermal waves could penetrate deeper into the ground during high obliquity conditions than is currently possible [*Mellon,* 1997], inducing more benign micro-climatic conditions within the ice-cemented subsurface soil. If the pingo-like features in UP were indeed formed by the growth of a massive ice-core (see above) they must be considered as landforms with very high potential for habitable conditions (Figure 4.4).

Our “dry” approach to Martian periglacial dynamics contradicts the “wet” periglacial evolution suggested by e.g., *Soare et al.* [2008] (see also Table 4.1). Besides the lack of geomorphological indicators of long-lived standing bodies of water in UP [*Lefort et al.,* 2009; *Ulrich et al.,* 2010], a wet scenario is also not likely because of the seasonal and diurnal temperature variations mentioned above. Since the periglacial landforms appear unaltered and well-preserved under the current atmospheric conditions, they must have been formed after the deposition of the latest ice-rich deposits. If the suggested periglacial landform evolution corresponds to the estimated periods of favorable climatic conditions (Figure 4.3), it appears unlikely that the last mantle deposition occurred during the most recent obliquity excursion around 0.4 – 2.1 Ma [*Head et al.,* 2003]. If the

surface age of the youngest mantle in UP is really only ~1.5 Ma, as determined by the analysis of crater size-frequency distributions [e.g., *Levy et al.*, 2009b], its thickness would have had to be very small to prevent it from obscuring the permafrost morphology in UP [see *Willmes et al.*, in revision]. This seems to be inconsistent with the thickness of the mantle material (Morgenstern et al., 2007), which suggests its deposition over tens of millions of years [e.g., *Madeleine et al.*, 2009]. *Levrard et al.* [2004] concluded that the latest mantle was formed between ~5-3 Ma ago. Moreover, recent crater dating of the DMT in Malea Planum (~55°-60°S), which is the closest morphological analogue landscape on Mars to UP, resulted in a mantle deposition age of ~3-5 Ma [*Willmes et al.*, in revision]. According to these chronological constraints, the latest major permafrost landform modification in UP should be considered to have occurred during periods when high obliquity and high eccentricity coincided, ~4.0 to 5.6 Ma ago (Figure 4.3).

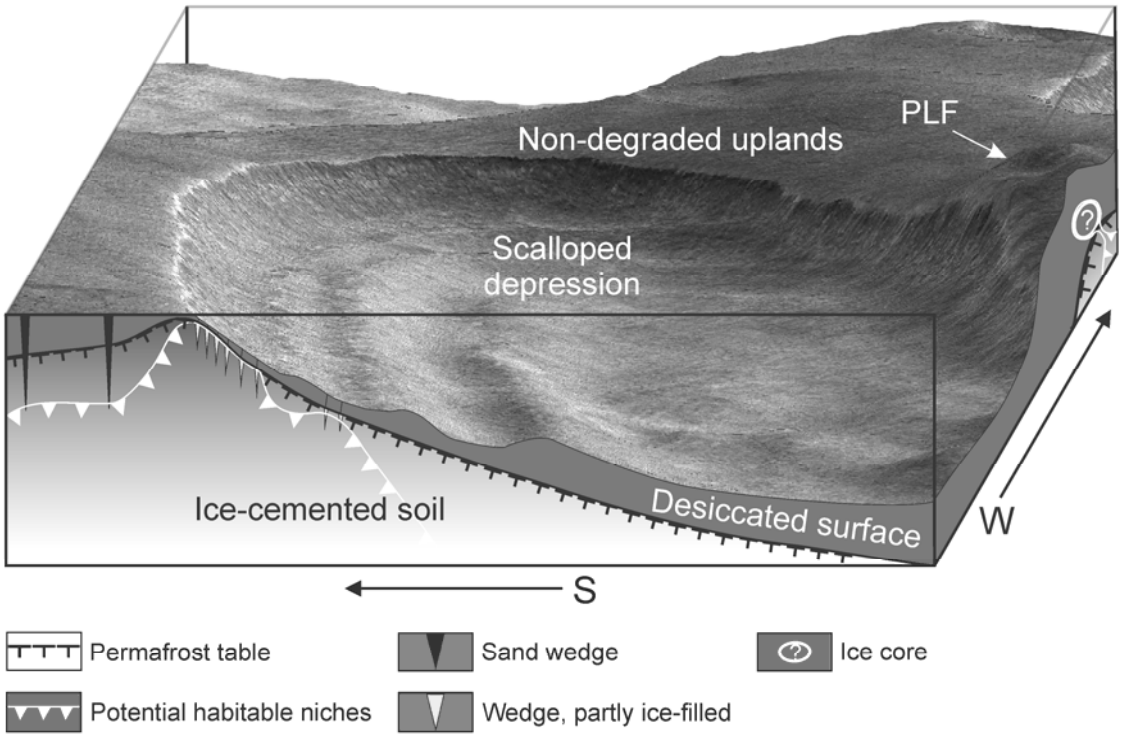

Figure 4.4: Block scheme of the periglacial landform assemblages in UP, in relation to estimated subsurface conditions and potential present-day habitable niches. Habitable niches could have resulted from regional habitable conditions in UP during landform formation under the climate periods highlighted in Figure 4.3. For further discussion see text. PLF, pingo-like feature (The question mark below indicate a hypothetical ice core). The depression is about 1000 m in diameter. Ground depth is not to scale. Portion of HiRISE image PSP_001938_2265 superposed on HiRISE DEM (stereo pair: PSP_001938_2265_PSP_002439_2265).

4.5 Could life have potentially survived during the last 10 Ma in UP?

Several paleoclimate models of early Mars have shown that, prior to 3.8 Ga ago, Mars was characterized by more moderate temperatures than today, the presence of liquid water, and an

anoxic atmosphere, conditions comparable to those extant on early Earth [*Durham et al.,* 1989; *McKay et al.,* 1992] at a time when the evolution of microorganisms had already started [*Schopf,* 1993]. Therefore, the possibility of finding present or past evidence of life (most likely microbial life) on Mars exists, hypothetically. Assuming that early life developed on Mars, Martian life must have either adapted to drastically changing environmental conditions or become extinct.

A basic requirement for any form of life as we know it is a biologically usable carbon and energy source. Since organic carbon has not been detected so far at the Martian surface [*Klein,* 1998], the most probable carbon source might be carbon dioxide, which can be used to generate biomass via autotrophic processes. Carbon dioxide can also be used as an electron donor for the oxidation of hydrogen or other inorganic electron acceptors (e.g., Fe^{3+}, MnO_2, SO_4^{2-}) to generate the energy necessary for life. In addition to carbon and energy, life requires some other specific elements to generate biomass, such as H, N, O, P, and S. Most of these elements can be found on Mars and in UP [reviewed in *Stoker et al.,* 2010] (see Table 4.2); therefore, this does not appear to be a problem for potential life on Mars.

Besides a carbon-based metabolism with an adequate source of energy, liquid water is considered to be one of the prerequisites for habitability. Several studies have indicated that water flowed on the surface of early Mars [e.g., *Carr,* 1996; *Baker,* 2001; *Squyres et al.,* 2004; *Andrews-Hanna and Lewis,* 2011]. The environmental conditions on present-day Mars do not allow liquid water to be permanently stable at the surface, but water could periodically become available for microorganisms under changing seasonal and diurnal temperature and pressure conditions as interfacial water or cryobrines [*Möhlmann,* 2010a]. One possibility for survival of Martian microorganisms could be subsurface ecosystems such as deep sediments, where liquid-like (‘unfrozen’) adsorption water could play a key role in allowing the transport of nutrients and the waste products of biological processes [*Möhlmann,* 2005].

Temperature is another important factor regulating the activity and survival of microorganisms. The minimum temperature for growth of microorganisms was recently reported to be −35°C (~238 K) [*Panikov and Sizova,* 2007]. Growth yields of isolated microorganisms were maintained down to −17°C; these yields were similar to those obtained from microorganisms kept at temperatures above the freezing point. Between −18°C and −35°C, growth was only detectable for three weeks after cooling. After that, metabolic activity declined to zero, and the microorganisms entered a state of reversible dormancy. These findings are in accordance with the grouping of microbial metabolic rates of cold-adapted microorganisms that was proposed by *Price and Sowers* [2004]: rates of their first group are sufficient for microbial growth; those of their second group are sufficient for metabolism but too low for growth; rates of their third group allow survival in a dormant state accompanied by macromolecular damage repair. Diurnal average subsurface temperature profiles calculated for the mid-latitudes on Mars indicated temperatures as low as around −90°C (~180 K) in an ice-cemented soil [*Mellon et al.,* 2004]. However, as mentioned

above (see also chapter 4.4), it seems feasible that higher temperatures could be reached in deeper subsurface layers because thermal waves follow deep contraction cracks [*Mellon,* 1997]. This offers an opportunity for microbial life, since it was shown in a Mars simulation experiment that microorganisms from terrestrial permafrost environments can survive a diurnal temperature profile between about −75°C and 20°C [*Morozova et al.,* 2007]. In addition, *McGrath et al.* [1994] showed that the intracellular water in fossil bacteria from permafrost soils was not crystallized as ice even at an extreme temperature of −150°C.

Regardless of the extreme conditions described for microbial life on present Mars, the present study showed that during the last 10 Ma distinct periods existed in the UP region which enabled liquid water to exist, depending on the obliquity and eccentricity of Mars (Figure 4.3). If life developed on early Mars during the first main climate stage, which was a water-rich and cold epoch (Noachian to Early Hesperian) [*Fairén et al.,* 2010], and this life survived by adaptation to the drastically changing environmental conditions, UP seems to provide some of the best isolated niches for life during the above-mentioned time period. Potential niches for microbial life include for instance, permafrost features such as polygonal structures with deep contraction cracks and ground ice as well as the pole-facing slopes of asymmetrically-shaped scalloped depressions, which are less thoroughly dried compared to the opposite sites (Figure 4.4).

Comparable environments exist in Arctic and Antarctic permafrost on Earth. From the microbiological point of view the best-studied terrestrial permafrost analogues are low-centered ice-wedge polygons, cryopegs (over-cooled water brine lenses), and Holocene to Pliocene permafrost deposits [reviewed in *Wagner,* 2008]. In spite of the harsh environmental conditions (e.g., low temperature, high salinity, low a_w, long-lasting background radiation resulting from accumulation over geological time-scales) of terrestrial permafrost, all the habitats are characterized by high cell numbers and a great diversity within the microbial communities [*Vishnivetskaya et al.,* 2006; *Steven et al.,* 2007; *Wagner et al.,* 2007; *Liebner et al.,* 2008; *Koch et al.,* 2009; *Yergeau et al.,* 2010].

Cryopegs, for example, which are lenses of ground containing over-cooled water brines that are perennially cryotic (–9°C to −11°C), are discussed as providing one potential niche for remaining life on Mars [*Gilichinsky et al.,* 2005]. Freezing of terrestrial cryopegs is prevented by freezing-point depression due to the high salt content (140-300 g l^{-1}) of the pore water. A variety of salt- (halophilic) and cold- (psychrophilic) adapted microorganisms isolated from cryopegs of Late Pleistocene age indicate the possibility of a trophic food chain within the microbial communities of this specific niche [*Gilichinsky et al.,* 2005; *Shcherbakova et al.,* 2005].

Viable microorganisms have survived even in several-million-years-old permafrost deposits [*Vorobyova et al.,* 1997; *Gilichinsky et al.,* 2007]. These microorganisms constitute the residue of the autochthon population within the paleosoils; this population was enclosed during deposition of fresh sediments. Survival could have been possible by anabiosis (living in a dormant stage) or by

reduced metabolic activity in unfrozen water films. The latter was recently shown for methane-producing microorganisms (methanogenic archaea, Figure 4.5) [*Wagner et al.*, 2007; *Koch et al.*, 2009; *Griess et al.*, in prep.]. Methanogenic archaea, which are considered to be one of the initial organisms of life on Earth, are strictly anaerobic microbes characterized by a lithoautotrophic metabolism [*Hedderich and Whiteman*, 2006]. They gain energy by the oxidation of inorganic substances such as hydrogen. Carbon dioxide can be used as the only carbon source. The existence of this kind of metabolism is one of the most important presumptions for long-term survival of microorganisms in extreme environments like terrestrial permafrost [*Morita*, 2000].

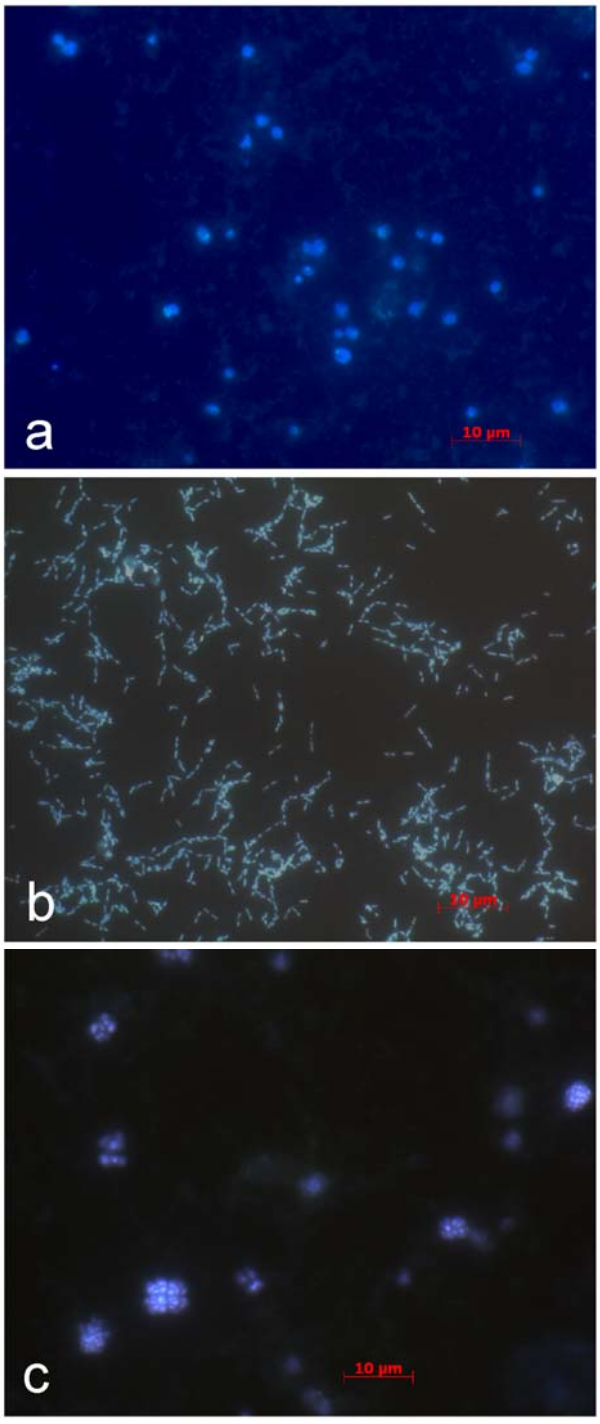

Figure 4.5:
DAPI stained fluorescence microscopic images of methanogenic archaea isolated from Siberian permafrost environments; (a) Candidatus *Methanosarcina gelisolum* SMA-21, (b) *Methanobacterium* SMA-26, (c) *Methanosarcina* SMA-17.

It was further shown that methanogens from Siberian permafrost are multi-tolerant against various stress conditions. For example, *Methanosarcina* SMA-21 (*Candidatus Ms. gelisolum*, Figure 4.5) [*Wagner et al.*, in prep.], isolated from Siberian permafrost-affected soils, is characterized by an extreme tolerance to low temperature (−78°C), high salinity (up to 6M NaCl), prolonged starvation, and desiccation (a_w shifts between 0.1 and 0.9) [*Morozova et al.*, 2007; *Morozova and Wagner*, 2007]. This strain also showed an extreme resistance to the effects of UV (F_{37} = 14-15 kJ m^{-2}) and ionizing radiation (D_{37} = 6-7 kGy; unpublished data), which is comparable to the most radiation-resistant bacteria *Deinococcus radiodurans* [*Ito et al.*, 1983]. Furthermore, *Methanosarcina* SMA-21 and other methanogens from Siberian permafrost (Figure 4.5) survived for 3 weeks under simulated thermo-physical Martian conditions, while the reference organisms from non-permafrost environments did not survive [*Morozova et al.*, 2007]. Additionally, *Kral et al.* [2004] showed that specific methanogens are able to grow on a Mars soil simulant when they are supplied with carbon dioxide, molecular hydrogen, and varying amounts of water.

All these pieces of evidence demonstrate the potential of a subsurface microbial community dominated by lithoautotrophic growing microorganisms (e.g., methanogens) [*Chapelle et al.*, 2002] to exist within the periglacial environments of the Martian mid-latitudes (i.e. UP). The results presented about the environmental conditions in UP during the last 10 Ma and the above-mentioned findings of other authors on the adaptation and survival of microorganisms, particularly methanogenic archaea, indicate that this region seems to be habitable at least for highly-specialized microorganisms comparable to methanogens from terrestrial permafrost. The special geomorphological and climatic situation of the Martian mid-latitudes generally, as was discussed for UP in particular, between the very cold polar regions and the deeply desiccated low-latitudes highly increases their potential habitability.

4.6 Conclusions

In this study we used an interdisciplinary approach to discuss the potential habitability of the Martian mid-latitudes with a focus on permafrost landforms in UP. Several past and present environmental ground-ice conditions, deduced from our own previous geomorphological studies and the literature, are synthesized with respect to the allowed environmental range for survival and even growth of microorganisms. Lithoautotrophic microorganisms seem to be the most likely and the best-adapted microbial communities to dominate such permafrost environments, as they dominate similar environments on Earth (Figure 4.5). It has been suggested that the short-lived trace gas methane exists in the Martian atmosphere [e.g., *Mumma et al.*, 2009]. This suggestions has not yet been sufficiently validated [see, e.g., *Zahnle et al.*, 2011], but if this methane exists, it could have originated from biological methane production similar to those performed by methanogenic archaea on Earth. Capillary waters or salt-rich undercooled solutions acting like pure

water could have provided physiology-supporting fluids, even at very low temperatures [*Möhlmann*, 2010a].

Liquid water involved in the evolution of permafrost landforms on Mars could have allowed the development of highly-specialized microorganisms; these microorganisms might have survived in micro-climatic permafrost niches, such as deep thermal contraction cracks, ground ice situated close to the surface on pole-facing slopes, or even pingo-like features. The numerical models by *Laskar et al.* [2004] extracted specific, but few periods during the last 10 Ma which meet the requirements of coinciding high obliquity (>35°), high eccentricity (>0.1), and northern summer at perihelion; at such times thaw processes and liquid water could have regionally existed in UP to influence periglacial landscape evolution in Martian mantle deposits.

Finally, *Kminek et al.* [2010] define a "special region" on Mars "as a region within which terrestrial organisms may be able to replicate, OR a region which is interpreted to have a high potential for the existence of extant Martian life". With respect to the past and present environmental conditions influencing permafrost landforms in UP, Martian periglacial features might be classified as special regions in future searches for evidence of life on Mars.

Acknowledgements

This research and all involved authors are supported by grants from the Helmholtz Association through the "Planetary Evolution and Life" research alliance. We thank Janosch Malaszkiewicz (AWI Potsdam, Germany) for kindly providing microscopic images of methanogenic archaea. The paper benefited by English proof-reading and valuable comments from Candace S. O'Connor (UAF, Fairbanks, Alaska).

5. Synthesis: The question about periglacial landscape evolution and habitability on Mars: Lessons learned from Earth

The major goal of this thesis was to deduce and reconstruct processes and environmental conditions responsible for the formation of periglacial landforms on Mars. It has already been suggested that these landforms were shaped by ground-ice (i.e. permafrost) dynamics. Therefore, the intention was, first, to understand the environmental conditions influencing certain permafrost features within arctic landscapes on Earth, and then to transfer this knowledge to Martian periglacial landscapes by analogical reasoning [*Baker,* 2008]. In addition, quantitative analyses of landform morphology were applied to extend the studies beyond the mostly descriptive (i.e. qualitative) previously published geomorphological comparisons between Earth and Mars. Depressions formed by permafrost degradation and polygonal patterned ground were selected as typical periglacial relief features for these morphometric analyses, modeling of process-controlling factors, and multivariate statistics.

5.1 Terrestrial periglacial landscape analogues to Mars

Detailed morphometric investigations comparing a large thermokarst depression in Siberian ice-rich deposits to scalloped depressions formed in Martian mid-latitude mantling deposits revealed a comparable asymmetrical morphology, which was interpreted as an indication of the lateral development of both kinds of depressions (Figure 5.1, Chapter 2). Insolation was identified as a major factor influencing retrogressive growth in both cases (Figures 2.9 and 2.17). Since size and depth of terrestrial thermokarst depressions are known to be related to the ice content of the deposits in which these depressions are formed (Figure 2.8), it was concluded that the development of the Martian scalloped depressions must be connected to ground-ice contents higher than the amounts indicated by remote-sensing measurements for the uppermost 1 m of sediments in the Utopia Planitia region (see Figure 1.2A) [*Boynton et al.,* 2002, *Mitrofanov et al.,* 2002, *Feldman et al.,* 2004]. Moreover, based on the knowledge of terrestrial thermokarst and on the specific morphology of the Martian scalloped terrain (Figure 2.14), the hypothesis that the Martian depressions are formed by thermokarst (i.e. wet periglacial) processes [e.g., *Soare et al.,* 2007, 2008] has been rejected (Figure 5.1).

Quantitative terrain analyses of ice-wedge polygons in the Adventdalen (Svalbard) and small-scale polygonal structures in Martian mid-latitudes revealed a comparable thermal contraction cracking genesis (Chapter 3), indicating that the seasonal variations in ground temperature that are essential for thermal contraction cracking existed in the Martian study area. Differences between the size and morphology of the polygons on Earth and on Mars are believed to reflect regional and local landscape dynamics (Table 3.5). In particular, the smallest studied Martian low-centered

polygons showed very close analogies to active ice-wedge polygons on Svalbard (Figure 5.2). It was thus concluded that thermal contraction cracking is very likely to be active currently only in certain micro-climatic niches (Figure 3.14) where fine-grained ice-rich deposits exist very close to the surface. Temperatures above the melting point of water are not necessary to enable this process to occur. If an occasional local liquid-water supply existed, however, it is conceivable that composite wedges were formed under past climate conditions (Figure 5.2, see Section 3.5.3). Under present-day hydrological and climatic conditions in Martian mid-latitudes (see Table 4.2), dry degradation processes are the dominant influence on polygon morphology in Utopia Planitia on a regional scale.

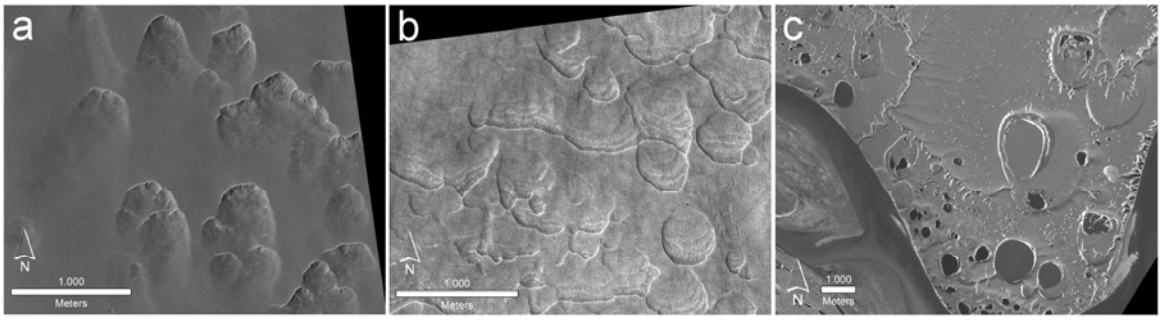

Figure 5.1: Comparison of the analogous ground-ice degradation features investigated on Mars and Earth. (a) Scalloped depressions on the southern hemisphere of Mars. (b) Scalloped depressions on the northern Martian hemisphere. Note the opposite asymmetrical shape of the southern and northern depressions. (c) Landscape characterized by thermokarst depressions on Kurungnakh Island (Lena Delta, NE Siberia). Note the channels connecting and draining the thermokarst depressions. Such features cannot be seen in *(a)* and *(b)*.

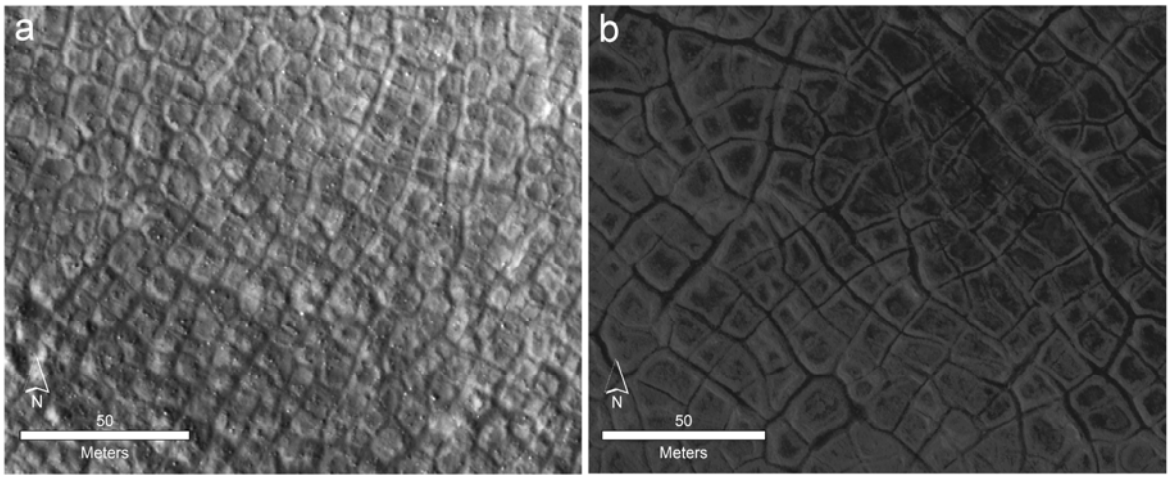

Figure 5.2: Comparison of the thermal contraction polygons investigated on Mars and Earth. (a) Small low- and high-centered polygons on the north-facing slope of a scalloped depression in Utopia Planitia. Thermal contraction cracking might be active here if an ice-table exists very close to the surface. The formation of composite wedges in the past might have affected the origin of the low-lying centers. (b) Active low-centered ice-wedge polygons in the Adventdalen (Central Spitsbergen).

Different scenarios for landscape evolution in Martian mid-latitude craters are discussed in the appendix of this thesis [Hauber et al., 2011], which are based on additional analogue studies of e.g. gullies, striped patterned ground, pingo mounds, and protalus ramparts in the Adventdalen (Svalbard). The differing interpretations of periglacial landscape evolution in Martian mid-latitude impact craters in a dry, wet, or snow scenario reveal the different possible implications for interpreting landscapes on Mars.

5.2 Liquid water and habitable zones on Mars

Generally, the existence of liquid water on present-day Mars facilitated by, e.g., the lowered melting point of brines, cannot be excluded. Although whether liquid water exists on Mars today remains an open question, it may be assumed that the thawing of ground-ice, if it were happening today, would be restricted to small micro-climatic niches (e.g., exposed slopes). In a regional context, ground ice in Utopia Planitia probably exists at greater depths than the depths to which thermal waves could penetrate into the subsurface. Furthermore, temperatures within the ice-cemented soil are probably at or below the current Martian freezing point (typically -72° C) [e.g., *Mellon et al.*, 2004] and even below the eutectic temperatures of several salty solutions [e.g., *Möhlmann and Thomsen*, 2011]. Therefore, it is obvious that in a regional context dry periglacial processes dominate the Martian permafrost geomorphology today and have done so throughout most recent times; this stands in clear contrast to the freeze-thaw conditions in the studied terrestrial analogue sites (Figure 5.3, see also Figure 1.3). However, it seems mandatory that the discussion on climate and subsurface conditions on Mars inferred from the study of specific morphological features requires a more integrated view of diverse landforms in a landscape context (Chapter 4 and Appendix). Unambiguous interpretations of Martian surface features as permafrost landforms, and even the influence of water in periglacial landscape evolution, is not without problems, because different processes acting in different environments can produce landforms that appear superficially similar. For example, it is shown in this thesis appendix that certain Martian landforms (e.g., fractured mounds) can easily be misinterpreted as periglacial landforms (e.g., open-system pingos, see Figure A13) if liquid water in the subsurface is presupposed. Thus, other scenarios for landscape evolution in the Martian northern mid-latitude lowlands cannot be excluded (Figure 1.2). Summarizing the insights from terrestrial analogue studies for periglacial landscape evolution on Mars, however, it was concluded in Section 4.4 that thaw processes and liquid water have played a role in the development of permafrost landforms in Utopia Planitia, but climate conditions allowing this to occur were rare in the Martian past and have been almost absent in the last 4 Ma (Figure 4.3). The results are consistent with estimations of rare times during which active-layer processes could have occurred on the Martian surface [*Kreslavsky et al.*, 2008]. It is also stated by *Kreslavsky et al.* [2008] that, in accordance with the modeled trend of Mars' orbital

parameters [*Laskar et al.*, 2004], it is not likely that conditions will be conducive to active-layer formation in the foreseeable future.

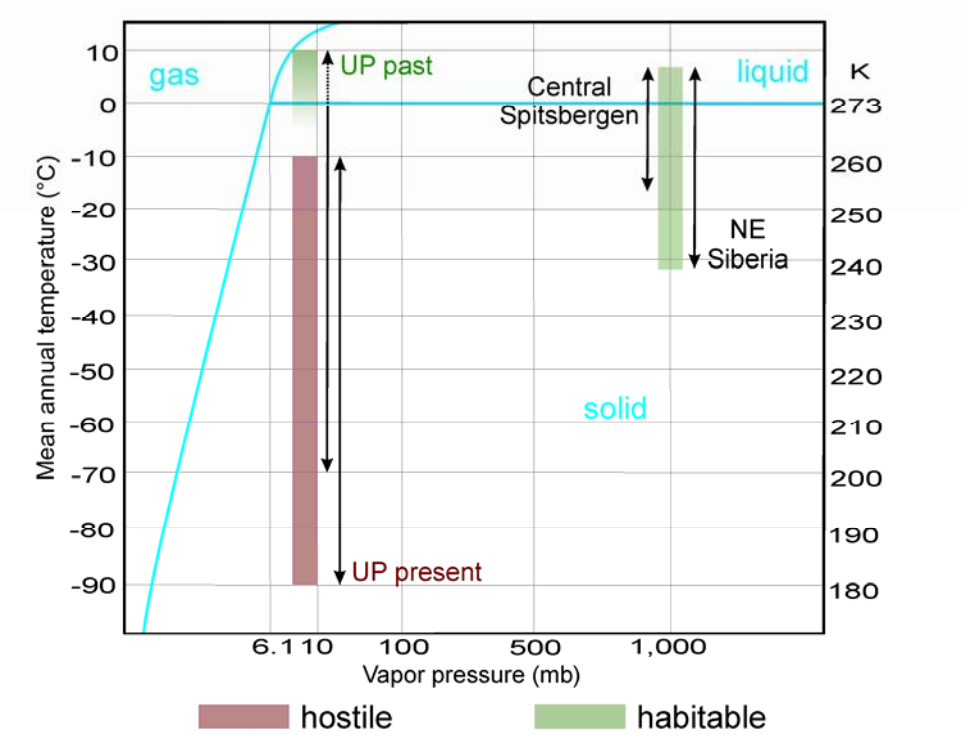

Figure 5.3: This water-phase diagram compares the current mean temperature and pressure ranges and habitability of the study regions investigated on Earth and Mars (Drawing is not to scale). Also shown is the Utopia Planitia (UP) temperature range that is suggested in this work to have existed in the past, during Late Amazonian periods of favorable orbital configurations (see also Figure 4.3). In accordance with *Phillips et al.* [2011] it is also likely that the pressure increased with increasing obliquity due to CO_2 release into the atmosphere from degrading Martian polar caps. Higher summer temperatures and pressures at those times, which rose above the triple point (~273 K, 6.1 mb), would increase potential UP habitability.

Although it is suggested here that transient liquid water and occasional thaw processes have influenced periglacial landscape evolution in Utopia Planitia in the past, the results from analogue studies and geomorphometric analyses presented in this thesis contradict the former existence of long-standing water bodies during the Late Amazonian [*Soare et al.*, 2008; *Soare and Osinski*, 2009], and it is equally unlikely that pure ice wedges, whose formation requires a substantial amount of water, could have existed [e.g., *Seibert and Kargel*, 2001; *Soare et al.*, 2005] (see also Table 3.1). As discussed in Section 4.4, these suggestions do not match with seasonal and diurnal temperature changes even if more benign climate periods occurred in the past (Figure 5.3). Moreover, the landscape assemblage in Utopia Planitia does not show any signs of wet periglacial processes (e.g., narrow channels connecting thermokarst-like depressions, Figure 5.1), although such processes have been suggested for the formation of equatorial periglacial landscapes on Mars [*Balme and Gallagher*, 2009; *Warner et al.*, 2010] (see also Section 2.5.2). However, some periglacial-like features in Utopia Planitia, in particular pingo-like features (see Figure 4.2b), cause questions to be raised about the influence of substantial amounts of liquid water, if these landforms

are really analogous to terrestrial pingos [e.g., *de Pablo and Komatsu*, 2009]. These questions may never be answered, because answering them would require ground truthing by robotic exploration or even field work.

Finally, it can be stated that the investigation of permafrost landforms on Mars in analogy to terrestrial periglacial features has enhanced our knowledge of current and past environmental conditions in Martian mid-latitudes. It has been shown that the present-day appearance of the landforms studied in Utopia Planitia is consistent with the effects of the current Martian climate conditions. The development of these landforms is currently stagnant and they are preserved by the cold desert climate. However, the permafrost landforms evolved in relation to high ground-ice contents under past climate conditions during which the Martian orbital configurations (i.e. high obliquity, high eccentricity, and Martian summer at perihelion) allowed temperatures to rise above the melting point of water and, therefore, thaw processes and occasional liquid water to be geomorphically active (Figure 5.3, see Section 4.4 and Figure 4.3).

How can all this be related to the second goal of this thesis, the identification of habitable zones on Mars? Answering this question is the main purpose of the paper presented in Chapter 4. Generally, this thesis has highlighted the wide distribution of permafrost landforms in Martian mid-latitudes, and has suggested that liquid water may have had a distinct influence on the evolution of these landforms. The source of this water is very likely to be ground ice, which exists or existed in high contents. While Mars transited through its three global climatic eras (Figure 1.1), from a relatively wet planet on which the basic requirements for life were present to the current extremely arid and cold climate which makes the surface generally uninhabitable [*Fairén et al.*, 2010], the subsurface permafrost has provided one environment where very specialized life forms could have survived in isolated niches until today (Sections 4.4, 4.5, and Figure 4.4). Beside the morphological evidence of past liquid water activity, ice may be present near the surface, on the pole-facing slopes of the scalloped depressions in Utopia Planitia, or perhaps on the pole-facing inner walls of craters (see Appendix); the presence of this ice enhances the potential habitability of a site [*Stoker et al.*, 2010]. Therefore, the studies presented in Chapter 2 and in Chapter 3 enable us to designate potential habitable niches (Figure 4.4), and thus contribute to answering the main questions of the Helmholtz research alliance, which framed this PhD thesis (see Chapter 1, Preface). However, many other key factors determine the habitability of a site (e.g., current evidence for liquid water, thermodynamic conditions, and stability of liquid water, energy, nutrients, etc.) [see *Stoker et al.*, 2010]. After computing a habitability index (HI) based on all these key factors for all known landing sites on Mars, it was suggested by *Stoker et al.* [2010] that the Phoenix Lander site in the northern polar region (~68°N) holds the highest potential for current habitability. This conclusion is based primarily on the *in-situ* observations and subsequent calculations of potential liquid water at the Phoenix Lander site [e.g., *Rennó et al.*, 2009; *Smith et al.*, 2009]. The lowest HI was computed for the Viking Lander 2 (VL2) site in eastern Utopia Planitia. Although no liquid water could be

observed at the VL2 site, the presence of winter frost [*Svitek and Murray,* 1990] increases the potential of its occurrence (see also Chapter A7 and Figure A14). As a final statement, considering liquid water activity in the evolution of the periglacial Utopia Planitia landscape as suggested in this work and the current environmental conditions at the VL2 site (see Table 4.2), which are, e.g., far closer to the triple point of water (Figure 5.3) than the extremely cold conditions in the polar regions, the habitability potential of the Utopia Planitia region (and even other mid-latitude periglacial regions) must be considered similar to or even higher than the potential computed for the Phoenix Lander site.

5.3 Limitation to and benefits of terrestrial analogue studies

Generally, there are no places on Earth which would perfectly match the past and present climate conditions on Mars (Figure 1.3). Nevertheless, there are terrestrial environments sufficiently similar to Martian climate conditions differing during Mars' geological history that the terrestrial and Martian environments can be compared [*Fairén et al.,* 2010]. Terrestrial polar regions are considered to be the closest environmental analogues to the Late Amazonian and to present-day Mars. However, compared to the dry polar deserts of the Antarctic Dry Valleys, it is far more difficult to consider arctic periglacial environments to be analogous to Martian landscapes, due to their comparatively wetter and warmer hydrological and climatic situation. In contrast to Antarctica, however, arctic landscapes often exhibit diverse periglacial landforms in close spatial proximity that are of different generations or exist in different stages of development, a situation which can be observed in particular at Martian mid-latitudes, thereby making it possible to investigate a large number of landforms in their geological and geomorphological context as well as the processes of periglacial landscape formation. For instance, the Ice Complex landscapes (i.e. Yedoma) in NE Siberia (Section 2.2.1) have allowed the interrelationships of active thermokarst processes, polygon development, and pingo evolution in fine-grained and very ice-rich sediments within an old permafrost environment to be explored; such an environment is characterized by long-term stable cold climate conditions and the absence of large Pleistocene ice sheets [*Hubberten et al.,* 2004; *Schirrmeister et al.,* in press]. On the other hand, the central regions of Spitsbergen provided insights into the relationships of numerous active mountainous periglacial processes with polygonal patterned ground and pingos within a comparatively dry and partly non-vegetated environment (Section 3.2.1) [e.g., *Hauber et al.,* in press]. The key aspect of this study was the analysis of the multiple factors responsible for forming terrestrial geomorphological systems and to extrapolate their relationships to the Martian landscapes, considering the prevailing atmospheric, hydrological, and geological conditions on Mars [*Baker,* 2008]. To go beyond this goal would be problematic, because it is clear that terrestrial periglacial analogues can only reflect individual processes or sub-aspects, which even on Earth are influenced by a complex of

environmental parameters that are, typically, not fully understood. These parameters, such as landscape, substrate, vegetation, and climate, are and were interrelated in a definitely different way on Mars or are not and were probably never an issue (e.g., vegetation). Furthermore, it may be assumed that periglacial processes on Earth take place comparatively quickly, on time scales of tens to 10^4 years, and the effect of these processes can be observed in a single person's lifetime [see e.g., *Mackay and Burn,* 2002, 2011], while comparable processes on Mars occur on very long time scales (approx. between 10^3 to 10^6 years and maybe more) due to the long-term cold and dry environment [e.g., *Baker,* 2001]. Therefore, the analogue studies presented in this thesis can only provide initial suggestions about the processes that may have influenced periglacial landform evolution on Mars, by making comparisons with the manifold processes which already exist on Earth.

The use of terrestrial analogues benefits from both field and remotely-sensed data (see Figure 1.5). While the former provides the necessary ground truth for remote-sensing analyses, increases the spatial resolution, and allows the subsurface to be sampled, the latter allows a more integrated view of large-scale relationships [*Sharp,* 1988; *Grosse et al.,* 2006; *Hauber et al.,* in press]. In particular, the application of remote-sensing data, which provide both high-resolution imagery and topographic information (i.e. HiRISE for Mars, HRSC-AX for Earth), was very helpful for quantitative terrain analyses. For successful terrestrial analogue studies it is necessary to use remote-sensing data that have a quality and scale comparable to that of planetary data. Interestingly, while very-high-resolution Martian satellite data (e.g. from HiRISE, MOC) are freely available online, terrestrial remote-sensing data at a comparable resolution are rare and, moreover, very expensive (e.g., GeoEye-1, Ikonos), which limits their potential for use in successful analogue studies. Within this work, different kinds of data were successfully implemented into GIS environments for each investigated site. Geomorphometric parameters were extracted from remote-sensing and topographic data, combined with field data, and used for various GIS-based spatial investigations and in numerical analyses. Nevertheless, the usefulness of remotely-sensed data is limited to analyzing the current evolutionary stage of a landscape, not least because remote sensing creates a snapshot of an ongoing process. Furthermore, the analysis of the Martian landscape, which lacks appropriate field data, is limited to the parameters which can be extracted from the available spacecraft data. For instance, the *in situ* data acquired by the Phoenix mission and previously by the Viking mission fostered the investigations of Martian mid- and high-latitude environments. Images taken by the landers' cameras allowed geomorphological features to be identified which cannot be analyzed even in the very-high-resolution (~30cm/pixel) HiRISE data [see *Levy et al.,* 2009c; *Marchant and Head,* 2010]. Finally, this thesis confirms that the combination of remote-sensing analysis with detailed analogue field studies is a promising approach to utilize in order to increase our knowledge of Martian landforms. Quantitative methods

are a useful tool; using such methods is necessary to reduce the ambiguity in interpreting analogous landforms.

5.4 Outlook and future prospectives

Although huge progress has been made in understanding the climatological, hydrological, geological, and astrobiological significance of Martian permafrost landforms, so far we have only rather randomly scratched the surface with respect to understanding the evolution of periglacial landscapes on Mars. Many questions remain open, providing rich potential for future investigations. The continuing study of analogous terrestrial landforms is necessary to increase our understanding of the terrestrial periglacial landscape systems, in order to enable an extrapolation of this knowledge to a specific extraterrestrial target. Detailed field studies should be extended to other Arctic regions as well; many such potential field sites are quite easily accessible and provide an environment that is closely analogous to that of Mars (e.g., Axel Heiberg Island in the Canadian high Arctic) [*Pollard et al.,* 2009]. More detailed investigations of physical properties and the individual subsurface and climatic conditions influencing different kinds of landforms should be performed and integrated in quantitative analyses. The application of more advanced techniques (e.g., ground-based geophysical methods, drilling, etc.) will help us to understand ground-ice conditions in relation to periglacial landforms on Earth, and could provide ground truth for understanding data detected by satellites orbiting Mars (e.g., radar sounder data) [*Clifford et al.*, 2010]. Furthermore, the better we understand the similarities and differences between terrestrial and Martian environments, the more effective will be the testing and certifying of such equipment and techniques, which are moreover often designed to study Martian permafrost landforms and cryosphere [e.g., *Frolov,* 2003; *Smith and McKay,* 2005; *Pfiffner et al.,* 2008; *Barfoot et al.,* 2010].

Extensive quantitative analyses of Martian landform geomorphometry in this work were limited by the availability of high-resolution topographic data. The ongoing acquisition of HiRISE data and the processing of appropriate DEMs [*Kirk et al.,* 2008; *McEwen et al.,* 2010] are necessary. These data will provide the possibility for more extensive and accurate studies. Comparative investigations must be extended to different latitudinal and altitudinal regions on Mars to understand individual morphological evolution with respect to the varying temperature, pressure, and geological setting. In addition, HiRISE DEMs provide more accurate input for thermal modeling; such modeling will become increasingly useful for understanding thermal variations related to certain periglacial features, and for estimating sublimation and/or melting of the ice therein over different Martian climatic periods. Finally, more *in situ* data of subsurface conditions at different latitudes gained by lander and rover missions would help us to achieve greater insights into the complex nature of Martian ground ice.

A particular intention of this thesis was to combine the results of geomorphological work with microbiological expertise, in order, ultimately, to determine habitable zones on Mars. Such an interdisciplinary approach was particularly suitable for those estimations and should be utilized more often in future astrobiological studies. The combination of different fields of expertise is the intention of astrobiology; this approach should be continued and intensified. An understanding of the complex interactions of biology, geology, chemistry, and physics is important for the study of the origin and evolution of life in the universe.

A Landscape evolution in Martian mid-latitude regions: insights from analogues periglacial landforms in Svalbard

Ernst Hauber[1], Dennis Reissr[2], Mathias Ulrich[3], Frank Preusker[1], Frank Trauthahn[1], Michael Zanetti[2], Harald Hiesinger[2], Ralf Jaumann[1], Lars Johansson[4], Andreas Johnsson[4], Stephan van Gasselt[5], Mats Olvmo[4]

[1]*Institute for Planetary Research, German Aerospace Center (DLR), Berlin, Germany*
[2]*Institut für Planetologie, Westfälische Wilhelms-Universität, Münster, Germany*
[3]*Alfred Wegener Institute for Polar and Marine Research, Research Unit Potsdam, Potsdam, Germany*
[4]*Department of Earth Science, University of Gothenburg, Göteborg, Sweden*
[5]*Institut für Geologische Wissenschaften, Freie Universität Berlin, Berlin, Germany*

Geological Society, London, Special Publications 356, 111-131. doi:10.1144/SP356.7.

Abstract

Periglacial landforms on Spitsbergen (Svalbard, Norway) are morphologically similar to landforms on Mars that are likely related to the past and/or present existence of ice at or near the surface. Many of these landforms, such as gullies, debris flow fans, polygonal terrain, fractured mounds, and rock glacier-like features, are observed in close spatial proximity in mid-latitude craters on Mars. On Svalbard, analogous landforms occur in strikingly similar proximity, which makes them useful study cases to infer the spatial and chronological evolution of Martian cold-climate surface processes. The analysis of the morphological inventory of analogous landforms on Svalbard and Mars allows constraining the processes operating on Mars. Different qualitative scenarios of landscape evolution on Mars help to better understand the action of periglacial processes on Mars in the recent past.

A1 Introduction

Many young landforms on Mars that were probably formed by exogenic processes show a latitude-dependent geographic distribution. They include surface mantling [*Kreslavsky & Head,* 2000*; Mustard et al.,* 2001; *Morgenstern et al.,* 2007], lobate debris aprons, lineated valley fill, and concentric crater fill [e.g., *Squyres,* 1978], viscous flow features *[Milliken et al.,* 2003], gullies [*Balme et al.,* 2006; *Kneissl et al.,* 2010], and patterned ground [*Mangold,* 2005]. Other landforms such as pedestal craters seem to indicate a preservation of near-surface ice and are latitude-dependent as well [*Kadish et al.,* 2009]. Collectively, these landforms are hypothesized to represent

the surface records of Martian ice ages [e.g., *Head et al.,* 2003] that were induced by astronomical forcing (*Laskar et al.* 2004) and associated climate changes [*Toon et al.,* 1980; *Jakosky & Carr,* 1985; *Mischna et al.,* 2003; *Forget et al.,* 2006; *Schorghofer,* 2007]. Previous authors often considered only one of such feature classes in isolation (e.g., gullies), without taking into account the geomorphologic context. It was not until the recent advent of high-resolution data from orbit and the *in situ* investigation of Martian high-latitude terrain by the Phoenix lander that allowed to develop a more integrated view of diverse landforms into a landscape evolution model [e.g., *Balme & Gallagher* 2009; *Levy et al.* 2009c]. A more comprehensive investigation of the full assemblage of landforms by means of landscape analysis, however, has the potential to reduce the ambiguity in interpreting landforms and to reveal the evolution of the climatic environment in more detail. The phenomenon of equifinality (i.e. similarly looking landforms resulting from diverse processes) is particularly problematic in planetary geomorphology, where the morphology as inferred from remote sensing data such as images and Digital Elevation Models (DEM) is the only observable component. An instructive example is the case of pitted mounds on Mars, which have been interpreted in the past as modified impact craters, rootless cones, cinder cones, and pingos. In some of the studies that favoured pingos, the interpretations were based on poor evidence and attracted criticism from terrestrial permafrost researchers [*Humlum & Christiansen,* 2008]. Here we present permafrost landforms of Svalbard (Norway) as useful terrestrial analogues for the suite of possible periglacial landforms that are typically found at mid-latitudes on Mars. We build on our previous investigations of gullies and fans [*Hauber et al.,* 2009], and include a number of classical periglacial landforms (patterned ground, rock glaciers, pingos) that all have close morphological analogues on Mars. Based on this comparison, we propose several evolutionary scenarios which could help to develop a better understanding of the sequential formation of the Martian landforms.

A2 Permafrost and periglacial features on Mars and Svalbard

Mars may be regarded as a permafrost planet, following the definition of permafrost as given by *Everdingen* [2005]: "Ground (soil or rock […]) that remains at or below 0°C for at least two consecutive years, regardless of the water content". In fact, the shallow subsurface of Mars probably experienced temperatures that were continuously below 0°C for most of its history [e.g., *Shuster & Weiss,* 2005]. In the current Martian climate, ground ice is thought to be stable only at higher latitudes [e.g., *Leighton & Murray,* 1966; *Smoluchowski,* 1968; *Fanale et al.,* 1986; *Mellon & Jakosky,* 1993], and indeed the Phoenix mission has provided unambiguous evidence for very shallow and rather pure ground ice at a latitude of 68.2°N [*Smith et al.,* 2009]. The latitudinal range of ice stability is, however, a function of the planet's obliquity (i.e. the tilt of the rotational axis). Mars` obliquity is assumed to vary widely [*Ward,* 1973; *Touma & Wisom,* 1993], and at an obliquity exceeding 32° (today: ~25°) ground ice becomes globally stable [*Mellon & Jakosky,*

1995]. An obliquity exceeding ~27° is required for ice to be stable at latitudes of 30° and higher [*Mellon & Jakosky,* 1995, their fig. 10d]. Other factors that affect the stability of ground ice are geographic variability, soil properties, rocks, and local slopes [see *Mellon et al.,* 2009, and references therein]. The large and frequent oscillations of Mars` obliquity [an obliquity cycle spans 117,000 years; *Laskar et al.,* 2004] should have a significant influence on the volatile distribution on the surface [*Jakosky et al.,* 1995], and climate modelling using Global Circulation Models (GCM) confirms this view [*Forget et al.,* 2006; *Levrard et al.,* 2004; *Madeleine et al.,* 2009]. It appears likely that water ice was frequently driven from the poles towards lower latitudes during periods of higher obliquities, when the polar regions received more incoming solar energy [*Forget et al.,* 2006]. In contrast, water ice was redistributed towards higher latitudes during following periods of lower obliquities [*Levrard et al.,* 2004]. Ground ice can thus be expected to be a significant factor in Martian landscape evolution. Recent observations indeed showed that near-surface water ice is present even in mid- and low-latitude regions [*Holt et al.,* 2008; *Byrne et al.,* 2009; *Vincendon et al.,* 2010a,b], in contrast to expectations from theoretical modelling (see above).

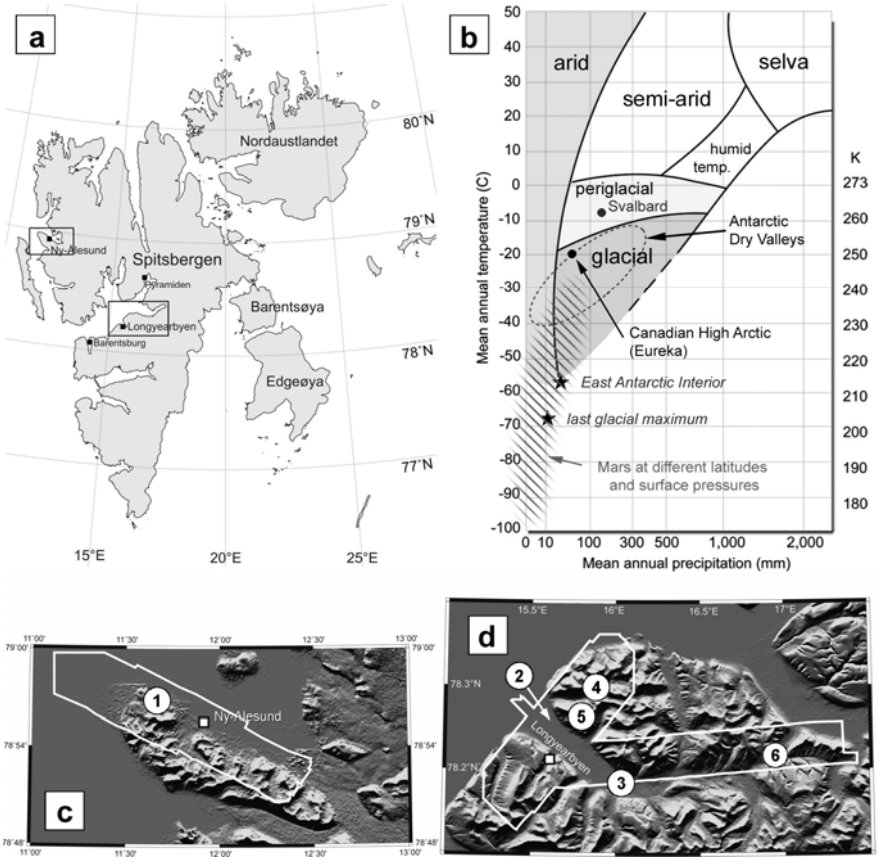

Figure A1: Location and climate of study areas on Svalbard. (a) Map of Svalbard with study areas (boxes, see *(c)* and *(d)*). (b) Climate zones and morphogenetic regions on Earth; modified from *Baker* [2001] and *Head & Marchant* [2007]. Climatic conditions on Mars (present and inferred past) are indicated by hatched area. (c) Study area on Brøgger peninsula (shaded elevation model derived from ASTER data). (d) Study area in Adventdalen (shaded elevation model derived from ASTER data). Numbers in *(c)* and *(d)* mark geographic locations mentioned in the text: 1-Stuphallet, 2-Adventfjord, 3-Adventdalen, 4-Hannaskogdalen, 5-Hiorthfjellet, 6-Eskerdalen.

To complement theoretical modelling, comparisons with terrestrial analogues are mandatory to constrain the action of periglacial processes and corresponding landscape evolution on Mars. Present-day Mars is cold and dry, so surface processes acting in terrestrial cold deserts should be considered as useful analogues. The closest cold-climate analogue to Mars on Earth are the Antarctic Dry Valleys [*Anderson et al.,* 1972; *Marchant & Head,* 2007, 2010], a polar desert environment with exceptionally cold and dry conditions [*Doran et al.,* 2002] and correspondingly small active layer depth [*Bockheim et al.,* 2007]. Other polar regions also display morphological analogues to Mars, however, and the archipelago of Svalbard and its largest island, Spitsbergen (Figure A1a), offer a diverse inventory of periglacial landforms in close spatial proximity. Terrain phenomena such as pingos, ice wedge polygons and rock glaciers are widespread, especially in the dry central regions of Spitsbergen. Periglacial features such as solifluction lobes occur primarily in the more humid western regions. Various forms of patterned ground, such as stone circles and stripes are widespread and well developed (see *Åkerman* [1987] for a review of periglacial landforms of Svalbard). Examples of periglacial morphologies are closely located to the settlements of Longyearbyen and Ny Ålesund on the main island, Spitsbergen, making them very useful morphological analogue to Martian cold-climate landforms. Major controls on permafrost aggradation are wind, snow, and avalanches [*Humlum,* 2005]. A particularly interesting aspect of permafrost on Svalbard is its interaction with glaciers [*Etzelmüller & Hagen,* 2005], because such interaction is often neglected in the literature [*Haeberli,* 2005] but may be highly important on Mars.

A3 Data

Martian surface features were analyzed using high-resolution images of the CTX (Context Camera) and HiRISE (High Resolution Imaging Science Experiment) cameras, which have spatial resolutions of 5-6 m/pixel and ~30 cm/pixel, respectively. An airborne version of the HRSC (High Resolution Stereo Camera) was used for the acquisition of stereo and color images of Spitsbergen. HRSC-AX is a multi-sensor push broom instrument with 9 CCD line sensors mounted in parallel. It simultaneously obtains high-resolution stereo, multicolour and multi-phase images. The particular value of HRSC-AX is the stereo capability, which allows to systematically produce high-resolution Digital Elevation Models (DEM) with grid sizes between 50 cm and 1 m [*Wewel et al.,* 2000; *Scholten & Gwinner,* 2004; *Scholten et al.,* 2005; *Gwinner et al.,* 2005, 2006, 2009, 2010]. The HRSC-AX flight campaign in July/August 2008 covered a total of seven regions in Svalbard: (i) Longyearbyen and the surroundings of Adventfjorden (all place names on Svalbard are as given as in the topographic map series, scale 1:100,000, published by the Norsk Polarinstitutt, Tromsø, Sheets C9 and A7), (ii) large parts of Adventdalen, (iii) large parts of the Brøggerhalvøya (*halvøya* = peninsula) in western Spitsbergen, (iv) the Bockfjorden area in northern Spitsbergen, (v) the

northeastern shore of the Palanderbukta and the margin of the adjacent ice cap in Nordaustlandet, (vi) an area on Prins Karls Forland, and (vii) the area of the abandoned Russian mining settlement of Pyramiden together with the nearby Ebbedalen. The landforms discussed in this study are located on the Brøgger peninsula and in Adventdalen and its vicinity (Figure A1a). In two field campaigns in 2008 and 2009, both areas covered by HRSC-AX were visited.

A4 The Svalbard Climate

The present climate of Svalbard is arctic (Figure A1b). The mean annual air temperature at the airport in Longyearbyen, which is located only a few kilometers from the study area of Adventdalen, ranges between about –6°C at sea level and –15°C in the high mountains [*Hanssen-Bauer & Førland,* 1998]. Annual precipitation is low and reaches only ~180 mm in central Spitsbergen (Table A1). The central part of Spitsbergen can therefore be considered to be a polar (semi)desert, which is defined as an area with annual precipitation less than 250 millimeters and a mean temperature during the warmest month of less than 10°C [*Walker,* 1997]. About 60% of Svalbard is covered by glaciers and ice caps, and relatively small glaciers and ice caps are situated on many massifs and valleys around Adventdalen. The unglaciated part of Svalbard is characterized by continuous permafrost, which has a thickness of 10-40 m in coastal regions, about 100 m in the major valleys, and >450 m in the highlands [*Listøl,* 1976; *Isaksen et al.,* 2000; *Sollid et al.,* 2000].

Table A1: Climate at Svalbard Airport. For the series of observed and modelled annual and seasonal precipitation sums from 1912 to 1993, the following values are given: mean, standard deviation, absolute minimum and absolute maximum. SD: Standard deviation; Corr.: correlation coefficient between observed and modelled precipitation series [data from *Hanssen-Bauer & Førland*, 1998]. For comparison, the mean annual air temperature at the floor of the Dry Valleys in Antarctica ranges from -14.8°C to -30°C, and the mean annual precipitation is <<100 mm, but can be as low as 13 mm [*Doran et al.,* 2002; *Campbell & Claridge,* 2004].

Season		Mean	SD	Min.	Max.	Mean	SD	Min.	Max.	
		Observed *T* [°C]				**Modelled *T* [°C]**				**Corr.**
Year		–6.3	1.7	–12.2	–3.1	–6.4	1.0	–8.9	–4.0	0.61
Winter	(DJF)	–14.0	3.6	–23.2	–7.6	–14.1	2.4	–19.1	–9.1	0.62
Spring	(MAM)	–10.8	2.4	–19.3	–6.7	–10.8	1.7	–15.2	–7.5	0.58
Summer	(JJA)	4.3	0.7	2.5	6.1	4.2	0.5	3.2	5.4	0.54
Autumn	(SON)	–4.8	2.0	–11.3	–1.3	–4.9	1.5	–8.7	–1.8	0.66
		Observed *P* [mm]				**Modelled *P* [mm]**				**Corr.**
Year		180.7	49.8	86.4	317.0	178.7	33.5	93.5	286.6	0.54
Winter	(DJF)	53.4	24.3	16.8	140.0	52.8	11.5	24.5	86.8	0.40
Spring	(MAM)	35.6	10.4	6.4	125.9	34.3	13.6	10.6	65.5	0.60
Summer	(JJA)	43.7	21.2	3.0	114.0	43.7	18.7	8.3	100.8	0.57
Autumn	(SON)	48.1	17.0	18.4	109.0	47.9	13.1	21.5	79.1	0.54

A5 Morphological comparisons between Mars and Svalbard

Many possible glacial and periglacial landforms are located in mid-latitude impact craters on Mars. This specific geologic setting provides ideal study cases, because there is high relief provided at the crater walls and the opportunity to study the effects of insolation variations, since craters are axisymmetric features and their inner walls have an azimuthal range of the entire 360°. It has been found by many previous researchers that the pole-facing walls of impact craters are particularly prone to be shaped by glacial and periglacial processes [e.g., *Dickson et al.,* 2007]. In this section, the inventory of such landforms is briefly reviewed and compared to analogous landforms on Svalbard. We note here that all of these features have been found in craters on Mars, sometimes several of them in the same crater, but so far no crater was found that would host all of them together.

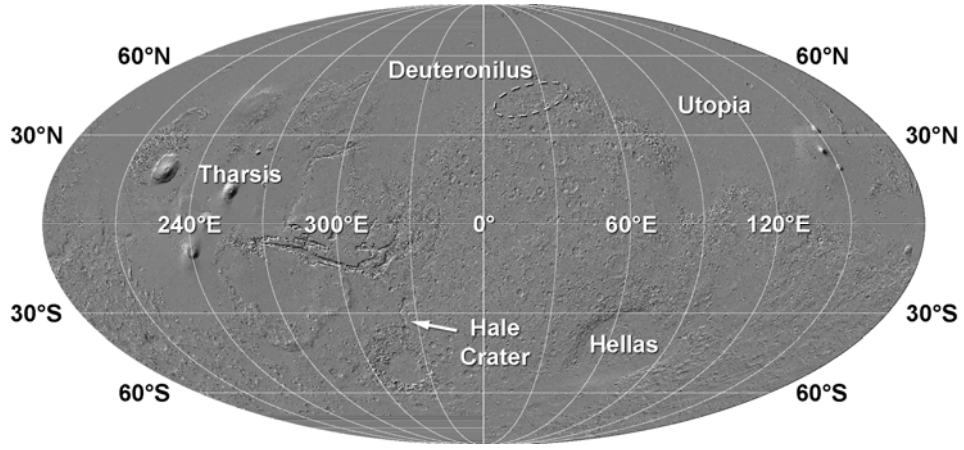

Figure A2: Locations of regional features on Mars mentioned in the text (shaded version of MOLA DEM).

A5.1 Martian landforms

Many landforms on Mars that are morphologically similar to terrestrial glacial and periglacial landforms occur in the middle latitudes, between ~30° and ~60° (Figure A2). They are situated along the high-relief belt of the Martian dichotomy boundary and other regions of high relief [e.g., *Head et al.,* 2006; *Pierce & Crown,* 2003; *Chuang & Crown,* 2005; *van Gasselt et al.,* 2010] as well as in flat-lying regions such as Utopia Planitia [*Morgenstern et al.,* 2007, *Lefort et al.,* 2009, *Soare et al.,* 2005]. A particularly interesting setting is the pole-facing inner wall of impact craters. Most gullies (Figure A3a) have been found on such walls, especially in the southern hemisphere [*Dickson et al.,* 2007]. On the base of some gullies, spatulate depressions are delineated towards the inner crater floor by arcuate ridges, which have been compared to moraines [e.g., *Berman et al.,* 2005, fig. 1]. Other landforms of possible periglacial origin have been observed in close spatial association with the crater wall-gullies, including polygons (Figure A4a) [*Levy et al.,* 2009d], patterned ground (Figure A5a) [*Mangold,* 2005], lobate features (Figure A6a and A7a) [*Milliken et al.,* 2003], and fractured mounds (Figure A8a) [*Dundas et al.,* 2008]. The unique occurrence of

diverse possible periglacial landforms within a small area with considerable relief makes such craters an ideal study case for the action of periglacial processes on Mars. In the following, they will be compared with terrestrial analogues on Spitsbergen. Based on this comparison, possible scenarios of landscape evolution on Mars will be outlined.

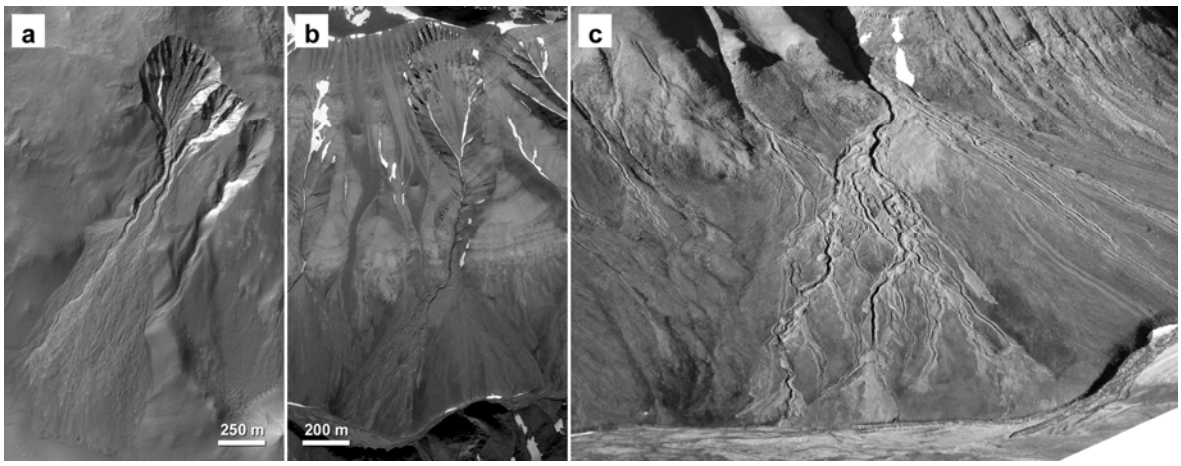

Figure A3: Gullies and fans on Mars and Svalbard. (a) Gully in Martian crater at 38.5°S/319.8°E (HiRISE PSP_006888_1410). (b) Gully and debris flow fan in Hannaskogdalen, Svalbard. Note the similarity in morphology and scale between the two systems. (c) Close-up field photo (taken from opposite mountain) of the fan surface shown in b. Note the morphological indicators of debris flows, such as large lateral levees and flow tongues.

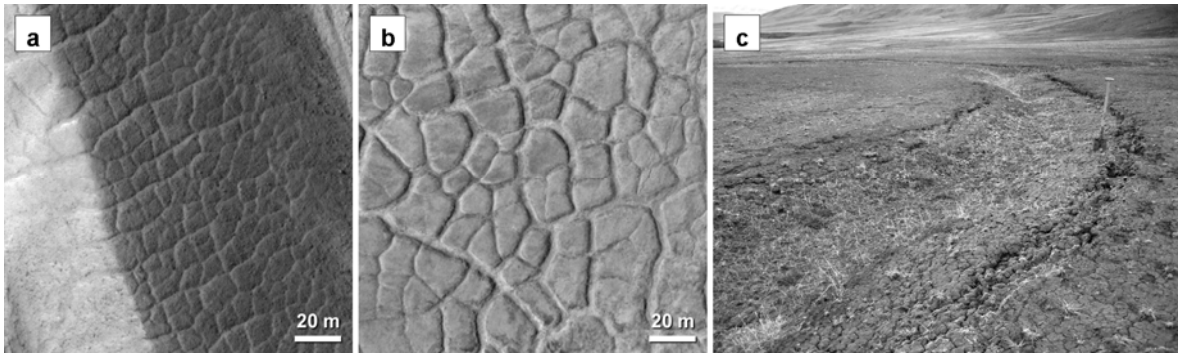

Figure A4: Polygons on Mars and Svalbard. (a) Oriented-orthogonal polygons pattern on a ridge between two gullies on the northern wall of Hale crater, Mars. The polygons have high centers and diameters between ~5 and ~10 meters (HiRISE image PSP_004072_1845; near 34.6°S, 323.1°E). (b) High-center orthogonal polygons in central Adventdalen (HRSC-AX image). The polygons have high centers and diameters between ~10 and ~20 meters. A trough which is typical for this type of polygons is shown in panel *(c)*. (c) Trough between high-center polygons in central Adventdalen. Note the fractured and degraded appearance of the trough shoulders. Spade for scale.

A5.2 Svalbard landforms

The main study site is Adventdalen, a ~40 km-long and up to ~3 km-wide valley in central Spitsbergen that was deglaciated about 10,000 years ago [*Mangerud et al.,* 1992]. The valley hosts a large number of periglacial landforms, both on the valley flanks and on the valley floor. The mountain massifs and the upper parts of many valleys are still partly covered by polythermal or

cold-based glaciers, which can be partly debris-covered [*Tolgensbakk et al.,* 2000]. Distinctive end moraines, which may be ice-cored [*Lukas et al.,* 2005], mark the former larger extent of the glaciers. Some tongue-shaped rock glaciers are perched in cirques and broad alcoves [*Isaksen et al.,* 2000; *Ødegård et al.,* 2003]. Protalus ramparts, defined as "ridges or ramps of debris formed at the downslope margin of a snowbed or firn field" [*Shakesby,* 1997], are well developed on the foot of high cliffs on the Brøgger peninsula (Figure A7b, c). Rock fall is frequent from the steep cliffs that mark the flat-topped summits of the mountains [*André,* 1995]. The flanks of the massifs bordering the valley are dissected by numerous gullies (Figure A3b, c), which are the transport pathways for debris flows. Debris flows can reach volumes of 50 to 500 m^3 in the Longyearbyen valley (*Larsson,* 1982), and their recurrence interval is 80 to 500 years (*André,* 1990).

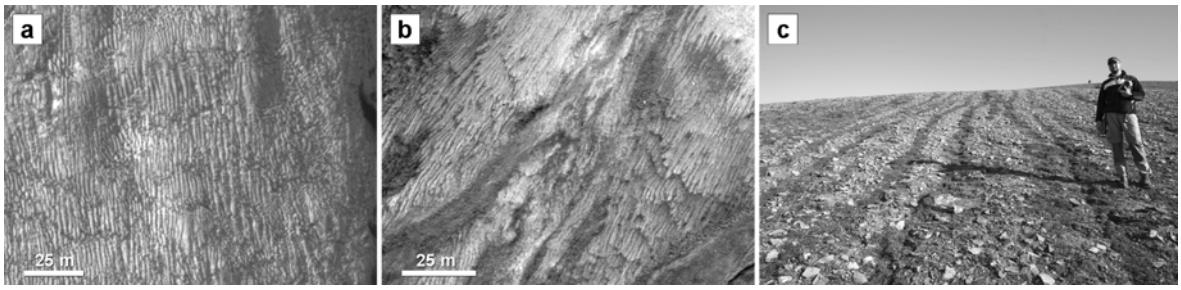

Figure A5: Comparison between alternating bright and dark stripes on Mars and sorted stripes on Svalbard. (a) Alternating dark and bright stripes near gullies on the inner wall of a Martian impact crater (HiRISE image PSP_001684_1410; near 38.9°S, 196.0°E). The orientation of the stripes is approximately downslope. (b) Sorted stripes on the western slopes of the Hiorthfjellet massif (east of Adventfjorden, Spitsbergen). Note the striking similarity in scale between a and b. (c) Sorted stripes in Adventdalen (Spitsbergen). Coarser and slightly elevated unvegetated stripes alternate with finer-grained and vegetated stripes (person for scale).

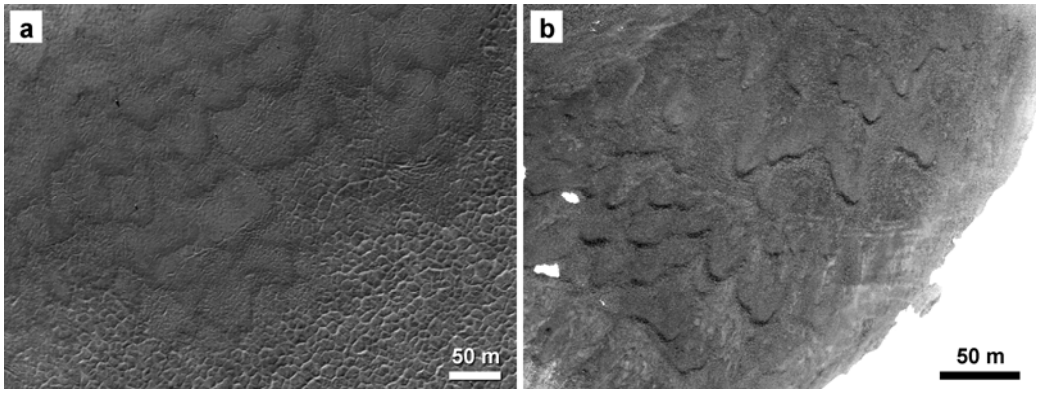

Figure A6: Comparison between lobate structures on Martian slopes and solifluction features on Svalbard. (a) Lobate features on the inner wall of an impact crater on Mars (near 71.9°N/344.5°E; HiRISE PSP_010077_2520). The morphology is identical to that of lobate solifluction sheets [cf. *Ballantyne & Harris,* 1994, fig. 11.1]. Although this particular example is on the wall of a crater in high latitudes, it is expected that such features might also be found in mid-latitude craters. (b) Solifluction lobes on the slopes of Louisfjellet (central Spitsbergen, Svalbard). Note the striking similarity in scale and morphology between *(a)* and *(b)*.

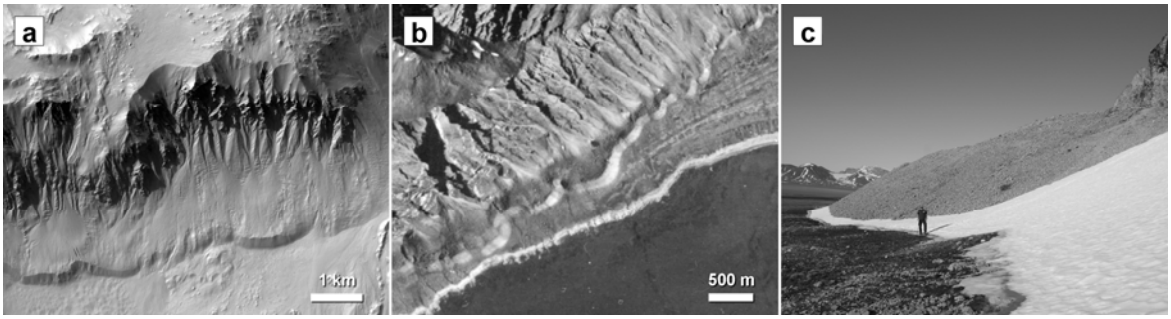

Figure A7: Possible protalus ramparts on Mars (left) and Svalbard (right). (a) Protalus lobe-like structures at the base of a large scarp on the northern wall of Hale Crater (CTX image P15_006756_1454; near 34.6°S, 323.1°E; North is up). The steep front is characterized by polygons [see *Reiss et al.,* 2009; their fig. 10b and c]. (b) Protalus lobes on the northern tip of Prins Karls Forland (Svalbard) [see *Berthling et al.,* 1998] at the western foot of the Fuglehukfjellet massif (aerial photo S 704128, Norsk Polarinstitutt, Oslo, Norway; from *André* [1994]; North is towards the left). (c) Close-up image of protalus rampart at Stuphallet, Brøgger peninsula (see person for scale). The surface of the steep front consists of very coarse blocks (diameters of up to tens of cm).

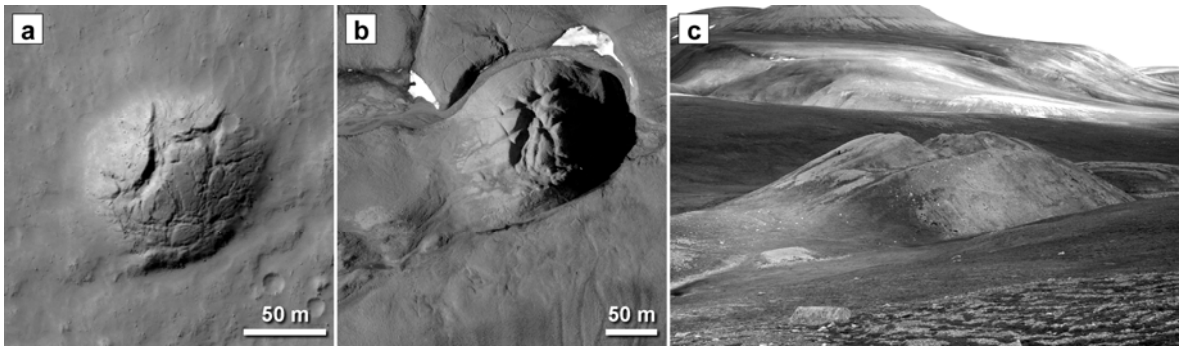

Figure A8: Comparison between fractured mound on Mars and pingo on Svalbard. (a) Fractured mound on floor of crater in southern hemisphere (detail of HiRISE image PSP_007533_1420; near 37.9°S, 347.2°E) [see *Dundas & McEwen,* 2010]. (b) Pingo in upper Eskerdalen (central Spitsbergen) with fractures on its top (HRSC-AX image, acquired in July 2008). Note the morphologic similarity to the shallow fractured mound shown in a. (c) Field photograph of pingo shown in *(b)*. North is up in panels *(a)* and *(b)*. View towards northeast in panel *(c)*.

Between the gullies, many slopes display evidence for solifluction (Figure A6b) and sorting processes (sorted and non-sorted nets and stripes; Figure A5b, c) [*Sørbel & Tolgensbakk,* 2002]. The debris flows build up fans, characterized by channels with lateral levees, flow tongues, and coarse sediment [for a description of an alluvial fan in a permafrost region see *Catto,* 1993]. Where fans extend to the shore of the estuary at the mouth of Adventdalen, they can form an arctic fan delta [*Lønne & Nemec,* 2004]. In the inland, debris flow fans at the downstream-end of the gullies coalesce along the valley to form bajadas. The valley floor is occupied by the large braided river, Adventelva, which often cuts the toes of the fans. Several open-system (hydraulic) pingos are located near the fans on the valley floor (Figure A8b, c) [*Listøl,* 1976; *Yoshikawa,* 1993; *Yoshikawa & Harada,* 1995]. River terraces are overprinted by thermal-contraction cracks that form widespread nets of ice-wedge polygons (Figure A4b, c) [*Christiansen,* 2005]. Most of the

landforms on the valley flanks can be considered to be part of an ice-debris transport system, where mass wasting takes place both by steady state processes (small-scale rockfall, avalanches, glacial and fluvial transport, and solifluction) and by more extreme short-lived processes (large-scale rockfall, landslides, debris flows) [*Haeberli,* 1985]. Figure A9 demonstrates the spatial arrangement of the landforms in Adventdalen in an idealized sketch, and Figure A10 shows a three-dimensional perspective view of the Hiorthfjellet massif exhibiting some of the features in their real setting.

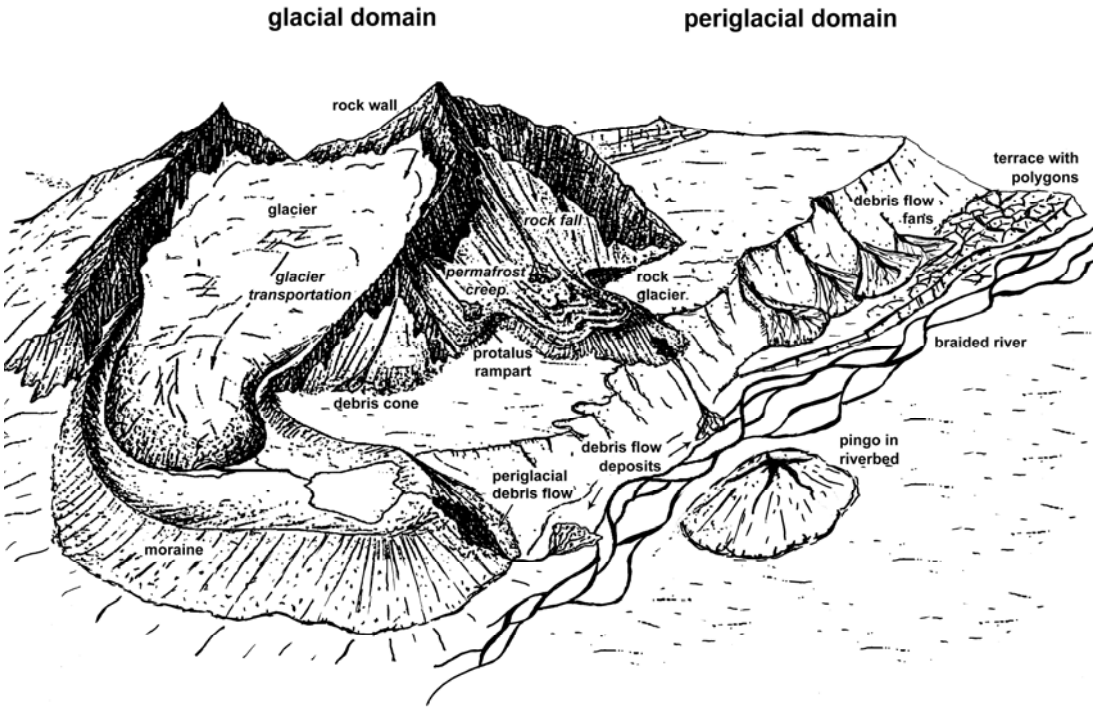

Figure A9: Ensemble of glacial and periglacial landforms observed in Adventdalen (central Spitsbergen, Svalbard [modified from *Haeberli,* 1985, fig. 1]. The qualitative sketch is not meant to represent the real situation in Adventdalen, but to illustrate the spatial arrangement of the landforms. Morphologically similar landforms have been observed in Martian mid-latitudes craters, often in comparably close spatial proximity. The unique advantage of such terrestrial analogues is their potential to provide constraints in the interpretation of planetary surface morphologies.

A6 Discussion

The above comparisons suggest that periglacial processes might have operated in Martian mid-latitude craters. However, the exact nature, intensity and sequence of these processes are unclear. We present three different models, which outline in a qualitative way some possible scenarios how mid-latitude craters were shaped in the recent Martian history by processes involving water ice and, to a lesser degree, liquid water. It is important to note that these models are not thought to be mutually exclusive, nor do they necessarily include all processes that operated on Mars. Instead, they are suggested as examples of how planetary landform analysis guided by terrestrial knowledge can yield improved insight into the evolution of complex landscapes.

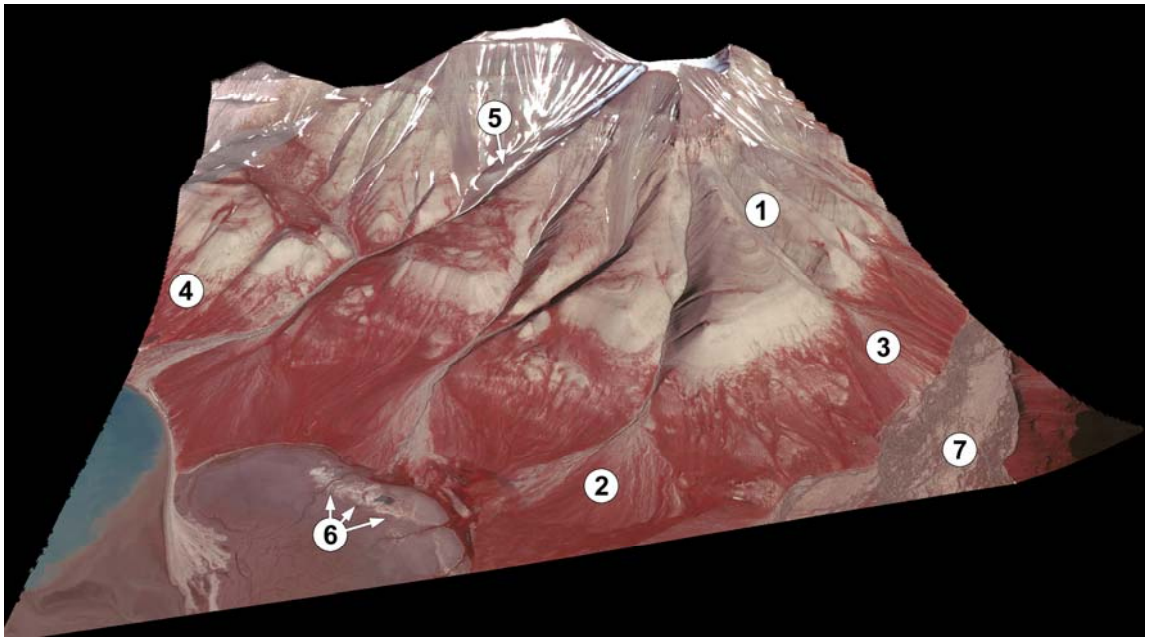

Figure A10: Example of close spatial proximity of glacial and periglacial landforms on Svalbard. The scene (width ~3.7 km; North is towards the background) was computed from HRSC-AX stereo images and shows the Hiorthfjellet mountain massif on the northern side of the Adventfjord. Numbers refer to specific landforms: 1-gullies; 2-alluvial fan; 3-debris flow fans merging along the valley wall into a bajada; 4-slope stripes; 5-rock glacier; 6-pingo; 7-braided river. All of these landforms have close morphological analogues in Martian mid-latitude craters.

The premise of the models is that during higher obliquity water ice is driven from the poles towards lower latitudes where it is precipitated as snow. During periods of lower obliquities, the precipitated snow would sublime or melt, and water vapour would be redistributed at higher latitudes. This basic pattern of volatile transport through the atmosphere as a function of obliquity has been modelled with GCM [*Mischna et al.,* 2003; *Levrard et al.,* 2004; *Forget et al.,* 2006; *Madeleine et al.,* 2009], and the modelling results successfully predict ice accumulation at places where indeed an increased frequency of possible glacial landforms have been observed (e.g., east of the Hellas basin, west of the Tharsis Montes, and at the Deuteronilus Mensae region). If this premise is accepted, it implies that the pattern of deposition and degradation of snow and the associated periglacial processes operate in cycles, as the obliquity varies cyclically. One of such cycles is discussed in the following for each of the scenarios.

Following the scheme of landscape evolution proposed by *Morgenstern et al.* [2007] for the lowlands of Utopia Planitia, the initial process in the cycle of deposition and degradation is the subaerial deposition of a volatile-rich mantle consisting of a layered mixture of dust and snow. Martian dust is suggested to origin from volcanic sources, meteoritic impact and rock erosion, and is redistributed by global dust storms [*Kahn et al.,* 1992]. The dust particles act as condensation nuclei for water-ice [e.g., *Gooding,* 1986]. The dusty snow mantle would be thicker at the pole-facing wall, but would also cover the crater interior and smaller crater therein. This stage is common to all three scenarios (Figure A11a-c, stage I). Such a mantling deposit has been suggested

already on the basis of Mariner 9 data [*Soderblom et al.,* 1973], and was later revealed in detail by high-resolution topography [*Kreslavsky & Head,* 2000] and images [*Mustard et al.,* 2001]. This mantling layer has a thickness in the order of tens of meters in lowlands [*Morgenstern et al.,* 2007], but it is not clear how much of this thickness is deposited during one obliquity cycle. The microclimatic conditions at pole-facing (inner) walls of craters are such that ice is preferentially accumulated and preserved in these locations, i.e., they function as cold traps for atmospheric water ice [*Hecht,* 2002; *Schorghofer & Edgett,* 2006; *Head et al.,* 2008].

A6.1 The 'dry' scenario

Over time, the accumulated snow pack would increase in thickness and eventually the lower portions would transform into glacier ice (Figure A11a, stage II). This glacier would probably contain a significant amount of dust (and perhaps wind-blown sand, but no or very few rock fragments), and we tentatively suggest the term "dust glacier". The plan-view shape of such glaciers would typically be tongue-shaped (length > width), as it is commonly observed on Earth (for a comparison between these shapes on Mars and Earth, see *Arfstrom & Hartmann* [2005] their fig. 2). If it were cold enough, this glacier would freeze to the underlying crater wall and be a cold-based glacier, as they were previously suggested for Mars [*Head & Marchant,* 2003]. A cold-based glacier would cause little or no erosion of the underlying crater wall, and therefore the slope of this wall might remain more or less unchanged. At the downslope termination of the glacier, thrust or push moraines could develop [e.g., *Berman et al.,* 2005], because even if there was no basal sliding of the glacier, it would deform internally and move downslope. The presence of push moraines in front of cold-based glaciers is well documented on Earth [e.g., *Haeberli,* 1979], where push moraines are the morphological result of permafrost deformation. These moraines would be piled up to ridges, which might contain some ice. In some cases, a lobate body might form at the base of the crater wall that has a width larger than its length (Figure A7a). This class of flow features exhibits a striking large-scale similarity to protalus ramparts on Svalbard (Figure A7b). The spatial proximity of "dust glaciers", (ice-cored) moraines, and permafrost features such protalus ramparts would not be surprising, since it was suggested that these landforms might be part of a morphological and developmental continuum [*Shakesby et al.,* 1987]. At smaller scales of observation, however, significant differences become obvious between the Martian and terrestrial features shown in Figure A7. The steep distal front of the Martian flow feature is overprinted by polygons [cf. *Reiss et al.,* 2009, fig. 10], which have likely be developed as thermal contraction cracks in fine-grained material. In contrast, the distal fronts of the protalus ramparts on Svalbard consist of coarse, decimetre-sized rocks derived from steep cliffs and mountain slopes. The difference is easily explained, however, if the relief above the features is taken into account. On Svalbard, the slopes are steep, and frequent mass wasting delivers copious amounts of coarse particles, which form the rocky part of the rock glacier. On the other hand, the lower slopes of large

and old craters on Mars (such as Hale Crater, in the example of Figure A7a) are much gentler, and the material being mixed with ice to form the protalus rampart-like feature would be fine-grained airborne dust. On the surface of such a body, it would be reasonable to expect the formation of sublimation polygons.

After the obliquity decreases, the ice would slowly become unstable and begin to sublimate. A lag deposit of dust and sand would form at the top of the glacier, decreasing the rate of sublimation [*Mellon & Jakosky,* 1993; *Chevrier et al.,* 2007]. Internally, the glacier might still be deformed. If the lag deposit has some cohesion, e.g., from cementation, the ongoing internal deformation of the glacier body might crack the lag deposit and form tension fractures, normal faults and grabens paralleling the topographic contours. When sublimation would have removed most of the ice, a thick and very fine-grained lag deposit (dominated by dust-sized particles) would remain above a thinned body of buried glacier ice. At the same time, the mantling deposit in the crater interior would also degrade and become thinner. Where this mantling filled a smaller impact crater, it might be preferentially preserved, leaving a high-standing mound of the mantling that could develop fractures at its top. As *Dundas & McEwen,* [2010] already discussed, such a fractured mound could easily be misinterpreted as a pingo (Figure A11a, stage III). Thermal contraction polygons could develop in the sublimation lag. In analogy to the McMurdo Dry Valleys in the Antarctica, these polygons could be sublimation polygons [*Marchant et al.,* 2002], as suggested for Mars by *Levy et al.* [2009a]. It has to be noted, however, that the exact nature of the polygons (ice wedge polygons, sand wedge polygons, or sublimation polygons) remains an open question, since the morphology alone does not allow for an unambiguous identification of either of these forms [e.g., *van Gasselt et al.,* 2005]. For example, degraded ice-wedge polygons in Adventdalen (Figure A4b, c) display a morphology that can hardly be distinguished from sublimation polygons in remote sensing imagery. With continual degradation, the volume of the remaining ice would be so small that scalloped depressions would form between the thrust moraines, left behind as arcuate ridges, and the remaining lag deposit on the crater walls (Figure A11a, stage III). Remnant thicker patches of near-surface ground ice [*Costard et al.,* 2002] or snow perched high in alcoves on the crater rim [*Head et al.,* 2008] might finally melt [*Hecht,* 2002; *Kossacki & Markiewicz,* 2004]. The meltwater could either run off surficially and initiate fluvial transport and downstream deposition, where an alluvial fan would form (Figure A11a, stage III). Alternatively, the meltwater could infiltrate into the lag deposit, saturate it, increase the pore pressure and thus reduce its shear strength, which would increase the susceptibility of the material to gravity-driven failure and debris flows [e.g., *Iverson et al.,* 1997]. The degree of saturation is commonly increased if a low permeability layer in the subsurface is present, which leads to the transient perching of the water table [*Reid et al.,* 1988], and the frozen underground would be such a hydrologic barrier. Another factor favouring the development of debris flows in this setting on Mars is the small grain size of the lag deposit, because clay-sized material is required to maintain the high pore pressures needed

during the flow [*Iverson,* 1997]. This mechanism of debris flow initiation has also been proposed by *Lanza et al.* [2010]. Unambiguous evidence for debris or mud flows on Mars has indeed been found by *Levy et al.* [2010b]. The debris flows and the fluvial processes would form a downstream fan, as it is typical for Earth. The fans have been dated by crater counting and have ages in the order of 10^5 to 10^6 years [*Reiss et al.,* 2004; *Schon et al.,* 2009a]. In the "dry" model, a transition takes place from glacial to periglacial processes, and the formation of gullies and fans from and on the lag deposit would be the final stage [*Dickson & Head,* 2009].

A6.2 The 'wet' scenario

The second scenario starts as the "dry" one, except that a warm-based or polythermal "dust glacier" would form. This glacier would experience basal melting and, therefore, the ice and subglacial meltwater would erode and steepen the crater wall (Figure A11b, stage II). Another difference to the first scenario would be the extent of the permafrost layer. Beneath the warm-based glacier, the permafrost would disappear, and liquid water generated by the basal melting of the glacier would infiltrate into the substrate. A similar scheme was proposed by *Carr & Head* [2003] and *Fassett & Head* [2006]. The groundwater would migrate down towards the interior of the crater. In the subsurface of the crater floor, beyond the extent of the glacier, there would be an impermeable permafrost layer above the groundwater, and the hydraulic head would pressurize the groundwater. At weak spots in the crater floor, which would be abundant due to the fracturing that was created at the impact, this groundwater could ascend as artesian water. Reaching the near surface, it would freeze and build a growing ice core. With time, a mound consisting of this ice core and some overlying mantle deposit would rise. This is how hydraulic (open-system) pingos grow on Earth, except that they do not form in craters, but in valleys where the hydraulic head has its source in nearby mountains [*Müller,* 1959; *Worsley & Gurney,* 1996; *Mackay,* 1998]. The pingos in the study area in Spitsbergen are also thought to form by this mechanism [*Listøl,* 1976, fig. 2]. If the same process applies to Mars, it would represent an example of glacier-permafrost interaction, which is also considered to be an important factor in landform evolution on Svalbard [*Etzelmüller & Hagen,* 2005]. The steepening of the crater wall by glacial erosion would increase the probability for rockfall, which was suggested as a triggering mechanism for debris flows on Earth, if the other requirements (saturated soil, positive pore pressure) are met [*Hsu,* 1975; *Johnson,* 1995]. Except for these differences, this "wet" scenario would otherwise be very similar to the "dry" scenario, and glacial processes (including surficial meltwater production and runoff; *Fassett et al.,* 2010) would be followed by the formation of periglacial landforms (polygons, solifluction lobes, rock glaciers, pingos) and, finally, paraglacial processes (avalanches, rock falls, debris flows, chemical denudation, mechanical fluvial denudation, surface movements/creep; Figure A11b, stage III).

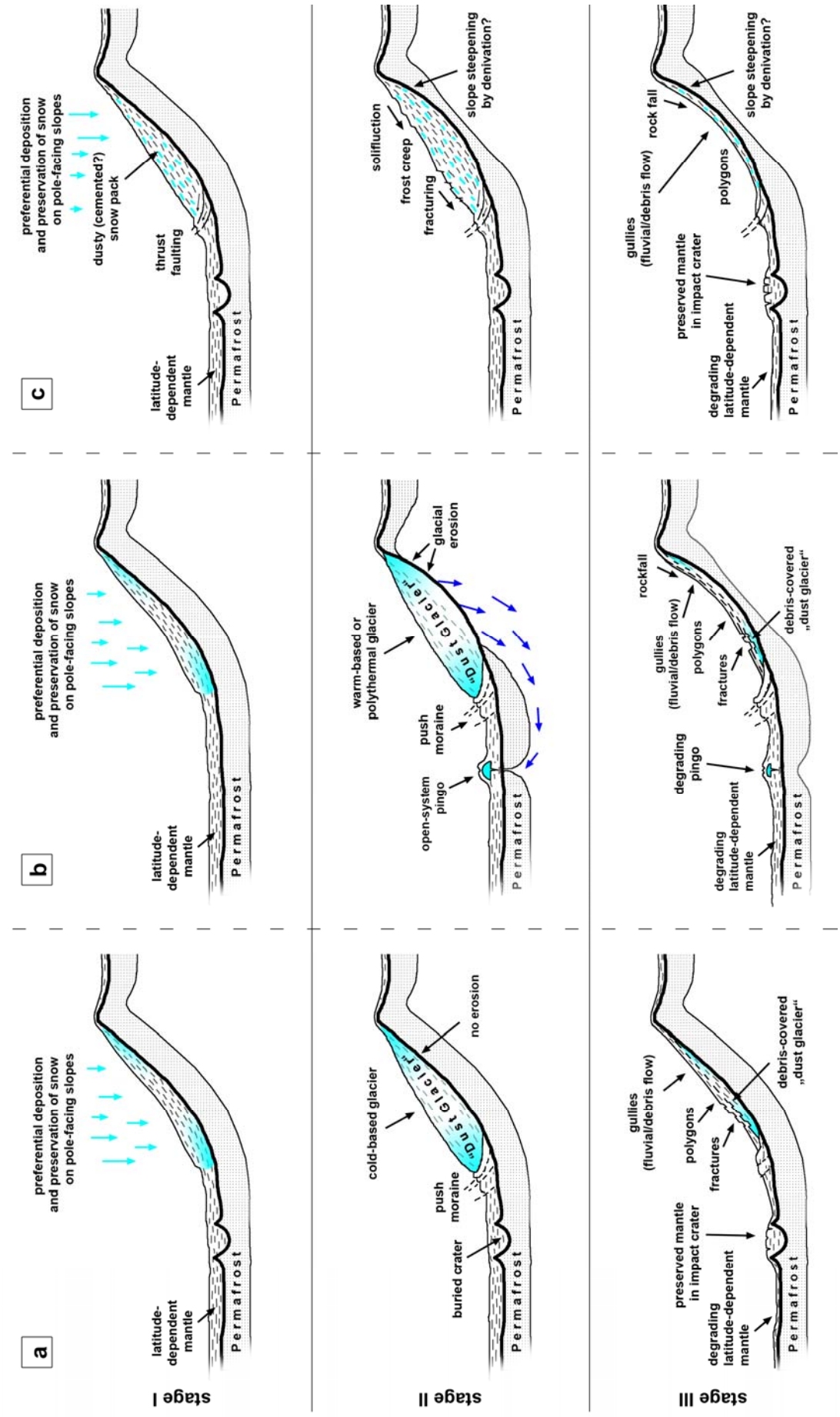

Figure A11: Qualitative scenarios of landscape evolution in Martian mid-latitude craters. See text for details.

A6.3 The 'snow' scenario

A thick snowpack might form instead of a glacier in the "snow" scenario (Figure A11c, stage I). The transition of snow (or rather firn) to glacier ice is defined by density and starts at ~830 kg m^{-3}, where interconnecting air passages between ice grains become sealed off [*Paterson,* 1994] and reaches a final value of 917 kg m^{-3} [*Knight,* 1999, tab. 3.3] (for an extended discussion of ice metamorphism, firnification, and ice formation see *Shumskii* 1964, p. 240-303). While it is known that many factors such as vapour transport, the diurnal and seasonal temperature variations and other factors control the snow densification on Mars [*Arthern et al.,* 2000], a clear difference between Earth and Mars is the rate of gravity-driven snow densification (sintering). Other factors being equal, the transition from snow (or rather firn) to glacier ice should therefore occur on Mars at a larger depth than on Earth (the Martian gravitational acceleration at its surface is about 38% of that on the Earth`s surface). Typical values for this depth on Earth are ~10 to 20 m in temperate areas, and >>50 m in cold continental areas [e.g., *Shumskii,* 1964, p. 275]. The timescales of this transformation are also vastly different, depending on the climate. In cold and dry climates such as in Antarctica, the transformation may require up to 2500 years [*Paterson,* 1994, tab. 2.2], while it can be as short as a few years only in more temperate regions such as in northwestern Canada. In summary, it can be expected that it takes longer in a very cold and presumably rather dry climate on Mars to transform snow to firn and finally to ice than on Earth. This should be true even for recent periods of higher obliquity. Similarly, one might expect snowpacks on Mars that reach larger thicknesses than on Earth before they transform to glacier ice. Based on these qualitative considerations, it seems likely that in many cases the accumulation of snow did not result in a glacier, but in a thick snowpack with intercalated layers of dust and perhaps wind-blown sand [cf. *Williams et al.,* 2008, fig. 3]. The snow scenario is perfectly in agreement with an interpretation of the features shown in Figure A7a as protalus ramparts, because such landforms on Earth are evidence for snow accumulation. Sublimation of snow would again favour the formation of a lag deposit on top of the snowpack. The slow downward creep [*Perron et al.,* 2003] in combination with compaction and sublimation of snow could induce fracturing of the overlying lag deposit (Figure A12a). A terrestrial analogue for this process was described by *Koster* [1988], who investigated niveo-aeolian forms in Alaska. He found that denivation of sand-covered snow on dunes can produce deformational structures such as tensional cracks and compressional features (Figure A11b) [see also *Dijkmans,* 1990; fig. 3B], which are morphologically similar to the contour-parallel fractures and grabens commonly seen on the lower slopes of mantling deposits and fans on Mars (cf. Figure A12a). The creep of the snowpack might also pile up some permafrost material at the base, analogous to the moraines as in the dry and wet scenarios (Figure A11c, stage II).

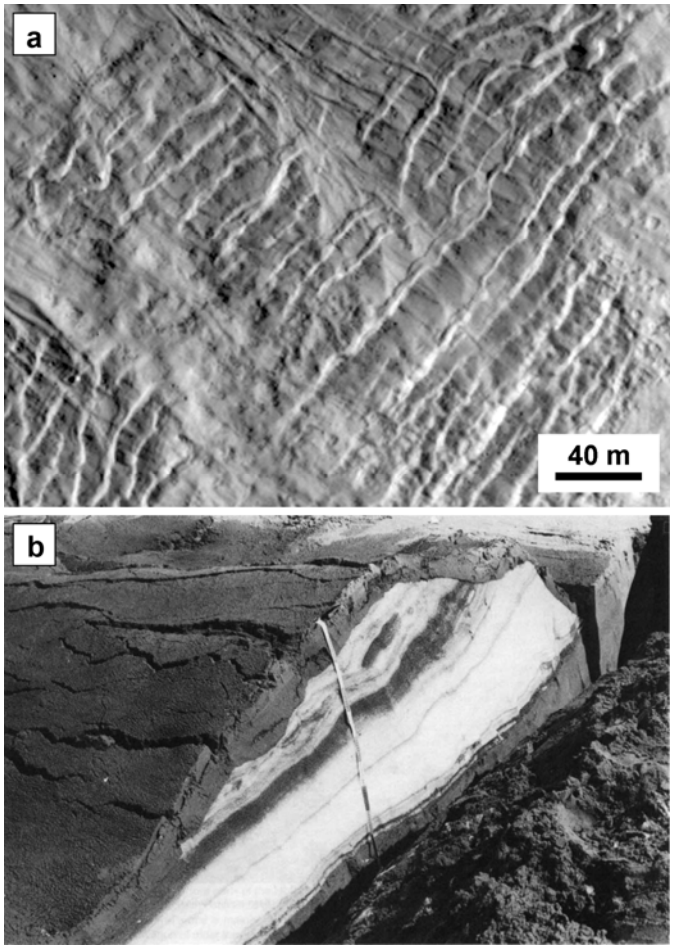

Figure A12: (a) Extensional features (normal faults and grabens) trending normal to the topographic gradient of the inner wall of an impact crater in the northern mid-latitudes (near 39.5°N, 105.4°E; detail of HiRISE PSP_001357_2200, North is up). (b) Niveo-aeolian sediment at the lee (slip) side of a transverse dune in the Great Kobuk Sand Dunes (NW Alaska, USA; from *Koster* [1988], photograph by J. Dijkmans).

The melting of a dusty snow pack has long been recognized as a potential source of liquid water on Mars [*Clow,* 1987], and more recent studies confirmed this possibility [*Williams et al.,* 2008]. While the results of *Williams et al.* [2008] apply only to periods of higher than today`s obliquity, *Möhlmann* [2010b] emphasizes the effect of the "solid-state greenhouse effect" in generating liquid water in snow packs and concludes that even in the current climate of Mars, liquid water can be produced. *Williams et al.* [2009] modelled snow melt at mid-latitudes on Mars and found that enough meltwater can be generated to produce gullies, an idea that had been previously suggested by *Christensen* [2003]. Whenever the snow melting occurred exactly, it would be a viable process to provide the required liquid water for gully and fan formation in the "snow" scenario. If an active layer existed in the past [*Kreslavsky et al.,* 2008], solifluction might occur in the form of frost creep or gelifluction, although the period of the freeze/thaw cycles is difficult to constrain (day-night or seasonal cycles). Fractured mounds would form as erosional forms, not as pingos. Where all the snow in the surrounding has decreased in height or disappeared, snow hummocks would remain, consisting of residual snow patches or ridges [*Koster & Dijkmans,* 1988]. When the tops of these denivation forms are broken up into radial patterns, they display a strikingly similar morphology to Martian fractured mounds (Figure A13). There is a huge difference in scale between the two types of fractured mounds shown in Figure A13, but the

principle should work for the larger fractured mounds on Mars as well. The other landforms would form very similarly as in the other scenarios (Figure A11c, stage III). An important aspect of this scenario and the associated snow melting would be intensified chemical weathering, the role of which has been underestimated in the past even on Earth [*Thorn,* 1988].

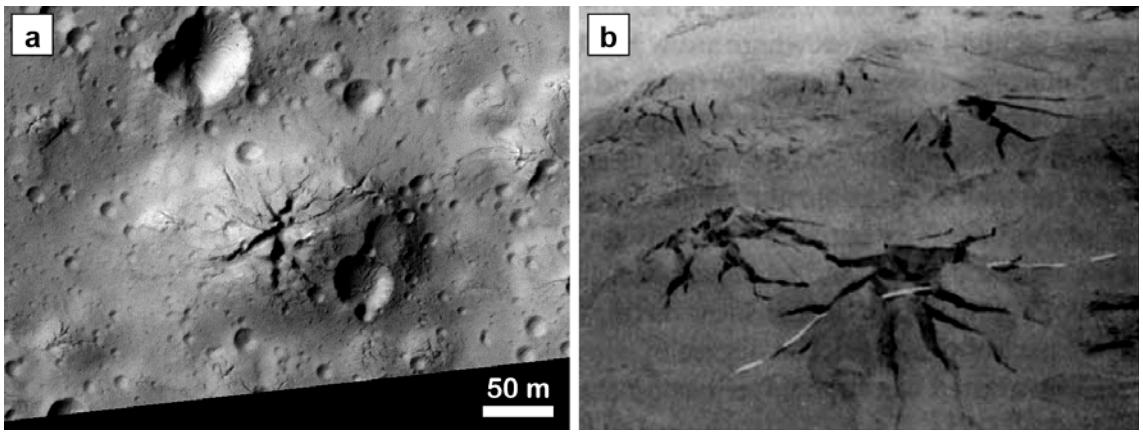

Figure A13: Comparison between fractured mound on Mars and niveo-eolian features on Earth. (a) Mound with radial fractures on the floor of an impact crater in the southern mid-latitudes. The surface of the mound is superposed by several round depressions, which might be due to collapse and/or impact cratering (near 33.6°S, 124°E; detail of HiRISE PSP_002135_1460; North is up). (b) Snow hummock with radial tensional cracks on the Great Kobuk Sand Dunes (Alaska, USA) [from *Koster & Dijkmans,* 1988]. The hummock is a denivation form that developed in niveo-eolian beds. Note the morphological similarity to *(a)*, but also note the large difference in scale (these hummocks are only a few decimetres to one meter wide). See text for details.

A7 Conclusions

Despite significant differences in the climates of Mars and Svalbard, a suite of very analogous landforms has developed, though perhaps over enormously different timescales. Attempts to reconstruct palaeo-climates on Mars have to take into account that different processes acting in different environments can produce similar results (equifinality). The integrated analysis of landscapes can reduce such ambiguities.

The landform inventory associated with pole-facing inner walls of impact craters in the Martian mid-latitudes (Figure A14) suggests the geologically recent action and interaction of glacial and periglacial processes. Based on terrestrial analogue landforms in similarly close spatial proximity on Svalbard, three scenarios of sequential landscape evolution are presented for Mars. All scenarios start with initial snow fall and the deposition of a dusty snow pack, and they all end with recent gully and fan formation. These scenarios are qualitative in the sense that none of them is expected to exactly represent the real situation on Mars. In fact, the scenarios are not mutually exclusive, and mixed cases (e.g., the dry and the snow scenarios) are very plausible. Dependent on latitude and insolation, some craters might have been shaped by the dry scenario, while craters at other latitudes might have been shaped by the wet scenario.

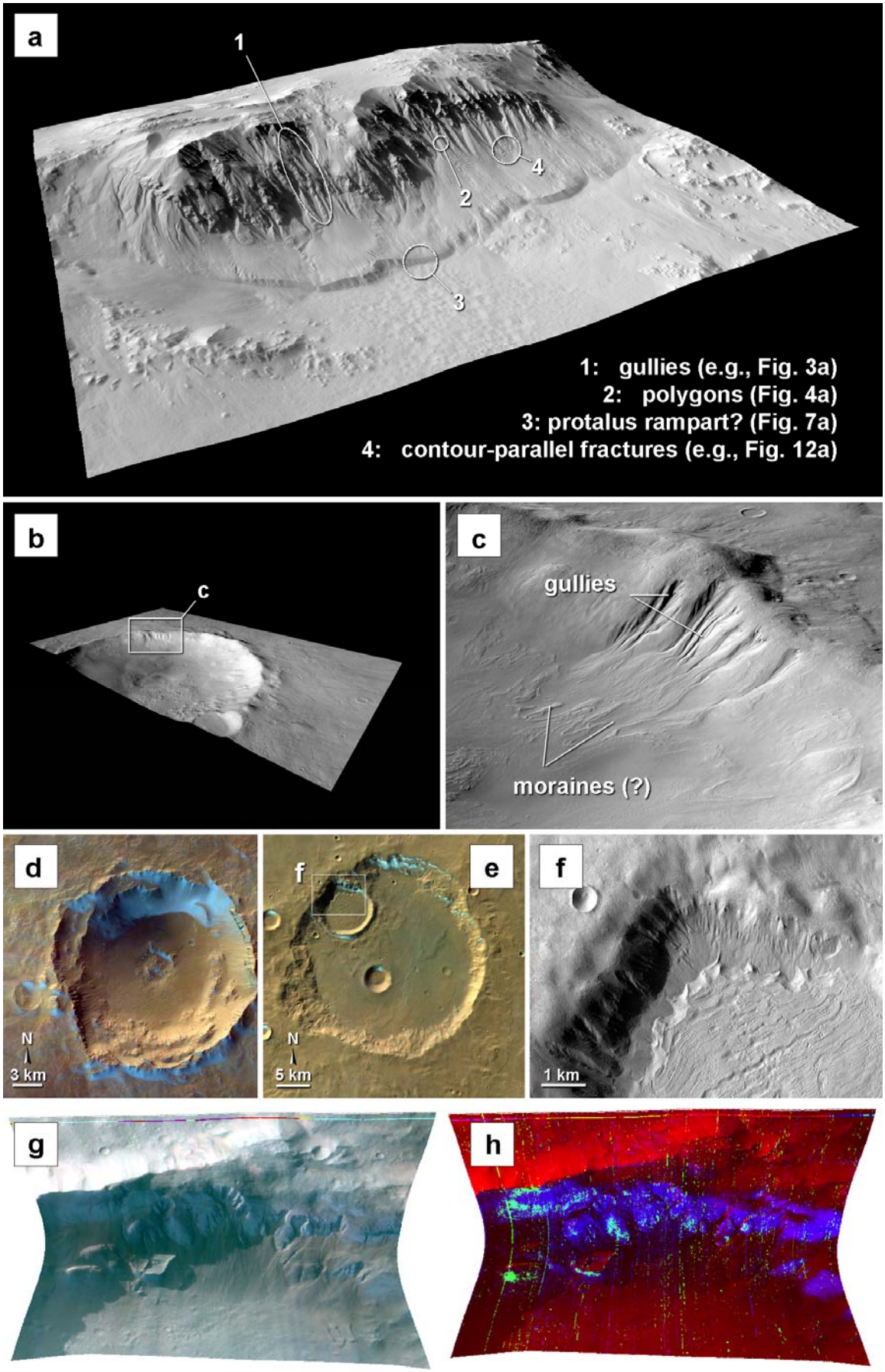
a
1
2
3
4
1: gullies (e.g., Fig. 3a)
2: polygons (Fig. 4a)
3: protalus rampart? (Fig. 7a)
4: contour-parallel fractures (e.g., Fig. 12a)
b
c
c
gullies
moraines (?)
d
N
3 km
f
e
N
5 km
f
1 km
g
h

Figure A.14

The different scenarios also have different implications for the interpretation of certain landforms. For example, fractured mounds are unlikely to be open-system pingos in the dry scenario, because that does not predict liquid water in the subsurface, a prerequisite for the growth of hydraulic pingos. On the other hand, basal melting of snow in the snow scenario could lead to infiltration of liquid water into the subsurface and the formation of a hydraulic pingo as in the wet scenario.

The landscape evolution proposed here would be controlled by obliquity and/or orbital parameters such as eccentricity or the position of perihelion, and is therefore assumed to be cyclic. Several successive episodes of deposition and removal have already been suggested by, e.g., *Kreslavsky & Head* [2002], *Schon et al.* [2009b], and *Morgan et al.* [2010]. Processes implying an active layer might have operated in the past, although an active layer does not exist today [*Kreslavsky et al.,* 2008]. It is thus important to realize that the Martian mid-latitude morphologies do not represent a stable situation over long periods. Instead, this is a dynamic landscape in constant, though perhaps very slow, transition, and patterns of sedimentation and erosion overprint each other repeatedly. Nevertheless, the associated rates for erosion (e.g., in the dry scenario) are likely to be very low, and not all traces of former ice ages are extinguished by later glaciations. Therefore, the spatial extent of former and more widespread glaciation can be identified by careful morphological analysis [*Hauber et al.,* 2008; *Dickson et al.,* 2008, 2010; *Head et al.,* 2010].

Figure A14: (*Continued*) Assemblages of possible periglacial landforms and water ice on Martian pole-facing crater walls. (a) Part of south-facing inner wall of Hale Crater, displaying several landforms that resemble periglacial landforms on Svalbard (CTX image P15_006756_1454 superposed on HRSCDEM, HRSC h0533_0000). View is towards the NE, no vertical exaggeration, image width is about 12 km. (b) Perspective view of a crater in the southern mid-latitudes (at 45.668S, 238.118E; CTX image B05_011519_1341 superposed on HRSC DEM, HRSC h0424_0000). View is towards the NE, no vertical exaggeration, crater diameter is 26 km. (c) Slightly rotated detail of the scene shown in (b), with gullies and possible moraines at the downward termination of the inferred location of former glaciers (view towards the north). (d) Snow and frost on pole-facing slopes (crater centre at 46.058S, 183.858E; detail of HRSC h8569_0000; image acquired during the southern winter at solar longitude (LS) 147.88). The bright material is likely to be water ice, as it was found by the Compact Reconnaissance Imaging Spectrometer (CRISM) at a similar latitude during the same season (see panels g and h). (e) Another example of snow and frost preferentially accumulated on pole-facing slopes (crater centre at 39.68S, 158.328E; detail of HRSC h8527_0000; image acquired during the southern winter at LS 141.68). The white box marks the location of panel (f) and corresponds to an area where bright material accumulated on the inner wall of a smaller impact crater. (f) Detail of the previous image. The area of snow accumulation corresponds exactly to sites where gullies, fans and moraine-like landforms are observed (detail of CTX B05_011746_1401). (g) CRISM false-colour image of a crater rim in Terra Sirenum (near 38.98S, 195.98E). Frost is characterized by a 'bluer' colour than the rock and soil. The image was taken during the Martian winter at LS 140.68 (image source: NASA PlanetaryPhotojournal, #PIA09101; image credit: NASA/JPL/JHUAPL). (h) Same scene as (g), with the colour indicating the depths of absorption bands of H20-frost at 1.50 μm (blue) and CO2-frost at 1.45 μm (green). While CO2-frost occurs only at the coldest, most shaded areas, water ice is more widespread and occurs on slopes incised by many gullies (image source: NASA PlanetaryPhotojournal, #PIA09101; image credit: NASA/JPL/JHUAPL) [see also *Vincendon et al.,* 2009].

Not all craters are necessarily expected to be exactly in the same stage of this landscape evolution. In general, however, the observations of gullies with very recent activity [e.g., *Reiss et al.,* 2010; *Dundas et al.,* 2010; *Diniega et al.,* 2010] point to a late stage situation for most mid-latitude craters at the present time. This is also in agreement with observations of current degradation of the mantling deposit in mid-latitudes [*Mustard et al.,* 2001; *Morgenstern et al.,* 2007; *Lefort et al.,* 2009; Zanetti *et al.,* 2010] and with theoretical modelling of ground ice stability in the recent history of Mars [*Chamberlain & Boynton,* 2007].

The importance of snow (Figures 12 and 13) should not be neglected in assessing the relative importance of glacial and periglacial processes on Mars. Snow and nivation processes are important factors in the geomorphology of polar and cold-climate regions [e.g., *Thorn,* 1978; *Christiansen,* 1998], and snowpacks might be viable alternatives to glacial interpretations of some Martian surface features. Wind should also be an important factor, as it can transport snow and accumulate it in protected regions [*Head et al.,* 2008], where it could act as a landscape forming agent.

Acknowledgements

This study would not have been possible without the logistical support by the German-French research station AWIPEV and the kind hospitality of their staff, in particular Marcus Schumacher and Damien Isambert. The generous help from UNIS and the Norwegian Polar Institute with transport and safety equipment for the field campaigns is highly appreciated. Ella Carlsson, Henrik Johansson, and Steve McDaniel joined the first field trip, and their companionship made it a wonderful experience. We thank the HiRISE and CTX teams for making their data publicly available. This research has been partly supported by the Helmholtz Association through the research alliance “Planetary Evolution and Life”. Constructive comments by Gareth Morgan and an anonymous reviewer are highly appreciated.

Bibliography

Åkerman, J., 1987. Periglacial forms of Svalbard: a review. In: Boardman, J. (ed.) *Periglacial processes and landforms in Britain and Ireland.* Cambridge University Press, Cambridge, 9-25.

Anderson, D.M., Tice, A.R., 1979. The analysis of water in the Martian regolith. *J. Mol. Evolv. 14,* 33-38.

Anderson, D.M., Gatto, L.W., Ugolini, F.C., 1972. An Antarctic analog of Martian permafrost terrain. *Antarctic J. US 7*, 114-116.

André, M.-F., 1990. Frequency of debris flows and slush avalanches in Spitsbergen: a tentative evaluation from lichenometry. *Polish Polar Research 11*, 345-363.

André, M.-F., 1994. Rock Glaciers in Svalbard - Tentative Dating and Inferred Long-Term Velocities. *Geografiska Annaler 76A*, 235-245.

André, M.-F., 1995. Holocene Climate Fluctuations and Geomorphic Impact of Extreme Events in Svalbard. *Geografiska Annaler 77A,* 241-250.

Andrews-Hanna J.C., Lewis K.W., 2011. Early Mars hydrology: 2. Hydrological evolution in the Noachian and Hesperian epochs. J. Geophys. Res., 116. doi:10.1029/2010JE003709

Anisimov, O., Reneva, S., 2006. Permafrost and changing climate: The Russian perpective. *Ambio 35(4)*, 169 – 176.

Arfstrom, J., Hartmann, W.K., 2005. Martian flow features, moraine-like ridges, and gullies: Terrestrial analogues and interrelationships. *Icarus 174,* 321-335.

Arthern, R.J., Winebrenner, D.P., Waddington, E.D., 2000. Densification of water ice deposits on the residual North Polar Cap of Mars. *Icarus 144,* 367-381.

Baker, V.R., 2001. Water and the Martian landscapes. Nature 412, 228-236.

Baker, V.R., 2008. Planetary landscape systems: a limitless frontier. Earth Surf. Proc. Land. 33, 1341–1353.

Ballantyne, C.K. Harris, C., 1994. *The periglaciation of Great Britain*. Cambridge University Press, Cambridge, 330 p.

Balme, M.R., Gallagher; C., 2009. An equatorial periglacial landscape on Mars. *Earth Planet. Sci. Lett. 285 (1-2)*, 1 – 15. doi:10.1016/j.epsl.2009.05.031.

Balme, M., Mangold, N., Baratoux, D., Costard, F., Gosselin, M., Masson, P., Pinet, P., Neukum, G., 2006. Orientation and distribution of recent gullies in the southern hemisphere of Mars: Observations from High Resolution Stereo Camera/Mars Express (HRSC/MEX) and Mars Orbiter Camera/Mars Global Surveyor (MOC/MGS) data. *Journal of Geophysical Research 111,* E05001. doi :10.1029/2005JE002607.

Balme, M.R., Gallagher, C., Page, D.P., Murray, J.B., Muller, J.-P., 2009. Sorted stone circles in Elysium Planitia, Mars: Implications for recent Martian climate. *Icarus 200,* 30-38.

Barfoot, T.D., Furgale, P.T., Osinski, G.R., Ghafoor, N., Williams, K.K., 2010. Field testing of robotic technologies to support ground ice prospecting in martian polygonal terrain. *Planet. Space Sci. 58,* 671-681.

Bauch, K.E., Hiesinger, H., Helbert, J., 2009. Estimation of Lunar surface temperatures: A numerical model. *Lunar Planet. Sci. XXXX*, Abstract 1789.

Beaty, D.W., Buxbaum, K., Meyer, M., Barlow, N., Boynton, W., Clark, B., Deming, J., Doran, P.T., Edgett, K., Hancock, S., Head, J., Hecht, M., Hipkin, V., Kieft, T., Mancinelli, R., McDonald, E., McKay, C., Mellon, M., Newson, H., Ori, G., Paige, D., Schuerger, A.C., Sogin, M., Spry, J.A., Steele, A., Tanaka, K., Voytek, M., 2006. Findings of the Mars special regions science analysis group. *Astrobiology 6,* 677–732.

Bibring, J.-P., Langevin, Y., Mustard, J.F., Poulet, F., Arvidson, R., Gendrin, A., Gondet, B., Mangold, N., Pinet, P., Forget, F., the OMEGA Team, 2006. Global mineralogical and aqueous Mars history derived from OMEGA/Mars Express data. *Science 312*, 400–404.

Berger, A., Loutre, M.F., 1991. Insolation values for the climate of the last 10 million years. *Quat. Sci. Rev. 10*, 297 – 317.

Berman, D.C., Hartmann, W.K., Crown, D.A., Baker, V.R., 2005. The role of arcuate ridges and gullies in the degradation of craters in the Newton Basin region of Mars. *Icarus 178,* 465-486.

Berthling, I., Etzelmüller, B., Eiken, T., Sollid, J.L., 1998, Rock glaciers on Prins Karls Forland, Svalbard. I: internal structure, flow velocity and morphology. *Permafrost Periglac. 9,* 135-145.

Black, R.F., 1976. Periglacial features indicative of permafrost: Ice and soil wedges. *Quat. Res. 6,* 3–26.

Bockheim, J.G., 1995. Permafrost distribution in the southern circumpolar region and ist relation to the environment: a review and recommendations for further research. *Permafrost Periglac. 6,* 27-45.

Bockheim, J.G., Campbell, I.B., McLeod, M., 2007. Permafrost distribution and active-layer depth in the McMurdo Dry Valleys, Antarctica. *Permafrost Periglac. 18*, 217-227.

Bockheim, J.G., Kurz, M.D., Soule, A., Burke, A., 2009. Genesis of active sand-filled polygons in lower and central Beacon Valley, Antarctica. *Permafrost Periglac. 20*, 295-308. doi:10.1002/ppp.661.

Boike, J., Wille, C., Abnizova, A., 2008. Climatology and summer energy and water balance of polygonal tundra in the Lena River Delta, Siberia. *J. Geophys. Res. 113*, G03025. doi:10.1029/2007JG000540.

Borcard, D., Legendre, P., 2002. All-scale spatial analysis of ecological data by means of principal coordinates of neighbor matrices. *Ecol. Model. 153,* 51-68.

Borcard, D., Legendre, P., Drapeau, P., 1992. Partialling out the spatial component of ecological variation. *Ecology 73 (3)*, 1045-1055.

Borcard, D., Legendre, P., Avois-Jacquet, C., Tuomisto, H., 2004. Dissecting the spatial structure of ecological data at multiple scales. *Ecology 87 (7),* 1826-1832.

Boynton, W.V., Feldman, W.C., Squyres, S.W., Prettyman, T.H., Brückner, J., Evans, L.G., Reedy, R.C., Starr, R., Arnold, J.R., Drake, D.M., Englert, P.A.J., Metzger, A.E., Mitrofanov, I., Trombka, J.I., d'Uston, C., Wänke, H., Gasnault, O., Hamara, D.K., Janes, D.M., Marcialis, R.L., Maurice, S., Mikheeva, I., Taylor, G.J., Tokar, R., Shinohara, C., 2002. Distribution of hydrogen in the near surface of Mars: Evidence for subsurface ice deposits. *Science 297,* 81-85. doi:10.1126/science.1073722.

Boytsov, M.N., 1965. Morphological evolution of thaw lake basins. In: *Anthropogenic period in the Arctic and Subarctic*. Papers of the Research Institute Geology of the Arctic, Moscow. Vol. 143, edited by NIEDRA, pp. 327 – 340, Moscow, Russia (in Russian).

Bridges, N.T., Lackner, C.N., 2006. Northern hemisphere Martian gullies and mantled terrain: Implications for near-surface water migration in Mars´ recent past. *J. Geophys. Res. 111*, E09014. doi:10.1029/2006JE002702.

Brown, J., Ferrians Jr., O.J., Heginbottom, J.A., Melnikov, E.S., 1998. *Circum-Arctic map of permafrost and ground-ice conditions*. National Snow and Ice Data Center/World Data Center for Glaciology, Boulder, CO.

Bryant, I.D., 1982. Loess deposits in lower Adventdalen, Spitsbergen. *Polar Res. 2,* 93-103.

Burr, D.M., Tanaka, K.L., Yoshikawa, K., 2009. Pingos on Earth and Mars. Planet. Space Sci. 57 (5-6), 541 – 555. doi:10.1016/j.pss.2008.11.003.Carr, M. H., and J. W. Head (2010),

Geologic history of Mars, *Earth Planet. Sci. Lett. 294 (3-4),* 185-203. doi:10.1016/j.epsl.2009.06.042.

Byrne, S. Dundas, C.M., Kennedy, M.R., Mellon, M.T., McEwen, A.S., Cull, S.C., Daubar, I.J., Shean, D.E., Seelos, K.D., Murchie, S.L., Cantor, B.A., Arvidson, R.E., Edgett, K.S., Reufer, A., Thomas, N., Harrison, T.N., Posiolova, L.V., Seelos5, F.P., 2009. Distribution of mid-latitude ground ice on Mars from new impact craters. *Science 325*, 1674-1676.

Campbell, I.B., Claridge, G.G.C., 2004. Cryosols in the extremely arid Transantarctic Mountains region of Antarctica. In: Kimble, J.M. (ed.) *Cryosols.* Springer, Berlin, 415-426.

Carr, M.H., 1996. *Water on Mars*. Oxford Univ. Press, New York, US.

Carr, M.H., Schaber, G.G., 1977. Martian permafrost features. J. Geophys. Res. 82, 4039-4054.

Carr, M.H., Head, J.W., 2003. Basal melting of snow on early Mars: A possible origin of some valley networks. *Geophys. Res. Lett. 30,* 2245. doi:10.1029/2003GL018575.

Carson, C. E., 2001. The oriented thaw lakes: A retrospective. In: *Fifty More Years Below Zero, Tributes and Meditations for the Naval Arctic Research Laboratory's First Half Century at Barrow, Alaska,* edited by Norton, D.W., pp. 129 – 137, Arctic Institute of North America, Calgary, AB, Canada.

Catto, N.R., 1993. Morphology and development of an alluvial fan in a permafrost region, Aklavik Range, Canada. *Geografiska Annaler 75A*, 83-93.

Chamberlain, M.A., Boynton, W.V., 2007. Response of Martian ground ice to orbit-induced climate change. *J. Geophys. Res. 112*, E06009. doi:10.1029/2006JE002801.

Chander, G., Markham, B.L., Helder, D.L., 2009. Summary of current radiometric calibration coefficients for Landsat MSS, TM, ETM+, and EO-1 ALI sensors. *Remote Sens. Environ. 113,* 893 – 903. doi:10.1016/j.rse.2009.01.007.

Chapelle, F., O'Neill, K., Bradley, P.M., Methe, B.A., Clufo, S.A., Knobel, L.L., Lovley, D.R., 2002. A hydrogen-based subsurface microbial community dominated by methanogens. *Nature 415*, 312-315.

Chevrier, V., Mathé, P.E., 2007. Mineralogy and evolution of the surface of Mars: A review. *Planet. Space Sci. 55*, 289-314.

Chevrier, V., Sears, D.W.G., Chittenden, J.D., Roe, L.A., Ulrich, R., Bryson, K., Billingsley, L., Hanley, J., 2007. Sublimation rate of ice under simulated Mars conditions and the effect of layers of mock regolith JSC Mars-1. *Geophys. Res. Lett. 34,* L02203. doi:10.1029/2006GL028401.

Christensen, P.R., 2003. Formation of recent Martian gullies through melting of extensive water-rich snow deposits. *Nature 422*, 45-48.

Christensen, P.R., Jakosky, B.M., Kieffer, H.H., Malin, M.C., McSween, H.Y., Nealson, K., Mehall, G.L., Silverman, S.H., Ferry, S., Caplinger, M., Ravine, M., 2004. The Thermal Emission Imaging System (THEMIS) for the Mars 2001 Odyssey Mission. *Space Sci. Rev. 110*, 85 – 130.

Christiansen, H.H., 1998. Nivation forms and processes in unconsolidated sediments, NE Greenland. *Earth Surf. Proc. Land. 23*, 751-760.

Christiansen, H.H., 2005. Thermal regime of ice-wedge cracking in Adventdalen, Svalbard. *Permafrost Periglac. 16,* 87-98. doi:10.1002/ppp.523.

Christiansen, H.H., Etzelmüller, B., Isaksen, K., Juliussen, H., Farbrot, H., Humlum, O., Johansson, M., Ingeman-Nielsen, T., Kristensen, L., Hjort, J., Holmlund, P., Sannel, A.B.K., Sigsgaard, C., Åkerman, H.J., Foged, N., Blikra, L.H., Pernosky, M.A., Ødegård, R.S., 2010. The thermal state of permafrost in the Nordic Area during the International Polar Year 2007–2009. *Permafrost Periglac. 21,* 156-181. doi:10.1002/ppp.687.

Chuang, F.C., Crown, D.A., 2005. Surface characteristics and degradational history of debris aprons in the Tempe Terra/Mareotis fossae region of Mars. *Icarus 179*, 24-42. doi:10.1016/j.icarus.2005.05.014.

Clifford, S.M., Lasue, J., Heggy, E., Boisson, J., McGovem, P., Max, M.D., 2010. Depth of the Martian cryosphere: Revised estimates and implications for the existence and detection of subpermafrost groundwater. *J. Geophys. Res. 115,* E07001. doi:10.1029/2009JE003462.

Clow, G.D., 1987. Generation of liquid water on Mars through the melting of a dusty snow pack. *Icarus 72,* 95-127.

Costard, F.M., Kargel J.S., 1995. Outwash plains and thermokarst on Mars. *Icarus 114*, 93 – 112. doi:10.1006/icar.1995.1046.

Costard, F.M., Forget, F., Mangold, N., Peulvast, J.P., 2002. Formation of recent Martian debris flows by melting of near-surface ground ice at high obliquity. *Science 295 (5552),* 110 – 113. doi:10.1126/science.1066698.

Côté, M.M., Burn, C.R., 2002. The oriented lakes of Tuktoyaktuk Peninsula, Western Arctic Coast, Canada – a GIS-based analysis. *Permafrost Periglac. 13*, 61 – 70.

Crampton, C.B., 1977. A note on asymmetric valleys in the central Mackenzie River catchment, Canada. *Earth Surf. Proc. 2*, 427 – 429.

Czudek, T., Demek, J., 1970). Thermokarst in Siberia and its influence on the development of lowland relief. *Quat. Res. 1*, 103 – 120.

Dallmann, W.K., Kjærnet, T., Nøttvedt, A., 2001. *Geomorphological and Quaternary Map of Svalbard.* 1:100,000, Sheet C9G Adventdalen, Temakart No.31/32. Norwegian Polar Institute, Tromsø.

de Pablo, M.A., Komatsu, G., 2009. Possible pingo fields in the Utopia basin, Mars: Geological and climatical implications. Icarus 199 (1), 49-74. doi:10.1016/j.icarus.2008.09.007.Dickson, J. L., J. W. Head, and M. Kreslavsky (2007), Martian gullies in the southern mid-latitudes of Mars: Evidence for climate-controlled formation of young fluvial features based upon local and global topography, *Icarus 188,* 315 – 323, doi:10.1016/j.icarus.2006.11.020.

Des Marais, D.J., et al., 2003. The NASA astrobiology roadmap. *Astrobiology 3*, 219-235.

de Vera, J.-P., Möhlmann, D., Butina, F., Lorek, A., Wernecke, R., Ott, S., 2010. Survival potential and photosynthetic activity of lichens under Mars-like conditions: A laboratory study. *Astrobiology 10,* 215-227.

Dickson, J.L., Head, J.W., 2009. The formation and evolution of youthful gullies on Mars: Gullies as the late-stage phase of Mars' most recent ice age. *Icarus 204,* 63-86.

Dickson, J.L., Head, J.W., Kreslavsky, M., 2007. Martian gullies in the southern mid-latitudes of Mars: Evidence for climate-controlled formation of young fluvial features based upon local and global topography. *Icarus 188,* 315-323.

Dickson, J.L., Head, J.W., Marchant, D.R. 2008. Late Amazonian glaciation at the dichotomy boundary on Mars: evidence for glacial thickness maxima and multiple glacial phases. *Geology 36,* 411-414.

Dickson, J. L., Head, J.W., Marchant, D.R. 2010. Kilometer-thick ice accumulation and glaciation in the northern mid-latitudes of Mars: Evidence for crater-filling events in the Late Amazonian at the Phlegra Montes. *Earth Planet. Sc. Lett 294*, 332-342.

Dijkmans, J.W.A., 1990. Niveo-aeolian sedimentation and resulting sedimentary structures; Søndre Strømfjord area, Western Greenland. *Permafrost Periglac 1,* 83-96.

Diniega, S., Byrne, S., Bridges, N.T., Dundas, C.M., McEwen, A.S., 2010. Present-day Martian dune gully activity. *Lunar and Planetary Science, XLI*, abstract 2216.

Doran, P.T., McKay, C.P., Clow, G.D., Dana, G.L., Fountain, A.G., Nylen, T., Lyons, W.B., 2002. Valley floor climate observations from the McMurdo Dry Valleys, Antarctica, 1986–2000. *J. Geophys. Res. 107(D24)*, 4772. doi:10.1029/2001JD002045.

Dundas, C.M., McEwen, A.S., 2010. An assessment of evidence for pingos on Mars using HiRISE. *Icarus 205*, 244-258.

Dundas, C.M., Mellon, M.T., McEwen, A.S., Lefort, A., Keszthelyi, L.P., Thomas, N., 2008. HiRISE observations of fractured mounds: Possible Martian pingos. *Geophys. Res. Lett. 35,* L04201. doi: 10.1029/2007GL031798.

Dundas, C.M., McEwen, A.S., Diniega, S., Byrne, S., Martinez-Alonso, S., 2010. New and recent gully activity on Mars as seen by HiRISE. *Geophys. Res. Lett. 37*, L07202. doi: 10.1029/2009GL041351.

Dutilleul, P., Haltigin, T.W., Pollard, W.H., 2009. Analysis of polygonal terrain landforms on Earth and Mars through spatial point patterns. *Environmetrics 20 (2),* 206–220.

Durham, R., Schmunk, R.B., Chamberlain, J.W., 1989. Comparative analysis of the atmospheres of early Earth and Mars. *Adv. Space Res. 9,* 139-42.

El Maarry, M.R., Markiewicz, W.J., Mellon, M.T., Goetz, W., Dohm, J.M., Pack, A., 2010. Crater floor polygons: Desiccation patterns of ancient lakes on Mars? *J. Geophys. Res. 115,* E10006. doi:10.1029/2010JE003609.

Etzelmüller, B., Hagen, J.O., 2005. Glacier-permafrost interaction in Arctic and alpine mountain environments with examples from southern Norway and Svalbard. In: Harris, C. & Murton, J.B. (eds.) *Cryospheric Systems: Glaciers and Permafrost.* Geological Society, London, Special Publication, 242, 11-27.

Everdingen, R. O. v. (Ed.) (2005), *Multi-Language Glossary of Permafrost and Related Ground-Ice Terms,* International Permafrost Association, Univ. of Calgary, Calgary, Canada (available at http://nsidc.org/fgdc/glossary).

Fairén, A.G., Davila, A.F., Lim, D., Bramali, N., Bonaccorsi, R., Zavaleta, J., Uceda, E.R., Stoker, C., Wierzchos, J., Dohm, J.M., Amils, R., Andersen, D., McKay, C.P., 2010. Astrobiology through the ages on Mars: The study of terrestrial analogues to understand the habitability of Mars. *Astrobiology 10(8)*, 821-843.

Fanale, F.P., Salvail, J.R., Zent, A.P., Postawko, S.E., 1986. Global distribution and migration of subsurface ice on Mars. *Icarus 67,* 1-18.

Farmer, J.D., Des Marais, D.J., 1999. Exploring for a record of ancient Martian life. *J. Geophys. Res. 104(E11)*, 26,977-26,995.

Fassett, C.I., Head, J.W. 2006. Valleys on Hecates Tholus, Mars: origin by basal melting of summit snowpack. *Planet. Space Sci. 54,* 370-378.

Fassett, C.I., Dickson, J.L., Head, J.W., Levy, J.S., Marchant, D.R., 2010. Supraglacial and proglacial valleys on Amazonian Mars. *Icarus 208,* 86-100.

Feldman, W.C., Prettyman, T.H., Maurice, S., Plaut, J.J., Bish, D.L., Vaniman, D.T., Mellon, M.T., Metzger, A.E., Squyres, S.W., Karunatillake, S., Boynton, W.V., Elphic, R.C., Funsten, H.O., Lawrence, D.J., Tokar, R.L., 2004. Global distribution of near-surface hydrogen on Mars. *J. Geophys. Res. 109,* E09006. doi: 10.1029/2003JE002160.

Forget, F., Haberle, R.M., Montmessin, F., Levrard, B., Head, J.W., 2006. Formation of Glaciers on Mars by Atmospheric Precipitation at High Obliquity. *Science 311,* 368–371.

Fortier, D., Allard, M., 2005. Frost-cracking conditions, Bylot Island, Eastern Canadian Artic archipelago. *Permafrost Periglac 16,* 145-161. doi:10.1002/ppp.504.

Fortier, D., Allard, M., Shur, Y., 2007. Observation of rapid drainage system development by thermal erosion of ice wedges on Bylot Island, Canadian Arctic Archipelago. *Permafrost Periglac. 18*, 229-243. doi:10.1002/ppp.595.

French, H.M., 1970. Soil temperatures in the active layer, Beaufort plain. *Arctic 23 (4),* 229 – 239.

French, H.M., 2007. *The Periglacial Environment*, 3rd ed., 458 pp., John Wiley, Chichester, U. K.

Frolov, A.D., 2003. A review of the nature and geophysical studies of the thick permafrost in Siberia: Relevance to exploration on Mars. *J. Geophys. Res. 108(E4),* 8039. doi:10.1029/2002JE001881.

Frouin, R., Gautier, C., Katsaros, K.B., Lind, R.J., 1988. A comparison of satellite and empirical formula techniques for estimating insolation over the oceans. *J. Meteorol. 27*, 1016 – 1023.

Fu, P., Rich, P.M., 1999. Design and implementation of the Solar Analyst: an ArcView extension for modeling solar radiation at landscape scales. In: *Proceedings of the Nineteenth Annual ESRI User Conference*, San Diego, USA. (available at http://proceedings.esri.com/library/userconf/proc99/proceed/papers/pap867/p867.htm).

Gallagher, C., Balme, M.R., Conway, S.J., Grindrod, P.M., 2011. Sorted clastic stripes, lobes and associated gullies in high-latitude craters on Mars: Landforms indicative of very recent, polycyclic ground-ice thaw and liquid flows *Icarus 211,* 458-471.

Gilichinsky, D.A., Wagener, S., 1995. Microbial life in permafrost: A historical review. *Permafrost Periglac. 6*, 243-250.

Gilichinsky, D.A., Wagener, S., Vishnevetskaya, T.A., 1995. Permafrost microbiology. *Permafrost Periglac. 6,* 281-291.

Gilichinsky, D.A., Rivkina, E., Bakermans, C., Shcherbakova, V., Petrovskaya, L., Ozerskaya, S., Ivanushkina, N., Kochkina, G., Laurinavichuis, K., Pecheritsina, S., Fattakhova, R., Tiedje, J.M., 2005. Biodiversity of cryopegs in permafrost. *FEMS Microbiol. Ecol. 53*, 117-128.

Gilichinsky, D.A., Wilson, G.S., Friedmann, E.I., McKay, C.P., Sletten, R.S., Rivkina, E.M., Vishnivetskaya, T.A., Erokhina, L.G., Ivanushkina, N.E., Kochkina, G.A., Shcherbakova, V.A., Soina, V.S., Spirina, E.V., Vorobyova, E.A., Fyodorov-Davydov, D.G., Hallet, B., Ozerskaya, S.M., Sorokovikov, V.A., Laurinavichyus, K.S., Shatilovich, A.V., Chanton, J.P., Ostroumov, V.E., Tiedje, J.M., 2007. Microbial Populations in Antarctic Permafrost: Biodiversity, State, Age, and Implication for Astrobiology. *Astrobiology 7(2),* 275-311. doi:10.1089/ast.2006.0012.

Griess, J., Mangelsdorf, K., Gattinger, A., Schloter, M., Kurchatova, A., Herzschuh, U., Wagner, D., in prep. Response of methanogenic archea to Holocene and Late Pleistocene climate changes in Siberian permafrost deposits. To be submitted to *The ISME Journal*.

Grigoriev, M.N., 1993. *Cryomorphogenesis in the Lena Delta*. 176 pp., Permafrost Institute Press, Yakutsk. (in Russian).

Gooding, J.L., 1986. Martian dust particles as condensation nuclei - A preliminary assessment of mineralogical factors. *Icarus 66*, 56-74.

Grom, J. D., Pollard, W.H., 2008. A study of high arctic retrogressive thaw slump dynamics, Eureka Sound Lowlands, Ellesmere Island. In: *Permafrost: Proceedings of the 9th International Conference on Permafrost 2008,* edited by Kane, D.L., and K.M. Hinkel, pp. 545-550, Institute of Northern Engineering, Univ. of Alaska Fairbanks.

Grosse, G., Jones, B.M., 2011. Spatial distribution of pingos in northern Asia. *The Cryosphere 5*, 13-33.

Grosse, G., Schirrmeister, L., Malthus, T.J., 2006. Application of Landsat-7 satellite data and a DEM for the quantification of thermokarst-effected terrain types in the periglacial Lena-Anabar coastal lowland. *Pol. Res. 25*, 51 – 67.

Grosse, G., Schirrmeister, L., Siegert, Ch., Kunitsky, V.V., Slagoda, E.A., Andreev, A.A., Dereviagyn, A.Y., 2007. Geological and geomorphological evolution of a sedimentary periglacial landscape in Northeast Siberia during the Late Quaternary. *Geomorphology 86(1-2)*, 25 – 51.

Günther, F., 2009. Untersuchung der Thermokarstentwicklung im südlichen Lena Delta anhand multitemporaler Fernerkundungs- und Felddaten, Dipl. thesis, 96 pp., Tech. Univ. of Dresden, Dresden, Germany. (in German).

Gurney, S.D., 1998. Aspects of the genesis and geomorphology of pingos: perennial permafrost mounds. Prog. *Phys. Geog. 22(3*), 307-324.

Gwinner, K., Scholten, F., Spiegel, M., Schmidt, R., Giese, B., Oberst, J., Jaumann, R., Neukum, G., the HRSC Co-Investigator Team, 2005. Hochauflösende Digitale Geländemodelle auf der Grundlage von Mars Express HRSC-Daten. *Photogrammetrie, Fernerkundung, Geoinformation 5/2005,* 387–394.

Gwinner, K., Coltelli, M., Flohrer, J., Jaumann, R., Matz, K.-D., Marsella, M., Roatsch, T., Scholten, F., Trauthan, F., 2006. The HRSC-AX Mt. Etna Project: High-Resolution Orthoimages and 1 m DEM at Regional Scale. *International Archives of Photogrammetry and Remote Sensing, XXXVI (Part 1)*. http://isprs.free.fr/documents/Papers/T05-23.pdf.

Gwinner, K., Scholten, F., Spiegel, M., Schmidt, R., Giese, B., Oberst, J., Heipke, C., Jaumann, R., Neukum, G., 2009. Derivation and Validation of High-Resolution Digital Elevation Models from Mars Express HRSC-Data. *Photogramm. Eng. Rem. S. 75*, 1127-1142.

Gwinner, K., Scholten, F., Preusker, F. Elgner, S., Roatsch, T., Spiegel, M., Schmidt, R., Oberst, J., Jaumann, R., Heipke, C., 2010. Topography of Mars from global mapping by HRSC high-resolution digital elevation models and orthoimages: characteristics and performance: *Earth Planet. Sc. Lett. 294,* 506-519.

Haberle, R.M., McKay, C.P., Schaeffer, J., Cabrol, N.A., Grin, E.A., Zent, A.P., Quinn, R., 2001. On the possibility of liquid water on present-day Mars. *J. Geophys. Res. 106*, E10, 23317-23326.

Haeberli, W., 1979. Holocene push-moraines in Alpine permafrost. *Geografiska Annaler 61A*, 43-48.

Haeberli, W., 1985. On the morphodynamics of ice/debris-transport systems in cold mountain areas. *Norsk Geografisk Tidsskrift 50*, 3-9.

Haeberli, W., 2005. Investigating glacier-permafrost relationships in high-mountain areas: historical background, selected examples and research needs. In: Harris, C. & Murton, J.B. (eds.) *Cryospheric Systems: Glaciers and Permafrost*, Geological Society, London, Special Publication, 242, 29-37.

Haltigin, T., Pollard, W., Dutilleul, P., 2010. Comparison of ground- and aerial-based approaches for quantifying polygonal terrain network geometry on Earth and Mars via spatial point pattern analysis. *Planet. Space Sci. 58,* 1636-1649.

Hanssen-Bauer, I., Førland, E.J., 1998. Long-term trends in precipitation and temperature in the Norwegian Arctic: Can they be explained by changes in atmospheric circulation patterns?. *Clim.Res. 10,* 143–153.

Härtel, S., Christiansen, H.H., 2010. Formation and dynamics of Holocene syngenetic ice-wedge polygons in Adventdalen, Svalbard. *Third European Conference on Permafrost*. The University Center in Svalbard, Longyearbyen, Svalbard, Norway, pp. 54.

Hartmann, W.K., Neukum, G., 2001. Cratering chronology and the evolution of Mars. *Space Sci. Rev. 96,* 165-194.

Hauber, E., van Gasselt, S., Chapman, M.G., and Neukum, G., 2008. Geomorphic evidence for former lobate debris aprons at low latitudes on Mars: Indicators of the Martian paleoclimate. *J. Geophys. Res. 113,* E02007, doi:10.1029/2007JE002897.

Hauber, E., Preusker, F., Trauthan, F., Reiss, D., Carlsson, A., Hiesinger, H., Jaumann, R., Johansson, H.A.B., Johansson, L., Johnsson, A., McDaniel, S., Olvmo, M., Zanetti, M., 2009. Morphometry of Alluvial Fans in a Polar Desert (Svalbard, Norway): Implications for Interpreting Martian Fans. *Lunar and Planetary Science Conference, 40,* abstract 1468.

Hauber, E., Reiss, D., Ulrich, M., Preusker, F., Trauthan, F., Zanetti, M., Hiesinger, H., Jaumann, R., Johansson, L., Johnsson, A., Gasselt, S. van, Olvmo, M., 2011. Landscape evolution in Martian mid-latitude regions: insights from analogous periglacial landforms in Svalbard. In: Balme, M.R., Bargery, A.S., Gallagher, C.J., Gupta, S. (Eds.), *Martian Geomorphology.* Geol. Soc., London, Special Publications, 356, 111-131. doi:10.1144/SP356.7.

Hauber, E., Reiss, D., Ulrich, M., Preusker, F., Trauthan, F., Zanetti, M., Hiesinger, H., Jaumann, R., Johansson, L., Johnsson, A., Olvmo, M., Carlsson, E., Johansson, H.A.B., McDaniel, S., in press. Periglacial landscapes on Svalbard: Terrestrial analogues for cold-climate landforms on Mars. In: Garry, B., Bleacher, J. (Eds.), *Analogs for planetary exploration.* GSA Special Papers, Geol. Soc. Amer, USA.

Head, J.W., Marchant, D.R., 2003. Cold-based mountain glaciers on Mars: Western Arsia Mons. *Geology 31,* 641–644.

Head, J.W., Kreslavsky, M.A., Pratt, S., 2002. Northern lowlands of Mars: Evidence for widespread volcanic flooding and tectonic deformation in the Hesperian period. *J. Geophys. Res. 107 (E1)*, 5003.

Head, J.W., Mustard, J.F., Kreslavsky, M.A., Milliken, R.E., Marchant, D.R., 2003. Recent ice ages on Mars. *Nature 426,* 797 – 802.

Head, J.W., Marchant, D.R., Agnew, M.C., Fassett, C.I., Kreslavsky, M.A., 2006. Extensive valley glacier deposits in the northern mid-latitudes of Mars: Evidence for Late Amazonian obliquity-driven climate change. *Earth Planet. Sci. Lett. 241,* 663–671.

Head, J.W., Marchant, D.R., Kreslavsky, M.A., 2008. Formation of gullies on Mars: Link to recent climate history and insolation microenvironments implicate surface water flow origin, *PNAS 105 (36)*, 13258 – 13263.

Head, J.W., Marchant, D.R., Dickson, J.L., Kress, A.M., Baker, D.M., 2010. Northern mid-latitude glaciation in the Amazonian period of Mars: Criteria for the recognition of debris-covered glacier and valley glacier landsystem deposits. *Earth Planet. Sci. Lett. 294,* 306-320.

Hecht, M., 2002. Metastability of liquid water on Mars. *Icarus 156*, 373 – 386, doi:10.1006/icar.2001.6794.

Hedderich, R., Whitman, W., 2006. Physiology and biochemistry of the methane-producing archaea. In: Dworkin, M., Falkow, S., Rosenberg, E., Schleifer, K.-H., Stackebrandt, E. (Eds.) *Prokaryotes,* vol 2, Springer, New York, pp. 1050–1079.

Hess, S.L., Ryan, J.A., Tillman, J.E., Henry, R.M., Leovy, C.B., 1980. The annual cycle of pressure on Mars measured by Viking Landers 1 and 2. *J. Geophys. Res. 7 (3),* 197-200.

Hiesinger, H., Head, J.W., 2000. Characteristics and origin of polygonal terrain in southern Utopia Planitia, Mars: Results from Mars Orbiter Laser Altimeter and Mars Orbiter Camera data. *J. Geophys. Res. 105,* 11999-12022.

Hill, P. R., Solomon, S., 1999. Geomorphologic and sedimentary evolution of a transgressive thermokarst coast, Mackenzie Delta Region, Canadian Beaufort Sea. *J. Coastal Res. 15*, 1011-1029.

Hinkel, K. M., Frohn, R.C., Nelson, F.E., Eisner, W.R., Beck, R.A., 2005. Morphometric and spatial analysis of thaw lakes and drained thaw lake basins in the western arctic coastal plain, Alaska. *Permafrost Periglac. 16,* 327 – 341.

Holt, J.W., Safaeinili, A., Plaut, J.J., Head, J.W., Phillips, R.J., Seu, R., Kempf, S.D., Choudhary, P., Young, D.A., Putzig, N.E., Biccari, D., Gim, Y., 2008. Radar Sounding Evidence for Buried Glaciers in the Southern Mid-Latitudes of Mars. *Science 322*, 1235-1238.

Horneck, G., 2000. The microbial world in case for Mars. *Planet. Space Sci. 48,* 1053-1063.

Hsu, K.J., 1975. Catastrophic debris streams (sturzstroms) generated by rockfalls. *Geological Society of America Bulletin 86,* 129–140.

Hubberten, H.W., Andreev, A., Astakhov, V.I., Demidov, I., Dowdeswell, J.A., Henriksen, M., Hjort, C., Houmark-Nielsen, M., Jakobsson, M., Kuzmina, S., Larsen, E., Lunkka, J.P., Lysså, A., Mangerud, J., Möller, P., Saarnisto, M., Schirrmeister, L., Sher, A.V., Siegert, C., Siegert, M.J., Svendsen, J.I., 2004. The periglacial climate and environment in northern Eurasia during the Last Glaciation. *Quat. Sci. Rev. 23,* 1333-1357.

Humlum, O., 2005. Holocene permafrost aggradation in Svalbard. In: Harris, C. & Murton, J.B. (eds.) *Cryospheric Systems: Glaciers and Permafrost,* Geological Society, London, Special Publication, 242, 11-27.

Humlum, O., Christiansen, H.H., 2008. Lowland periglacial research: a review of published advances 2003-2007. *Permafrost Periglac. 19*, 211-235.

Humlum, O., Instanes, A., Sollid, J.L., 2003. Permafrost in Svalbard: A review of research history, climatic background and engineering challenges. *Polar Res. 22 (2),* 191-215.

Hutchinson, M.F., 1989. A new procedure for gridding elevation and stream line data with automatic removal of spurious pits. *J. Hydrol. 106*, 211 – 232.

Isaksen, K., Ødegård, R.S., Eiken, T., Sollid, J.L., 2000. Composition, flow and development of two tongue-shaped rock glaciers in the permafrost of Svalbard. *Permafrost Periglac. 11*, 241-257.

Isaksen, K., Holmlund, P., Sollid, J.L., Harris, C., 2001. Three deep alpine boreholes in Svalbard and Scandinavia. *Permafrost Periglac. 12,* 13-25. doi:10.1002/ppp.380.

Ito, H., Watanabe, H., Takehisa, M., and Iizuka, H., 1983. Isolation and identification of radiation-resistant cocci belonging to the genus Deinococcus from sewage sludges and animal feeds. *Agric. Biol. Chem. 47,* 1239–1247.

Iverson, R.M., Reid, M.E., Lahusen, R.G., 1997. Debris-flow mobilization from landslides. *Annu. Rev. Earth Pl. Sc. 25*, 85–138.

Jakosky, B.M., Carr, M.H., 1985. Possible precipitation of ice at low latitudes of Mars during periods of high obliquity. *Nature 315*, 559-561.

Jakosky, B.M., Henderson, B.G., Mellon, M.T., 1995. Chaotic obliquity and the nature of the Martian climate. *J. Geophys. Res. 100*, 1579-1584.

Jakosky, B., Nealson, K, Bakermans, C., Ley, R., Mellon, M., 2003. Subfreezing activity of microorganisms and the potential habitability of Mars' polar regions. *Astrobiology 3,* 34-350.

Jaumann, R., Neukum, G., Behnke, T., Duxbury, T.C., Eichentopf, K., Flohrer, J., Gasselt, S. van, Giese, B., Gwinner, K., Hauber, E., Hoffmann, H., Hoffmeister, A., Köhler, U., Matz, K.-D., McCord, T.B., Mertens, V., Oberst, J., Pischel, R., Reiss, D., Ress, E., Roatsch, T., Saiger, P., Scholten, F., Schwarz, G., Stephan, K., Wählisch, M., the HRSC Co-Investigator Team, 2007. The high-resolution stereo camera (HRSC) experiment on Mars Express: Instrument aspects and experiment conduct from interplanetary cruise through the nominal mission. *Planet. Space Sci. 55,* 928-952.

Jeppesen, J.W., 2001. Palæoklimatiske indikatorer for central Spitsbergen, Svalbard. Eksemplificeret ved studier af iskiler og deres værtssediment (Ice wedges and host sediments as palaeoclimatic indicators in central Spitsbergen, Svalbard) MSc thesis. University of Copenhagen, Denmark. (in Danish).

Johnson, P.G., 1995. Debris transfer and sedimentary environments: Alpine glaciated areas. In: Slaymaker, O. (ed.) *Steepland Geomorphology*, Wiley, Chichester, 27-44.

Kadish, S.J., Head, J.W., Barlow, N.G., Marchant, D.R., 2008. Martian pedestal craters: Marginal sublimation pits implicate a climate-related formation mechanism. *Geophys. Res. Lett. 35*, L16104. doi.10.1029/2008GL034990.

Kadish, S.J., Barlow, N.G., Head, J.W., 2009. Latitude dependence of Martian pedestal craters: Evidence for a sublimation-driven formation mechanism. *J. Geophys. Res. 114,* E10001. doi:10.1029/2008JE003318.

Kahn, R.A., Martin, T.Z., Zurek, R.W., Lee, S.W., 1992. The Martian dust cycle. In: Kieffer, H.H. et al. (eds.) *Mars*. Univ. of Ariz. Press, Tucson, 1017-1053.

Kieffer, H.H., 1976. Soil and surface temperatures at the Viking landing sites. *Science 194*, 1344-1346.

Kieffer, H. H., Titus, T.N., Mullins, K.F., Christensen, P.R., 2000. Mars south polar spring and summer behavior observed by TES: Seasonal cap evolution controlled by frost grain size. *J. Geophys. Res. 105 (E4),* 9653 – 9700, doi:10.1029/1999JE001136.

Kirk, R.L., Howington-Kraus, E., Rosiek, M.R., Anderson, J.A., Archinal, B.A., Becker, K.J., Cook, D.A., Galuszka, D.M., Geissler, P.E., Hare, T.M., Holmberg, I.M., Keszthelyi, L.P., Redding, B.L., Delamere, W.A., Gallagher, D., Chapel, J.D., Eliason, E.M., King, R., McEwen, A.S., 2008. Ultrahigh resolution topographic mapping of Mars with MRO HiRISE stereo images: Meter-scale slopes of candidate Phoenix landing sites. *J. Geophys. Res. 113,* E00A24. doi:10.1029/2007JE003000.

Klein, H.P., 1998. The search for life on Mars: What we learned from Viking. *J. Geophys. Res. 103(E12),* 28,463-28,466.

Kminek, G., Rummel, J.D., Cockell, C.S., Atlas, R., Barlow, N., Beaty, D., Boynton, W., Carr, M., Clifford, S., Conley, C.A., Davila, A.F., Debus, A., Doran, P., Hecht, M., Heldmann, J., Helbert, J., Hipkin, V., Horneck, G., Kieft, T.L., Klingelhoefer, G., Meyer, M., Newson, H., Ori, G.G., Parnell, J., Prieur, D., Raulin, F., Schulze-Makuch, D., Spry, J.A., Stabekis, P.E., Stackebrandt, E., Vago, J., Viso, M., Voytek, M., Wells, L., Westall, F., 2010. Report of the COSPAR Mars special regions colloquium. *Adv. Space Res. 46,* 811-829.

Kneissl, T., Reiss, D., van Gasselt, S., Neukum, G., 2010. Distribution and orientation of northern-hemisphere gullies on Mars from the evaluation of HRSC and MOC-NA data. *Earth Planet. Sci. Lett. 294 (3-4),* 357-367. doi:10.1016/j.epsl.2009.05.018.

Koch, K., Knoblauch, C., Wagner, D., 2009. Methanogenic community composition and anaerobic carbon turnover in submarine permafrost sediments of the Siberian Laptev Sea. *Environmental Microbiology 11,* 657-668.

Kossacki, K.J., Markiewicz, W.J., 2004. Seasonal melting of surface water ice condensing in Martian gullies. *Icarus 171*, 272-283.

Koster, E.A., 1988. Ancient and modern cold-climate aeolian sand deposition: a review. *J. Quat. Sci. 3,* 69-83.

Koster, E.A., Dijkmans, J.W.A., 1988. Niveo-aeolian deposits and denivation forms, with special reference to the Great Kobuk Sand Dunes, Northwestern Alaska. *Earth Surf. Proc. Land. 13,* 153-170.

Kral, T.A., Bekkum, C.R., McKay, C.P., 2004. Growth of methanogens on a Mars soil simulant. *Origins Life Evol. B. 34,* 615-626.

Krbetschek, M.R., Gonser, G., Schwamborn, G., 2002. Luminescence dating results on sediment sequences of the Lena Delta. *Polarforschung 70,* 83 – 88.

Kreslavsky, M.A., Head, J.W., 2000. Kilometer-scale roughness of Mars: Results from MOLA data analysis*. J. Geophys. Res. 105(E11),* 26695-26711.

Kreslavsky, M.A., Head, J.W., 2002. Mars: Nature and evolution of young latitude dependent water-ice-rich mantle. *Geophys. Res. Lett. 29(15)*. doi:10.1029/2002GL015392.

Kreslavsky, M.A., Head, J.W., Marchant, D.R., 2008. Periods of active permafrost layer formation during the geological history of Mars: Implications for circum-polar and mid.latitudes surface processes. *Planet. Space Sci. 56*, 289-302.

Kumar, P.V.H., Kumar, N.M., Mathew, B., 1991. Insolation over the Arabian Sea during the southwest monsoon. *Boundary-Layer Meteorol. 56*, 197 – 203.

Lachenbruch, A.H., 1962. Mechanics of thermal contraction cracks and ice-wedge polygons in permafrost. *Spec. Pap. Geol. Soc. Am. 70.*

Lachenbruch, A.H., 1966. Contraction theory of ice-wedge polygons: A qualitative discussion. *Proc. Permafrost Int. Conf.,* Lafayette, Indiana. Publ. 1287. U.S. Natl. Acad. Sci., Washington, D. C. pp. 63-71.

Laevastu, T., 1960. Factors affecting the temperature of the surface 1ayer of the sea. *Comment. Phys. Math. 25*, 1 – 136.

Lanza, N.L., Meyer, G.A., Okubo, C.H., Newsom, H.E., Wiens, R.C., 2010. Evidence for debris flow gully formation initiated by shallow subsurface water on Mars. *Icarus 205*, 103-112.

Larsson, S., 1982. Geomorphological effects on the slopes of Longyear Valley, Spitsbergen, after a heavy rainstorm in July 1972. *Geografiska Annaler 64 A,* 105-125.

Laskar, J., Levrard, B., Mustard, J.F., 2002. Orbital forcing of the martian polar layered deposits. *Nature 419*, 375-377.

Laskar, J., Correia, A.C.M., Gastineau, M., Joutel, F., Levrard, B., Robutel, P., 2004. Long term evolution and chaotic diffusion of the insolation quantities of Mars. *Icarus 170*, 343 – 364. doi:10.1016/j.icarus.2004.04.005.

Lefort, A., Russell, P.S., Thomas, N., McEwen, A.S., Dundas, C.M., Kirk, R.L., 2009. Observations of periglacial landforms in Utopia Planitia with the High Resolution Imaging Science Experiment (HiRISE*). J. Geophys. Res. 114,* E04005. doi:10.1029/2008JE003264.

Lefort, A., Russell, P.S., Thomas, N., 2010. Scalloped terrain in Peneus and Amphitrites Paterae region of Mars as observed by HiRISE. *Icarus 2005(1)*, 259 – 268. doi:10.1016/j.icarus.2009.06.005.

Leighton, R.R., Murray, B.C., 1966. Behavior of carbon dioxide and other volatiles on Mars. *Science 153,* 136-144.

Levrard, B., Forget, F., Montmessin, F., Laskar, J., 2004. Recent ice-rich deposits formed at high latitudes on Mars by sublimation of unstable equatorial ice during low obliquity. *Nature 431,* 1072–1075.

Levy, J., Head, J., Marchant, D., 2009a. Thermal contraction crack polygons on Mars: Classification, distribution, and climate implications from HiRISE observations. *J. Geophys. Res. 114,* E01007. doi:10.1029/2008JE003273.

Levy, J, Head, J.W., Marchant, D.R., 2009b. Concentric crater fill in Utopia Planitia: History and interaction between glacial “brain terrain” and periglacial processes. *Icarus 202,* 462-476.

Levy, J.S., Head, J.W., Marchant, D.R., 2009c. Cold and dry processes in the Martian Arctic: Geomorphic observations at the Phoenix landing site and comparisons with terrestrial cold desert landforms. *Geophys. Res. Lett. 36,* L21203. doi: 10.1029/2009GL040634.

Levy, J.S., Head, J.W., Marchant, D.R., Dickson, J.L., Morgan G.A., 2009d. Geologically recent gully-polygon relationships on Mars: Insights from the Antarctic Dry Valleys on the roles of permafrost, microclimates, and water sources for surface flow. *Icarus 201,* 113-126.

Levy, J., Marchant, D.R., Head, J.W., 2010a. Thermal contraction crack polygons on Mars: A synthesis from HiRISE, Phoenix, and terrestrial analog studies. *Icarus 206,* 229-252.

Levy, J.S., Head, J.W., Dickson, J.L., Fassett, C.I., Morgan G.A., Schon, S.C., 2010b. Identification of gully debris flow deposits in Protonilus Mensae, Mars: Characterization of a water-related, energetic gully-forming process. *Earth Planet. Sci. Lett. 294,* 368-377.

Lewkovicz, A.G., 1986. Headwall retreat of ground-ice slumps, Bank Island, Northwest Territories. *Can. J. Earth Sci. 24*, 1077 – 1085.

Liebner, S., Harder, J, Wagner, D., 2008. Bacterial diversity and community structure in polygonal tundra soils from Samoylov Island, Lena Delta, Siberia. *Int. Microbiol. 11*, 195-202.

Liestøl, O., 1976. Pingos, springs and permafrost in Spitsbergen. *Norsk Polarinstitutt Árb. 1975*, 7-29.

Lobitz, B., Wood, B.L., Averner, M.M., McKay, C.P., 2001. Use of spacecraft data to derive regions on Mars where liquid water would be stable. *PNAS 98 (5),* 2132-2137.

Lønne, I., Nemec, W., 2004. High-arctic fan delta recording deglaciation and environment disequilibrium. *Sedimentology 51*, 553-589.

Lukas, S., Nicholson, L.I., Ross, F.H., Humlum, O., 2005. Formation, meltout processes and landscape alteration of high-arctic ice-cored moraines - examples from Nordenskiöld land, Central Spitsbergen. *Polar Geogr. 29*, 157-187.

Lucchitta, B.K., 1981. Mars and Earth-Comparison of cold-climate features. *Icarus 45,* 264-303.

Mackay, J.R., 1974. Ice-wedge cracks, Garry Island, Northwest Territories. *Can. J. Earth. Sci. 11,* 1366–1383.

Mackay, J.R., 1980. Deformation of ice-wedge polygons, Garry Island, Northwest Territories. *Geol. Surv. Can. 80-1A*, 287–291.

Mackay, J.R., 1987. Pingo collapse and paleoclimatic reconstruction. *Can. J. Earth Sci. 25*, 495-511.

Mackay, J.R., 1992. The frequency of ice-wedge cracking (1967– 1987) at Garry Island, western Arctic Coast, Canada. *Can. J. Earth Sci. 29*, 236– 248.

Mackay, J.R., 1998. Pingo growth and collapse, Tuktoyaktuk Peninsula area, Western Arctic Coast, Canada: A long term field study. *Geographique physique et Quaternaire 52*, 271–323.

Mackay, J.R., 2000. Thermally induced movements in ice-wedge polygons, Western Arctic Coast: A long-term study. *Géographie physique et Quaternaire 54 (1),* 41-68.

Mackay, J.R., Burn, C.R., 2002. The first 20 years (1978-1979 to 1998-1999) of ice-wedge growth at the Illisarvik experimental drained lake site, western Arctic coast, *Canada. Can. J. Earth Sci. 39,* 95-111.

Mackay, J.R., Burn, C.R., 2011. A century (1910-2008) of change in a collapsing pinog, Parry Peninsula, Western Arctic Coast, Canada. *Permafrost Periglac.* online available. doi:10.1002/ppp.723.

Madeleine, J.-B., Forget, F., Head, J.W., Levrard, B., Montmessin, F., Millour, E., 2009. Amazonian northern mid-latitude glaciation on Mars: A proposed climate scenario. *Icarus 203,* 390-405.

Malin, M.C., Edgett, K.S., 2000. Evidence for recent groundwater seepage and surface runoff on Mars. *Science 288,* 2330–2335. doi:10.1126/science.288.5475.2330.

Malin, M.C., Bell, J.F., Cantor, B.A., Caplinger, M.A., Calvin, W.M., Clancy, R.T., Edgett, K.S., Edwards, L., Haberle, R.M., James, P.B., Lee, S.W., Ravine, M.A., Thomas, P.C., Wolff, M.J., 2007. Context Camera investigation on board the Mars Reconnaissance Orbiter, *J. Geophys. Res. 112,* E05S04. doi:10.1029/2006JE002808.

Malmström, B., Nordström, S., Palmér, O., 1973. Iskilpolygoner i Adventdalen, Spetsbergen (Ice-wedge polygons in Adventdalen, Spitsbergen). In: Svensson, H., Hellden, U., Malmström, B., Nordström, S., Palmér, O., Åhman, R., Åkerman, J. (Eds.), *Studier i periglacial geomorfologi på Spetsbergen.* Rapporter och notiser 15. Lunds Univerisitets, Naturgeografiska Institution, 4-26 (in Swedish).

Mangerud, J., Bolstad, M., Elgersma, A., Helliksen, D., Landvik, J.Y., Lønne, I., Lycke, A.K., Salvigsen, O., Sandahl, T., Svendsen, J.I., 1992. The last glacial maximum on Spitsbergen, Svalbard. *Quaternary Res. 38,* 1-39.

Mangold, N., 2005. High latitude patterned grounds on Mars: Classification, distribution and climatic control. *Icarus 174,* 336-359.

Mangold, N., Maurice, S., Feldman, W.C., Costard, F., Forget, F., 2004. Spatial relationships between patterned ground and ground ice detected by the neutron spectrometer on Mars. *J. Geophys. Res. 109,* E8. doi:10.1029/2004JE002235.

Marchant, D.R., Head, J.W., 2007. Antarctic Dry Valleys: Microclimate zonation, variable geomorphic processes, and implications for assessing climate change on Mars*. Icarus 192,* 187-222.

Marchant, D.R., Head, J.W., 2010. Geologic analogies between the surface of Mars and the McMurdo Dry Valleys: microclimate-related geomorphic features and evidence for climate change. In: Doran, P.T., Lyons, W.B. & McKnight, D.M. (eds.) *Life in Antarctic Deserts and other Cold Dry Environments.* Cambridge University Press, Cambridge, 9-77.

Marchant, D.R., Lewis, A., Phillips, W.C., Moore, E.J., Souchez, R., Landis, G.P., 2002. Formation of patterned-ground and sublimation till over Miocene glacier ice in Beacon Valley, Antarctica. *Geological Society of America Bulletin 114,* 718-730.

Matsuoka, N., 1999. Monitoring of thermal contraction cracking at an ice-wedge site, central Spitsbergen. *Polar Geosci. 12,* 258–271.

Matsuoka, N., Hirakawa K., 1993. Critical polygon size for ice-wedge formation in Svalbard and Antarctica. *Proceedings of the Sixth International Conference on Permafrost,* Vol. 1. Beijing. pp. 449–454.

McEwen, A.S., Eliason, E.M., Bergstrom, J.W., Bridges, N.T., Hansen, C.J., Delamere, W.A., Grant, J.A., Gulick, V.C., Herkenhoff, K.E., Keszthelyi, L., Kirk, R.L., Mellon, M.T., Squyres, S.W., Thomas, N., Weitz, C.M., 2007. Mars Reconnaissance Orbiter's High-Resolution Imaging Science Experiment (HiRISE). *J. Geophys. Res. 112,* E05S02. doi:10.1029/2005JE002605.

McEwen, A.S., 69 co-authors, 2010. The High Resolution Imaging Science Experiment (HiRISE) during MRO's Primary Science Phase (PSP). *Icarus 205,* 2-37.

McGill, G.E., 1989. Buried topography of Utopia, Mars: Persistence of a giant impact depression. *J. Geophys. Res. 94,* 2753 – 2759.

McGrath, J., Wagener, S., Gilichinsky, D.A., 1994. Cryobiological studies of ancient microorganisms isolated from the Siberian permafrost. In: Gilichinsky, D. A. (ed.), *Viable Microorganisms in Permafrost.* Pushchino, Russia, 74-82.

McKay, C.P., 1997. The search for life on Mars. *Origins Life Evolv. B. 27*, 263-289.

McKay, C.P., Stoker, C.R., 1989. The early environment and its evolution on Mars: Implications for life. *Rev. Geophysics 27(2),* 189-214.

McKay, C.P., Friedman, E.I., Wharton, R.A., Davies, W.L., 1992. History of water on Mars: A biological perspective. *Adv. Space Res. 12,* 231-238.

Meier, K.D., Thannheiser, D., 2009. Gletscher und Permafrost in Nordenskiøldland, Spitzbergen, als potentielle Klimaindikatoren (Glacier and permafrost in Nordenskiøldland, Spitsbergen, as potential climate indicators). *Hamburger Beiträge zur Physischen Geographie und Landschaftsökologie 20.* (in German).

Mellon, M.T., 1997. Small-scale polygonal features on Mars: Seasonal thermal contraction cracks in permafrost. *J. Geophys. Res. 102,* E11, 25617-25628.

Mellon, M.T., Jakosky, B.M., 1993. Geographic variations in the thermal and diffusive stability of ground ice on Mars. *J. Geophys. Res. 98 (E2)*, 3345-3364. doi:10.1029/92JE02355.

Mellon, M.T.; Jakosky, B.M., 1995. The distribution and behavior of Martian ground ice during past and present epochs. J. Geophys. Res. 100(E6), 11,781-11,799.

Mellon, M. T., Jakosky, B.M., Kieffer, H.H., Christensen, P.R., 2000. High resolution thermal inertia mapping from the Mars Global Surveyor Thermal Emission Spectrometer. *Icarus 148*, 437 – 455. doi:10.1006/icar.2000.6503.

Mellon, M.T., Feldman, W.C., Prettyman, T.H., 2004. The presence and stability of ground ice in the southern hemisphere of Mars. *Icarus 169,* 324-340. doi:10.1016/j.icarus.2003.10.022.

Mellon, M.T., Arvidson, R.E., Marlow, J.J., Phillips, R.J., Asphaug, E., 2008. Periglacial landforms at the Phoenix landing site and the northern plains of Mars. *J. Geophys. Res. 113.* doi:10.1029/2007JE003039.

Mellon, M. T. Arvidson, R.E., Sizemore, H.G., Searls, M.L., Blaney, D.L., Cull, S., Hecht, M.H., Heet, T.L., Keller, H.U., Lemmon, M.T., Markiewicz, W.J., Ming, D.W., Morris, R.V., Pike, W.T., Zent, A.P., 2009. Ground ice at the Phoenix Landing Site: Stability state and origin. *J. Geophys. Res*. 114, E00E07. doi: 10.1029/2009JE003417.

Milliken, R.E., Mustard, J.F., 2003. Erosional morphologies and characteristics of latitude dependent surface mantles on Mars. *Sixth International Conference on Mars.* Abstract #3240.

Milliken, R.E. Mustard, J.F., Goldsby, D.L., 2003. Viscous flow features on the surface of Mars: Observations from high-resolution Mars Orbiter Camera (MOC) images. *J. Geophys. Res. 108(E6),* 5057, doi: 10.1029/2002JE002005.

Mischna, M.A., Richardson, M.I., Wilson, R.J., McCleese, D.J., 2003. On the orbital forcing of Martian water and CO2 cycles: A general circulation model study with simplified volatile schemes. *J. Geophys. Res. 108,* 5062. doi: 10.1029/2003JE002051.

Mitrofanov, I., Anfimov, D., Kozyrev, A., Litvak, M., Sanin, A., Tret'yakov, V., Krylov, A., Shvetsov, V., Boynton, W., Shinohara, C., Hamara, D., Saunders, R.S., 2002. Maps of subsurface hydrogen from the High Energy Neutron Detector, Mars Odyssey. *Science 297*, 78-81.

Möhlmann, D., 2005. Adsorption water-related potential chemical and biological processes in the upper Martian surface. *Astrobiology 5 (6),* 770-777.

Möhlmann, D., 2010a. The three types of liquid water in the surface of present Mars. *Int. J. Astrobiol 9 (1),* 45-49.

Möhlmann, D., 2010b. Temporary liquid water in upper snow/ice sub-surfaces on Mars? *Icarus 207*, 140-148.

Möhlmann, D., Thomsen, K., 2011. Properties of cryobrines on Mars. *Icarus 212,* 123-130.

Morgan, G., Head, J.W., Forget, F., Madeleine, J.-B., Spiga, A., 2010. Gully formation on Mars: Two recent phases of formation suggested by links between morphology, slope orientation and insolation history. *Icarus 208(2)*, 658-666. doi:10.1016/j.icarus.2010.02.019.

Morgenstern, A., Hauber, E., Reiss, D., van Gasselt, S., Grosse, G., Schirrmeister, L., 2007. Deposition and degradation of a volatile-rich layer in Utopia Planitia and implications for climate history on Mars. *J. Geophys. Res. 112,* E06010. doi:10.1029/2006JE002869.

Morgenstern, A., Ulrich, M., Guenther, F., Roessler, S., Lantuit, H., 2008a. Combining ALOS data and field investigations for the reconstruction of thermokarst evolution in the North Siberian Lena Delta. In: *Proceedings of the 'Second ALOS PI 2008 Symposium'*, ESA SP-664 (CD-ROM), ESA Communication Production Office, European Space Agency, Noordwijk, The Netherlands. http://hdl.handle.net/10013/epic.31924.

Morgenstern, A., Grosse, G., Schirrmeister, L., 2008b. Genetic, morphological, and statistical characterization of lakes in the permafrost-dominated Lena Delta. In: *Permafrost: Proceedings of the 9th International Conference on Permafrost 2008,* edited by Kane, D.L., and K.M. Hinkel, pp. 1239 – 1244, Institute of Northern Engineering, Univ. of Alaska Fairbanks.

Morita, R.Y., 2000. Is H2 the universal energy source for long-term survival? *Microb. Ecol. 38*, 307-320.

Morozova, D., Wagner, D., 2007. Stress response of methanogenic archea from Siberian permafrost compared with methanogens from nonpermafrost habitats. *FEMS Microbiol. Ecol. 61,* 16-25.

Morozova, D., Möhlmann, D., Wagner, D., 2007. Survival of methanogenic archea from Siberian permafrost under simulated Martian thermal conditions. *Orig. Life Evol. Biosph. 37,* 189-200.

Murton, J.B., 1996. Morphology and paleoenvironmental significance of Quarternary sand veins, sand wedges, and composite wedges, Tutktoyaktuk coastland, western Arctic Canada. *J. Sediment. Res. 66,* 17-25.

Mustard, J.F., Cooper, C.D., Rifkin, M.K., 2001. Evidence for recent climate change on Mars from the identification of youthful near-surface ground ice. *Nature 412,* 411-414.

Müller, F. 1959. Beobachtungen über Pingos. *Meddelelser om Grønland 153*, 1-127.

Mumma, M.J., Villanueva, G.L., Novak, R.E., Hewagama, T., Bonev, B.P., DiSanti, M.A., Mandell, A.M., Smith, M.D., 2009. Strong release of methane on Mars in northern summer 2003. *Science 323,* 1041-1045.

Ødegård, R.S., Isaksen, K., Eiken, T., Sollid, J.-L. 2003. Terrain analyses and surface velocity measurements of the Hiorthfjellet rock glacier, Svalbard. *Permafrost Periglac. 14*, 359-365.

Overduin, P.P., Kane, D.L., 2006. Frost boils and soil ice content: Field observations. *Permafrost Periglac. 17,* 291 – 307.

Paige, D.A., 2002. Near-surface liquid water on Mars. *Lunar Planet. Sci. XXXIII*, Abstract 2049.

Panikov, N.S., Sizova, M.V., 2007. Growth kinetics of microorganisms isolated from Alaskan soil and permafrost in solid media frozen down to −35°C. *FEMS Microbiol Ecol 59*, 500-512.

Paterson, W.S.B., 1994. *The Physics of Glaciers (3rd ed.),* Pergamon/Elsevier, Oxford.

Pearce, G., Osinski, G.R., Soare, R.J., 2011. Intra-crater glacial processes in central Utopia Planitia, Mars. *Icarus 212*, 86-95.

Perron, J.T., Dietrich, W.E., Howard, A.D., McKean, J.A., Pettinga, J.R., 2003. Ice-driven creep on Martian debris slopes. *Geophys. Res. Lett. 30*, 1747. doi:10.1029/2003GL017603.

Péwé, T.L., 1959. Sand wedge polygons (Tesselations) in the McMurdo Sound Region, Antarctica. *Am. J. Sci. 257*, 545-552.

Pfiffner, S.M., Onstott, T.C., Ruskeeniemi, T., Talikka, M., Bakermans, C., McGown, D., Chan, E., Johnson, A., Phelps, T.J., Le Puil, M., Difurio, S.A., Pratt, L.M., Stotler, R., Frape, S., Telling, J., Sherwood Lollar, B., Neill, I., Zerbin, B., 2008. Challenges for coring deep permafrost on Earth and Mars. *Astrobiology 8(3)*, 623-638.

Phillips, R.J., Davis, B.J., Tanaka, K.L., Byrne, S., Mellon, M.T., Putzig, N.E., Haberle, R.M., Kahre, M.A., Campbell, B.A., Carter, L.M., Smith, I.B., Holt, J.W., Smrekar, S.E., Nunes, D.C., Plaut, J.J., Egan, A.F., Titus, T.N., Seu, R., 2011. Massive CO2 ice deposits sequestered in the south polar layered deposits of Mars. *Science 332*, 838-841.

Pierce, T.L., Crown, D.A., 2003. Morphologic and topographic analyses of debris aprons in the eastern Hellas region, Mars. *Icarus 163*, 46-65.

Pina, P., Saraiva, J., Bandeira, L., Antunes, J., 2008. Polygonal terrains on Mars: A contribution to their geometric and topological characterization. Planet. *Space Sci. 56,* 1919-1924.

Plug, L.J., Werner, B.T., 2001. Fracture networks in frozen ground. *J. Geophys. Res. 106*, B5, 8599-8613.

Pollard, W., Haltigin, T., Whyte, L., Niederberger, T., Andersen, D., Omelon, C., Nadeau, J., Ecclestone, M., Lebeuf, M., 2009. Overview of analogue science activities at the McGill Arctic Research Station, Axel Heilberg Island, Canadian High Arctic. *Planet. Space Sci. 57,* 646-659.

Price, P.B., Sowers T, 2004. Temperature dependence of metabolic rates for microbial growth, maintenance, and survival. *Proc Natl Acad Sci. 101*, 4631-4636.

Putzig, N. E., M. T Mellon, K. A. Kretke, and R. E. Arvidson (2005), Global thermal inertia and surface properties of Mars from the MGS mapping mission, *Icarus 173*, 325 – 341, doi:10.1016/j.icarus.2004.08.017.

Reed, R.K., 1977. On estimating insolation over the ocean. *J. Phys. Oceanogr. 7,* 482–485.

Reid, M.E., Nielsen, H.P., Dreiss, S.J., 1988. Hydrologic factors triggering a shallow hillslope failure. *Bulletin of the Association of Engineering Geologists 25*, 349-61.

Reiss, D., van Gasslet, S., Neukum, G., Jaumann, R., 2004. Absolute dune ages and implications for the time of formation of gullies in Nirgal Vallis, Mars. *J. Geophys. Res. 109.* doi:10.1029/2004JE002251.

Reiss, D., Hiesinger, H., Hauber, E., Gwinner, K., 2009. Regional differences in gully occurrence on Mars: A comparison between the Hale and Bond craters. *Planet. Space Sci. 57*, 958-974.

Reiss, D., Erkeling, G., Bauch, K.E., Hiesinger, H., 2010. Evidence for present day gully activity on the Russell crater dune field, Mars. *Geophys. Res. Lett. 37*, L06203. doi:10.1029/2009GL042192.

Rennó, N.O., Bos, B.J., Catling, D., Clark, B.C., Drube, L., Fisher, D., Goetz, W., Hviid, S.F., Keller, H.U., Kok, J.F., Kounaves, S.P., Leer, K., Lemmon, M., Madsen, M.B., Markiewicz, W.J., Marshall, J., McKay, C., Mehta, M., Smith, M., Zorzano, M.P., Smith, P.H., Stoker, C., Young, S.M.M., 2009. Possible physical and thermodynamical evidence for liquid water at the Phoenix landing site. *J. Geophys. Res. 114,* E00E03. doi:10.1029/2009JE003362.

Rich, P.M., Dubayah, R., Hetrick, W.A., Saving, S.C., 1994. Using viewshed models to calculate intercepted solar radiation: Applications in ecology. *American Society for Photogrammetry and Remote Sensing Technical Papers*, 524 – 529. (available at http://libraries.maine.edu/Spatial/gisweb/spatdb/acsm/ac94060.html).

Rivkina, E.M., Friedman, E.I., McKay, C.P., Gilichinsky, D.A., 2000. Metabolic activity of permafrost bacteria below the freezing point. *Appl. Environ. Microb. 66 (8),* 3230-3233.

Roberts, D.W., 1986. Ordination on the basis of fuzzy set theory. *Vegetatio 66,* 123-131.

Romanovskii, N.N., 1977. *Formirovanie poligonal'no-zhil'nykh struktur* (Formation of polygonal wedge-structures). Novosibirsk, Nauka. (in Russian).

Romanovskii, N.N., 1985. Distribution of recently active ice and soil wedges in the USSR. In: Church, M., Slaymaker, O. (Eds), *Field and Theory; Lectures in Geocryology*. University of British Columbia Press, Vancouver. pp. 154-165.

Romanovskii, N.N., Hubberten, H.W., Gavrilov, A.V., Tumskoy, V.E., Tipenko, G.S., Grigoriev, M.N., Siegert, Ch., 2000. Thermokarst and land-ocean interactions, Laptev Sea Region, Russia. *Permafrost Periglac. 11*, 137 – 152.

ROSHYDROMET, 2009. Weather Information for Tiksi. (available at http://www.worldweather.org/107/c01040.htm). Russian Federal Service for Hydrometeorology and Environmental Monitoring, Moscow.

Ross, N., Brabham, P.J., Harris, C., Christiansen, H.H., 2007. Internal structure of open system pingos, Adventdalen, Svalbard: The use of resistivity tomography to assess ground-ice conditions. *J. Environ. Eng. Geoph. 12,* 113-126.

Rossbacher, L.A., 1986. Nearest-neighbour analysis: a technique for quantitative evaluation of polygonal ground patterns. *Geogr. Ann. A 68 (1/2),* 101-105.

Rossbacher, L.A., Judson, S., 1981. Ground ice on Mars: Inventory, distribution, and resulting landforms. *Icarus 45,* 39-59.

Rothschild, L.J., Mancinelli, R.L., 2001. Life in extreme environments. *Nature 409*, 1092-1101.

Schirrmeister, L., Kunitsky, V.V., Grosse, G., Schwamborn, G., Andreev, A.A., Meyer, H., Kuznetsova, T., Bobrov, A., Oezen, D., 2003. Late Quaternary history of the accumulation plain north of the Chekanovsky Ridge (Lena Delta, Russia): A multidisciplinary approach. *Pol. Geogr. 27,* 277 – 319.

Schirrmeister, L., Kunitsky, V.V., Grosse, G., Kuznetsova, T.V., Derevyagin, A.Y., Wetterich, S., Siegert, Ch., 2008. The Yedoma Suite of the northeastern Siberian shelf region – characteristics and concept of formation. In: *Permafrost: Proceedings of the 9th International Conference on Permafrost 2008,* edited by Kane, D.L., and K.M. Hinkel, pp. 1595 – 1601, Institute of Northern Engineering, Univ. of Alaska Fairbanks.

Schirrmeister, L., Kunitsky, V., Grosse, G., Wetterich, S., Meyer, H., Schwamborn, G., Babiy, O., Derevyagin, A., Siegert, C., in press. Sedimentary characteristics and origin of the Late Pleistocene Ice Complex on the north-east Siberian Arctic coastal lowlands and islands – A review. *Quatern. Int.*

Scholten, F., Gwinner, K., 2004. Operational parallel processing in digital photogrammetry – strategy and results using different multi-line cameras. *International Archives of Photogrammetry and Remote Sensing, XXXIV,* 408-413.

Scholten, F., Gwinner, K., Roatsch, T., Matz, K.-D., Wählisch, M., Giese, B., Oberst, J., Jaumann, R., Neukum, G., the HRSC Co-Investigator Team, 2005. Mars Express HRSC data processing - methods and operational aspects. *Photogramm. Eng. Rem. S. 71,* 1143-1152.

Schon, S.C., Head, J.W., Fassett, C.I., 2009a. Unique chronostratigraphic marker in depositional fan stratigraphy on Mars: Evidence for ca. 1.25 Ma gully activity and surficial meltwater origin. *Geology 37,* 207–210.

Schon, S.C., Head, J.W., Milliken, R.E., 2009b. A recent ice age on Mars: Evidence for climate oscillations and the buried ice hypothesis revealed by regional layering in dissected mid-latitude mantling deposits. *Geophys. Res. Lett. 36,* L15202, doi:10.1029/2009GL038554.

Schopf, J.W., 1993. Microfossils of the early Archean Apex chert: new evidence of the antiquity of life. Science 260, 640-646.

Schorghofer, N., 2007. Dynamics of ice ages on Mars. Nature 449, 192-194.

Schorghofer, N., Edgett, K.S., 2006. Seasonal surface frost at low latitudes on Mars. *Icarus 180,* 321-334.

Schorghofer, N., Aharonson, O., 2005. Stability and exchange of subsurface ice on Mars. *J. Geophys. Res. 110,* E05003. doi:10.1029/2004JE002350.

Schwamborn, G., Rachold, V., Grigoriev, M.N., 2002. Late Quaternary sedimentation history of the Lena Delta. *Quat. Int. 89,* 119 – 134.

Seibert, N.M., Kargel, J.S., 2001. Small-scale Martian polygonal terrain: Implications for liquid surface water. *Geophys. Res. Lett. 28*, 899-902.

Séjourné A., Costard, F., Gargani, J., Soare, R.J., Fedorov, A., Marmo, C., 2011. Scalloped depressions and small-sized polygons in western Utopia Planitia, Mars: A new formation hypothesis. *Planet. Space Sci. 59 (5/6),* 412-422. doi:10.1016/j.pss.2011.01.007.

Shakesby, R.A., 1997. Pronival (protalus) ramparts: a review of forms, processes, diagnostic criteria and palaeoenvironmental implications. *Prog. Phys. Geog. 21*, 394-418.

Shakesby, R.A., Dawson, A.G., Matthews, J.A., 1987. Rock glaciers, protalus ramparts and related phenomena, Rondane, Norway: a continuum of large-scale talus-derived landforms. *Boreas 16,* 305-317.

Sharp, R.P., 1973. Mars: Fretted and chaotic terrain. *J. Geophys. Res. 78*, 4073 – 4083.

Sharp, R.P., 1988. Earth science field work: Role and status. *Annu. Rev. Earth Pl. Sc. 16*, 1-19.

Shcherbakova, V.A., Chuvilskaya, N.A., Rivkina, E.M., Pecheritsyna, S.A., Laurinavichius, K.S., Suzina, N.E., Osipov, G.A., Lysenko, A.M., Gilichinsky, D.A., Akimenko, V.K., 2005. Novel psychrophilic anaerobic spore-forming bacterium from the overcooled water brine in permafrost: Description Clostridium algoriphilum sp. nov. *Extremophiles 9*, 239-246.

Shumskii, P.A., 1964. *Principles of Structural Glaciology.* Dover Publications, New York.

Shuster, D.L., Weiss, B.P., 2005. Martian surface paleotemperatures from thermochronology of meteorites. *Science 309,* 597.

Sletten, R.S., Hallet, B., Fletcher, R.C., 2003. Resurfacing time of terrestrial surfaces by the formation and maturation of polygonal patterned ground. *J. Geophys. Res. 108(E4),* 8044. doi:10.1029/2002JE001914.

Smith, D.E., Zuber, M.T., Frey, H.V., Garvin, J.B., Head, J.W., Muhleman, D.O., Pettengill, G.H., Phillips, R.J., Solomon, S.C., Zwally, H.J., Banerdt, W.B., Duxbury, T.C., Golombek, M.P., Lemoine, F.G., Neumann, G.A., Rowlands, D.D., Aharonson, O., Ford, P.G., Ivanov, A.B., Johnson, C.L., McGovern, P.J., Abshire, J., Afzal, R.S., Sun, X., 2001. Mars Orbiter Laser Altimeter: Experiment summary after the first year of global mapping of Mars. *J. Geophys.Res. 106(E10),* 23, 689 – 23, 722. doi:10.1029/2000JE001364.

Smith, H.D., McKay, C.P., 2005. Drilling in ancient permafrost on Mars for evidence of a second genesis for life. *Planet. Space Sci. 53,* 1302-1308.

Smith, P.H., Tamppari, L.K., Arvidson, R.E., Bass, D., Blaney, D., Boynton, W.V., Carswell, A., Catling, D.C., Clark, B.C., Duck, T., DeJong, E., Fisher, D., Goetz, W., Gunnlaugsson, H.P., Hecht, M.H., Hipkin, V., Hoffman, J., Hviid, S.F., Keller, H.U., Kounaves, S.P., Lange, C.F., Lemmon, M.T., Madsen, M.B., Markiewicz, W.J., Marshall, J., McKay, C.F., Mellon, M.T., Ming, D.W., Morris, R.V., Pike, W.T., Renno, N., Staufer, U., Stoker, C., Taylor, P., Whiteway, J.A., Zent, A.P., 2009. H2O at the Phoenix landing site. *Science 325,* 58-61.

Smoluchowski, R., 1968. Mars: Retention of Ice. *Science 159,* 1348-1350.

Soare, R.J., Osinski, G.R., 2009. Stratigraphical evidence of late Amazonian periglaciation and glaciation in the Astapus Colles region on Mars. *Icarus 202,* 17-21.

Soare, R.J., Burr, D.M., Wan Bun Tseung, J.M., 2005. Possible pingos and a periglacial landscape in northwest Utopia Planitia. *Icarus 174,* 373-382. doi:10.1016/j.icarus.2004.11.013.

Soare, R. J., Kargel, J.S., Osinski, G.R., Costard, F., 2007. Thermokarst processes and the origin of crater-rim gullies in Utopia and western Elysium Planitia. *Icarus 191*, 95 – 112. doi:10.1016/j.icarus.2007.04.018.

Soare, R. J., Osinski, G.R., Roehm, C.L., 2008. Thermokarst lakes and ponds on Mars in the very recent (late Amazonian) past. *Earth Planet. Sci. Lett. 272,* (382 – 393). doi:10.1016/j.epsl.2008.05.010.

Soderblom, L.A., Kreidler, T.J., Masursky, H., 1973. Latitudinal distribution of a debris mantle on the Martian surface. *J. Geophys. Res. 78,* 4117–4122.

Sollid, J.L., Holmlund, P., Isaksen, K., Harris, C., 2000. Deep permafrost boreholes in western Svalbard, northern Sweden and southern Norway. *Norsk Geografisk Tidsskrift 54*, 186-191.

Soloviev, P.A., 1962. Alas relief of Central Yakutia and its formation, in *Permafrost and Accompanying phenomena in the territory of the Yakutian ASSR*, pp. 38 – 53, Academy of Sciences of the USSR, Moscow (in Russian).

Soloviev, P.A., 1973. Thermokarst phenomena and landforms due to frostheaving in Central Yakutia, *Biuletyn Peryglacjalny 23*, 135 – 155.

Sørbel L, Tolgensbakk J., 2002. Ice-wedge polygons and solifluction in the Adventdalen area, Spitsbergen, Svalbard. *Norsk Geografisk Tidsskrift 56*, 62-66.

Sørbel, L., Tolgensbakk, J., Hagen, J.O., Høgvard, K., 2001. *Geomorphological and Quaternary Map of Svalbard.* 1:100,000, Sheet C9Q Adventdalen, Temakart No.31/32. Norwegian Polar Institute, Tromsø.

Squyres, S.W., 1978. Martian fretted terrain - Flow of erosional debris. *Icarus 34,* 600-613.

Squyres, S.W., Grotzinger, J.P., Arvidson, R.F., Bell, J.F., Calvin, W., Christensen, P.R., Clark, B.C., Crisp, L.A., Farrand, W.H., Herkenhoff, K.E., Johnson, J.R., Klingelhofer, G., Knoll, A.H., McLennan, S.M., McSween, H.Y., Morris, R.V., Rice, J.W., Rieder, R., Soderblom, L.A.,2004. In situ evidence for an ancient aqueous environment at Meridiani Planum, Mars. *Science 306*, 1709-1714.

Steven, B., Briggs, G., McKay, C.P., Pollard, W.H., Greer, C.W., Whyte, L.G., 2007. Characterization of the microbial diversity in a permafrost sample from the Canadian high Arctic using culturedependent and culture-independent methods. *FEMS Microbiol Ecol 59,* 513-523.

Stoker, C.R., Zent, A., Catling, D.C., Douglas, S., Marshall, J.R., Archer Jr., D., Clark, B., Kounaves, S.P., Lemmon, M.T., Quinn, R., Renno, N., Smith, P.H., Young, S.M.M., 2010. Habitability of the Phoenix landing site. *J. Geophys. Res. 115,* E00E20. doi:10.1029/2009JE003421.

Svensson, H., 1971. Pingos i yttre delen av Adventdalen (Pingos in outermost Adventdalen valley). *Norsk Polarinstitutt Árbok 1969,* Oslo, 168-174. (in Norwegian).

Svitek, T., Murray, B., 1990. Winter frost at the Viking Lander 2 site. *J. Geophys. Res. 95(B2),* 1485-1510.

Sweetman, J.N., Rühland, K.M., Smol, J.P., 2010. Environmental and spatial factors influencing the distribution of cladocerans in lakes across the central Canadian Acrtic treeline region. *J. Limnol. 69 (1),* 76-87.

Tanaka, K.L., Skinner, J.A., Hare, T.M., 2005. *Geologic map of the northern plains of Mars.* 1:15,000,000, U. S. Geol. Surv. Sci. Invest. Map 2888.

Thomson, B.J., Head, J.W., 2001. Utopia Basin, Mars: Characterization of topography and morphology and assessment of the origin and evolution of basin internal structure. *J. Geophys. Res.106 (E10),* 232009-23230.

Thorn, C.E., 1978. The geomorphic role of snow. *Ann. Associ. Ame. Geogr. 68,* 414-425.

Thorn, C.E., 1988. Nivation: a geomorphic chimera. In: Clark, M.J. (ed.) *Advances in Periglacial Geomorphology*. Wiley, Chichester, 3-31.

Tolgensbakk, J., Sørbel, L., Høgvard, K., 2001. *Adventdalen, geomorphological and quaternary geological map of Svalbard.* 1:100,000, Spitsbergen sheet C9Q. Temakart No.32. Norwegian Polar Institute, Tromsø.

Toon, O.B., Pollack, J.B., Ward, W., Burns, J.A., Bilski, K., 1980. The astronomical theory of climatic change on Mars. *Icarus 44,* 552-607.

Tosca, N.J., McLennan, S.M., Lamb, M.P., Grotzinger, J.P., 2011. Physicochemical properties of concentrated Martian surface waters. *J. Geophys. Res. 116*, E05004. doi:10.1029/2010JE003700.

Touma, J., Wisdom, J., 1993. The chaotic obliquity of Mars. *Science 259*, 1294–1297.

Ulrich, M., Grosse, G., Chabrillat, S., Schirrmeister, L., 2009. Spectral characterization of periglacial surfaces and geomorphological units in the Arctic Lena Delta using field spectrometry and remote sensing. *Remote Sens. Environ. 113*, 1220 – 1235. doi:10.1016/j.rse.2009.02.009.

Ulrich, M., Morgenstern, A., Günther, F., Reiss, D., Bauch, K.E., Hauber, E., Rössler, S., Schirrmeister, L., 2010. Thermokarst in Siberian ice-rich permafrost: Comparison to asymmetric scalloped depressions on Mars. *J. Geophys. Res. 115*, E10009. doi:10.1029/2010JE003640.

Ulrich, M., Hauber, E., Herzschuh, U., Härtel, S., Schirrmeister, L., in press. Polygon pattern geomorphometry on Svalbard (Norway) and western Utopia Planitia (Mars) using high-resolution stereo remote-sensing data. *Geomorphology*.

Ulrich, M., Wagner, D., Hauber, E., de Vera, J.-P., Schirrmeister, L., submitted. Habitable periglacial landscapes in Martian mid-latitudes. *Icarus.*

van Gasselt, S., Reiss, D., Thorpe, A.K., Neukum, G., 2005. Seasonal variations of polygonal thermal contraction crack patterns in a south polar trough, Mars. *J. Geophys. Res. 110 (E8),* E08002. doi: 10.1029/2004JE002385.

van Gasselt, S., Hauber, E., Neukum, G., 2010. Lineated valley fill at the Martian dichotomy boundary: Nature and history of degradation. *J. Geophys. Res. 115*, E08003. doi:10.1029/2009JE003336.

Vincendon, M., Mustard, J., Forget, F., Kreslavsky, M., Spiga, A., Murchie, S., Bibring, J.-P., 2009. Mid latitude CO2 ice deposits analyzed with CRISM and OMEGA. In: *Third International Workshop on Mars Polar Energy Balance and the CO2 Cycle*. held July 21–24, 2009 in Seattle, Washington. Lunar and Planetary Institute, Houston, TX. LPI Contribution No. 1494, abstract 7021, pp. 61–62.

Vincendon, M., Mustard, J., Forget, F., Kreslavsky, M., Spiga, A., Murchie, S., Bibring, J.-P., 2010a. Near-tropical subsurface ice on Mars. *Geophys. Res. Lett. 37,* L01202. doi:10.1029/2009GL041426.

Vincendon, M., Forget, F., Mustard, J., 2010b. Water ice at low to mid latitudes on Mars. *J. Geophys. Res. 115*, E10001 doi: 10.1029/2010JE003584.

Vishnivetskaya, T.A., Kathariou, S., McGrath, J., Gilichinsky, D., Tiedje, J.M., 2000. Low-temperature recovery strategies for the isolation of bacteria from ancient permafrost sediments. *Extremophiles 4,* 165-173.

Vishnivetskaya, T.A., Petrova, M.A., Urbance, J, Ponder, M, Moyer, C.L, Gilichinsky, D.A, Tiedje, J.M., 2006. Bacterial community in ancient Siberian permafrost as characterized by culture and culture-independent methods. *Astrobiology 6,* 400-414.

Vorobyova, E., Soina, V., Gorlenko, M., Minkovskaya, N., Zalinova, N., Mamukelashvih, A., Gilichinsky, D., Rivkina, E., Vishnivetskaya, T., 1997. The deep cold biosphere: Facts and hypothesis. *FEMS Microbiol Rev, 20*, 277-290.

Wagner, D., 2008. Microbial communities and processes in Arctic permafrost environments. In: Dion, P., Nautiyal, C.S. (Eds.), *Microbiology of Extreme Soils*. Soil Biology 13, Springer-Verlag Berlin. pp. 133-154.

Wagner, D., Lipski, A., Embacher, A., Gattinger, A., 2005. Methane fluxes in permafrost habitats of the Lena Delta: Effects of microbial community structures and organic matter quality. *Environ. Microbiol. 7 (10),* 1582-1592.

Wagner D., Gattinger A., Embacher A., Pfeiffer E.-M., Schloter M., Lipski A., 2007. Methanogenic activity and biomass in Holocene permafrost deposits of the Lena Delta, Siberian Arctic and its implication for the global methane budget. *Global Change Biology 13*, 1089-1099.

Wagner, D., Malaszkiewicz, J., Ganzert, L., Morozova, D. in prep. Methanosarcina gelisolum sp. nov., a multi-tolerant methanogenic archaeon isolated from a Siberian permafrost-affected soil. To be submitted to *Int. J. Sys. Evol. Microbiol.*

Walker, A.S., 1997. *Deserts – Geology and Resources*. USGS Online Book. http://pubs.usgs.gov/gip/deserts/.

Ward, W.R., 1973. Large-scale variations in the obliquity of Mars. *Science 181*, 260-262.

Warner, N., Gupta, S., Kim, J.-R., Lin, S.-Y., Muller, J.-P., 2010. Hesperian equatorial thermokarst lakes in Ares Vallis as evidence for transient warm conditions on Mars. *Geology 38*, 71 – 74. doi:10.1130/G30579.1.

Washburn, A.L., 1979. *Geocryology - A Survey of Periglacial Processes and Environments*. E. Arnold Ltd., London.

Wetterich, S., Kuzmina, S., Andreev, A.A., Kienast, F., Meyer, H., Schirrmeister, L., Kuznetsova, T., Sierralta, M., 2008. Palaeoenvironmental dynamics inferred from late Quaternary permafrost deposits on Kurungnakh Island (Lena Delta, Northeast Siberia, Russia). *Quat. Sci. Rev. 27,* 1523 – 1540.

Wewel, F., Scholten, F., Gwinner, K., 2000. High Resolution Stereo Camera (HRSC) – Multispectral 3D-data acquisition and photogrammetric data processing. *Can J. Remote Sens. 26,* 466-474.

Williams, K.E., Toon, O.B., Heldmann, J.L., McKay, C., Mellon, M.T., 2008. Stability of mid-latitude snowpacks on Mars. *Icarus 196,* 565-577.

Williams, K.E., Toon, O.B., Heldmann, J.L., Mellon, M.T., 2009. Ancient melting of mid-latitude snowpacks on Mars as a water source for gullies. *Icarus 200,* 418-425.

Williams, P.J., Smith, M. W., 1989. *The Frozen Earth: Fundamentals of Geocryology*. Cambridge Univ. Press., Cambridge.

Willmes, M., Reiss, D., Hiesinger, H., Zanetti, M., in revision. Surface age of the ice-dust mantle in Malea Planum, Mars. Submitted to *Planet. Space Sci.*

Worsley, P., Gurney, S.D., 1996. Geomorphology and hydrogeological significance of the Holocene pingos in the Karup Valley area, Traill Island, northern east Greenland. *J. Quat. Sci. 11,* 249-262.

Yergeau, E., Hogues, H., Whyte, L.G., Greer, C.W., 2010. The functional potential of high Arctic permafrost revealed by metagenomic sequencing, qPCR and microarray analyses. The ISME Journal, 4, 1206-1214.

Yershov, E.D., 2004. *General Geocryology; Studies in Polar Research.* Cambridge Univ. Press, New York.

Yoshikawa, K., 1993. Notes on open-system pingo ice, Adventdalen, Spitsbergen. *Permafrost Periglac. 4,* 327-334.

Yoshikawa, K., 2003. Origin of the polygons and thickness of Vastitas Borealis Formation in Western Utopia Planitia on Mars. *Geophys. Res. Lett. 30(12*), 1603. doi:10.1029/2003GL017165.

Yoshikawa, K., Harada, K., 1995. Observations on nearshore pingo growth, Adventdalen, Spitsbergen. *Permafrost Periglac. 6,* 361-372.

Yoshikawa, K., Nakamura, T., 1996. Pingo growth ages in the delta area, Adventdalen, Spitsbergen. *Polar Record 32,* 347-352.

Zahnle, K., Freedman, R.S., Catling, D.C., 2011. Is there methane on Mars? Icarus 212, 493-503.

Zanetti, M., Hiesinger, H., Reiss, D., Hauber, E., Neukum, G., 2010. Distribution and evolution of scalloped terrain in the southern hemisphere, Mars. *Icarus 206(2),* 691 – 706. doi:10.1016/j.icarus.2009.09.010.

Zhang, T., Barry, R.G., Knowles, K., Heginbottom, J.A., Brown, J., 2005. Statistics and characteristics of permafrost and ground-ice distribution in the northern hemisphere. *Polar Geogr. 23 (2),* 132-154.

Zuur, A.F., Ieno, E.N., Smith, G.M., 2007. *Statistics for Biology and Health; Analyzing Ecological Data.* Springer, New York.

Note: The reference list has been updated and arranged in accordance to the structures of the thesis.

Therefore, slight differences to citations in the already published original papers may occur.

Acknowledgements

This thesis and the work at the Alfred Wegener Institute (AWI) Potsdam during the last years could not have realized without the support and patience of many people from my scientific and private environment. I really enjoyed the time in Potsdam at the AWI and the very friendly working atmosphere. I would like to thank you all very warmly.

This research has been partly supported by the German Helmholtz Association through the "Planetary Evolution and Life" research alliance.

Lutz Schirrmeister – Thank you for your excellent guidance, enthusiasm and continual support throughout the work at the AWI and beyond. Thank you for being there, helping me to be content and positive when I was in doubt even when things were tough for yourself. I am really glad and proud that I could work with you all the time since 2003 and I hope that we can continue the work together.

Ernst Hauber – Thank you for letting me part of your enormous knowledge and experience in planetary geomorphology and for providing me always with critical comments and fruitful ideas. This thesis has not been possible without your patient support and interests in the work we did together.

Hans-Wolfgang Hubberten – I am very grateful for the general supervision of this thesis and the opportunity to conduct this work at the AWI Potsdam. Many thanks also for the unique chance of doing field work at amazing places in Siberia and Spitsbergen and for enabling my participations at overseas conferences.

Ute Bastian – Thank you for providing me with your valuable support in the lab and your special sympathy and warmth.

I would like to thank many others who support my work at the AWI and within the HGF research alliance. **Dennis Reiss** provided valuable help and support with Martian remote sensing data. My statistical analyses were highly supported by the expertise of **Ulrike Herzschuh**. **Dirk Wagner** guided and supported my side trip into the microbiology. Thank you very much.

The field teams in particular **Anne Morgenstern, Frank Günther, Sebastian Rössler, Fabian Beermann, Sebastian Zybrzycki, Ernst Hauber, Dennis Reiss, Harald Hiesinger, Michael Zanetti, Andreas Johnsson, and Lars Johansson** – Thank you all for your engagement during the field work in Siberia and Spitsbergen and for making the trips to wonderful and exciting experiences.

All co-authors and reviewers of relevant papers – I really appreciate your contributions, ideas and valuable comments. The publications and this thesis highly benefited by English proof-reading and valuable comments from Candace S. O'Connor (UAF, Fairbanks, Alaska). Thank you.

All AWI colleagues (Lars Ganzert, Michael Fritz, Anne Morgenstern, Andreas Borchers, Sebastian Wetterich, Thomas Opel, Frank Günther, Hugues Lantuit, Jens Strauss, Stephan Opitz, Francisco Fernandoy, Boris Biskaborn, Birgit Heim, and all other AWI geo- and bio- PhD students and seniors) – Many thanks for the wonderful times which I had at the AWI. Thank you very much for the creative scientific and non-scientific discussions, the friendship, and lots of fun.

Mein besonderer und herzlichster Dank gilt meiner Familie für die liebevolle und ausdauernde Unterstützung meiner Arbeit, insbesondere meinen Eltern, welche mich immer und nicht nur finanziell unterstützt haben und am Fortgang der Arbeit interessiert waren.

Zu guter Letzt aber besonders wichtig, danke Katja für Milla, für deine Liebe, für deine Geduld, Unterstützung und Motivation während der letzten Jahre und dein Verständnis dafür, dass ich soviel Zeit mit meinem Computer verbracht habe, die ich eigentlich mit euch hätte verbringen sollen. Danke, dass du zusammen mit mir so manche Schwierigkeit ausgehalten hast.

Eidesstattliche Erklärung

Hiermit versichere ich an Eides statt, dass die vorliegende Arbeit selbstständig und ohne unerlaubte Hilfsmittel angefertigt wurde.

Die kumulative Dissertation wurde von mir am Alfred-Wegener Institut für Polar- und Meeres-forschung in Potsdam bearbeitet, in englischer Sprache verfasst und wird erstmalig und nur an der Universität Potsdam eingereicht.

Die dem Verfahren zugrunde liegende Promotionsordnung ist mir bekannt.

Mathias Ulrich
Potsdam, 6. Juli 2011